



Contents lists available at ScienceDirect



Highlighting coupling effects in ionic diffusion

Rajamani Krishna

Van't Hoff Institute for Molecular Sciences, University of Amsterdam, Science Park 904, 1098 XH Amsterdam,
The Netherlands

ARTICLE INFO

Article history:

Received 2 May 2016

Received in revised form 2 August 2016

Accepted 4 August 2016

Available online 11 August 2016

Keywords:

Ion diffusion

Ion exchange

Nernst–Planck equations

Diffusion asymmetry

Uphill diffusion

Transient overshoots

ABSTRACT

The proper description of ion diffusion fluxes is important in the design and development of separation processes such as ion exchange, electrodialysis, metals extraction and fuel cells. The primary objective of this article is to highlight the several distinguishing characteristics of ionic diffusion. Due to the requirements of electro-neutrality and the no-current prescription, an electrostatic potential gradient is induced that tends to accelerate or decelerate ions depending on the sign of their charges. Furthermore, for mixed ion systems the diffusion fluxes are strongly coupled to one another. Diffusional coupling effects result in overshoots and uphill ion diffusion in bulk electrolytes and within charged ion-exchange particles. The induced electrostatic potential also cause forward and reverse ion exchange processes to proceed at significantly different rates, i.e. these are asymmetric. For exchange of three counter-ions, the transient adsorption/desorption trajectories follow completely different equilibration trajectories in composition space. The Nernst–Planck equation is found to be of sufficient accuracy to capture all of the essential features of mixed ion diffusion in the variety of systems examined.

© 2016 The Institution of Chemical Engineers. Published by Elsevier B.V. All rights reserved.

1. Introduction

A wide variety of processes of importance in the chemical process industries involve the transport of ionic species in bulk electrolyte liquid mixtures, within charged particles, and across charged membranes. Examples include electrolysis, electrodialysis, ion exchange, metals extraction, and fuel cells (Buck, 1984; Franzreb et al., 1993; Helfferich, 1962a,b, 1983; Jones and Carta, 1993; Lightfoot, 1974; Lito et al., 2012; Newman, 1991; Rodriguez et al., 1998; Seader et al., 2011; Sirkar, 2014; Wankat, 2012; Wesselingh and Krishna, 2000; Yoshida and Kataoka, 1987). Ion exchange separations, for example, have applications in water treatment, water softening, water demineralization, decolorization of sugar solutions, and recovery of trace metal ions from acid leach solutions.

The design and development of ionic separation processes requires a proper model description for the ionic diffusion fluxes. The application of the Fick's law of diffusion

to relate the ion diffusion flux, N_i , to its concentration gradient by defining an effective ion diffusivity, $D_{i,\text{eff}}$ is fraught with complications and ambiguities. One of the earliest demonstrations of the limitations of Eq. (1) is to be found in the experimental data for the effective ionic diffusivities reported by (Vinograd and McBain, 1941). The effective diffusivities $D_{i,\text{eff}}$ were determined in a two-compartment diffusion cell, shown schematically in Fig. 1a. Diffusion takes place through the pores of a sintered glass disc that separates the two compartments. Each of the two compartments is well-mixed, and the concentration gradients are restricted to the disc of thickness, δ . The bottom compartment contains pure water while the top compartment contains a mixture of aqueous solutions of HCl and BaCl_2 . Let c_{HCl} and c_{BaCl_2} denote the molar concentrations, expressed in mol L^{-1} of solution. Total ionization takes place and the system is a quaternary mixture: $1 = \text{H}^+$, $2 = \text{Cl}^-$, $3 = \text{Ba}^{++}$, $4 = \text{H}_2\text{O}$; the ionic charges are $z_1 = +1$; $z_2 = -1$, $z_3 = +1$; $z_4 = 0$. The concentrations of ions are: $c_{\text{H}^+} = c_{\text{HCl}}$; $c_{\text{Ba}^{++}} = c_{\text{BaCl}_2}$; $c_{\text{Cl}^-} = (c_{\text{HCl}} + 2c_{\text{BaCl}_2})$. In one set of experiments reported by (Vinograd and McBain, 1941), the ratio of the concentrations $c_{\text{HCl}}/c_{\text{BaCl}_2}$ was varied. The experimentally

$$N_i = -D_{i,\text{eff}} \frac{\partial c_i}{\partial z} \quad (1)$$

E-mail address: r.krishna@contact.uva.nl
<http://dx.doi.org/10.1016/j.cherd.2016.08.009>

0263-8762/© 2016 The Institution of Chemical Engineers. Published by Elsevier B.V. All rights reserved.

Nomenclature

A	transfer area, m ²
c_i	molar concentration, mol m ⁻³
c_{fixed}	molar concentration of fixed charges in ion exchanger particle, mol m ⁻³
D_i	ion diffusivity, m ² s ⁻¹
$D_{i,\text{eff}}$	effective ion diffusivity, m ² s ⁻¹
[D]	matrix of diffusivities, m ² s ⁻¹
F	Faraday constant, 9.65 × 10 ⁴ C mol ⁻¹
m	number of counter-ions, dimensionless
n	number of species in the mixture, dimensionless
r	radial direction coordinate, m
r_c	radius of ion-exchanger particle, m
R	gas constant, 8.314 J mol ⁻¹ K ⁻¹
t	time, s
T	absolute temperature, K
V	compartment volume, m ³
X_i	ionic equivalent fraction of species i inside IEX particle, dimensionless
z	distance coordinate, m
z_i	charge on species i, dimensionless
 Greek letters	
β	cell constant, m ⁻²
δ	diffusion film or membrane thickness, m
δ_{ij}	Kronecker delta, dimensionless
Φ	electrostatic potential, V
μ_i	molar chemical potential of component i, J mol ⁻¹
σ	rate of entropy production, J m ⁻³ s ⁻¹ K ⁻¹

observed ionic effective diffusivities $D_{i,\text{eff}}$ are shown in Fig. 1b as function of the square root of the ratio of the initial ionic concentrations of H^+ and Ba^{2+} in the top compartment $\sqrt{c_{HCl}/c_{BaCl_2}} = \sqrt{c_{H^+}/c_{Ba^{2+}}}$. With increasing values of $\sqrt{c_{H^+}/c_{Ba^{2+}}}$, it is observed that both D_{H^+} and $D_{Ba^{2+}}$ decreases while D_{Cl^-} increases. An exactly analogous set of results is obtained for $H^+/K^+/Cl^-$ mixed ion-system (cf. Fig. 1b); in this case, with increasing values of $\sqrt{c_{H^+}/c_{K^+}}$, both D_{H^+} and D_{K^+} decrease, while D_{Cl^-} increases. The experimental data on the effective ionic diffusivities leads us to conclude that the $D_{i,\text{eff}}$ is influenced by the signs of the ionic charges.

Let us consider diffusional effects in ion exchange processes that are commonly carried out in fixed bed devices, loaded with the ion exchanger resin particles, and operated in transient mode with adsorption and regeneration cycles. The ion-exchange resins are usually solid gels, consisting of a polymeric matrix produced by co-polymerization of styrene and a cross-linking agent, divinylbenzene, to produce a three-dimensional cross-linked structure with ionic functional groups attached to the polymeric network (Seader et al., 2011). A cation exchange particle, for example, consists of fixed negative charges (e.g. HSO_3^-) on a polymer matrix; see schematic in Fig. 2. Positively charged counter-ions such as H^+ , Na^+ , Ba^{2+} , Zn^{2+} and Cs^+ can exchange between the IEX particle and the surrounding bulk electrolyte liquid, but co-ions such as Cl^- , SO_4^{2-} , and NO_3^- are virtually excluded from participation in the forward/reverse exchanges. If the styrene-divinylbenzene copolymer is chloromethylated and aminated, a strong-base, anionic exchange resin is formed that contains

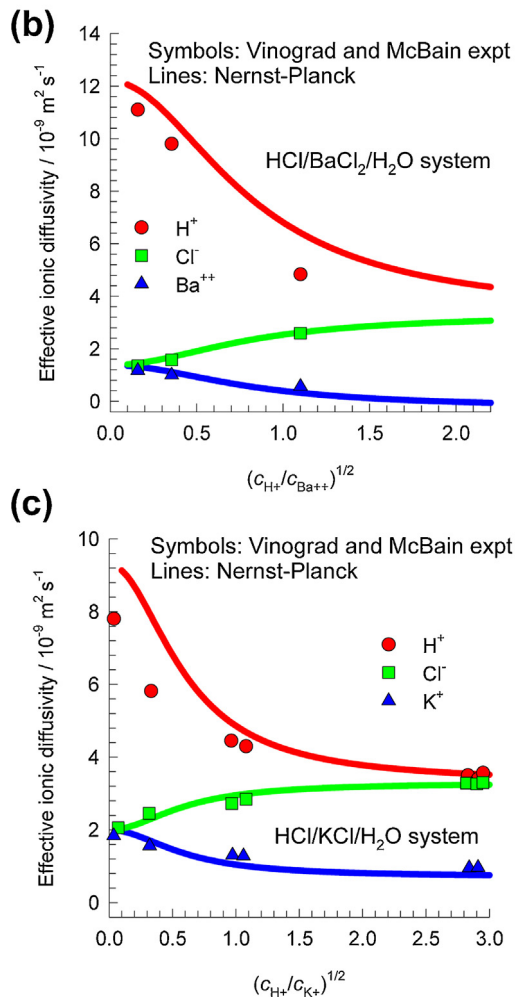
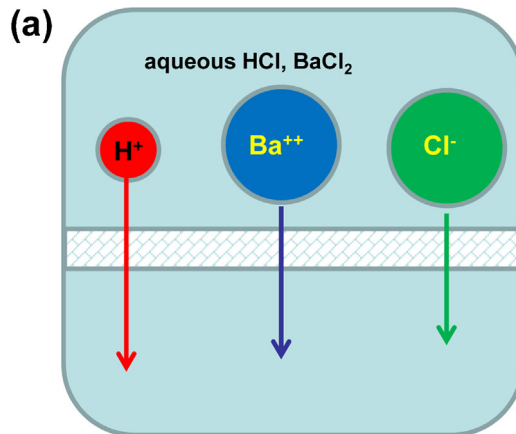


Fig. 1 – (a) Schematic of diaphragm cell used for investigation of co-diffusion of mixed ions between two well-mixed compartments. Experimental data of (Vinograd and McBain, 1941) for effective diffusivities of (b) $H^+/Ba^{2+}/Cl^-$ and (c) $H^+/K^+/Cl^-$ mixed ion-systems. The continuous solid lines represent calculations using Eqs. (13)–(15); details are provided in the Supplementary material.

fixed positive charges, RN^+ . The design and development of ion exchange separation devices require the description of both ion exchange equilibria between the IEX particle, and the ion exchange kinetics. Depending on the set of operating conditions used (concentration of ions in the bulk electrolyte), and the particle properties (pore size of particles, intra-particle diffusivities), two scenarios for diffusion limitations are

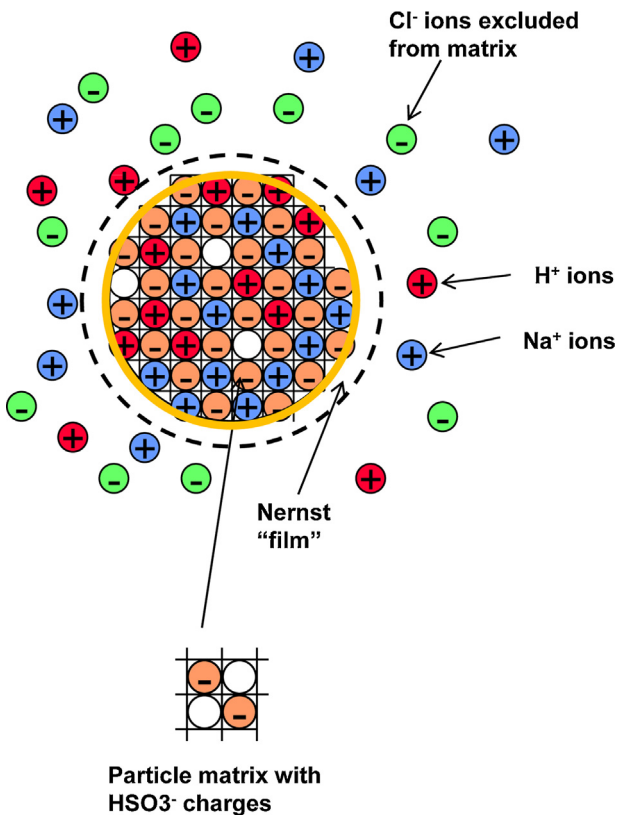


Fig. 2 – Schematic showing an ion exchanger particle with fixed HSO_3^- charges. The surrounding liquid phase consists of a solution of HCl and NaCl . The electrolytes are fully ionized and the bulk liquid phase contains H^+ , Na^+ , Cl^- ions along with unionized water molecules.

possible: (a) the ion exchange process is limited by transfer from the bulk liquid phase to the external surface of the particle, and (b) the ion exchange process is limited by intra-particle diffusion. Generally speaking, for low concentrations of electrolytes in the bulk liquid, typically $<0.01 \text{ mol L}^{-1}$, the exchange process is governed by the diffusion through the “film” surrounding the particle. For high external concentrations, typically $>0.1 \text{ mol L}^{-1}$, the exchange process is governed by intra-particle diffusion.

Experimentally, it has been found that loading Na^+ into the particle while removing H^+ from particle, occurs at a significantly different rate than loading H^+ into the particle while removing Na^+ from particle. In other words, the diffusion process is asymmetric. This directional influence of the diffusion potential is illustrated in the experiments of (Kraaijeveld and Wesselingh, 1993a) for external mass transfer limited ion exchange. Exchanging Na^+ within the ion exchange bead with H^+ from the bulk chloride solution proceeds at a significantly higher rate than for the reverse exchange process; see Fig. 3a. Fig. 3b shows experimental data for analogous asymmetry for $\text{H}^+/\text{Ca}^{++}$ exchanges.

The asymmetry in the forward/reverse exchanges also persists when the diffusion resistance is located within the IEX particle. Fig. 4a presents the experimental data for H^+/Na^+ exchange in phenolsulphonic acid cation exchangers as reported by (Helfferich, 1962b, 1983) for two scenarios: (1) initially the particle is loaded with H^+ and is brought into contact with NaCl in the surrounding bulk liquid phase, and (2) initially the particle is loaded with Na^+ and is brought into contact with HCl in the surrounding bulk liquid phase. The

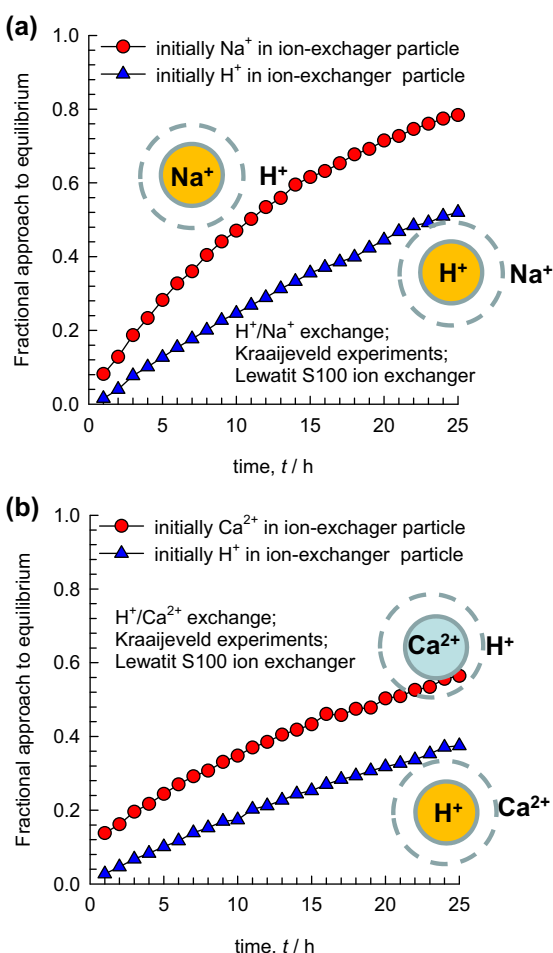


Fig. 3 – Experimental data of (Kraaijeveld and Wesselingh, 1993a) demonstrating asymmetry in forward/reverse (a) H^+/Na^+ , and (b) $\text{H}^+/\text{Ca}^{++}$ exchanges. These systems are limited by diffusion from bulk liquid electrolyte to the surface of the particle.

experiments show that Scenario 1 leads to significantly faster equilibration than observed in Scenario 2. Remarkably, the hierarchy of equilibration rates is opposite to that experienced for the case in which the diffusion limitation is outside the particle (cf. Fig. 3a).

The experimental data of (Varshney and Pandith, 1999) for forward/reverse $\text{H}^+/\text{Ca}^{++}$ exchanges in zirconium (IV) aluminophosphate IEX particles at 298 K are shown Fig. 4b. The equilibration is significantly faster when the IEX is initially loaded with the more mobile H^+ ; this hierarchy is opposite to the hierarchy observed in Fig. 3b when the diffusion resistance is located outside the IEX particle.

The forward and reverse cation exchanges in FAU zeolite are also determined to be asymmetric (Shunong et al., 1994).

To cater for asymmetrical cation exchanges, the effective diffusivity, $D_{i,\text{eff}}$, defined in Eq. (1), must be dependent on the direction of movement of mobile and tardy cations.

A different kind of asymmetry manifests for transient exchange of $\text{H}^+/\text{Na}^+/\text{Zn}^{++}$ exchange in DOWEX 50WX10. When the IEX particle is loaded with H^+ and is replaced $\text{Na}^+/\text{Zn}^{++}$, the experimental data of (Yoshida and Kataoka, 1987) show a pronounced overshoot in the uptake of Na^+ ; see Fig. 5a. The achievement of supra-equilibrium signals the phenomenon of uphill diffusion, implying that $D_{i,\text{eff}} < 0$ for Na^+ . The experimental data for the reverse exchange process in which the particle is loaded with $\text{Na}^+/\text{Zn}^{++}$ and is replaced H^+ are shown in Fig. 5b.

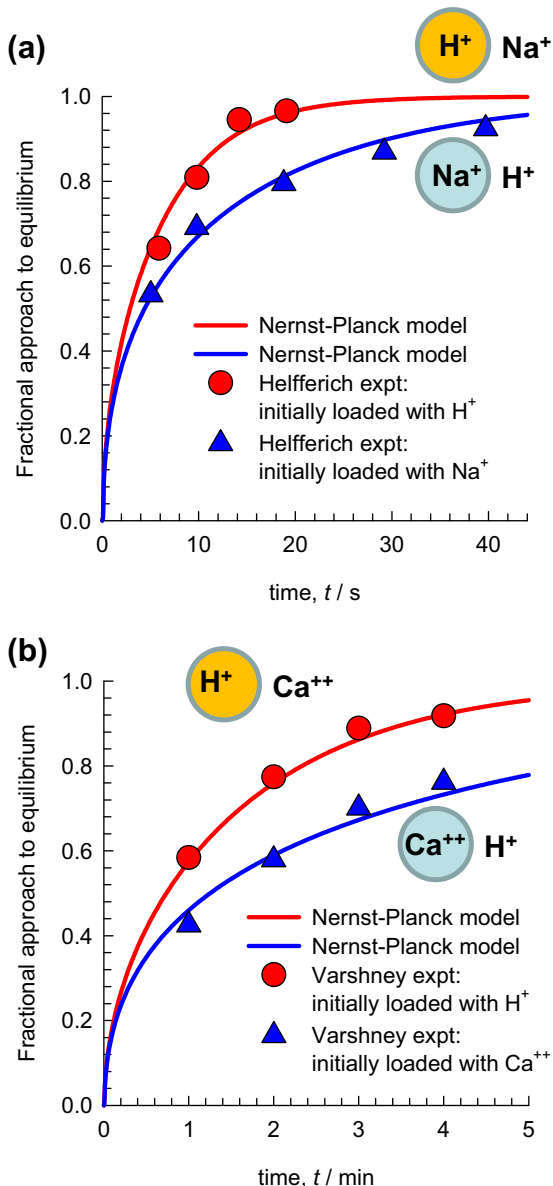


Fig. 4 – (a) Experimental data for H^+ / Na^+ exchange reported by (Helfferich, 1962b, 1983) for phenolsulphonic acid cation exchangers. **(b)** Experimental data of (Varshney and Pandith, 1999) for H^+ / Ca^{++} exchange in zirconium (IV) aluminophosphate cation exchanger particle.

No overshoots or undershoots are experienced in this scenario. The data in Fig. 5 also imply that the effective diffusivity of Na^+ must change sign for forward/reverse exchange.

(Yang and Pintauro, 2000) report experimental data for transient transport of H^+ , Na^+ , and Cs^+ ions across a Nafion cation exchange membrane separating the acid and salt compartments; see Fig. 6. In the reported experiments, the initial concentrations are: salt compartment: $\text{Na}_2\text{SO}_4 = 0.125 \text{ mol L}^{-1}$; $\text{Cs}_2\text{SO}_4 = 0.0054 \text{ mol L}^{-1}$; acid compartment: $\text{H}_2\text{SO}_4 = 0.125 \text{ mol L}^{-1}$. The H^+ ions transfer from the acid to the salt compartment. Both Na^+ , and Cs^+ ions transfer from the salt to the acid compartment. The SO_4^{2-} ions cannot cross the membrane because of the fixed negative charges in the membrane. While the transient equilibration of H^+ , and Na^+ ions occurs in normal manner with an exponential approach to equilibrium, Cs^+ displays a concentration overshoot during the earlier stages of the transience. The manifestation of transient overshoots for Cs^+ indicates that

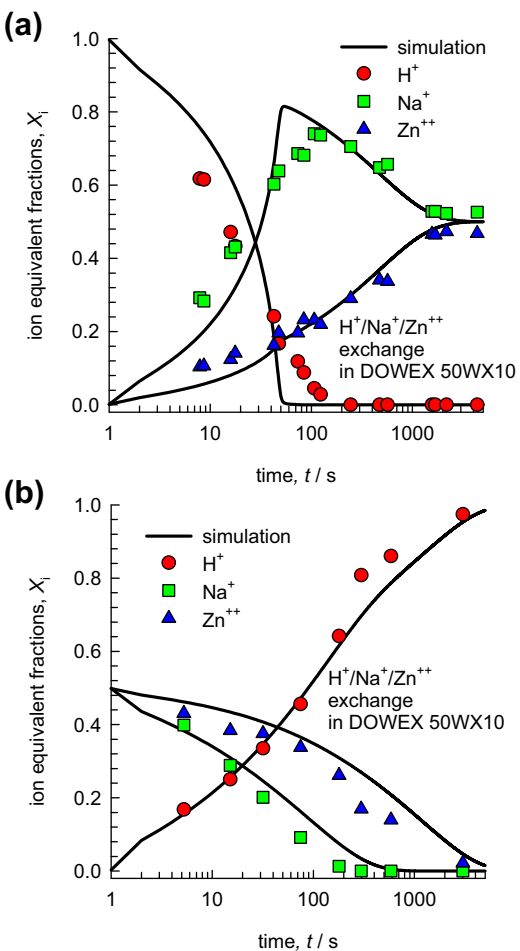


Fig. 5 – (a, b) Experimental data of (Yoshida and Kataoka, 1987) (indicated by symbols) with Nernst-Planck simulations for transient exchange of H^+ / Na^+ / Zn^{++} within DOWEX 50WX10 cation exchanger particle. **(a)** Initially the particle is loaded with H^+ and is replaced Na^+ / Zn^{++} . **(b)** Initially the particle is loaded with Na^+ / Zn^{++} and is replaced H^+ . The continuous solid lines in (a, b) are the simulations using the Nernst-Planck model; simulation details are provided in the Supplementary material.

the flux of Cs^+ is coupled to the transport of the two counter-ions H^+ and Na^+ . The data in Fig. 6 underscore the limitations of the uncoupled flux Eq. (1).

The experimental data in Figs. 1 and 3–6 lead to the following set of conclusions regarding the characteristics of the effective ionic diffusivity, $D_{i,\text{eff}}$, defined by Eq. (1): (a) it is strongly concentration dependent, (b) has values that are dependent on whether the ionic charge z_i is positive or negative, (c) can assume negative values, and (d) depends on the direction of movement relative to the other ions in the mixture.

The primary objective of this article is to analyze the diverse set of experiments discussed above using the Nernst-Planck equations for ion diffusion. We investigate the root causes for transient overshoots, uphill diffusion, and asymmetry in forward/reverse ion exchanges.

The Supplementary material accompanying this publication, available for download in the online version of this article, provides detailed derivations of model equations, solution methodology, and data inputs.

We begin by setting up the proper description of ion diffusion fluxes.

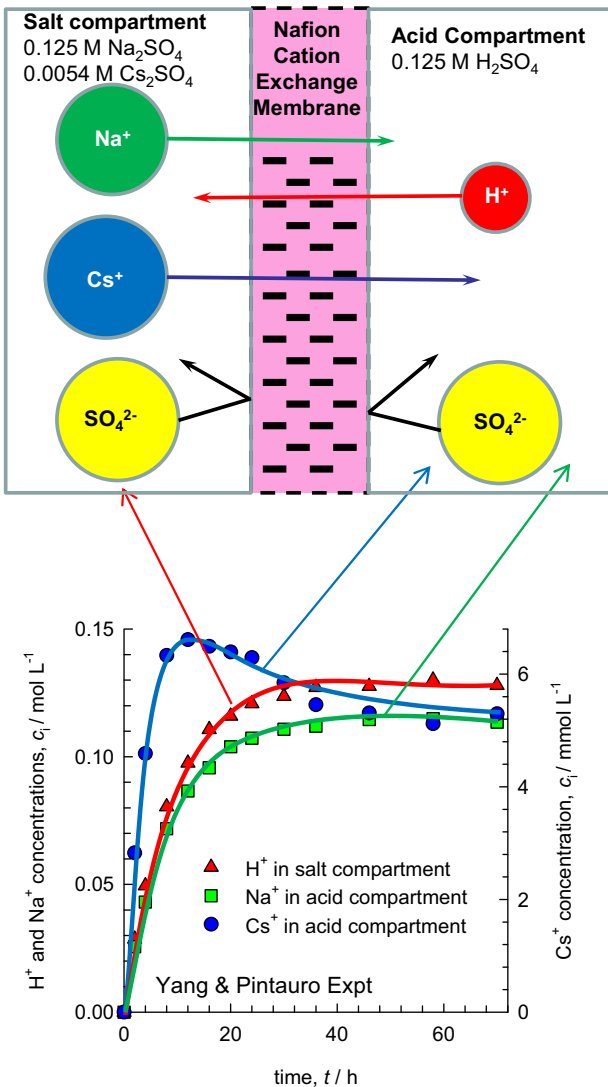


Fig. 6 – Experimental data of (Yang and Pintauro, 2000) for the transient equilibration of H^+ , Na^+ , and Cs^+ in the salt and acid compartments that are separated by a Nafion cation exchange membrane.

2. The Maxwell–Stefan–Nernst–Planck equations for ion diffusion

For diffusion in n -component fluid mixtures consisting of neutral, uncharged species, the Maxwell–Stefan (M–S) equations (Krishna, 2015a,b; Krishna and van Baten, 2016) are normally written as

$$-\frac{x_i}{RT} \frac{\partial \mu_i}{\partial z} = \sum_{j=1}^n \frac{x_i x_j (u_i - u_j)}{D_{ij}}; \quad i = 1, 2, \dots, n \quad (2)$$

In Eq. (2), u_i is the velocity of species i in a laboratory fixed reference frame, and D_{ij} is the diffusivity of $i-j$ pair in the n -component mixture. The M–S formulation is essentially a friction formulation, and D_{ij} is to be interpreted as the inverse drag coefficient for the $i-j$ pair. The Onsager reciprocal relations demand the symmetry constraint

$$D_{ij} = D_{ji}; \quad i = 1, 2, \dots, n \quad (3)$$

For diffusion of ionic species, the M–S formulation needs to be extended to include the contribution due to electrostatic potential gradients that serve as additional driving forces for ionic species with charge numbers z_i (Graham and Dranoff, 1982a,b; Krishna, 1987; Krishna and Wesselingh, 1997; Lightfoot, 1974; Lito et al., 2012; Newman, 1991; Taylor and Krishna, 1993; Wesselingh and Krishna, 2000). We modify the M–S Eq. (2) by including the additional driving force in the left member of Eq. (2)

$$-\frac{x_i}{RT} \frac{\partial \mu_i}{\partial z} - x_i z_i \frac{F}{RT} \frac{\partial \Phi}{\partial z} = \sum_{j=1}^n \frac{x_i x_j (u_i - u_j)}{D_{ij}}; \quad i = 1, 2, \dots, n \quad (4)$$

The second law of thermodynamics demands that the rate of entropy production be positive definite (Standart et al., 1979)

$$\sigma = \frac{1}{2} c_t R \sum_{i=1}^n \sum_{j=1}^n \frac{x_i x_j |(u_i - u_j)|^2}{D_{ij}} \geq 0 \quad (5)$$

The second law constraint does not require each of the pair M–S diffusivities to be positive definite. Indeed, (Kraaijeveld and Wesselingh, 1993b) present experimental evidence to suggest that cation–cation diffusivities could assume negative values without violation of the second law of thermodynamics. For molten salt mixtures $\text{LiF}-\text{BeF}_2$, the MD simulation data of (Chakraborty, 2015) show negative values of the ion pair diffusivities, without violation of the second law constraint (5).

An important, persuasive, advantage of the M–S formulation is that the drag between the $i-j$ pair is not affected by the introduction of the additional driving force in the left member of Eq. (4).

As illustration, let us consider diffusion in an aqueous solution of H_2SO_4 ; the transport properties for this system have been collected by (Umino and Newman, 1993). The system consists of three species: H^+ (=1), SO_4^{2-} (=2) and H_2O (=3). The charges are $z_1 = 1$, $z_2 = -2$ and $z_3 = 0$. Let $c_{\text{H}_2\text{SO}_4}$ represent the concentration of the electrolyte in the aqueous solution and c_3 the molar concentration of water. The concentrations of the ions are $c_1 = 2c_{\text{H}_2\text{SO}_4}$; $c_2 = c_{\text{H}_2\text{SO}_4}$ and the corresponding mole fractions are $x_1 = (2c_{\text{H}_2\text{SO}_4})/(3c_{\text{H}_2\text{SO}_4} + c_3)$; $x_2 = (c_{\text{H}_2\text{SO}_4})/(3c_{\text{H}_2\text{SO}_4} + c_3)$. The values of the three M–S diffusivities D_{13} , D_{23} and D_{12} as function of the sulfuric acid concentration are shown in Fig. 7a. The diffusivity of H^+ ion in water, D_{13} , is about ten times higher than that of the SO_4^{2-} ion, D_{23} . Let us now examine the relative importance of the contributions of the two frictional terms on the right members of Eq. (4). For hydrogen ion H^+ in aqueous sulphuric acid solutions, the relative friction experienced with the sulphate ions to that with water is $((x_2/D_{12})/(x_3/D_{13}))$; similarly for the sulphate ion SO_4^{2-} the relative friction experienced with the hydrogen ion to that with water is $((x_1/D_{12})/(x_2/D_{23}))$. These relative values have been calculated using the data of (Umino and Newman, 1993) and presented in Fig. 7b.

For further discussions on diffusion in concentrated ionic systems, the reader is referred to (Samson et al., 1999), and (Dufrêche et al., 2002).

We note that for electrolyte concentrations smaller than about 0.01 mol L^{-1} , the cation–anion friction is less than 20%

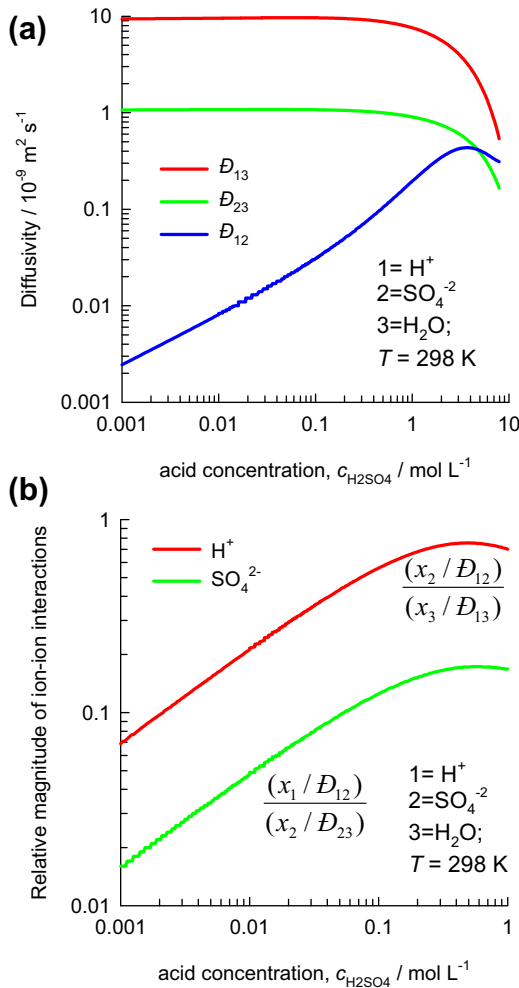


Fig. 7 – (a) Maxwell-Stefan diffusivities in aqueous sulphuric acid system; the data from (Umino and Newman, 1993) are re-plotted here. (b) Relative contributions of ion-ion friction and ion-water friction in aqueous solution of sulphuric acid.

of the ion–water friction. If ion–ion interactions are neglected, the M–S formulation reduce to

$$N_i = -D_i \frac{c_i}{RT} \frac{\partial \mu_i}{\partial z} - c_i z_i D_i \frac{F}{RT} \frac{\partial \Phi}{\partial z} + c_i u_n; \quad i = 1, 2, \dots, n-1 \quad (6)$$

where the D_i are the ion–solvent M–S diffusivities and the ionic diffusion fluxes are defined as

$$N_i = c_i u_i; \quad i = 1, 2, \dots, n \quad (7)$$

The species n is often water, that is usually present in significantly large proportions, and can often be considered stagnant, $N_n = c_n u_n = 0$. For dilute aqueous solutions of electrolytes, the activity coefficients are approximately unity, so $(c_i/RT)(\partial \mu_i/\partial z) \approx (\partial c_i/\partial z)$. The D_i are practically independent of electrolyte concentration for dilute solutions; cf. Fig. 7a. For dilute solutions, Eq. (6) reduce to the Nernst–Planck equations

$$N_i = -D_i \frac{\partial c_i}{\partial z} - c_i z_i D_i \frac{F}{RT} \frac{\partial \Phi}{\partial z}; \quad i = 1, 2, \dots, n-1 \quad (8)$$

Except in regions close to electrode surfaces, where there will be charge separation (the double layer phenomena), the condition of electro-neutrality is met

$$\sum_{i=1}^n z_i c_i = 0; \quad \sum_{i=1}^{n-1} z_i \frac{\partial c_i}{\partial z} = 0; \quad \text{electroneutrality constraint} \quad (9)$$

The total current carried by the electrolyte is $F \sum_{i=1}^n z_i N_i$. In many chemical process applications such as ion exchange, no external electrical field is imposed on the system, and also there is no flow of current, i.e.

$$\sum_{i=1}^n z_i N_i = 0; \quad \text{no current prescription} \quad (10)$$

Combining Eqs. (8) and (10) we obtain the following expression for the diffusion potential that is engendered due to ionic diffusion

$$\frac{\partial \Phi}{\partial z} = - \frac{\sum_{k=1}^{n-1} z_k D_k (\partial c_k / \partial z)}{RT \sum_{j=1}^{n-1} c_j z_j^2 D_j} \quad (11)$$

and therefore there are only $(n-2)$ independent concentration gradients, and $(n-2)$ independent fluxes N_i .

Combining Eqs. (8), (9) and (11), we derive

$$N_i = -D_i \frac{\partial c_i}{\partial z} + \frac{c_i z_i D_i}{\sum_{j=1}^{n-1} c_j z_j^2 D_j} \sum_{k=1}^{n-2} z_k (D_k - D_{n-1}) \frac{\partial c_k}{\partial z}; \\ i = 1, 2, \dots, n-2 \quad (12)$$

Eq. (12) can be conveniently cast into $(n-2)$ dimensional matrix notation

$$(N) = -[D] \frac{\partial(c)}{\partial z} \quad (13)$$

The elements of the $(n-2) \times (n-2)$ dimensional square matrix are

$$D_{ik} = D_i \delta_{ik} - \frac{c_i z_i D_i (D_k - D_{n-1})}{\sum_{j=1}^{n-1} c_j z_j^2 D_j}; \quad i, k = 1, 2, \dots, n-2 \quad (14)$$

where δ_{ik} is the Kronecker delta. The second member of the right of Eq. (14) quantifies the contribution of the electrostatic “leash” that serves to enhance, or diminish, the ionic mobilities. Whether an ion is accelerated or decelerated depends on the species charges, z_i , and whether we have co-diffusion or counter-diffusion.

The Nernst–Planck equations help explain the Vinograd–McBain experiments in Fig. 1. At the start of the diffusion process, the highly mobile H^+ diffuses ahead of its companion ions into the pure water compartment, creating an excess of positive charge. This induces an electrostatic potential gradient $\partial \Phi / \partial z$, also called the diffusion potential, which acts in such a way as to comply with the no-current and electro-neutrality prescriptions. The consequence is that the Cl^- experiences an extra electrostatic “pull”, enhancing its effective diffusivity value. The electrical potential gradient also serves to retard the motion of the positive ions H^+ and Ba^{++} or in other words these ions experience a “push” in a direction opposite to that dictated by their composition gradient

driving forces. For $\sqrt{c_{H^+}/c_{Ba^{2+}}}=2$, the electrostatic “push” on Ba^{2+} is such as to result in a vanishing value for $D_{Ba^{2+}}$. The continuous solid lines in Fig. 1 are the calculations of the effective diffusivities

$$D_{i,\text{eff}} = \frac{N_i}{(c_{i0} - c_{i\delta})/\delta} \quad (15)$$

wherein the fluxes are determined from Eq. (12). The continuous solid lines in Fig. 1 are the calculations using Eqs. (13)–(15). The essential diffusion characteristics for the $HCl/BaCl_2/H_2O$ and $HCl/KCl/H_2O$ mixtures are properly captured by the Nernst–Planck equation. The Nernst–Planck model calculations anticipate negative values of $D_{Ba^{2+}}$ for $\sqrt{c_{H^+}/c_{Ba^{2+}}}>2$ due to a strong electrostatic “push”; see Fig. 1b. Negative effective diffusivities signal the possibility of uphill diffusion for Ba^{2+} (Krishna, 2015a).

3. Transient overshoots during counter-diffusion of mixed ions

We shall demonstrate the possibility of transient overshoots in counter-diffusion of mixed electrolyte solutions. For this purpose, we consider counter-diffusion of $1=H^+$, $2=Cl^-$, $3=Ba^{2+}$ between the two compartments; see Fig. 8a. We assume that each of the two compartments is well mixed and the concentration gradients are restricted to the thickness of the porous diaphragm separating the two compartments. Initially, the left compartment contains HCl with a concentration of 0.04 mol L^{-1} ; the right compartment contains $BaCl_2$ with a concentration of 0.02 mol L^{-1} . In 3-dimensional vector notation, the initial concentrations in the left and right compartments are ($1=H^+$, $2=Cl^-$, $3=Ba^{2+}$)

$$(c_{L0}) = \begin{pmatrix} 0.04 \\ 0.04 \\ 0 \end{pmatrix}; \quad (c_{R0}) = \begin{pmatrix} 0.0 \\ 0.04 \\ 0.02 \end{pmatrix} \quad (16)$$

It is noteworthy, that there is no driving force for transport of chloride ions across the porous membrane.

The transient equilibration process in the left and right compartments (with volumes V , and interfacial area A) is described in matrix notation by $V(d(c_L)/dt) = -V(d(c_R)/dt) = -(N_i)A$. The molar flux N_i is taken to be positive if directed from left to right. At any instant of time, t , we have $V(d(c_L)/dt) = -[D]/(\delta)(c_L - c_{eq})/A$ where δ is the effective thickness of the diffusion layer. We define a cell constant $\beta = (A\delta/V)$, and write $(d(c_L)/dt) = -\beta[D](c_L - c_{eq})$. If the diffusivity matrix is considered constant for a short discretized interval of time, this matrix differential equation may be integrated to obtain

$$(c_L - c_{eq}) = \exp[-\beta[D]t](c_{L0} - c_{eq}) \quad (17)$$

where the vector $(c_{eq}) = \frac{(c_{L0} + c_{R0})}{2} = \begin{pmatrix} 0.02 \\ 0.04 \\ 0.01 \end{pmatrix}$. An analogous expression holds for the right compartment. In our calculations, we take $\beta = 10^4\text{ m}^{-2}$. The Sylvester theorem, detailed in Appendix A of (Taylor and Krishna, 1993) is required for explicit determination of the transient equilibration trajectories described by Eq. (17); the calculations are easily implemented in MathCad 15; see Supplementary material.

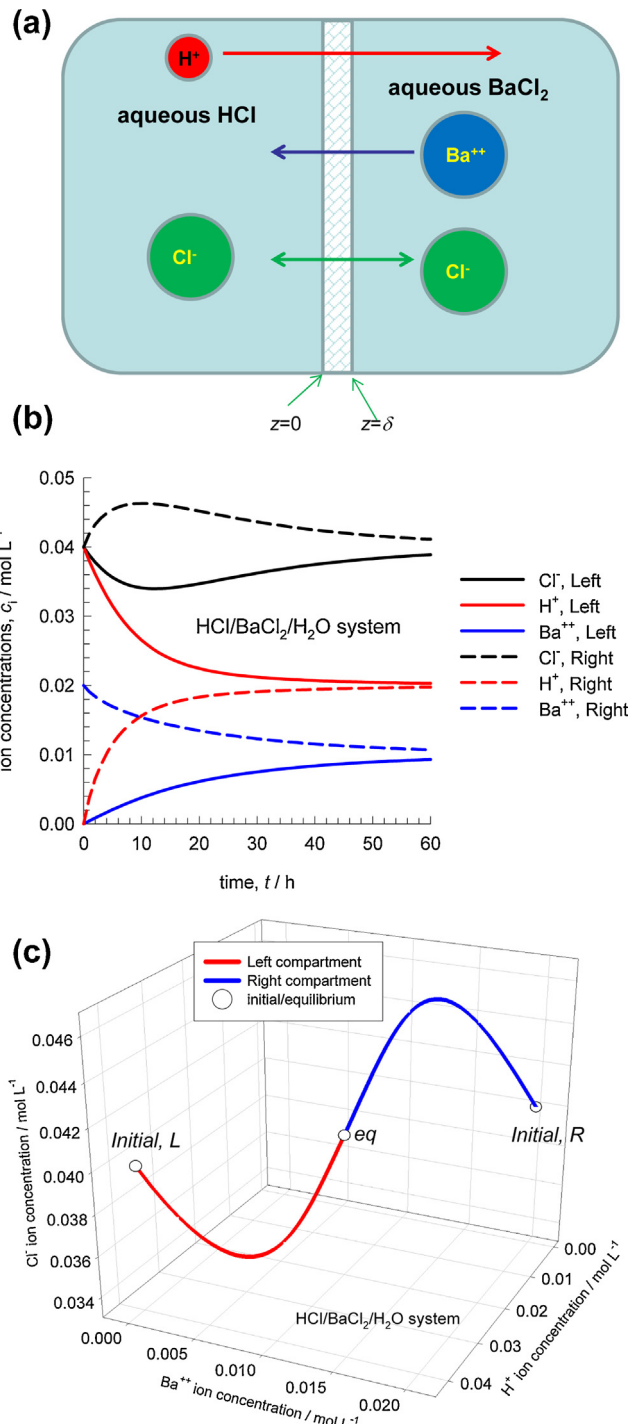


Fig. 8 – (a) Schematic showing counter-diffusion between two well-mixed compartments. (b) Simulations of transient counter-diffusion of H^+ , Ba^{2+} , and Cl^- between two well-mixed compartments. (c) Equilibration trajectories plotted in composition space.

The composition trajectories in the left and right compartments during transient equilibration are presented in Fig. 8b. The diffusion equilibration of H^+ , and Ba^{2+} proceeds in a “normal” manner, i.e. the transport is from higher to lower concentration regions with exponential decay. The equilibration of chloride ions is remarkable in that a concentration overshoot is experienced in the right compartment with concomitant undershoot in the left compartment. Let us explain the concentration overshoot in physical terms. The more mobile H^+ rapidly diffuses into the right compartment; this

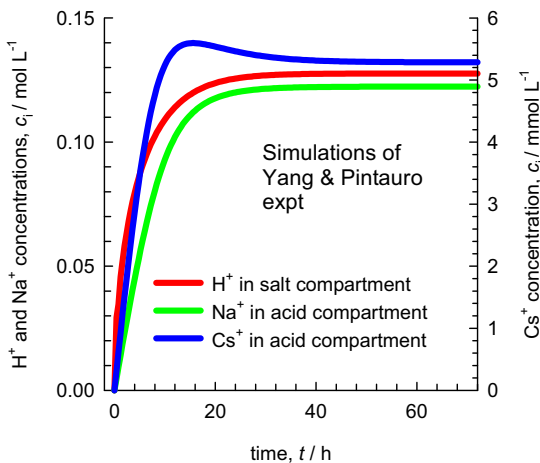


Fig. 9 – Simulations of experiments shown in Fig. 6, for the transient equilibration of H^+ , Na^+ , and Cs^+ in the salt and acid compartments that are separated by a Nafion cation exchange membrane. The simulation details are provided in the Supplementary material.

creates an excess of positive charge. The necessity of maintaining electro-neutrality demands the presence of Cl^- that gets transported from left to right in order to negate the charge imbalance. The trans-membrane transport of Cl^- occurs even though its ion concentrations are the same in the two compartments; this is because of electro-static coupling. It is also interesting to note that the equilibration process follows serpentine trajectories in composition space; see Fig. 8c.

The simulations of experiments shown in Fig. 6, for the transient equilibration of H^+ , Na^+ , and Cs^+ in the salt and acid compartments that are separated by a Nafion cation exchange membrane proceeds along similar lines as in the foregoing example. In this case, however, the SO_4^{2-} ions cannot transfer across the membrane and its flux must be constrained to zero; the simulation results are presented in Fig. 9. The overshoots in Cs^+ concentration during the early stages of the transience are essentially captured in the simulations. Other experimental evidence is also available for transient overshoots for ion transport across cation exchange membranes (Neihof and Sollner, 1957; Soddy et al., 2006).

4. Asymmetry in forward/reverse ion-exchange: diffusion resistance outside the IEX particle

We examine forward and reverse ion exchange for the situation in which the transfer resistance is located external to the particle; specifically, we seek to rationalize the asymmetry observed in Fig. 3 for forward/reverse $H^+(1)/Na^+(2)$ exchanges. We rationalize these experiments using the penetration model for transfer of ions from the resin phase (left compartment in Fig. 10a) into the bulk electrolyte (right compartment in Fig. 10a). The exclusion of the chloride ions (species 3) from the IEX particles implies

$$N_3 = -D_3 \frac{\partial c_3}{\partial z} - c_3 z_3 D_3 \frac{F}{RT} \frac{\partial \Phi}{\partial z} = 0; \quad \frac{\partial c_3}{\partial z} = -c_3 z_3 \frac{F}{RT} \frac{\partial \Phi}{\partial z};$$

(18)

anion exclusion from IEX

Exclusion of the chloride ions from the ion exchanger particle does not imply that the concentration gradient of

chloride ion vanishes; the concentration gradient of chloride ion must balance the electrostatic potential gradient. Combining Eqs. (8) and (18) with the electro-neutrality and no-current prescriptions leads to the following expressions for effective diffusivities, $D_{i,eff}$ (defined as in Eq. (1)), of the univalent counter-ions H^+ and Na^+ (Smith and Dranoff, 1964; Turner and Snowdon, 1968) (detailed derivations are provided in the Supplementary material)

$$D_{1,eff} = \frac{2(c_1 + c_2)}{\left[\frac{c_1}{D_1} + \frac{c_1}{D_2} + \frac{2c_2}{D_1} \right]}; \quad D_{2,eff} = \frac{2(c_1 + c_2)}{\left[\frac{c_2}{D_1} + \frac{c_2}{D_2} + \frac{2c_1}{D_2} \right]} \quad (19)$$

The IEX resin phase is maintained at a constant concentration $c_{i,LO}$ by through-flow of the resin particles in the left compartment. We focus on the transient equilibration in the right compartment, $z \geq 0$; the transient development of concentrations of the ions in the right compartment is described by the following expression

$$c_i(z, t) = c_{i,LO} + erf \left[\frac{z}{\sqrt{4D_{i,eff} t}} \right] (c_{i,RO} - c_{i,LO}); \quad i = 1, 2 \quad (20)$$

where the effective ionic diffusivities $D_{i,eff}$ are given by Eq. (19).

For the Scenario 1: exchange H^+ within the ion exchange resin with Na^+ from the bulk electrolyte outside the IEX particle we use the following set of conditions:

$$(c_{L0}) = \begin{pmatrix} 0.0 \\ 0.01 \end{pmatrix}; \quad (c_{R0}) = \begin{pmatrix} 0.01 \\ 0.00 \end{pmatrix}; \quad \text{Scenario 1}$$

For the Scenario 2: exchange Na^+ within the ion exchange bead with H^+ from the bulk electrolyte outside the IEX particle we use the following set of conditions:

$$(c_{L0}) = \begin{pmatrix} 0.01 \\ 0.0 \end{pmatrix}; \quad (c_{R0}) = \begin{pmatrix} 0.0 \\ 0.01 \end{pmatrix}; \quad \text{Scenario 2}$$

It is to be noted that in the step-wise numerical procedure used (details provided in the Supplementary material), the calculations of the effective diffusivities are constantly updated and evaluated at the concentrations at the previous time step.

Fig. 10b shows the ionic concentration profiles for the scenario 1: exchanging H^+ within the ion exchange resin with Na^+ from the bulk solution. The fast motion of H^+ away from the particle into the bulk liquid engenders a gradient $\partial\Phi/\partial z$ that effectively pushes the chloride ion away from the particle/solution interface. This is evidenced by the undershoot in the chloride concentration near the particle/liquid interface. Fig. 10c shows the ionic concentration profiles for the scenario 2: exchanging Na^+ within the ion exchange bead with H^+ from the bulk solution. The fast motion of H^+ from the bulk liquid towards the particle engenders a gradient $\partial\Phi/\partial z$ that effectively pushes the chloride ion towards the particle/solution interface. This is evidenced by the overshoot in the chloride concentration near the particle/liquid interface.

Fig. 10d compares the equilibration trajectories; we note that the ingress Na^+ into the liquid is faster than the ingress of H^+ ; this is in accord with the experiments of (Kraaijeveld and Wesselingh, 1993a); cf. Fig. 3a.

The generalization of Eq. (19) for the general case of ions with charges z_i is

$$D_{1,eff} = \frac{c_1 z_1^2 + c_2 z_2^2 + c_3 z_3^2}{\frac{c_1 z_1^2}{D_2} + \frac{(c_2 z_2^2 + c_3 z_3^2)}{D_1}}, \quad D_{2,eff} = \frac{c_1 z_1^2 + c_2 z_2^2 + c_3 z_3^2}{\frac{(c_1 z_1^2 + c_3 z_3^2)}{D_2} + \frac{c_2 z_2^2}{D_1}} \quad (21)$$

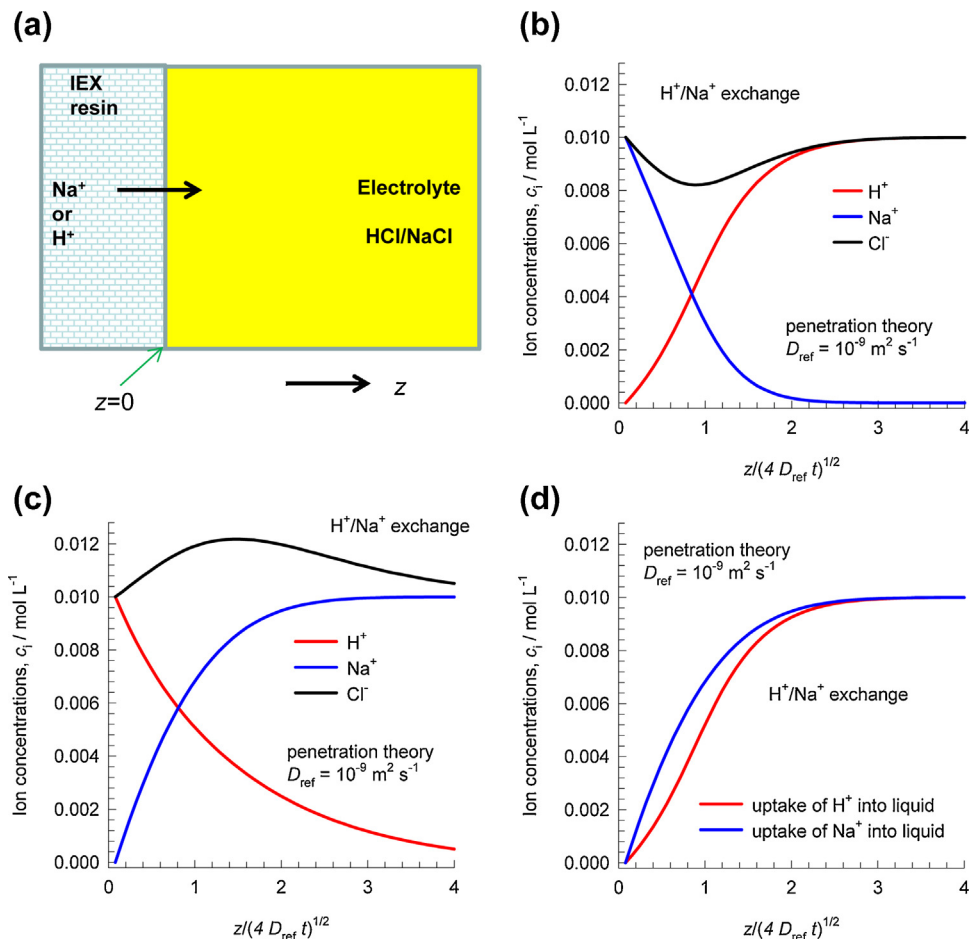


Fig. 10 – (a) Schematic showing forward and reverse H^+/Na^+ exchange from ion exchange resin (left compartment) to bulk electrolyte HCl/NaCl (right compartment). **(b)** Penetration model calculations for IEX particle loaded with H^+ . **(c)** Penetration model calculations for IEX particle loaded with Na^+ . **(d)** Comparison of the transient equilibrations of H^+ and Na^+ in the two scenarios shown in **(b)** and **(c)**.

where the concentration of component 3 is restrained by electro-neutrality

$$c_1 z_1 + c_2 z_2 = -c_3 z_3; \quad \text{electroneutrality constraint} \quad (22)$$

The limiting values of the effective diffusivities:

$$\begin{aligned} c_1 \rightarrow 0; \quad & D_{1,\text{eff}} \rightarrow D_1 \\ c_2 \rightarrow 0; \quad & D_{2,\text{eff}} \rightarrow D_2 \end{aligned} \quad (23)$$

are counter-intuitive because the limiting $D_{i,\text{eff}}$ values equal the value of the ion-diffusivity of the component that is present in the smaller concentration. The use of Eq. (21) helps to rationalize the asymmetry in observed in Fig. 3b for $\text{H}^+/\text{Ca}^{++}$ exchanges limited by "film" diffusion; see Figs. S20, S21, and S22 of Supplementary material.

5. Asymmetry in forward/reverse ion-exchange: diffusion resistance inside the IEX particle

We now turn our attention to forward/reverse exchanges in which the diffusion resistance is located within the particle. Let us assume that the total concentration of negative charges inside the matrix is c_{fixed} , expressed say as mole equivalent per volume. Typically, the concentration of fixed

negative charges is in the range of $1\text{--}4 \text{ mol L}^{-1}$ (Wesselingh and Krishna, 2000); this value is considerably higher than the molar concentrations of ions in the bulk electrolyte solutions surrounding the particle. The concentration of counter ions within the particle must balance c_{fixed} and therefore we have $\sum_{i=1}^m z_i c_i = c_{\text{fixed}}$ where m is the total number of counter-ions. The quantity $(z_i c_i)/c_{\text{fixed}} \equiv X_i$ is the ionic equivalent fraction. The ionic equivalent fractions of the m counter ions sum to unity $\sum_{i=1}^m X_i = 1$. The flux relations for m counter-ions in IEX resin can be written as

$$z_i N_i = -c_{\text{fixed}} D_i \frac{\partial X_i}{\partial z} - c_{\text{fixed}} X_i z_i D_i \frac{F}{RT} \frac{\partial \Phi}{\partial z}; \quad i = 1, 2, \dots, m; \quad (24)$$

The fluxes are defined in a reference frame with respect to the IEX particle. The corrective action of the induced potential gradient $\partial \Phi / \partial z$ is mainly directed *against* the species that is present in the higher equivalent fraction X_i .

It is convenient to define an $(m-1) \times (m-1)$ dimensional square matrix $[D_{\text{eff}}]$ (Jones and Carta, 1993; Rodriguez et al., 1998; Yoshida and Kataoka, 1987)

$$z_i N_i = -c_{\text{fixed}} \sum_{k=1}^{m-1} D_{ik,\text{eff}} \frac{\partial X_k}{\partial z}; \quad i = 1, 2, \dots, m-1 \quad (25)$$

The elements of $[D_{eff}]$ can be derived by applying the no-current $\sum_{i=1}^m z_i N_i = 0$ and electro-neutrality $\sum_{i=1}^m z_i \frac{\partial X_i}{\partial z} = 0$ constraints for intra-particle diffusion; the result is

$$D_{ik,eff} = D_i \delta_{ik} - \frac{(X_i z_i D_i)}{\sum_{j=1}^m X_j z_j D_j} (D_k - D_m) \quad (26)$$

For binary cation exchange, there is only one independent flux, N_1 , and one effective diffusivity, D_{eff} . Eqs. (24)–(26) simplify to yield (Helfferich, 1983):

$$z_1 N_1 = -z_2 N_2 = -c_{fixed} D_{eff} \frac{\partial X_1}{\partial z}; \quad D_{eff} = \frac{X_1 z_1 + X_2 z_2}{\left(\frac{X_1 z_1}{D_2} + \frac{X_2 z_2}{D_1}\right)} \quad (27)$$

Eq. (27) is to be contrasted with the corresponding equations for the effective ionic diffusivities in the bulk electrolyte liquid, Eq. (21). The differences arise because the negative charges within the IEX particle are immobile and therefore electro-neutrality can only be maintained if both the effective diffusivities of the counter-ions are identical. For bulk electrolytes, the flux of the chloride ion is zero, but its concentration gradient adjusts itself in such a manner as to counteract the influence of the electrostatic potential gradient; see Eq. (18).

Eq. (27) is a remarkable result because the limiting values are:

$$\begin{aligned} X_1 \rightarrow 0; \quad D_{eff} &\rightarrow D_1; \\ X_2 \rightarrow 0; \quad D_{eff} &\rightarrow D_2 \end{aligned} \quad (28)$$

In other words, the effective intra-particle diffusivity is closer in magnitude to the diffusivity of the ion that is present in the smaller quantity. Helfferich, perhaps the most influential researcher in ion exchange, has termed this the “minority rule”. To quote (Helfferich, 1983): *binary interdiffusion is not a democratic process but, in the parlance of the activist 1960’s, is ruled by a participating minority!*

We can use Eq. (27) for quantitative modelling of the experiments in Fig. 4. For an IEX particle of radius r_c , the transient equilibration in terms of ionic equivalent fractions is described by the classic Geddes model (Geddes, 1946)

$$\begin{aligned} \bar{X}_i(t) &= X_{i,r=r_c} + Q_i(X_{i,0} - X_{i,r=r_c}); \\ Q_i &= \frac{6}{\pi^2} \sum_{m=1}^{\infty} \frac{1}{m^2} \exp \left[-m^2 \pi^2 \frac{D_{eff}}{r_c^2} t \right]; \quad i = 1, 2 \end{aligned} \quad (29)$$

In Eq. (29), the $\bar{X}_i(t)$ are radial-averaged equivalent fractions, along direct comparison with the experimental results. The computational details of the numerical implementation are provided in the *Supplementary material*. The continuous solid lines in Fig. 4a and b are the simulation results. The asymmetry in the forward and reverse exchanges in the two experimental sets are properly captured by the combination of Eqs. (27) and (29). In both cases, the equilibration is significantly faster when the IEX is initially loaded with the more mobile H^+ . A qualitative rationalization of the experimental data is provided by the minority rule. To rationalize the asymmetry, the calculations of the effective diffusivities for the forward and reverse H^+/Ca^{++} exchanges are shown in Fig. 11. The desorption of H^+ is a faster process because D_{eff} progressively increases during equilibration. Conversely, the desorption of Ca^{++} is a slower process because D_{eff}

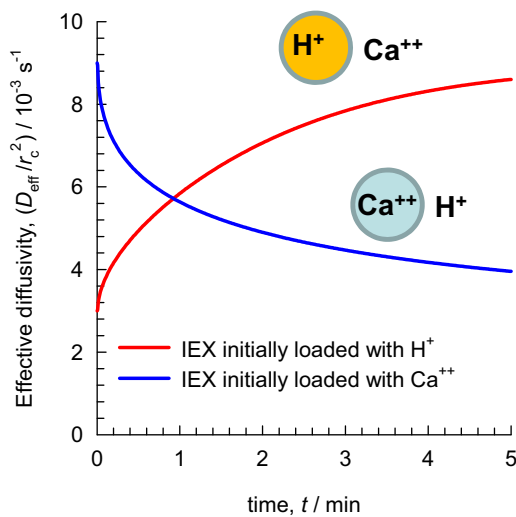


Fig. 11 – Effective diffusivities for the forward and reverse H^+/Ca^{++} exchanges exchange in zirconium (IV) aluminophosphate cation exchanger particle.

progressively decreases during equilibration. The agreement of the Nernst–Planck model with the experimental results is remarkably good; similar good agreement is obtained for the simulations of the experimental data of (Varshney and Pandith, 1999) for forward/reverse H^+/Li^+ , H^+/Mg^{++} and H^+/Sr^{++} exchanges; see Fig. S28 of *Supplementary material*.

For uptake of ternary counter-cations $H^+/Na^+/Zn^{++}$ in DOWEX 50WX10, the transfer fluxes are described by a square 2-dimensional matrix of effective diffusivities; see Eq. (26). This implies that the diffusion flux of any ion is also coupled to the driving forces of the other counter-ions within the particle. The diffusional coupling effects cause uphill ion diffusion and overshoots during transient uptake. Analogous transient overshoots in microporous and mesoporous materials are observed in a variety of non-ionic systems but in these cases the origins of the overshoots can be traced to coupled mixture adsorption thermodynamics (Krishna, 2015a, 2016a,b,c).

The continuous solid lines in Fig. 5a and b are the transient equilibration of radial-averaged equivalent fractions $\bar{X}_i(t)$, obtained by incorporation of Eq. (26) into the Geddes model for transient uptake into a spherical IEX particle. The overshoot in the uptake of Na^+ observed in the experiments of (Yoshida and Kataoka, 1987) is properly captured by the simulations; the input data for the ionic diffusivities inside the pores of the ion exchanger are taken from Table III of their paper. The rapid efflux of H^+ causes steep electrostatic potential gradients to develop during the early stages of the transience (see Fig. S38 of *Supplementary material*). The steep gradients $\partial\phi/\partial r$ serve to enhance the influx of Na^+ , causing supra-equilibrium loadings to be achieved.

For the reverse exchange process in which the particle is loaded with Na^+/Zn^{++} and is replaced H^+ ; the simulations do not show any overshoots, in good agreement with experimental data; see Fig. 5b.

In Fig. 12, the trajectories followed during transient equilibration of the forward and reverse $H^+/Na^+/Zn^{++}$ exchanges are plotted in ternary composition space. It is noteworthy that the two equilibration trajectories follow completely different paths.

A total of seven different experimental campaigns of (Yoshida and Kataoka, 1987) for forward/reverse $H^+/Na^+/Zn^{++}$

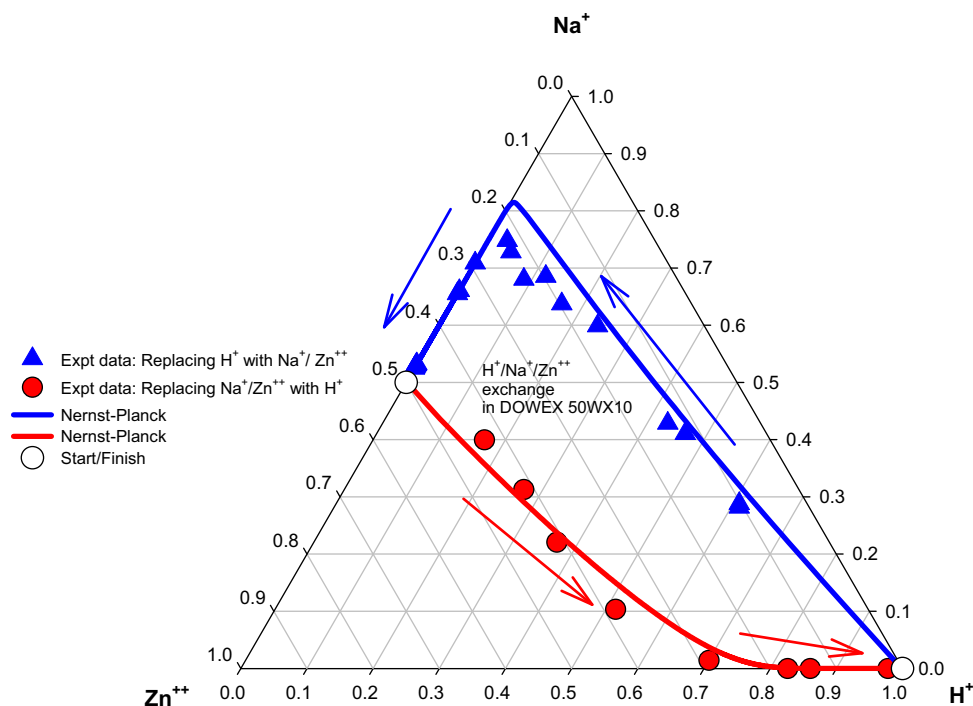


Fig. 12 – The experimental data on $\text{H}^+/\text{Na}^+/\text{Zn}^{++}$ exchange within DOWEX 50WX10, along with the simulation results are plotted in ternary composition (equivalent fractions X_i) space.

exchanges in DOWEX 50WX8, DIAION SK116, and DOWEX 50WX10 IEX particles were simulated with good accuracy using the same approach as in the foregoing example; the results are available in Figs. S32–S38 of the Supplementary material. In all cases transient overshoots are properly captured by the Nernst–Planck model.

6. Conclusions

The following conclusions can be drawn on the basis of detailed analyses of experimental data on ionic diffusion.

- (1) For ionic diffusion, an electro-static potential gradient $z_i F(\partial\phi/\partial z)$ is engendered due to the requirements of electro-neutrality and the no-current prescription. This additional potential gradient serves to either accelerate or decelerate an ionic species, depending on the species charge and operating conditions.
- (2) For diffusion in both bulk electrolyte solutions and within ion-exchange particles, transient overshoots and uphill diffusion are often encountered.
- (3) Forward and reverse ion exchange processes are almost invariably asymmetric in nature and proceed at different rates. When the diffusion resistance is within the particle, the Helfferich minority rule applies for binary exchanges: the effective diffusivity is closer in magnitude to the ionic diffusivity of the component that is present in smaller quantity. The minority rule is the root cause of the asymmetry in the forward and reverse exchange rates.
- (4) For uptake of ternary cations, the equilibration trajectories in ternary composition space follow entirely different paths.
- (5) The Nernst–Planck equations allow all the essential characteristics of ionic diffusion to be essentially captured in the wide variety of processes that are analyzed. For all of the examples discussed in this article analytic, or

semi-analytic, solutions to the Nernst–Planck equations have been used.

Appendix A. Supplementary data

Supplementary material related to this article can be found, in the online version, at doi:10.1016/j.cherd.2016.08.009.

References

- Buck, R.P., 1984. Kinetics of bulk and interfacial ionic motion: microscopic bases and limits for the Nernst–Planck equation to membrane systems. *J. Membr. Sci.* 17, 1–62.
- Chakraborty, B., 2015. Sign crossover in all Maxwell–Stefan diffusivities for molten salt LiF–BeF₂: a molecular dynamics study. *J. Phys. Chem. B* 119, 10652–10663.
- Dufrêche, J.-F., Bernard, O., Turq, P., 2002. Ionic self-diffusion in concentrated aqueous electrolyte solutions. *Phys. Rev. Lett.* 88, 095902.
- Franzreb, M., Höll, W.H., Sontheimer, H., 1993. Liquid-phase mass transfer in multi-component ion exchange. I. Systems without chemical reactions in the film. *React. Polym.* 21, 117–133.
- Geddes, R.L., 1946. Local efficiencies of bubble-plate fractionators. *Trans. Am. Inst. Chem. Eng.* 42, 79–105.
- Graham, E.E., Dranoff, J.S., 1982a. Application of the Stefan–Maxwell equations to diffusion in ion exchangers. 1. Theory. *Ind. Eng. Chem. Res.* 21, 360–365.
- Graham, E.E., Dranoff, J.S., 1982b. Application of the Stefan–Maxwell equations to diffusion in ion exchangers. 2. Experimental results. *Ind. Eng. Chem. Res.* 21, 365–369.
- Helfferich, F.G., 1962a. *Ion Exchange*. McGraw Hill, New York, U.S.A.
- Helfferich, F.G., 1962b. Ion exchange kinetics. III. Experimental test of the theory of particle-diffusion controlled ion exchange. *J. Phys. Chem.* 66, 39–42.
- Helfferich, F.G., 1983. Ion exchange kinetics – evolution of a theory. In: Liberti, L., Helfferich, F.G. (Eds.), *Mass Transfer and Kinetics of Ion Exchange*, Vol. Martinus Nijhoff Publishers, The Hague, pp. 157–179.

- Jones, I.L., Carta, G., 1993. Ion exchange of amino acids and dipeptides on cation resins with varying degree of cross-linking. 2. Intraparticle transport. *Ind. Eng. Chem. Res.* 32, 117–125.
- Kraaijeveld, G., Wesselingh, J.A., 1993a. The kinetics of film-diffusion-limited ion exchange. *Chem. Eng. Sci.* 48, 467–473.
- Kraaijeveld, G., Wesselingh, J.A., 1993b. Negative Maxwell-Stefan diffusion coefficients. *Ind. Eng. Chem. Res.* 32, 738–742.
- Krishna, R., 1987. Diffusion in multicomponent electrolyte systems. *Chem. Eng. J.* 35, 19–24.
- Krishna, R., 2015a. Uphill diffusion in multicomponent mixtures. *Chem. Soc. Rev.* 44, 2812–2836.
- Krishna, R., 2015b. Serpentine diffusion trajectories and the ouzo effect in partially miscible ternary liquid mixtures. *Phys. Chem. Chem. Phys.* 17, 27428–27436.
- Krishna, R., 2016a. Diffusing uphill with James Clerk Maxwell and Josef Stefan. *Curr. Opin. Chem. Eng.* 12, 106–119.
- Krishna, R., 2016b. Investigating the validity of the Knudsen diffusivity prescription for mesoporous and macroporous materials. *Ind. Eng. Chem. Res.* 55, 4749–4759.
- Krishna, R., 2016c. Tracing the origins of transient overshoots for binary mixture diffusion in microporous crystalline materials. *Phys. Chem. Chem. Phys.* 18, 15482–15495.
- Krishna, R., van Baten, J.M., 2016. Describing diffusion in fluid mixtures at elevated pressures by combining the Maxwell-Stefan formulation with an equation of state. *Chem. Eng. Sci.* 153, 174–187.
- Krishna, R., Wesselingh, J.A., 1997. The Maxwell-Stefan approach to mass transfer. *Chem. Eng. Sci.* 52, 861–911.
- Lightfoot, E.N., 1974. *Transport Phenomena and Living Systems*. John Wiley, New York.
- Lito, P.F., Cardoso, S.P., Loureiro, J.M., Silva, C.M., 2012. Ion exchange equilibria and kinetics, Chapter 3. In: Imamuddin, M., Luqman (Eds.), *Ion Exchange Technology I*, Vol. Marcel Dekker, New York, pp. 51–120.
- Neihof, R., Sollner, K., 1957. The transitory overshooting of final equilibrium concentrations in membrane systems which drift toward the Gibbs-Donnan membrane equilibrium. *J. Phys. Chem.* 61, 159–163.
- Newman, J., 1991. *Electrochemical Systems*, 2nd ed. Prentice Hall, Inc., Englewood Cliffs, NJ, USA.
- Rodriguez, J.F., Valverde, J.L., Rodrigues, A.E., 1998. Measurements of effective self-diffusion coefficients in a gel-type cation exchanger by the zero-length-column method. *Ind. Eng. Chem. Res.* 37, 2020–2028.
- Samson, E., Lemaire, G., Marchand, J., Beaudoin, J.J., 1999. Modeling chemical activity effects in strong ionic solutions. *Comput. Mater. Sci.* 15, 285–294.
- Seader, J.D., Henley, E.J., Roper, D.K., 2011. *Separation Process Principles*, 3rd ed. John Wiley, New York.
- Shunong, F., Yilu, F., Peiyan, L., 1994. Application of an ion selective electrode to study in-situ in kinetics of cations exchange in Zeolite Y. *Talanta* 41, 155–157.
- Sirkar, K.K., 2014. *Separation of Molecules, Macromolecules and Particles. Principles, Phenomena and Processes*. Cambridge University Press, Cambridge.
- Smith, T.G., Dranoff, J.S., 1964. Film diffusion-controlled kinetics in binary ion exchange. *Ind. Eng. Chem. Fundam.* 5, 195–200.
- Sodaye, S., Agarwal, C., Goswami, A.N., 2006. Study on multicomponent diffusion of ions in poly(perfluorosulfonated) ion-exchange membrane using radiotracers. *J. Membr. Sci.* 314, 221–225.
- Standart, G.L., Taylor, R., Krishna, R., 1979. The Maxwell-Stefan formulation of irreversible thermodynamics for simultaneous heat and mass transfer. *Chem. Eng. Commun.* 3, 277–289.
- Taylor, R., Krishna, R., 1993. *Multicomponent Mass Transfer*. John Wiley, New York.
- Turner, J.C.R., Snowdon, C.B., 1968. Liquid-side mass-transfer coefficients in ion exchange: an examination of the Nernst-Planck Model. *Chem. Eng. Sci.* 23, 221–230.
- Umino, S., Newman, J., 1993. Diffusion of sulfuric acid in concentrated solutions. *J. Electrochem. Soc.* 140, 2217–2221.
- Varshney, K.G., Pandith, A.H., 1999. Forward and reverse ion-exchange kinetics for some alkali and alkaline earth metal ions on amorphous zirconium(IV) aluminophosphate. *Langmuir* 15, 7422–7425.
- Vinograd, J.R., McBain, J.W., 1941. Diffusion of electrolytes and ions in their mixtures. *J. Am. Chem. Soc.* 63, 2008–2015.
- Wankat, P.C., 2012. *Separation Process Engineering*, 3rd ed. Prentice-Hall, Upper Saddle River, New Jersey, USA.
- Wesselingh, J.A., Krishna, R., 2000. *Mass Transfer in Multicomponent Mixtures*. VSSD, Delft.
- Yang, Y., Pintauro, P.N., 2000. Multicomponent space-charge transport model for ion-exchange membranes. *A.I.Ch.E.J.* 46, 1177–1190.
- Yoshida, H., Kataoka, T., 1987. Intraparticle ion-exchange mass transfer in ternary system. *Ind. Eng. Chem. Res.* 26, 1179–1184.

Supplementary material to accompany

Highlighting Coupling Effects in Ionic Diffusion

Rajamani Krishna

Van 't Hoff Institute for Molecular Sciences, University of Amsterdam, Science Park 904,
1098 XH Amsterdam, The Netherlands

Email: r.krishna@contact.uva.nl

Table of Contents

1.	Preamble.....	3
2.	The Maxwell-Stefan diffusion formulation for ionic diffusion	3
3.	Ion-water and ion-ion Maxwell-Stefan diffusivities	6
4.	Effective ion diffusivities calculated from the Nernst-Planck equations.....	9
5.	Simulation of Vinograd-McBain experiments	10
6.	Taylor dispersion of mixed ions for laminar flow in a circular tube.....	14
7.	Transient overshoots during counter-diffusion of mixed ions	15
8.	Transient overshoots for permeation across cation exchange membranes	17
9.	Forward/Reverse Ion-Exchanges	20
10.	Asymmetry in Forward/Reverse Ion-Exchange: Diffusional limitation outside IEX particle	21
11.	Minority rule for diffusion of counter ions within ion exchanger particle.....	29
12.	Asymmetry in Forward/Reverse Ion-Exchange: Diffusional limitation inside particle.....	35
13.	Transient overshoots and asymmetry for uptake of ternary cations in cation exchange particles	40
14.	Simulation of the transient overshoots in Yoshida-Kataoka experiments.....	43
15.	A simplified transient model for the Kraaijeveld-Wesselingh experiments.....	47
16.	Notation	51
17.	References	54
18.	Caption for Figures	56

1. Preamble

This Supplementary material accompanying the article *Highlighting Coupling Effects in Ionic Diffusion* provides details of (a) derivations of the Nernst-Planck equations starting from the Maxwell-Stefan equations, (b) some background information and insights on diffusivities, (d) calculation of effective diffusivities, (e) simulations of transient diffusion of ions across membranes, and within ion-exchanger particles, and (f) all input data used in the simulations of transient diffusion.

All the calculations and simulations were performed using MathCad 15.¹ The printouts of the MathCad files used in the calculations are at the end of this document.

For ease of reading, this Supplementary material is written as a stand-alone document; as a consequence, there is some overlap of material with the main manuscript.

2. The Maxwell-Stefan diffusion formulation for ionic diffusion

For diffusion in n -component fluid mixtures consisting of neutral, uncharged species, the Maxwell-Stefan (M-S) equations^{2,3} are normally written as

$$-\frac{x_i}{RT} \frac{\partial \mu_i}{\partial z} = \sum_{\substack{j=1 \\ j \neq i}}^n \frac{x_i x_j (u_i - u_j)}{D_{ij}}; \quad i = 1, 2, \dots, n \quad (1)$$

In equation (1), u_i is the velocity of species i in a laboratory fixed reference frame, and D_{ij} is the diffusivity of $i-j$ pair in the n -component mixture. The M-S formulation is essentially a friction formulation, and D_{ij} is to be interpreted as the inverse drag coefficient for the $i-j$ pair. The Onsager reciprocal relations demand the symmetry constraint

$$D_{ij} = D_{ji}; \quad i = 1, 2, \dots, n \quad (2)$$

We may also define the diffusion fluxes

$$N_i = c_i u_i; \quad i = 1, 2, \dots, n \quad (3)$$

where c_i is the molar concentration of species i . The total molar concentration of the mixture is

$$c_t = \sum_{i=1}^n c_i \quad (4)$$

A wide variety of processes of importance in the process industries involve the transport of ionic species in bulk electrolyte liquid mixtures, within charged particles, and across charged membranes. Examples include electrolysis, electrodialysis, ion exchange, and fuel cells.⁴⁻⁹ For design and development of such processes, it is essential to have adequate models to describe the transport fluxes. For transport of ionic species in electrolyte solutions, we need to consider as an additional driving force, expressed in Joules per mole of mixture, caused by the electrostatic potential gradient

$$F_i = -z_i F \frac{\partial \Phi}{\partial z} \quad (5)$$

where z_i is the ionic charge of species i and F is the Faraday constant. Except in regions close to electrode surfaces, where there will be charge separation (the double layer phenomena), the condition of electro-neutrality is met

$$\sum_{i=1}^n c_i z_i = 0; \quad \text{electroneutrality constraint} \quad (6)$$

and therefore

$$\sum_{k=1}^n c_k F_k = \left(\sum_{k=1}^n c_k z_k \right) F \frac{\partial \Phi}{\partial z} = 0 \quad (7)$$

Adding the contribution of the external forces, described by equation (5), to the left member of equation (1) yields

$$-\frac{x_i}{RT} \frac{\partial \mu_i}{\partial z} - x_i z_i \frac{F}{RT} \frac{\partial \Phi}{\partial z} = \sum_{\substack{j=1 \\ j \neq i}}^n \frac{x_i x_j (u_i - u_j)}{D_{ij}}; \quad i = 1, 2, \dots, n \quad (8)$$

It is convenient to define a generalized driving force

$$d_i \equiv \frac{x_i}{RT} \frac{\partial \mu_i}{\partial z} + x_i z_i \frac{F}{RT} \frac{\partial \Phi}{\partial z} \quad (9)$$

The second law of thermodynamics demands that the rate of entropy production be positive definite¹⁰

$$\sigma = \frac{1}{2} c_t R \sum_{i=1}^n \sum_{j=1}^n \frac{x_i x_j |(u_i - u_j)|^2}{D_{ij}} \geq 0 \quad (10)$$

The division by 2 is required because of the application of the Onsager reciprocal relations (2).

The second law constraint does not require each of the pair M-S diffusivities to be positive definite. Indeed, Kraaijeveld and Wesselingh¹¹ experimental evidence to suggest that cation-cation diffusivities could assume negative values without violation of the second law of thermodynamics. For molten salt mixtures LiF-BeF₂, the MD simulation data of Chakraborty¹² show negative values of the ion pair diffusivities, without violation of the second law constraint (10).

Written in terms of the fluxes, $N_i = c_i u_i$, we may re-write equation (8) as

$$-\frac{x_i}{RT} \frac{\partial \mu_i}{\partial z} - x_i z_i \frac{F}{RT} \frac{\partial \Phi}{\partial z} = \sum_{\substack{j=1 \\ j \neq i}}^n \frac{x_j N_i - x_i N_j}{c_t D_{ij}}; \quad i = 1, 2, \dots, n \quad (11)$$

The total current carried by the electrolyte is $F \sum_{i=1}^n z_i N_i$. In many chemical process applications such as

ion exchange, no external electrical field is imposed on the system, and also there is no flow of current, i.e.

$$\sum_{i=1}^n z_i N_i = \sum_{i=1}^n c_i z_i u_i = 0; \quad \text{no current prescription} \quad (12)$$

For aqueous electrolyte solutions, the n^{th} component is usually taken to be water, that is often considered to be stagnant, i.e.

$$u_n = 0; \quad N_n = 0; \quad \text{stagnant solvent water prescription} \quad (13)$$

3. Ion-water and ion-ion Maxwell-Stefan diffusivities

Let us first consider ion-water diffusivities. Figure 1 presents a comparison of cation-water and anion-water diffusivities for various electrolyte systems at 293 K. The decrease in the diffusivities for salt concentration above about 1 mol L⁻¹ is mainly due to increased viscosity of the solution. The H⁺ and OH⁻ have considerably higher mobilities than other ions in solution. Wesselingh and Krishna⁸ provide the following explanation: “These ions propagate through water by “bumping off” new ions from the other side of the water molecule”.

Let us now compare cation-water, anion-water, and cation-anion diffusivity values. As illustration, let us consider diffusion in an aqueous solution of H₂SO₄; the transport properties for this system have been collected by Umino and Newman.¹³ The system consists of three species: H⁺ (= 1), SO₄²⁻ (= 2) and H₂O (= 3). The charges are z₁ = 1, z₂ = -2 and z₃ = 0. Let c_{H₂SO₄} represent the concentration of the electrolyte in the aqueous solution and c₃ the molar concentration of water. The concentrations of the ions are c₁ = 2c_{H₂SO₄}; c₂ = c_{H₂SO₄} and the corresponding mole fractions are

$$x_1 = \frac{2c_{H_2SO_4}}{3c_{H_2SO_4} + c_3}; \quad x_2 = \frac{c_{H_2SO_4}}{3c_{H_2SO_4} + c_3}.$$

Equation (1) can be written explicitly for the ionic species in the system as follows

$$\begin{aligned} -\frac{x_1}{RT} \frac{\partial \mu_1}{\partial z} - x_1 z_1 \frac{F}{RT} \frac{\partial \Phi}{\partial z} &= \frac{x_1 x_2 (u_1 - u_2)}{D_{12}} + \frac{x_1 x_3 (u_1 - u_3)}{D_{13}} \\ -\frac{x_2}{RT} \frac{\partial \mu_2}{\partial z} - x_2 z_2 \frac{F}{RT} \frac{\partial \Phi}{\partial z} &= \frac{x_2 x_1 (u_2 - u_1)}{D_{12}} + \frac{x_2 x_3 (u_2 - u_3)}{D_{23}} \end{aligned} \quad (14)$$

The values of the three Maxwell-Stefan diffusivities D₁₃, D₂₃ and D₁₂ as function of the sulphuric acid concentration are shown in Figure 2. The diffusivity of H⁺ ion in water, D₁₃, is about ten times higher than that of the SO₄²⁻ ion, D₂₃. However, due to the requirement of electro-neutrality (6), an electric field Φ is set up, called the diffusion potential, which tends to slow down the H⁺ ions and accelerate the SO₄²⁻ ions so that they move in unison. The effective Maxwell-Stefan diffusivity of H₂SO₄, considered as a whole, can be defined by

$$-\frac{1}{RT} \frac{\partial \mu_{H_2SO_4}}{\partial z} = \frac{x_3(u_{H_2SO_4} - u_3)}{D_{H_2SO_4}} \quad (15)$$

where the chemical potential of H₂SO₄ is

$$\mu_{H_2SO_4} = (2)\mu_1 + (1)\mu_2 \quad (16)$$

in which the individual ionic chemical potentials have been multiplied by the corresponding stoichiometric coefficients for the H⁺ and SO₄²⁻ ions respectively. Combining equations (14) - (16) allows us to obtain the following expression for the Maxwell-Stefan diffusivity D_{H₂SO₄}

$$D_{H_2SO_4} = \frac{D_{13}D_{23}(z_1 - z_2)}{z_1D_{13} - z_2D_{23}} \quad (17)$$

whose value lies between D₁₃ and D₂₃; see Figure 2.

At a concentration of 0.1 mol L⁻¹, the diffusivity values are

$$D_{12} = 0.03 \times 10^{-9}$$

$$D_{13} = 9.63 \times 10^{-9} \quad m^2 s^{-1}$$

$$D_{23} = 1.08 \times 10^{-9}$$

$$D_{H_2SO_4} = 2.63 \times 10^{-9}$$

It is interesting to note that the diffusivity of the neutral electrolyte D_{H₂SO₄} is closer to the diffusivity of the tardier SO₄²⁻ ion in water, D₂₃, than that of the more mobile H⁺ in water, D₁₃.

Figure 3 presents the data on Maxwell-Stefan diffusivities in aqueous NaCl system: Na⁺ (= 1), Cl⁻ (= 2) and H₂O (= 3).⁸ In this case, the diffusivity of the cation in water, D₁₃, is lower than that of the anion in water, D₂₃.

We also note from equation (17) that the ion-ion interaction coefficient D₁₂ (i.e. plus-minus diffusivities) has no influence on the diffusivity of the neutral electrolyte. The values of D₁₂, which represents the long-range cation - anion interaction, are typically one or two orders of magnitude lower than the ion-water diffusivities (cf. Figure 2) and vanish as the concentration approaches zero with a

\sqrt{c} dependence in accordance with Debye-Hückel-Onsager theory for ion-ion interactions in dilute solution; see Newman.⁵

A series of cation-anion diffusivities, D_{12} , is plotted in Figure 4. For all species, the diffusivity increases approximately with the square root of the salt concentration. The diffusivities increase strongly with increasing charge numbers. Interactions between pairs of ions with the same charge numbers are almost identical.

Let us now examine the relative importance of the contributions of the two frictional terms on the right members of equation (14).

For hydrogen ion H^+ in aqueous sulphuric acid solutions, the relative friction experienced with the sulphate ions to that with water is $\frac{(x_2 / D_{12})}{(x_3 / D_{13})}$; similarly for the sulphate ion SO_4^{2-} the relative friction experienced with the hydrogen ion to that with water is $\frac{(x_1 / D_{12})}{(x_2 / D_{23})}$. These relative values have been calculated using the data of Umino and Newman¹³ and presented in Figure 5.

We see that for electrolyte concentrations smaller than about 0.01 mol L^{-1} , the cation-anion friction is less than 20% of the ion - water friction and the first right members of eq. (14) can be ignored giving for ionic species i

$$N_i = -D_i \frac{c_i}{RT} \frac{\partial \mu_i}{\partial z} - c_i z_i D_i \frac{F}{RT} \frac{\partial \Phi}{\partial z} + c_i u_n; \quad i = 1, 2, \dots, n-1 \quad (18)$$

where the D_i in equation (18) are the ionic diffusivities. The three contributions to the molar flux of ionic species i are usually termed “diffusion”, “migration” and “convection”.

The species n is usually water, that is usually present in significantly large proportions, and can often be considered stagnant, $N_n = c_n u_n = 0$. The ion-water diffusivities are practically independent of electrolyte concentration for dilute solutions (cf. Figure 1). For dilute aqueous solutions of electrolytes,

the activity coefficients are approximately unity, so $\frac{c_i}{RT} \frac{\partial \mu_i}{\partial z} \approx \frac{\partial c_i}{\partial z}$. With these assumptions and

simplifications, equations (18) reduce to the Nernst-Planck equation for the flux of individual ionic species

$$N_i = -D_i \frac{\partial c_i}{\partial z} - c_i z_i D_i \frac{F}{RT} \frac{\partial \Phi}{\partial z}; \quad i = 1, 2, \dots, n-1 \quad (19)$$

4. Effective ion diffusivities calculated from the Nernst-Planck equations

Combining equations (12), and (19), we obtain the following expression for the diffusion potential that is engendered due to ionic diffusion

$$\frac{\partial \Phi}{\partial z} = - \frac{\sum_{k=1}^{n-1} z_k D_k \frac{\partial c_k}{\partial z}}{\frac{F}{RT} \sum_{j=1}^{n-1} c_j z_j^2 D_j} \quad (20)$$

Inserting equation (20) for the diffusion potential into equation (19) we obtain

$$N_i = -D_i \frac{\partial c_i}{\partial z} + \frac{c_i z_i D_i}{\sum_{j=1}^{n-1} c_j z_j^2 D_j} \sum_{k=1}^{n-1} z_k D_k \frac{\partial c_k}{\partial z}; \quad i = 1, 2, \dots, n-1 \quad (21)$$

The requirement of electro-neutrality places a constraint on the ionic concentration gradients

$$\sum_{i=1}^{n-1} z_i \frac{\partial c_i}{\partial z} = 0; \quad \text{electroneutrality constraint} \quad (22)$$

This means that the $(n-1)$ th gradient can be eliminated

$$\sum_{i=1}^{n-2} z_i \frac{\partial c_i}{\partial z} = -z_{n-1} \frac{\partial c_{n-1}}{\partial z}; \quad \text{electroneutrality constraint} \quad (23)$$

Combining equations (12), (19), and (23) we obtain the following expression for the diffusion potential that is engendered due to ionic diffusion

$$\frac{\partial \Phi}{\partial z} = - \frac{\sum_{k=1}^{n-2} z_k D_k \frac{\partial c_k}{\partial z} + z_{n-1} D_{n-1} \frac{\partial c_{n-1}}{\partial z}}{\frac{F}{RT} \sum_{j=1}^{n-1} c_j z_j^2 D_j} = - \frac{\sum_{k=1}^{n-2} z_k (D_k - D_{n-1}) \frac{\partial c_k}{\partial z}}{\frac{F}{RT} \sum_{j=1}^{n-1} c_j z_j^2 D_j} \quad (24)$$

Inserting equation (24) for the diffusion potential into equation (19) we obtain

$$N_i = -D_i \frac{\partial c_i}{\partial z} + \frac{c_i z_i D_i}{\sum_{j=1}^{n-1} c_j z_j^2 D_j} \sum_{k=1}^{n-2} z_k (D_k - D_{n-1}) \frac{\partial c_k}{\partial z}; \quad i = 1, 2, \dots, n-2 \quad (25)$$

Equation (25) can be conveniently cast into $(n-2)$ dimensional matrix notation

$$(N) = -[D] \frac{\partial(c)}{\partial z} \quad (26)$$

The elements of the $(n-2) \times (n-2)$ dimensional square matrix are

$$D_{ik} = D_i \delta_{ik} - \frac{c_i z_i z_k D_i (D_k - D_{n-1})}{\sum_{j=1}^{n-1} c_j z_j^2 D_j}; \quad i, k = 1, 2, \dots, n-2 \quad (27)$$

where δ_{ik} is the Kronecker delta. The second member of the right of equation (27) quantifies the electrostatic “leash” that serves to enhance, or diminish, the ionic mobilities. Whether an ion is accelerated or decelerated depends on the species charges, z_i , and whether we have co-diffusion or counter-diffusion.

The elements of the matrix $[D]$ are strongly concentration dependent; the off-diagonal elements are non-zero, i.e. *ionic diffusion is always coupled even for dilute solutions.*

5. Simulation of Vinograd-McBain experiments

To illustrate diffusional coupling effects, consider the experimental results of Vinograd and McBain¹⁴ in a two-compartment diffusion cell, shown schematically in Figure 6. Diffusion takes place through the pores of a sintered glass disk that separate the two compartments. Each of the two compartments is well-mixed, and the concentration gradients are restricted to disk thickness, δ . The bottom compartment contains pure water while the top compartment contains a mixture of aqueous solutions of HCl and BaCl₂. Let c_{HCl} and c_{BaCl_2} denote the molar concentrations, expressed in mol L⁻¹ of solution. Total ionization takes place and the system is a quaternary mixture: 1 = H⁺, 2 = Cl⁻, 3 = Ba⁺⁺, 4 = H₂O. The concentrations of ions are: $c_{\text{H}^+} = c_{\text{HCl}}$; $c_{\text{Ba}^{++}} = c_{\text{BaCl}_2}$; $c_{\text{Cl}^-} = (c_{\text{HCl}} + 2 c_{\text{BaCl}_2})$. In one set of experiments

reported by Vinograd and McBain,¹⁴ the ratio of the concentrations $c_{\text{HCl}}/c_{\text{BaCl}_2}$ was varied. By monitoring the concentrations of the three ionic species as a function of time, Vinograd and McBain¹⁴ obtained the effective ionic diffusivities $D_{i,\text{eff}}$ for H^+ , Cl^- and Ba^{2+} . The experimentally observed ionic diffusivities are shown in Figure 6 as function of the square root of the ratio of the initial ionic concentrations of H^+ and Ba^{2+} in the top compartment $\sqrt{c_{\text{HCl}}/c_{\text{BaCl}_2}} = \sqrt{c_{\text{H}^+}/c_{\text{Ba}^{2+}}}$. With increasing values of $\sqrt{c_{\text{H}^+}/c_{\text{Ba}^{2+}}}$, it is observed that both D_{H^+} and $D_{\text{Ba}^{2+}}$ decrease while D_{Cl^-} increases. At the start of the diffusion process, the highly mobile H^+ diffuses ahead of its companion ions into the pure water compartment, creating an excess of positive charge. This induces a diffusion potential $\partial\Phi/\partial z$ which acts in such a way as to comply with the no-current and electro-neutrality prescriptions. The consequence is that the Cl^- experiences an extra electrostatic “pull”, enhancing its effective diffusivity value. The electrical potential gradient also serves to retard the motion of the positive ions H^+ and Ba^{++} or in other words these ions experience a “push” in a direction opposite to that dictated by their composition gradient driving forces. For $\sqrt{c_{\text{H}^+}/c_{\text{Ba}^{2+}}} = 2$, the electrostatic “push” on Ba^{++} is such as to result in a vanishing value for $D_{\text{Ba}^{2+}}$. The continuous solid lines in Figure 6 are the calculations of the effective diffusivities

$$D_{i,\text{eff}} = \frac{N_i}{-\frac{\partial c_i}{\partial z}} \quad (28)$$

wherein the fluxes are determined from Equation (25).

The values of the effective diffusivities $D_{i,\text{eff}}$ for H^+ , Cl^- and Ba^{++} can be determined explicitly from equations (26) and (27) by approximating the concentration gradients $-\frac{\partial c_i}{\partial z} = \frac{c_{i0} - c_{i\delta}}{\delta}$; $i = 1, 2, \dots, n-1$.

The concentrations c_{i0} correspond to those in the top well-stirred compartment.

$$c_{10} = c_{\text{HCl}}; \quad c_{20} = c_{\text{HCl}} + 2c_{\text{BaCl}_2}; \quad c_{30} = c_{\text{BaCl}_2}$$

In the bottom compartment, we have pure water; all the ionic concentrations are zero $c_{i\delta} = 0$. We use the ionic diffusivities provided in Example 2.4.2 of Taylor and Krishna:¹⁵

$$D_1 = 9.3 \times 10^{-9}; \quad D_2 = 2 \times 10^{-9}; \quad D_3 = 0.85 \times 10^{-9} \text{ m}^2 \text{ s}^{-1}.$$

The continuous solid lines in Figure 6 are the calculations using equations (26), (27), and (28). The elements of the matrix $[D]$ are determined at the *average* concentration in the top and bottom compartments; this allows explicit evaluation of the fluxes and the effective ionic diffusivities. The essential diffusion characteristics for the HCl/BaCl₂/H₂O mixture are properly captured by the analytic solution to the Nernst-Planck equation.

The Nernst-Planck model calculations anticipate negative values of $D_{\text{Ba}^{2+}}$ for $\sqrt{c_{\text{H}^+}/c_{\text{Ba}^{2+}}} > 2$ due to a strong electrostatic “push”; see Figure 6. Negative effective diffusivities signal the possibility of uphill diffusion for Ba²⁺.

Figure 7 compares the experimental data of Vinograd and McBain¹⁴ for ionic diffusivities of H⁺, K⁺, and Cl⁻ in a two-compartment diffusion cell with the calculations using equations (26), (27), and (28). We use the ionic diffusivities¹⁵ (1 = H⁺, 2 = Cl⁻, 3 = K⁺)

$$D_1 = 9.3 \times 10^{-9}; \quad D_2 = 2 \times 10^{-9}; \quad D_3 = 2 \times 10^{-9} \text{ m}^2 \text{ s}^{-1}.$$

In this case, the Cl⁻ is accelerated, while both cations H⁺, and K⁺ are retarded due to the electrostatic leash. The essential diffusion characteristics for the HCl/KCl/H₂O mixture are properly captured by the analytic solution to the Nernst-Planck equation.

The calculations presented in Figure 6 and Figure 7 are for steady-state conditions. The influence of electrostatic coupling effects are also clearly demonstrated by transient diffusion calculations for a diffusion “couple” as described by Krishna.² A HCl/BaCl₂/H₂O electrolyte mixture, maintained at constant composition (0.02 mol L⁻¹ HCl; 0.01 mol L⁻¹ BaCl₂) is brought into contact with liquid water at time $t = 0$. The transient development of concentrations of the ions in the Left and Right compartments (denoted by subscripts L and R) is described by the matrix equation

$$(c(z,t)) = \frac{(c_{L0} + c_{R0})}{2} + erf\left[\frac{z}{\sqrt{4t}}[D]^{-1/2}\right] \frac{(c_{R0} - c_{L0})}{2} \quad (29)$$

The matrix of diffusivities $[D]$ is given by equation (27). The Sylvester theorem, detailed in Appendix A of Taylor and Krishna,¹⁵ is required for explicit determination of the 3-dimensional square matrix

$$[Q] = erf\left[\frac{z}{\sqrt{4t}}[D]^{-1/2}\right].$$

For the case of three distinct eigenvalues, λ_1 , λ_2 , and λ_3 of the 3-dimensional square matrix $[D]$, the Sylvester theorem yields

$$\begin{aligned} [Q] = & \frac{f(\lambda_1)[D] - \lambda_2[I][D] - \lambda_3[I]}{(\lambda_1 - \lambda_2)(\lambda_1 - \lambda_3)} + \\ & \frac{f(\lambda_2)[D] - \lambda_1[I][D] - \lambda_3[I]}{(\lambda_2 - \lambda_1)(\lambda_2 - \lambda_3)} + \frac{f(\lambda_3)[D] - \lambda_1[I][D] - \lambda_2[I]}{(\lambda_3 - \lambda_1)(\lambda_3 - \lambda_2)} \end{aligned} \quad (30)$$

In equation (30), $[I]$ is the identity matrix with elements δ_{ik} . The functions $f(\lambda_i)$ are calculated from

$$f(\lambda_i) = erf\left[\frac{z}{\sqrt{4t}} \lambda_i^{-1/2}\right] \quad (31)$$

Figure 8a shows the transient development of the concentrations of H^+ , Cl^- and Ba^{++} . The concentration profiles are presented as a function of a distance coordinate $\left[\frac{z}{\sqrt{4D_{ref}t}}\right]$ where the

reference value of the scalar diffusivity $D_{ref} = 10^{-9} \text{ m}^2 \text{ s}^{-1}$. Due to the higher mobility of H^+ , it penetrates deep into the aqueous phase in the Right compartment. The electrostatic potential gradient serves to retard the mobility of H^+ , while enhance the mobility of Cl^- . We note that the penetration of

H^+ and Cl^- goes hand-in-hand, for $\left[\frac{z}{\sqrt{4D_{ref}t}}\right] > 1$, in order to maintain electroneutrality. The

requirement of electroneutrality also serves to retard the motion of the tardiest Ba^{++} . The penetration of Ba^{++} into the right compartment lags far behind that of the co-ions H^+ , and Cl^- .

Figure 8b presents the results for transient co-diffusion of H^+ , NO_3^- , Na^+ , and Cl^- . A bulk HNO_3/NaCl electrolyte solution, maintained at constant composition ($0.1 \text{ mol L}^{-1} \text{ HNO}_3$; $0.1 \text{ mol L}^{-1} \text{ NaCl}$) in the Left compartment, is brought into contact with NaCl solution (also of concentration 0.1 mol L^{-1}) in the Right compartment at time $t = 0$. There is no concentration driving force for either Na^+ , or Cl^- . However, due to electrostatic coupling, we note that Na^+ , and Cl^- undergo overshoots, and undershoots during the transient diffusion process. Due to the rapid diffusion of H^+ into the right compartment, there is a charge imbalance. This causes Cl^- to diffuse into the right compartment to maintain electro-neutrality, causing an overshoot. Concomitantly, the Na^+ diffuses into the left compartment to maintain electro-neutrality. A further noteworthy point is that the penetration of H^+ into the right compartment lags slightly behind the penetration of NO_3^- .

6. Taylor dispersion of mixed ions for laminar flow in a circular tube

A different demonstration of coupling effects in ionic diffusion is provided by consideration of Taylor dispersion in a tube. For laminar flow in a circular tube of length L , and radius R the concentration development following the (Dirac delta) δ -pulse injection of a tracer of a *binary* mixture with Fick diffusivity D is

$$C = \frac{M}{2\pi R^2 \sqrt{\pi \frac{u^2 R^2}{48D} t}} \exp\left(-\frac{(L-ut)^2}{4 \frac{u^2 R^2}{48D} t}\right) \quad (32)$$

In equation (32), M is the excess amount of component (moles) injected, above the concentration in the flowing stream at the inlet. The details of the derivation are provided, for example, by Price¹⁶ and Rutten;¹⁷ these authors also provide details of the extension of the model to multicomponent mixtures.

Following, Rutten,¹⁷ our Taylor dispersion calculations are for the following set of conditions:

Length of tube, $L = 15 \text{ m}$;

Cross-sectional averaged velocity in tube, $u = 0.01 \text{ m s}^{-1}$;

Radius of tube, $R = 0.265 \text{ mm}$

The liquid flowing through the tube consists of a mixture containing HCl (with a concentration of 0.01 mol L⁻¹) and BaCl₂ (with a concentration of 0.01 mol L⁻¹). The diffusivity matrix [D] can be calculated at this composition using equation (27). At time $t = 0$, a δ -pulse containing 10⁻⁹ moles of HCl and 10⁻⁹ moles of BaCl₂ is injected; in terms of the ionic species, the δ -pulse contains 10⁻⁹ moles of H⁺, 3 × 10⁻⁹ moles of Cl⁻, and 10⁻⁹ moles of Ba⁺⁺. The transient concentration at the exit of the tube ($L = 15$ m) is shown in Figure 9a. The undershoot in the H⁺ concentration is due to the retarding influence of the electrostatic leash as quantified by the second right member of equation (27).

Figure 9b presents the dispersion calculations in which the electrostatic leash is neglected and the diffusivity matrix is calculated using $D_{ik} = D_{iw}\delta_{ik}$. In this scenario, the undershoot in H⁺ concentration disappears.

7. Transient overshoots during counter-diffusion of mixed ions

We demonstrate the possibility of transient overshoots in counter-diffusion of mixed electrolyte solutions. For this purpose, we consider counter-diffusion of 1 = H⁺, 2 = Cl⁻, 3 = Ba⁺⁺ between the two compartments as shown in Figure 10. We assume that each of the two compartments is well mixed and the concentration gradients are restricted to the thickness of the porous diaphragm separating the two compartments. Initially, the left compartment contains HCl with a concentration of 0.04 mol L⁻¹; the right compartment contains BaCl₂ with a concentration of 0.02 mol L⁻¹. In 3-dimensional vector notation, the initial concentrations in the left and right compartments are (1 = H⁺, 2 = Cl⁻, 3 = Ba⁺⁺)

$$(c_{L0}) = \begin{pmatrix} 0.04 \\ 0.04 \\ 0 \end{pmatrix}; \quad (c_{R0}) = \begin{pmatrix} 0.0 \\ 0.04 \\ 0.02 \end{pmatrix} \quad (33)$$

It is noteworthy, that there is no driving force for transport of chloride ions across the porous membrane.

The transient equilibration process in the left and right compartments (with volumes V , and interfacial area A) is described in matrix notation by $V \frac{d(c_L)}{dt} = -V \frac{d(c_R)}{dt} = -(N_i)A$. The molar flux N_i is taken to

be positive if directed from left to right. At any instant of time, t , we have $V \frac{d(c_L)}{dt} = -[D] \frac{(c_L - c_{eq})}{\delta} A$

where δ is the effective thickness of the diffusion layer. We define a cell constant $\beta = \frac{A\delta}{V}$, and write

$\frac{d(c_L)}{dt} = -\beta[D](c_L - c_{eq})$. If the diffusivity matrix is considered constant for a short discretized interval

of time, this matrix differential equation may be integrated to obtain

$$(c_L - c_{eq}) = \exp[-\beta[D]t](c_{L0} - c_{eq}) \quad (34)$$

where the vector $(c_{eq}) = \frac{(c_{L0} + c_{R0})}{2} = \begin{pmatrix} 0.02 \\ 0.04 \\ 0.01 \end{pmatrix}$. An analogous expression holds for the right compartment..

In our calculations, we take $\beta = 10^4 \text{ m}^{-2}$. The square matrix $[Q] = \exp[-\beta[D]t]$ quantifies the transient departure from equilibrium. The Sylvester theorem, detailed in Appendix A of Taylor and Krishna,¹⁵ is required for explicit determination of $[Q] = \exp[-\beta[D]t]$.

For the case of three distinct eigenvalues, λ_1 , λ_2 , and λ_3 of the 3-dimensional square matrix $[D]$, the Sylvester theorem yields

$$[Q] = \frac{f(\lambda_1)[D] - \lambda_2[I][D] - \lambda_3[I]}{(\lambda_1 - \lambda_2)(\lambda_1 - \lambda_3)} + \frac{f(\lambda_2)[D] - \lambda_1[I][D] - \lambda_3[I]}{(\lambda_2 - \lambda_1)(\lambda_2 - \lambda_3)} + \frac{f(\lambda_3)[D] - \lambda_1[I][D] - \lambda_2[I]}{(\lambda_3 - \lambda_1)(\lambda_3 - \lambda_2)} \quad (35)$$

In equation (35), $[I]$ is the identity matrix with elements δ_{ik} . The functions $f(\lambda_i)$ are calculated from

$$f(\lambda_i) = \exp[-\beta\lambda_i t] \quad (36)$$

The elements of the matrix $[D]$ are determined at the *average* concentration in the left and right compartments at any instant of time. In other words, the solution to the matrix equation (34) is carried out in time-discretized form. By choosing sufficiently small time intervals, sufficiently good accuracy in the calculations is achieved.

The composition trajectories in the left and right compartments during transient equilibration are presented in Figure 10. The diffusion equilibration of H^+ , and Ba^{++} proceeds in a “normal” manner, i.e. the transport is from higher to lower concentration regions with exponential decay. The equilibration of chloride ions is remarkable in that a concentration overshoot is experienced in the right compartment with concomitant undershoot in the left compartment. Let us explain the concentration overshoot in physical terms. The more mobile H^+ rapidly diffuses into the right compartment; this creates an excess of positive charge. The necessity of maintaining electroneutrality demands the presence of Cl^- that gets transported from left to right in order to negate the charge imbalance.

The equilibration process follows serpentine trajectories in composition space.

Figure 11 presents the analogous results for counter-diffusion of H^+ , K^+ , and Cl^- between two well-mixed compartments. The continuous solid lines are the calculations using equations (26), (27), and (34). In this case too, the chloride ion experiences overshoot/undershoot characteristics, that characterize uphill diffusion.²

8. Transient overshoots for permeation across cation exchange membranes

There is experimental evidence of transient overshoots such as that demonstrated in Figures 10 and 11. Yang and Pintauro¹⁸ report an interesting set of experimental data for transient transport of H^+ , Na^+ , and Cs^+ ions across a Nafion cation exchange membrane separating the acid and salt compartments; see Figure 12a. In the reported experiments, the initial concentrations are:

Left: salt compartment: $\text{Na}_2\text{SO}_4 = 0.125 \text{ mol L}^{-1}$; $\text{Cs}_2\text{SO}_4 = 0.0054 \text{ mol L}^{-1}$

Right: acid compartment: $\text{H}_2\text{SO}_4 = 0.125 \text{ mol L}^{-1}$

The H^+ ions transfer from the acid to the salt compartment. Both Na^+ , and Cs^+ ions transfer from the salt to the acid compartment. The SO_4^{2-} ions cannot cross the membrane. Due to the significantly higher mobility of the H^+ ions, there is a significant influence of the diffusion potential $\frac{\partial\Phi}{\partial z}$ that tends to influence the mobility of the Na^+ , and Cs^+ ions during the initial stages of the transience. Since the

concentration driving force of Cs^+ ions is very small, the initial transience is strongly dictated by the diffusion potential $\frac{\partial\Phi}{\partial z}$; this results in the observed overshoot in the transient equilibration of Cs^+ . Yang and Pintauro¹⁸ present a detailed simulation model for the experiments. For our purposes here, we wish to demonstrate that the overshoot in the transient equilibration of Cs^+ ions can be rationalized by a simplified analytic solution of the Nernst-Planck equations using matrix calculus.

Assuming total ionization, the total ionic concentrations in the left and right compartments are ($1 = \text{H}^+$, $2 = \text{Na}^+$; $3 = \text{Cs}^+$, $4 = \text{SO}_4^{2-}$)

$$c_{1L0} = 0; \quad c_{2L0} = 0.25; \quad c_{3L0} = 0.0108; \quad c_{4L0} = 0.1304 \text{ mol L}^{-1}$$

$$c_{1R0} = 0.25; \quad c_{2R0} = 0.0; \quad c_{3R0} = 0.0; \quad c_{4R0} = 0.125$$

The equilibrated ionic concentrations are the arithmetic averages

$$c_{1eq} = 0.125; \quad c_{2eq} = 0.125; \quad c_{2eq} = 0.0054 \text{ mol L}^{-1}$$

The cation exchange membrane prevents the transport of SO_4^{2-} ions; and therefore the compositions in the left and right compartments of SO_4^{2-} ions will remain 0.1304 and 0.125, respectively. In order to take account of the exclusion of SO_4^{2-} ions from the matrix of the cation exchange membrane, we need to impose the additional constraint for the $(n-1)^{\text{th}}$ species, i.e. the 4th species.

$$N_{n-1} = 0 \tag{37}$$

This implies that the no-current relation (12) must simplify to

$$\sum_{i=1}^{n-2} z_i N_i = \sum_{i=1}^{n-2} c_i z_i u_i = 0; \quad \text{no current prescription} \tag{38}$$

The expression for the electrostatic potential gradient also reduces to

$$\frac{\partial\Phi}{\partial z} = -\frac{\sum_{k=1}^{n-2} z_k D_k \frac{\partial c_k}{\partial z}}{\frac{F}{RT} \sum_{j=1}^{n-2} c_j z_j^2 D_j} \tag{39}$$

The $(n-2)$ non-zero flux relations are

$$N_i = -D_i \frac{\partial c_i}{\partial z} + \frac{c_i z_i D_i}{\sum_{j=1}^{n-2} c_j z_j^2 D_j} \sum_{k=1}^{n-2} z_k D_k \frac{\partial c_k}{\partial z}; \quad i = 1, 2, \dots, n-2 \quad (40)$$

We define a $(n-2) \times (n-2)$ dimensional square matrix

$$D_{ik} = D_i \delta_{ik} - \frac{(c_i z_i D_i z_k D_k)}{\sum_{j=1}^{n-2} c_j z_j^2 D_j}; \quad i, k = 1, 2, \dots, n-2 \quad (41)$$

The explicit expression for the $(n-2)$ non-zero fluxes can be written in $(n-2)$ dimensional matrix notation

$$(N) = -[D] \frac{\partial(c)}{\partial z} \quad (42)$$

The transient equilibration process in the left and right compartments is described by the $(n-2)$

dimensional matrix equations (34) where the vector $(c_{eq}) = \frac{(c_{L0} + c_{R0})}{2} = \begin{pmatrix} 0.125 \\ 0.125 \\ 0.0054 \end{pmatrix}$, and β is the cell

constant. The 3×3 dimensional square matrix $\exp[-\beta[D]t]$ quantifies the transient approach to equilibrium. In our calculations, we take $\beta = 2 \times 10^4 \text{ m}^{-2}$, that is representative of the experimental set-up. The Sylvester theorem, detailed in Appendix A of Taylor and Krishna,¹⁵ is required for explicit determination of $[Q] = \exp[-\beta[D]t]$. Equation (41) is used to determine the diffusivity matrix $[D]$.

For simulations of the transient equilibration process, we use the ionic diffusivities provided in Table 3 of Yang and Pintauro¹⁸ ($1 = \text{H}^+$, $2 = \text{Na}^+$; $3 = \text{Cs}^+$, $4 = \text{SO}_4^{2-}$)

$$D_1 = 9.3 \times 10^{-9}; \quad D_2 = 1.33 \times 10^{-9}; \quad D_3 = 2.06 \times 10^{-9}; \quad D_4 = 1.33 \times 10^{-9} \text{ m}^2 \text{ s}^{-1}.$$

The elements of the matrix $[D]$ are determined at the *average* concentration in the left and right compartments at any instant of time. In other words, the solution to the matrix equation (34) is carried out in time-discretized form. By choosing sufficiently small time intervals, a good accuracy in the calculations is achieved. The simulation results, obtained by combination of equations (26), and (34), and (41) are shown in Figure 12b. Our simple model is able to capture the overshoot in the transient

equilibration of Cs^+ ions. The physical reasoning for the overshoot is as follows. The more mobile H^+ ions vacate the right (acid) compartment rapidly. This creates a rapid reduction in the positive charge in the right compartment. The SO_4^{2-} are non-diffusing and cannot participate in redressing this charge imbalance. Electroneutrality is restored by the enhanced influx of Na^+ , and Cs^+ from the salt compartment. Consequently, both Na^+ , and Cs^+ get accelerated by electrostatic effects. The influence of the second member of the right of equation (41) is relatively large for Cs^+ because its concentration driving force is small.

The reasonably good match between model simulations and experiments is also indicative of the fact that the transmembrane permeation fluxes are dictated by diffusion in the electrolyte solutions in either compartment.

In Figure 13 the equilibration trajectories followed by H^+ , Na^+ , and Cs^+ in the salt and acid compartments, plotted in composition space. In Figure 13a, the left compartment contains Na_2SO_4 and Cs_2SO_4 and the right compartment contains H_2SO_4 . The undershoot and overshoot in Cs^+ correspond to the Yang-Pintauro experimental observations.

We also carried out simulations for a set of different concentrations in the left and right compartments. The results are presented in Figure 13b for the scenario in which the left compartment contains Na_2SO_4 and the right compartment contains H_2SO_4 and Cs_2SO_4 ; in this case no overshoot or undershoot is experienced by Cs^{++} because it diffuses in the same direction as H^+ .

Transient overshoots for Cs^+/Na^+ permeation across a cation-exchange membrane have been reported by Sodaye et al.¹⁹ These overshoots are most likely caused by a combination of electrostatic and thermodynamic coupling effects.

9. Forward/Reverse Ion-Exchanges

Ion exchange is a sorption separation process that is carried out in fixed bed units in a transient manner. Most commonly, the ion-exchange resins are solid gels, consisting of a polymeric matrix produced by co-polymerization of styrene and a cross-linking agent, divinylbenzene, to produce a three-dimensional cross-linked structure with ionic functional groups attached to the polymeric network.⁴ As

illustration, Figure 14 shows a schematic showing an ion exchanger (IEX) particle with fixed HSO_3^- charges. The liquid phase surrounding the particles consists of a bulk electrolyte solution e,g, HCl and NaCl. The electrolytes are fully ionized and the bulk liquid phase contains H^+ , Na^+ , Cl^- ions along with unionized water molecules. The cation exchange particle is negative charged and disallows the influx of Cl^- ions; only the positively charged cations, called counter-ions, are allowed to enter or leave the particle. If the styrene-divinylbenzene copolymer is chlormethylated and aminated, a strong-base, anionic exchange resin is formed that contain fixed positive charges, RN^+ .⁴ In all of the examples considered below, we consider cation-exchange resins only.

Experimentally, it has been found that loading Na^+ *into the particle* while removing H^+ from particle, occurs at a significantly different rate than loading H^+ *into the particle* while removing Na^+ from particle. In other words, the diffusion process is asymmetric.

Depending on the set of operating conditions used (concentration of ions in the bulk electrolyte), and the properties (pore size of particles, intra-particle diffusivities), two scenarios for diffusion limitations are possible: (a) the ion exchange process is limited by transfer from the bulk liquid phase to the external surface of the particle, and (b) the ion exchange process is limited by intra-particle diffusion. Generally speaking, for low concentrations of electrolytes in the bulk liquid, typically $< 0.01 \text{ mol L}^{-1}$, the exchange process is governed by the diffusion through the “film” surrounding the particle. For high external concentrations, typically $> 0.1 \text{ mol L}^{-1}$, the exchange process is governed by intra-particle diffusion. Each of these scenarios needs to be analyzed and discussed separately because the physico-chemical principles are different.

10. Asymmetry in Forward/Reverse Ion-Exchange: Diffusional limitation outside IEX particle

We first examine forward and reverse ion exchange for the situation in which the transfer resistance is located external to the particle. The diffusion process is dictated by physico-chemical phenomena external to the particle in the bulk liquid phase; the diffusion process was first analysed by Schlögl and Helfferich.²⁰ This directional influence of the diffusion potential is illustrated clearly by the experiments

of Kraaijeveld and Wesselingh²¹ for external mass transfer limited ion exchange. Exchanging Na⁺ within the ion exchange bead with H⁺ from the bulk chloride solution proceeds at a significantly higher rate than for the reverse exchange process; see Figure 15a. Figure 15b shows experimental data for analogous asymmetry for H⁺/Ca⁺⁺ exchanges.

Smith and Dranoff²² also present experimental evidence of asymmetry in H⁺/Na⁺ exchange when controlled by external mass transfer resistance.

The exclusion of the co-ions from the particle implies the condition $N_3 = 0$

$$N_3 = -D_3 \frac{\partial c_3}{\partial z} - c_3 z_3 D_3 \frac{F}{RT} \frac{\partial \Phi}{\partial z} = 0; \quad \frac{\partial c_3}{\partial z} = -c_3 z_3 \frac{F}{RT} \frac{\partial \Phi}{\partial z}; \quad \text{anion exclusion from IEX} \quad (43)$$

It is also important to stress that even though the flux of the chloride ion (species 3) is zero, because of the exclusion from the ion exchanger particle, this does not imply that the concentration gradient of chloride ion vanishes.

Combining equations (19) and (43) with the no-current prescription

$$z_1 N_2 + z_2 N_2 = 0; \quad \text{no current prescription} \quad (44)$$

leads to the following explicit expressions for the ionic fluxes

$$N_i = -D_{i,\text{eff}} \frac{\partial c_i}{\partial z}; \quad i = 1, 2 \quad (45)$$

where the effective ionic diffusivities are

$$N_1 = -D_{1,\text{eff}} \frac{\partial c_1}{\partial z}; \quad D_{1,\text{eff}} = \frac{c_1 z_1^2 + c_2 z_2^2 + c_3 z_3^2}{\frac{c_1 z_1^2}{D_2} + \frac{(c_2 z_2^2 + c_3 z_3^2)}{D_1}} \quad (46)$$

and

$$N_2 = -D_{2,\text{eff}} \frac{\partial c_2}{\partial z}; \quad D_{2,\text{eff}} = \frac{c_1 z_1^2 + c_2 z_2^2 + c_3 z_3^2}{\frac{(c_1 z_1^2 + c_3 z_3^2)}{D_2} + \frac{c_2 z_2^2}{D_1}} \quad (47)$$

where the concentration of component 3 is restrained by electro-neutrality

$$c_1 z_1 + c_2 z_2 = -c_3 z_3; \quad \text{electroneutrality constraint} \quad (48)$$

Equation (46) is equivalent to equation 12 of Turner and Snowdon.²³

An alternative expression for the fluxes is in terms of the gradients of the equivalent fractions X_i that are defined as follows

$$X_1 = \frac{z_1 c_1}{-z_3 c_3}; \quad X_2 = \frac{z_2 c_2}{-z_3 c_3}; \quad X_1 + X_2 = 1 \quad (49)$$

In terms of the equivalent fractions, the flux expressions are

$$\begin{aligned} z_1 N_1 &= \frac{X_1(z_1 - z_2) + (z_2 - z_3)}{\frac{z_1 X_1}{D_2} + \frac{(z_2 - z_3 - z_2 X_1)}{D_1}} z_3 c_3 \frac{\partial X_1}{\partial z} = D_{1,eff} z_3 c_3 \frac{\partial X_1}{\partial z} \\ z_2 N_2 &= \frac{X_2(z_2 - z_1) + (z_1 - z_3)}{\frac{(z_1 - z_3 - z_1 X_2)}{D_2} + \frac{X_2 z_2}{D_1}} z_3 c_3 \frac{\partial X_2}{\partial z} = D_{2,eff} z_3 c_3 \frac{\partial X_2}{\partial z} \end{aligned} \quad (50)$$

The expressions for the effective diffusivities, expressed in terms of the equivalent fractions are

$$\begin{aligned} D_{1,eff} &= \frac{X_1(z_1 - z_2) + (z_2 - z_3)}{\frac{z_1 X_1}{D_2} + \frac{(z_2 - z_3 - z_2 X_1)}{D_1}} \\ D_{2,eff} &= \frac{X_2(z_2 - z_1) + (z_1 - z_3)}{\frac{(z_1 - z_3 - z_1 X_2)}{D_2} + \frac{X_2 z_2}{D_1}}; \quad X_1 + X_2 = 1 \end{aligned} \quad (51)$$

The limiting values of the effective diffusivities are

$$\begin{aligned} X_1 \rightarrow 0; \quad D_{1,eff} &\rightarrow D_1 \\ X_2 \rightarrow 0; \quad D_{2,eff} &\rightarrow D_2 \end{aligned} \quad (52)$$

The effective diffusivities at limiting concentrations are counter-intuitive.

For the special case of univalent ions, $z_1 = 1; z_2 = 1; z_3 = -1$, the expressions (46) and (47) for the effective diffusivities simplify to yield

$$D_{1,eff} = \frac{2(c_1 + c_2)}{\left[\frac{c_1}{D_2} + \frac{2c_2 + c_1}{D_1} \right]} = \frac{2}{\left[\frac{X_1}{D_2} + \frac{2X_2 + X_1}{D_1} \right]}; \quad X_1 + X_2 = 1 \quad (53)$$

$$D_{2,eff} = \frac{2(c_1 + c_2)}{\left[\frac{c_2}{D_1} + \frac{2c_1 + c_2}{D_2} \right]} = \frac{2}{\left[\frac{X_2}{D_1} + \frac{2X_1 + X_2}{D_2} \right]}; \quad z_1 = 1; z_2 = 1; z_3 = -1$$

Equations (53) are equivalent to equations 21 and 22, as derived by Smith and Dranoff²²; these are valid only for univalent ions.

For the H⁺/Na⁺ exchange in the bulk electrolyte containing four species: 1 = H⁺, 2 = Na⁺; 3 = Cl⁻, 4 = water, the calculations of the effective diffusivities of 1 = H⁺, and 2 = Na⁺ for a total molar concentration $c_t = c_1 + c_2 = c_3 = 0.05 \text{ mol L}^{-1}$ and varying equivalent fractions $X_1 = \frac{z_1 c_1}{-z_3 c_3} = \frac{c_1}{c_1 + c_2}$ are

shown in Figure 16a. The input data for ion diffusivities used are (1 = H⁺, 2 = Na⁺, 3 = Cl⁻)

$D_1 = 9.3 \times 10^{-9}$; $D_2 = 1.3 \times 10^{-9}$; $D_3 = 2 \times 10^{-9} \text{ m}^2 \text{ s}^{-1}$. These values are taken from Kraaijeveld and Wesselingh.²¹

The obtained results for effective diffusivities of H⁺, and Na⁺ in bulk electrolyte phase surrounding ion exchanger particle are quite remarkable because both effective diffusivities are *reduced* when the proportion of the more mobile H⁺ *increases*. This result is counter-intuitive; we shall discuss a similar phenomenon for exchange of H⁺, and Na⁺ within the IEX particle in the subsequent section.

Figure 16b presents the corresponding results for the calculations of the effective diffusivities of 1 = H⁺, and 2 = Ca⁺ for a total molar concentration $c_t = c_1 + c_2 = c_3 = 0.05 \text{ mol L}^{-1}$ and varying equivalent fractions $X_1 = \frac{z_1 c_1}{-z_3 c_3} = \frac{c_1}{c_1 + 2c_2}$. The input data for ion diffusivities used are (1 = H⁺, 2 = Ca⁺⁺, 3 = Cl⁻) $D_1 = 9.3 \times 10^{-9}$; $D_2 = 0.792 \times 10^{-9}$; $D_3 = 2 \times 10^{-9} \text{ m}^2 \text{ s}^{-1}$. These values are taken from Kraaijeveld and Wesselingh.²¹ The effective diffusivities also illustrate the non-intuitive characteristics of equation (52) for the limiting values.

For the special case of univalent ions, $z_1 = 1; z_2 = 1; z_3 = -1$, Turner and Snowdon²³ have obtained analytic solutions for steady-state transfer fluxes across a film of thickness δ . The flux expressions are

$$N_1 = \frac{D_1}{\delta} \frac{2c_{3\delta}(X_{10} - X_{1\delta})}{\left(1 + \left(\frac{D_1}{D_2} - 1\right)X_{10}\right) + \sqrt{\left(1 + \left(\frac{D_1}{D_2} - 1\right)X_{10}\right)\left(1 + \left(\frac{D_1}{D_2} - 1\right)X_{1\delta}\right)}} \quad (54)$$

$$N_2 = \frac{D_2}{\delta} \frac{2c_{3\delta}(X_{20} - X_{2\delta})}{\left(1 + \left(\frac{D_2}{D_1} - 1\right)X_{20}\right) + \sqrt{\left(1 + \left(\frac{D_2}{D_1} - 1\right)X_{20}\right)\left(1 + \left(\frac{D_2}{D_1} - 1\right)X_{2\delta}\right)}} \quad (55)$$

Because of the electrostatic potential field, the concentrations of the anions vary along the distance, z , of the diffusion layer

$$\frac{c_{3z}}{c_{3\delta}} = \sqrt{\frac{1 + \left(\frac{D_1}{D_2} - 1\right)X_{1\delta}}{1 + \left(\frac{D_1}{D_2} - 1\right)X_{1z}}} = \sqrt{\frac{1 + \left(\frac{D_1}{D_2} - 1\right)(1 - X_{2\delta})}{1 + \left(\frac{D_1}{D_2} - 1\right)(1 - X_{2z})}} \quad (56)$$

At $z = 0$, we have

$$\frac{c_{30}}{c_{3\delta}} = \sqrt{\frac{1 + \left(\frac{D_1}{D_2} - 1\right)X_{1\delta}}{1 + \left(\frac{D_1}{D_2} - 1\right)X_{10}}} = \sqrt{\frac{1 + \left(\frac{D_1}{D_2} - 1\right)(1 - X_{2\delta})}{1 + \left(\frac{D_1}{D_2} - 1\right)(1 - X_{20})}} \quad (57)$$

The Turner-Snowdon analytic solutions above are restricted in their applicability to univalent ions.

Let us first offer a simple qualitative explanation for the experimental observations in Figure 15a for the system: 1 = H^+ , 2 = Na^+ ; 3 = Cl^- , 4 = water. Following the illustration in Figure 20.8 of Wesselingh and Krishna,⁸ Figures 17a,b show the calculations of typical concentration profiles for H^+/Na exchanges that are limited by transfer to/from the IEX particle; in other words the transfer resistance is in a thin film surrounding the IEX particle. These steady-state calculations are based on the flux expressions (54), (55), along with equation (56). The effective thickness of the film surrounding the particle is

assumed as $\delta = 20 \mu\text{m}$. The fluxes of the two counter cations ($1 = \text{H}^+$, $2 = \text{Na}^+$) must satisfy the relation

$$N_1 = -N_2.$$

The two sets of calculations shown in Figures 17a,b are shown for the case in which the concentrations of the counter ions in the bulk electrolyte (position $z = \delta$), and at the surface of the particle (position $z = 0$) are (a) $c_{1\delta} = 0.0$; $c_{2\delta} = 0.05$; $c_{20} = 0 \text{ mol L}^{-1}$ and (b) $c_{1\delta} = 0.05$; $c_{2\delta} = 0.0$; $c_{10} = 0 \text{ mol L}^{-1}$.

Consider the scenario in which we exchange H^+ within the ion exchange bead with Na^+ from the bulk electrolyte outside the particle. The calculated profiles shown in Figure 17a are for specific case in which the concentrations chosen are $c_{1\delta} = 0.0$; $c_{2\delta} = 0.05$; $c_{20} = 0 \text{ mol L}^{-1}$. The concentration c_{30} must satisfy Equation (57); the value determined is $c_{30} = 0.01869 \text{ mol L}^{-1}$. To satisfy electroneutrality, we must therefore have also $c_{10} = 0.01869 \text{ mol L}^{-1}$. The calculated fluxes are $N_1 = -N_2 = 4.73 \times 10^{-6} \text{ mol m}^{-2} \text{ s}^{-1}$. The fast motion of H^+ away from the particle into the bulk liquid causes an electrostatic potential gradient $\frac{\partial \Phi}{\partial z}$. This gradient acts in a way so as to push the chloride ion away from the particle/solution interface.

In the second scenario we exchange Na^+ within the ion exchange bead with H^+ from the bulk electrolyte outside the particle. The calculated profiles shown in Figure 17a are for specific case in which the concentrations chosen are $c_{1\delta} = 0.05$; $c_{2\delta} = 0.0$; $c_{10} = 0 \text{ mol L}^{-1}$. The concentration c_{30} must satisfy Equation (57); the value determined is $c_{30} = 0.13373 \text{ mol L}^{-1}$. To satisfy electroneutrality, we must therefore have also $c_{20} = 0.13373 \text{ mol L}^{-1}$. The calculated fluxes are $-N_1 = N_2 = 12.65 \times 10^{-6} \text{ mol m}^{-2} \text{ s}^{-1}$. The fast motion of H^+ toward the particle from the bulk liquid causes an electrostatic potential gradient $\frac{\partial \Phi}{\partial z}$; this gradient acts in a way so as to push the chloride ion toward the particle/solution interface. In this second scenario, the concentration gradients are higher. Larger

concentration gradients cause higher fluxes and faster equilibration. The magnitude of the fluxes in the second scenario are a factor 2.67 larger than the magnitude of the fluxes in the first scenario.

A different procedure for calculating the steady-state fluxes are to use the combination of equations (45), (46), and (47), along with the flux constraint on two counter cations ($1 = \text{H}^+$, $2 = \text{Na}^+$)

$$N_1 = \frac{D_{1,\text{eff}}}{\delta} (c_{10} - c_{1\delta}) = -N_2 = -\frac{D_{2,\text{eff}}}{\delta} (c_{20} - c_{2\delta}).$$

The effective diffusivities may be evaluated at the

arithmetic averaged concentrations within the film using Equation (53). These calculations yield identical results to those obtained using the Turner-Snowdon analytic solutions. The approach using the effective diffusivities are not restricted to univalent ions. Furthermore, the effective diffusivities can be inserted into transient diffusion models, as illustrated in the examples below.

The calculations presented in Figure 17 are for steady-state conditions. The asymmetry in the forward/reverse exchanges can also be demonstrated by transient diffusion calculations for a diffusion “couple”. The left compartment is the IEX resin and the right compartment is the bulk electrolyte solution. In contrast to the earlier discussions in the context of Figures 8a, and 8b, the left compartment is maintained at a constant composition (c_{L0}) by maintaining a “through flow” of the resin phase. We focus on the transient equilibration in the right compartment, $z \geq 0$. The transient development of concentrations of the ions in the Right compartment is described by

$$c_i(z, t) = c_{i,L0} + \operatorname{erf} \left[\frac{z}{\sqrt{4D_{i,\text{eff}}t}} \right] (c_{i,R0} - c_{i,L0}); \quad i = 1, 2 \quad (58)$$

Equations (46), and (47) are used for the calculations of the effective diffusivities of H^+ , and Na^+ .

For the Scenario 1: exchange H^+ within the ion exchange resin with Na^+ from the bulk electrolyte outside the IEX particle we use the following set of conditions:

$$(c_{L0}) = \begin{pmatrix} 0.0 \\ 0.01 \end{pmatrix}; \quad (c_{R0}) = \begin{pmatrix} 0.01 \\ 0.00 \end{pmatrix}; \quad \text{Scenario 1}$$

For the Scenario 2: exchange Na^+ within the ion exchange bead with H^+ from the bulk electrolyte outside the IEX particle we use the following set of conditions:

$$(c_{L0}) = \begin{pmatrix} 0.01 \\ 0.0 \end{pmatrix}; \quad (c_{R0}) = \begin{pmatrix} 0.0 \\ 0.01 \end{pmatrix}; \quad \text{Scenario 2}$$

The concentration profiles are presented as a function of a distance coordinate $\left[\frac{z}{\sqrt{4D_{ref}t}} \right]$ where the

reference value of the scalar diffusivity $D_{ref} = 10^{-9} \text{ m}^2 \text{ s}^{-1}$. The ionic concentration profiles for the two scenarios are presented in Figures 18a, and 18b. We note that the Scenario 2, the uptake of Na^+ is faster than the uptake of H^+ for Scenario 1 (see comparison of the two uptakes in the inset to Figure 18). Figure 19 presents calculations using equations (46) and (47) of the effective diffusivities for forward and reverse H^+/Na^+ exchange in the two scenarios shown in Figure 18. We note that for Scenario 2, the effective diffusivities of both components increase during the transient diffusion; in contrast the

effective diffusivities decrease with $\left[\frac{z}{\sqrt{4D_{ref}t}} \right]$ for scenario 1.

The transient diffusion calculations in Figure 18 and Figure 19 provide a rationalization of the experimental data shown in Figure 15a.

Figures 20a, and 20b present the corresponding results for forward and reverse $\text{H}^+/\text{Ca}^{++}$ exchange from ion exchange resin to bulk electrolyte HCl/CaCl_2 liquid. Note that in this case the ionic concentrations are plotted as $z_i c_i$ in order to properly compare the development of the concentration profiles for univalent H^+ with divalent Ca^{++} . The uptake of Ca^{++} into the liquid occurs faster than the uptake of H^+ into the liquid; see comparison of the two uptakes in the inset to Figures 20.

Figure 21 presents calculations using equations (46) and (47) of the effective diffusivities for forward and reverse H^+/Na^+ exchange in the two scenarios shown in in Figure 20. We note that for Scenario 2, the effective diffusivities of both components increase during the transient diffusion; in contrast the

effective diffusivities decrease with $\left[\frac{z}{\sqrt{4D_{ref}t}} \right]$ for scenario 1.

The uptake profiles provide a rationalization of the experimental data shown in Figure 15b.

Figure 22 provides a comparison of the concentration trajectories followed during forward and reverse (a) H^+/Na^+ , and (b) $\text{H}^+/\text{Ca}^{++}$ exchange from ion exchange resin to bulk electrolyte liquid. The trajectories follow different paths in composition space.

A further point to emphasize in the results presented for the steady-state and transient profiles in Figure 17, and Figure 18 is that even though the flux of chloride ions is zero, $N_3 = 0$ this does *not* imply that the corresponding concentration gradient also vanishes, i.e. $\frac{\partial c_3}{\partial z} \neq 0$. Indeed, the profiles of the excluded chloride ion shown in Figures 18, and 20 demonstrate that the chloride ion exhibits an undershoot or overshoot, depending on whether the more mobile H^+ is transported into the liquid, or out of the liquid into the adjoining resin IEX particle. This is an important feature that is quite different for diffusion within the IEX particle, as discussed in the following section.

11. Minority rule for diffusion of counter ions within ion exchanger particle

We now turn our attention to forward/reverse exchanges in which the diffusion resistance is within the particle. The IEX particle matrix consists of fixed negative charges. Let us assume that the total concentration of negative charges inside the matrix is c_{fixed} , expressed say as equivalent (mole) per volume of particle. Typically, the concentration of fixed negative charges is in the range of 1 to 4 equiv L^{-1} ;⁸ this value is considerably higher than the molar concentrations of ions in the bulk electrolyte solutions surrounding the particle. The concentration of counter ions within the particle must balance

c_{fixed} and therefore we have $\sum_{i=1}^m z_i c_i = c_{\text{fixed}}$. The quantity

$$\frac{z_i c_i}{c_{\text{fixed}}} \equiv X_i \quad (59)$$

is the ionic equivalent fraction. The ionic equivalent fractions of all the counter ions sum to unity

$\sum_{i=1}^m X_i = 1$. Please note that the ionic equivalent fractions for the solid particle phase is defined different

than the corresponding ion equivalent fractions in the bulk electrolytes surrounding the particle, equation (49).

For HCl/NaCl exchange, the negative chloride ion is excluded from the particle. The fluxes of $\text{H}^+(1)$, and $\text{Na}^+(2)$ are

$$\begin{aligned} N_1 &= -D_1 \frac{\partial c_1}{\partial z} - c_1 z_1 D_1 \frac{F}{RT} \frac{\partial \Phi}{\partial z} \\ N_2 &= -D_2 \frac{\partial c_2}{\partial z} - c_2 z_2 D_2 \frac{F}{RT} \frac{\partial \Phi}{\partial z} \end{aligned} \quad (60)$$

There is no flow of current

$$z_1 N_1 + z_2 N_2 = 0 \quad (61)$$

Combining equations (60) and (61), allows the determination of the electrostatic potential gradient engendered by intra-particle diffusion

$$\frac{F}{RT} \frac{\partial \Phi}{\partial z} = \frac{-z_1 D_1 \frac{\partial c_1}{\partial z} - z_2 D_2 \frac{\partial c_2}{\partial z}}{(c_1 z_1^2 D_1 + c_2 z_2^2 D_2)} \quad (62)$$

Introducing equation (62) into equation (60) yields the flux relations

$$\begin{aligned} N_1 &= -D_1 \frac{\partial c_1}{\partial z} + c_1 z_1 D_1 \frac{z_1 D_1 \frac{\partial c_1}{\partial z} + z_2 D_2 \frac{\partial c_2}{\partial z}}{(c_1 z_1^2 D_1 + c_2 z_2^2 D_2)} \\ N_2 &= -D_2 \frac{\partial c_2}{\partial z} + c_2 z_2 D_2 \frac{z_1 D_1 \frac{\partial c_1}{\partial z} + z_2 D_2 \frac{\partial c_2}{\partial z}}{(c_1 z_1^2 D_1 + c_2 z_2^2 D_2)} \end{aligned} \quad (63)$$

For electro-neutrality:

$$z_1 \frac{\partial c_1}{\partial z} + z_2 \frac{\partial c_2}{\partial z} = 0 \quad (64)$$

In view of equation (64), we can simplify equations (63) as follows

$$N_1 = -D_{1,\text{eff}} \frac{\partial c_1}{\partial z}; \quad N_2 = -D_{2,\text{eff}} \frac{\partial c_2}{\partial z} \quad (65)$$

where the effective ionic diffusivities are

$$D_{1,eff} = \frac{c_1 z_1^2 + c_2 z_2^2}{(c_1 z_1^2 D_1 + c_2 z_2^2 D_2)} D_1 D_2 = D_{2,eff} = D_{eff} = \frac{c_1 z_1^2 + c_2 z_2^2}{\left(\frac{c_1 z_1^2}{D_2} + \frac{c_2 z_2^2}{D_1} \right)} \quad (66)$$

Equation (66) is to be contrasted with the corresponding equations for the effective ionic diffusivities in the bulk electrolyte liquid, Equations (46), and (47). The differences arise because the negative charges within the IEX particle are immobile and therefore electro-neutrality can only be maintained if both the effective diffusivities of the counter-ions are identical. For bulk electrolytes, the flux of the chloride ion is zero, but its concentration gradient adjusts itself in such a manner as to counteract the influence of the electrostatic potential gradient; see Equation (43).

Equation (66) is a remarkable result because the limiting values are:

$$\begin{aligned} c_1 \rightarrow 0; \quad D_{eff} &\rightarrow D_1 \\ c_2 \rightarrow 0; \quad D_{eff} &\rightarrow D_2 \end{aligned} \quad (67)$$

In other words, the intra-particle effective diffusivity corresponds to the diffusivity of the ion that is present in the *smaller* quantity. Helfferich, perhaps the most influential researcher, in ion exchange has termed this the “minority rule”. To quote Helfferich⁷ *binary interdiffusion is not a democratic process but, in the parlance of the activist 1960's, is ruled by a participating minority!*

For the cases such as for $H^+(1)/Na^+(2)$, in which $z_1 = z_2$, we obtain

$$D_{1,eff} = \frac{1}{\frac{c_1}{D_2} + \frac{c_2}{D_1}} = D_{2,eff} = D_{eff}; \quad \text{special case of equal charges } z_1 = z_2 \quad (68)$$

As illustration, Figure 23a presents the calculations of the effective diffusivity of $H^+(1)/Na^+(2)$ in an ion exchanger particle, using the following input data for ion diffusivities ($1 = H^+$, $2 = Na^+$) divided by the square of the radius of the IEX particle

$$D_1/r_c^2 = 0.015; \quad D_2/r_c^2 = 0.006 \text{ s}^{-1}.$$

$$\frac{z_1 c_1}{c_{fixed}} \rightarrow 0; \quad D_{eff}/r_c^2 \rightarrow D_1/r_c^2 = 0.015$$

We note that ; this result is counter-intuitive.

$$\frac{z_2 c_2}{c_{fixed}} \rightarrow 0; \quad D_{eff}/r_c^2 \rightarrow D_2/r_c^2 = 0.006$$

Figure 23b presents the calculations of the effective diffusivity of $\text{Na}^+(1)/\text{Sr}^{++}(2)$ in an ion exchanger particle, using the input data for ion diffusivities ($1 = \text{Na}^+$, $2 = \text{Sr}^{++}$) divided by the square of the radius of the IEX particle

$$D_1/r_c^2 = 0.006; \quad D_2/r_c^2 = 4 \times 10^{-4} \text{ s}^{-1}.$$

$$\frac{z_1 c_1}{c_{fixed}} \rightarrow 0; \quad D_{eff}/r_c^2 \rightarrow D_1/r_c^2 = 0.006$$

We note that ; this result is counter-intuitive.

$$\frac{z_2 c_2}{c_{fixed}} \rightarrow 0; \quad D_{eff}/r_c^2 \rightarrow D_2/r_c^2 = 4 \times 10^{-4}$$

We will use the above set of values of D_i/r_c^2 in the subsequent section to model the transient $\text{H}^+(1)/\text{Na}^+(2)$, and $\text{Na}^+(1)/\text{Sr}^{++}(2)$ exchanges within IEX particle.

We can also extend the foregoing analysis to diffusion of m different counter ions within the IEX particle. Equation (60) is extended as follows

$$N_i = -D_i \frac{\partial c_i}{\partial z} - c_i z_i D_i \frac{F}{RT} \frac{\partial \Phi}{\partial z}; \quad i = 1, 2, \dots, m \quad (69)$$

For no flow of current, the electrostatic diffusion potential gradient that is engendered by diffusion is

$$\frac{F}{RT} \frac{\partial \Phi}{\partial z} = \frac{-z_1 D_1 \frac{\partial c_1}{\partial z} - z_2 D_2 \frac{\partial c_2}{\partial z} - \dots - z_m D_m \frac{\partial c_m}{\partial z}}{\sum_{k=1}^m c_k z_k^2 D_k} \quad (70)$$

Electro-neutrality demands

$$z_1 \frac{\partial c_1}{\partial z} + z_2 \frac{\partial c_2}{\partial z} + \dots + z_m \frac{\partial c_m}{\partial z} = 0 \quad (71)$$

so we can eliminate the concentration gradient of the m th component and write

$$\frac{F}{RT} \frac{\partial \Phi}{\partial z} = \frac{- \sum_{k=1}^{m-1} z_k (D_k - D_m) \frac{\partial c_k}{\partial z}}{\sum_{k=1}^m c_k z_k^2 D_k} \quad (72)$$

Combining equation (69) and (72) we obtain

$$N_i = -D_i \frac{\partial c_i}{\partial z} + c_i z_i D_i \frac{\sum_{j=1}^{m-1} z_j (D_k - D_m) \frac{\partial c_k}{\partial z}}{\sum_{j=1}^m c_j z_j^2 D_j}; \quad i = 1, 2, \dots, m-1 \quad (73)$$

We may cast equation (73) into $(m-1)$ -dimensional matrix notation

$$(N) = -[D] \frac{\partial(c)}{\partial z} \quad (74)$$

Where the elements of the $(m-1) \times (m-1)$ dimensional square matrix $[D]$ are

$$D_{ik} = D_i \delta_{ik} - \frac{(c_i z_i D_i) z_k (D_k - D_m)}{\sum_{j=1}^m c_j z_j^2 D_j}; \quad i, k = 1, 2, \dots, m-1 \quad (75)$$

For the case in which we have 3 counter-ions within the IEX particle, $m = 3$, and equation (73) degenerates to yield

$$N_1 = -D_1 \frac{\partial c_1}{\partial z} + c_1 z_1 D_1 \frac{z_1 (D_1 - D_3) \frac{\partial c_1}{\partial z} + z_2 (D_2 - D_3) \frac{\partial c_2}{\partial z}}{(c_1 z_1^2 D_1 + c_2 z_2^2 D_2 + c_3 z_3^2 D_3)} \quad (76)$$

$$N_2 = -D_2 \frac{\partial c_2}{\partial z} + c_2 z_2 D_2 \frac{z_1 (D_1 - D_3) \frac{\partial c_1}{\partial z} + z_2 (D_2 - D_3) \frac{\partial c_2}{\partial z}}{(c_1 z_1^2 D_1 + c_2 z_2^2 D_2 + c_3 z_3^2 D_3)}$$

We may cast equation (76) into 2-dimensional matrix notation

$$(N) = -[D] \frac{\partial(c)}{\partial z} \quad (77)$$

in which the 2×2 dimensional square matrix $[D]$ has the elements

$$\begin{aligned}
D_{11} &= D_1 - c_1 z_1 D_1 \frac{z_1 (D_1 - D_3)}{(c_1 z_1^2 D_1 + c_2 z_2^2 D_2 + c_3 z_3^2 D_3)} \\
D_{12} &= -c_1 z_1 D_1 \frac{z_2 (D_2 - D_3)}{(c_1 z_1^2 D_1 + c_2 z_2^2 D_2 + c_3 z_3^2 D_3)} \\
D_{21} &= -c_2 z_2 D_2 \frac{z_1 (D_1 - D_3)}{(c_1 z_1^2 D_1 + c_2 z_2^2 D_2 + c_3 z_3^2 D_3)} \\
D_{22} &= D_2 - c_2 z_2 D_2 \frac{z_2 (D_2 - D_3)}{(c_1 z_1^2 D_1 + c_2 z_2^2 D_2 + c_3 z_3^2 D_3)}
\end{aligned} \tag{78}$$

It is noteworthy that Yoshida and Kataoka²⁴ and Jones and Carta²⁵ have set up in a different manner using the gradients of the ionic equivalent fractions, $\frac{\partial X_k}{\partial z}$ as driving forces, where X_k defined by equation (59).

$$z_i N_i = -c_{fixed} \sum_{k=1}^{m-1} D_{ik,eff} \frac{\partial X_k}{\partial z}; \quad i = 1, 2, \dots, m-1 \tag{79}$$

The elements of the $(m-1) \times (m-1)$ dimensional square matrix $[D_{eff}]$ is defined by

$$D_{ik,eff} = D_i \delta_{ik} - \frac{(X_i z_i D_i)}{\sum_{j=1}^m X_j z_j D_j} (D_k - D_m) \tag{80}$$

For the special case $m=2$, we have only one independent flux, and equations (59), (79), and (80) degenerate to yield

$$\begin{aligned}
z_1 N_1 &= -c_{fixed} D_1 \frac{\partial X_1}{\partial z} - c_{fixed} X_1 z_1 D_1 \frac{F}{RT} \frac{\partial \Phi}{\partial z} = -c_{fixed} D_{eff} \frac{\partial X_1}{\partial z}; \\
z_2 N_2 &= -c_{fixed} D_2 \frac{\partial X_2}{\partial z} - c_{fixed} X_2 z_2 D_2 \frac{F}{RT} \frac{\partial \Phi}{\partial z} = -c_{fixed} D_{eff} \frac{\partial X_2}{\partial z}; \\
D_{eff} &= \frac{X_1 z_1 + X_2 z_2}{\left(\frac{X_1 z_1}{D_2} + \frac{X_2 z_2}{D_1} \right)}
\end{aligned} \tag{81}$$

The corrective action of the induced potential gradient $\frac{\partial \Phi}{\partial z}$ is mainly directed *against* the species that is present in the *higher* equivalent fraction X_i .

For the limiting scenario $X_1 \rightarrow 0$, Equation (81) yields the minority rule

$$\begin{aligned} X_1 &\rightarrow 0; \quad D_{\text{eff}} \rightarrow D_1 \\ X_2 &\rightarrow 0; \quad D_{\text{eff}} \rightarrow D_2 \end{aligned} \tag{82}$$

The minority rule for diffusion within the ion exchanger particle leads to asymmetry in forward and reverse exchanges, as shall be demonstrated below.

12. Asymmetry in Forward/Reverse Ion-Exchange: Diffusional limitation inside particle

Consider the scenario in which the ion exchange process is limited by intra-particle diffusion.

Figure 24a presents the experimental data for H^+/Na^+ exchange in phenolsulphonic acid cation exchangers as reported by Helfferich^{6, 7} for two scenarios: (1) initially the particle is loaded with H^+ and is brought into contact with NaCl in the surrounding bulk liquid phase, and (2) initially the particle is loaded with Na^+ and is brought into contact with HCl in the surrounding bulk liquid phase. The experiments show that Scenario 1 leads to significantly faster equilibration than observed in Scenario 2. Remarkably, the hierarchy of equilibration rates is *opposite* to that experienced for the case in which the diffusion limitation is outside the particle (cf. Figure 15a, 15b).

Figure 24b presents the experimental data for $\text{Na}^+/\text{Sr}^{++}$ exchange in phenolsulphonic acid cation exchangers as reported by Helfferich^{6, 7} for two scenarios: (1) initially the particle is loaded with Na^+ and is brought into contact with SrCl_2 in the surrounding bulk liquid phase, and (2) initially the particle is loaded with Sr^{++} and is brought into contact with NaCl in the surrounding bulk liquid phase. The experiments show that Scenario 1 leads to significantly faster equilibration than observed in Scenario 2.

Figure 24c presents a comparison of the data for H^+/Na^+ exchange, with $\text{Na}^+/\text{Sr}^{++}$ exchanges. An interesting observation is that the replacement of Na^+ with H^+ occurs significantly faster than the replacement of Na^+ with Sr^{++} .

We rationalize these experimental observations using the explicit solution to the Nernst-Planck equations described in a foregoing section.

For transient unary uptake within a spherical IEX particle of radius r_c , the radial distribution of ion concentrations, c_i , is obtained from a solution of a set of differential equations describing the uptake

$$\frac{\partial c_i(r,t)}{\partial t} = -\frac{1}{r^2} \frac{\partial}{\partial r} \left(r^2 N_i \right) \quad (83)$$

Combining equations (77) and (83) we obtain the following expression describing the uptake transience

$$\frac{\partial c_i(r,t)}{\partial t} = \frac{1}{r^2} \frac{\partial}{\partial r} \left(r^2 \sum_{k=1}^{m-1} D_{ik} \frac{\partial c_k}{\partial r} \right) \quad (84)$$

where the elements of the $(m-1) \times (m-1)$ dimensional square matrix $[D]$ are given by equation (75).

Written in terms of the ionic mole fractions, equations (84) take the form

$$\frac{\partial X_i(r,t)}{\partial t} = \frac{1}{r^2} \frac{\partial}{\partial r} \left(r^2 \sum_{k=1}^{m-1} D_{ik}^* \frac{\partial X_k}{\partial r} \right) \quad (85)$$

where the elements of the $(m-1) \times (m-1)$ dimensional square matrix $[D^*]$ are given by equation (80).

At any time t , during the transient approach to thermodynamic equilibrium, the spatially averaged concentration within the particle of radius r_c is obtained by integration of the radial loading profile

$$\bar{c}_i(t) = \frac{3}{r_c^3} \int_0^{r_c} c_i(r,t) r^2 dr \quad (86)$$

An analytical solution to equation (83) is only possible for the special case in which the matrix $[D]$, defined by equation (27), can be considered constant for the range of concentrations encountered within the particle. In our simulations, we calculate the matrix $[D]$ at the spatially averaged value $\bar{x}_i(t)$, i.e. the diffusivity matrix is constantly updated in the time-discretized calculations.

Let us consider a particle that has the uniform concentrations (c_0). At time $t = 0$, the external surface is brought into contact with the bulk electrolyte solution with a different composition. The surface concentrations ($c_{r=r_c}$) is maintained for the entire duration of the equilibration process; this concentration is dictated by the ion exchange equilibrium (for further details see Wesselingh and Krishna⁸).

The expression for fractional *departure* from equilibrium is given by the matrix equation

$$(\bar{c}(t) - c_{r=rc}) = [Q](c_0 - c_{r=rc}); \quad [Q] \equiv \frac{6}{\pi^2} \sum_{m=1}^{\infty} \frac{1}{m^2} \exp\left[-m^2 \pi^2 \frac{[D]t}{r_c^2}\right] \quad (87)$$

Using time discretization, typically over a few thousand steps, the equation (87) can be written as

$(\bar{c}(t_j)) = [Q_{j-1}](c_0 - c_{r=rc}) + c_{r=rc}$ where $[Q_{j-1}]$ is evaluated using the concentrations at the time step t_{j-1} , $(c(t_{j-1}))$ that are known from the previous time step. The numerical procedure is easily implemented in MathCad 15. The same procedure applies to the determination of the spatial-averaged ionic equivalent fractions, $(\bar{X}(t_j))$:

$$(\bar{X}(t) - X_{r=rc}) = [Q](X_0 - X_{r=rc}); \quad [Q] \equiv \frac{6}{\pi^2} \sum_{m=1}^{\infty} \frac{1}{m^2} \exp\left[-m^2 \pi^2 \frac{[D]t}{r_c^2}\right] \quad (88)$$

The accuracy of our methodology for determination of the spatial-averaged concentrations $(\bar{X}(t_j))$ was established by comparison with the results of Hwang and Helfferich²⁶, for ternary ion uptake obtained using an exact numerical procedure; the results reported in their Figure 1 could be matched exactly using our procedure; see comparisons in Figure 25.

For the $\text{H}^+(1)/\text{Na}^+(2)$ exchange, the matrix $[D]$ is simply a scalar diffusivity D_{eff} , calculated from Equation (68), times the identity matrix.

For the simulations of transient forward/reverse exchange the following parameter values were used:

Ion diffusivities: (1 = H^+ , 2 = Na^+)

$$D_1/r_c^2 = 0.015; \quad D_2/r_c^2 = 0.006 \text{ s}^{-1}.$$

For the Scenario 1 we use the following set of conditions:

$$\frac{z_1 c_{1,0}}{c_{\text{fixed}}} = 1; \quad \frac{z_2 c_{2,0}}{c_{\text{fixed}}} = 0; \quad \frac{z_1 c_{1,r=rc}}{c_{\text{fixed}}} = 0; \quad \frac{z_2 c_{2,r=rc}}{c_{\text{fixed}}} = 1; \quad \text{particle initially loaded with } \text{H}^+$$

For the Scenario 2 we use the following set of conditions:

$$\frac{z_1 c_{1,0}}{c_{\text{fixed}}} = 0; \quad \frac{z_2 c_{2,0}}{c_{\text{fixed}}} = 1; \quad \frac{z_1 c_{1,r=rc}}{c_{\text{fixed}}} = 1; \quad \frac{z_2 c_{2,r=rc}}{c_{\text{fixed}}} = 0; \quad \text{particle initially loaded with } \text{Na}^+.$$

For both scenarios, the values of the ionic equivalent fractions $\frac{z_i c_{i,r=rc}}{c_{fixed}}$ correspond to those *at the surface, within the particle* and therefore take implicit account of the ion exchange equilibrium.

From the calculated spatial-averaged mole fractions, the fractional approach to equilibrium can be determined; these are plotted in Figures 26a, and 26b.

The results in Figure 26a are precisely opposite to the two corresponding scenarios considered in Figures 18, when the transfer resistance is external to the IEX resin particle.

The uptake simulations for fractional approach to equilibrium (cf. Figure 26b) are in good quantitative agreement with the Helfferich experiments. They show that the efflux of H^+ from the particle occurs much more rapidly than the efflux of Na^+ from the particle. Figure 26c shows the variation of the effective diffusivities for the two scenarios. Figure 26d shows the variation of the electrostatic potential differences.

It is quite remarkable to note that the analytic solution to the Nernst-Planck equation captures all of the essential features of the transient equilibration process. In the words of Helfferich⁷: *A remarkable prediction from the Nernst-Planck equations is that forward and reverse exchange of two ions of different mobilities should occur at different rates and with different behavior of the concentration profiles. With particle diffusion controlling, the rate is higher and concentrations in the particle are more sharply stepped if the counterion initially in the ion exchanger is the faster of the two. Surprisingly, no such direct comparisons between forward and reverse exchange has been made before this asymmetry in behavior was predicted. Its experimental verification may thus be viewed as strong evidence for the basic soundness of the Nernst-Planck approach.*

Figure 27 presents the simulations of the Na^+ / Sr^{++} exchange within cation exchanger particle of radius 0.55 mm, compared with Helfferich^{6, 7} experiments. Two scenarios are considered: (i) initially the particle is loaded with Na^+ and is brought into contact with $SrCl_2$ in the surrounding bulk liquid phase, and (ii) initially the particle is loaded with Sr^{++} and is brought into contact with $NaCl$ in the

surrounding bulk liquid phase. Ionic mole fractions for the two scenarios are compared with experiments.

For the $\text{Na}^+(1)/\text{Sr}^{++}(2)$ exchange, the matrix $[D]$ is simply a scalar diffusivity D_{eff} , calculated from Equation (68), times the identity matrix.

For the simulations of transient forward/reverse exchange the following parameter values were used:

Ion diffusivities: (1 = Na^+ , 2 = Sr^{++})

$$D_1/r_c^2 = 0.006; \quad D_2/r_c^2 = 4 \times 10^{-4} \text{ s}^{-1}.$$

For the Scenario 1 we use the following set of conditions:

$$\frac{z_1 c_{1,0}}{c_{\text{fixed}}} = 1; \quad \frac{z_2 c_{2,0}}{c_{\text{fixed}}} = 0; \quad \frac{z_1 c_{1,r=rc}}{c_{\text{fixed}}} = 0; \quad \frac{z_2 c_{2,r=rc}}{c_{\text{fixed}}} = 1; \quad \text{particle initially loaded with } \text{Na}^+$$

For the Scenario 2 we use the following set of conditions:

$$\frac{z_1 c_{1,0}}{c_{\text{fixed}}} = 0; \quad \frac{z_2 c_{2,0}}{c_{\text{fixed}}} = 1; \quad \frac{z_1 c_{1,r=rc}}{c_{\text{fixed}}} = 1; \quad \frac{z_2 c_{2,r=rc}}{c_{\text{fixed}}} = 0; \quad \text{particle initially loaded with } \text{Sr}^{++}$$

For both scenarios, the values of the ionic equivalent fractions $\frac{z_i c_{i,r=rc}}{c_{\text{fixed}}}$ correspond to those *at the*

surface, within the particle and therefore take implicit account of the ion exchange equilibrium.

The simulations are in reasonable agreement with the corresponding Helfferich^{6, 7} experiments. The physical reasoning is analogous to that for $\text{H}^+(1)/\text{Na}^+(2)$ exchange. In this case, Na^+ has the higher mobility. When the IEX particle is initially loaded with Na^+ (Scenario 1), the efflux of Na^+ occurs rapidly and vacant sites are created for occupation by the tardier Sr^{++} ions. However, when the IEX particle is initially loaded with Sr^{++} (scenario 2) the influx of Na^+ is only feasible when the tardier Sr^{++} ions vacate the IEX particle. Consequently, Scenario 2 occurs much slower as compared to scenario 1.

The experimental data of Varshney and Pandith²⁷ for forward/reverse exchanges of (a) H^+/Li^+ , (b) $\text{H}^+/\text{Ca}^{++}$, (c) $\text{H}^+/\text{Mg}^{++}$ and (d) $\text{H}^+/\text{Sr}^{++}$ in zirconium (IV) aluminophosphate IEX at 298 K are shown in Figure 28. In conformity with the Helfferich experiments, the equilibration is faster when the IEX is initially loaded with the more mobile H^+ . The continuous solid lines in Figure 28 are the Nernst-Planck model calculations using ion diffusivities:

$$\begin{aligned} D_{H^+}/r_c^2 &= 9 \times 10^{-4}; \quad D_{Li^+}/r_c^2 = 1.7 \times 10^{-4}; \\ D_{Ca^{++}}/r_c^2 &= 3 \times 10^{-4}; \quad D_{Mg^{++}}/r_c^2 = 2 \times 10^{-4}; \quad D_{Sr^{++}}/r_c^2 = 4 \times 10^{-4} \text{ s}^{-1}. \end{aligned}$$

For Na^+ / Cs^+ exchange within cation exchanger DOWEX 50X8 particle of radius 0.44 mm, the experiments of Graham and Dranoff^{28, 29} experiments show that the forward and reverse exchanges are practically indistinguishable from each other; see Figure 29. For rationalization of the results, the Maxwell-Stefan diffusivities of Na^+ , and Cs^+ within the particle were determined to be $\approx 2 \times 10^{-10} \text{ m}^2 \text{s}^{-1}$.^{28, 29}

13. Transient overshoots and asymmetry for uptake of ternary cations in cation exchange particles

We shall demonstrate the possibility of overshoots in ionic concentration during transient uptake of ternary counter-ions within cation exchanger particles.

The intra-particle diffusion is described by the 2×2 dimensional square matrix $[D]$ with elements given by equation (78). The transient uptake of the three cations is described by a two-dimensional matrix equation (88) for the fractional departure from equilibrium; the matrix $[Q]$ quantifies the departure from equilibrium. The Sylvester theorem, detailed in Appendix A of Taylor and Krishna,¹⁵ is required for explicit calculation of the elements of $[Q]$. Using time discretization, typically over a few thousand steps, the equation (88) can be written as $(\bar{X}(t_j)) = [Q_{j-1}] (X_0 - X_{r=rc}) + X_{r=rc}$ where $[Q_{j-1}]$ is evaluated using the equivalent fractions at the time step t_{j-1} : $(\bar{X}(t_{j-1}))$ that are known from the previous time step.

We first investigate the uptake of $\text{Na}^+(1)/\text{Cs}^+(2)/\text{Zn}^{2+}(3)$ in IEX particle. The ion exchanger particle is DOWEX 50 (of radius $r_c = 0.4$ mm) with fixed HSO_3^- charges. The cation exchange particle prevents the influx of anions from the bulk electrolyte surrounding the particle. The zero-flux constraint of Equation (37) applies to anions.

Two scenarios are simulated.

- (a) Initially the particle is loaded with Na^+ and is replaced by $\text{Cs}^+/\text{Zn}^{2+}$

$$\frac{z_1 c_{1,0}}{c_{fixed}} = 1; \quad \frac{z_2 c_{2,0}}{c_{fixed}} = 0; \quad \frac{z_3 c_{3,0}}{c_{fixed}} = 0; \quad \text{particle initially loaded with Na}^+$$

The surface of the particle in contact with bulk electrolytes such that the surface ion fractions are maintained at

$$\frac{z_1 c_{1,r=rc}}{c_{fixed}} = 0; \quad \frac{z_2 c_{2,r=rc}}{c_{fixed}} = 0.5; \quad \frac{z_3 c_{3,r=rc}}{c_{fixed}} = 0.5$$

(b) Initially the particle is loaded with $\text{Cs}^+/\text{Zn}^{2+}$ and is replaced by Na^+

$$\frac{z_1 c_{1,0}}{c_{fixed}} = 0; \quad \frac{z_2 c_{2,0}}{c_{fixed}} = 0.5; \quad \frac{z_3 c_{3,0}}{c_{fixed}} = 0.5; \quad ; \quad \text{particle initially loaded with } \text{Cs}^+/\text{Zn}^{2+}$$

The surface of the particle in contact with bulk electrolytes such that the surface ion fractions are maintained at

$$\frac{z_1 c_{1,r=rc}}{c_{fixed}} = 1; \quad \frac{z_2 c_{2,r=rc}}{c_{fixed}} = 0; \quad \frac{z_3 c_{3,r=rc}}{c_{fixed}} = 0$$

The intra-particle ion diffusivities: ($1 = \text{Na}^+$, $2 = \text{Cs}^+$, $3 = \text{Zn}^{2+}$) are taken from Boyd and Soldano³⁰

$D_1 = 9.44 \times 10^{-11}$; $D_2 = 17.7 \times 10^{-11}$; $D_3 = 6.3 \times 10^{-12} \text{ m}^2 \text{ s}^{-1}$. The ion diffusivity of Zn^{2+} is about an order of magnitude lower than that of Na^+ , and Cs^+ .

The simulation results are shown in Figure 30a for scenario (a), and Figure 30b for scenario (b). Figure 30c compares the electrostatic potential differences during the transient uptake in the two scenarios

$$\Delta\Phi = \frac{-z_1(D_1 - D_3)(x_1 - x_{1,0}) - z_2(D_2 - D_3)(x_2 - x_{2,0})}{\frac{F}{RT} \sum_{k=1}^3 x_k z_k^2 D_k} \quad (89)$$

A visual inspection of the two scenarios shows that the equilibration in scenario (a) proceeds faster than the equilibration in scenario (b). The rationalization of this can be found in the transient potential differences for the two scenarios (cf. Figure 30c). For scenario (a), $\Delta\Phi < 0$ during the transience and this accelerates the influx of Cs^+ , and Zn^{2+} . The accelerated influx of Cs^+ ion is of such a magnitude as

to cause an overshoot in the ionic equivalent fraction $\frac{z_i c_i}{c_{fixed}}$ of Cs^+ . For scenario (b), $\Delta\Phi > 0$ during the transience and this decelerates the influx of Na^+ . Consequently, the equilibration in scenario (b) is slower as compared to scenario (a).

Figure 30d compares the equilibration trajectories followed in the forward/reverse ion exchanges. We note that completely difference equilibration trajectories are followed in the two scenarios, i.e. the forward/reverse ion exchanges are asymmetric.

We now examine the possibility of overshoots in ionic concentration during transient uptake of ternary $\text{Na}^+(1)/\text{Cs}^+(2)/\text{La}^{3+}(3)$ cations within DOWEX 50 (of radius $r_c = 0.4$ mm) with fixed HSO_3^- charges. Two scenarios are simulated.

(a) Initially the particle is loaded with Na^+ and is replaced by $\text{Cs}^+/\text{La}^{3+}$

$$\frac{z_1 c_{1,0}}{c_{fixed}} = 1; \quad \frac{z_2 c_{2,0}}{c_{fixed}} = 0; \quad \frac{z_3 c_{3,0}}{c_{fixed}} = 0; \quad \text{particle initially loaded with } \text{Na}^+$$

The surface of the particle in contact with bulk electrolytes such that the surface ion fractions are maintained at

$$\frac{z_1 c_{1,r=rc}}{c_{fixed}} = 0; \quad \frac{z_2 c_{2,r=rc}}{c_{fixed}} = 0.5; \quad \frac{z_3 c_{3,r=rc}}{c_{fixed}} = 0.5$$

(b) Initially the particle is loaded with $\text{Cs}^+/\text{La}^{3+}$ and is replaced by Na^+

$$\frac{z_1 c_{1,0}}{c_{fixed}} = 0; \quad \frac{z_2 c_{2,0}}{c_{fixed}} = 0.5; \quad \frac{z_3 c_{3,0}}{c_{fixed}} = 0.5; \quad ; \quad \text{particle initially loaded with } \text{Cs}^+/\text{La}^{3+}$$

The surface of the particle in contact with bulk electrolytes such that the surface ion fractions are maintained at

$$\frac{z_1 c_{1,r=rc}}{c_{fixed}} = 1; \quad \frac{z_2 c_{2,r=rc}}{c_{fixed}} = 0; \quad \frac{z_3 c_{3,r=rc}}{c_{fixed}} = 0$$

The intra-particle ion diffusivities: (1 = Na^+ , 2 = Cs^+ , 3 = La^{3+}) are taken from Boyd and Soldano³⁰ $D_1 = 9.44 \times 10^{-11}$; $D_2 = 17.7 \times 10^{-11}$; $D_3 = 9.2 \times 10^{-13} \text{ m}^2 \text{ s}^{-1}$. The ion diffusivity of La^{3+} is about two orders of magnitude lower than that of Na^+ , and Cs^+ .

The simulation results are shown in Figure 31a for scenario (a), and Figure 31b for scenario (b). Figure 31c compares the electrostatic potential differences during the transient uptake in the two scenarios

A visual inspection of the two scenarios shows that the equilibration in scenario (a) proceeds faster than the equilibration in scenario (b). The rationalization of this can be found in the transient potential differences for the two scenarios (cf. Figure 31c). For scenario (a), $\Delta\Phi < 0$ during the transience and this accelerates the influx of Cs^+ , and La^{3+} . The accelerated influx of Cs^+ ion is of such a magnitude as to cause an overshoot in the ionic equivalent fraction $\frac{z_i c_i}{c_{fixed}}$ of Cs^+ . For scenario (b), $\Delta\Phi > 0$ during the transience and this decelerates the influx of Na^+ . Consequently, the equilibration in scenario (b) is slower as compared to scenario (a).

Figure 31d compares the equilibration trajectories followed in the forward/reverse ion exchanges. We note that completely difference equilibration trajectories are followed in the two scenarios, i.e. the forward/reverse ion exchanges are asymmetric.

14. Simulation of the transient overshoots in Yoshida-Kataoka experiments

The experimental data of Yoshida and Kataoka²⁴ for transient uptake of H^+ , Na^+ , and Zn^{++} within DOWEX 50WX8, DIAION SK116, and DOWEX 50WX10 cation exchangers provide experimental confirmation of intra-particle overshoots and asymmetries in the forward/reverse ion exchanges.

They present a set of 7 experimental data sets as specified in Table 1.

We simulated each of the seven experimental data sets by using the matrix equation (87) to quantify the transient uptake of H^+ , Na^+ , and Zn^{++} .

The input data for the ionic diffusivities inside the pores of the ion exchanger are taken from Table III of Yoshida and Kataoka.²⁴ The data are provided below.

DOWEX 50WX8: $D_1 = 2.42 \times 10^{-9}$; $D_2 = 1.61 \times 10^{-10}$; $D_3 = 1.8 \times 10^{-11} \text{ m}^2 \text{ s}^{-1}$.

DIAION SK116: $D_1 = 7.51 \times 10^{-10}$; $D_2 = 4.17 \times 10^{-11}$; $D_3 = 1.72 \times 10^{-12} \text{ m}^2 \text{ s}^{-1}$.

$$\text{DOWEX 50WX10: } D_1 = 1.65 \times 10^{-9}; \quad D_2 = 1.1 \times 10^{-10}; \quad D_3 = 9.62 \times 10^{-12} \text{ m}^2 \text{ s}^{-1}.$$

In our simulations we used a particle radius $r_c = 0.4$ mm, an average value of the sizes reported in Table II of Yoshida and Kataoka.²⁴

Figure 32 shows the simulations of the transient exchange of $\text{H}^+/\text{Na}^+/\text{Zn}^{++}$ within DOWEX 50WX8 cation exchanger particle. Two scenarios are simulated. Figure 32a shows the results of the simulations when the particle is loaded with H^+ and is replaced $\text{Na}^+/\text{Zn}^{++}$. Also shown in Figure 32a are the experimental data from Figure 3 of Yoshida and Kataoka²⁴ for this scenario. There is good agreement between the experimental data and the simulated uptakes. The overshoot in the uptake of Na^+ is properly captured by the simulations. Figure 32b shows the simulations for the scenario in which the particle is loaded with $\text{Na}^+/\text{Zn}^{++}$ and is replaced H^+ . No overshoots or undershoots are experienced in this scenario. Figure 32c compares the diffusion equilibration trajectories in composition space. The two scenarios follow completely different paths in composition space.

Figure 33 shows the simulations of the transient exchange of $\text{H}^+/\text{Na}^+/\text{Zn}^{++}$ within DIAION SK116 cation exchanger particle. Two scenarios are simulated. Figure 33a shows the results of the simulation when the particle is loaded with H^+ and is replaced $\text{Na}^+/\text{Zn}^{++}$. Also shown in Figure 33a are the experimental data from Figure 5 of Yoshida and Kataoka²⁴ for this scenario. There is reasonable agreement between the experimental data and the simulated uptakes. The overshoot in the uptake of Na^+ is properly captured by the simulations. Figure 33b shows the simulations for the scenario in which the particle is loaded with $\text{Na}^+/\text{Zn}^{++}$ and is replaced H^+ . No overshoots or undershoots are experienced in this scenario. Figure 33c compares the diffusion equilibration trajectories in composition space. The two scenarios follow completely different paths in composition space.

Figure 34 shows the simulations of the transient exchange of $\text{H}^+/\text{Na}^+/\text{Zn}^{++}$ within DOWEX 50WX10 cation exchanger particle. Two scenarios are simulated. Figure 35a shows the results of the simulation when the particle is loaded with Zn^{++} and is replaced H^+/Na^+ . Also shown in Figure 34a are the experimental data from Figure 7 of Yoshida and Kataoka²⁴ for this scenario. There is reasonably agreement between the experimental data and the simulated uptakes. Figure 34b shows the simulations

for the scenario in which the particle is loaded with H^+/Na^+ and is replaced Zn^{++} . No overshoots or undershoots are experienced in this scenario. Interestingly, Na^+ exhibits an overshoot during the desorption phase, but no experimental data is available to test the anticipations of the simulations. Figure 34c compares the diffusion equilibration trajectories in composition space. The two scenarios follow completely different paths in composition space.

Figure 35 shows the simulations of the transient exchange of $\text{H}^+/\text{Na}^+/\text{Zn}^{++}$ within DOWEX 50WX10 cation exchanger particle. Two scenarios are simulated. Figure 35a shows the results of the simulation when the particle is loaded with Na^+ and is replaced $\text{H}^+/\text{Zn}^{++}$. Also shown in Figure 35a are the experimental data from Figure 6 of Yoshida and Kataoka²⁴ for this scenario. There is good agreement between the experimental data and the simulated uptakes. The overshoot in the uptake of H^+ is properly captured by the simulations. Figure 35b shows the simulations for the scenario in which the particle is loaded with $\text{H}^+/\text{Zn}^{++}$ and is replaced Na^+ . No overshoots or undershoots are experienced in this scenario. Also shown in Figure 35b are the experimental data in Figure 9 of Yoshida and Kataoka²⁴ for this scenario; there is good agreement between simulations and experiment. Figure 35c compares the diffusion equilibration trajectories in composition space. The two scenarios follow completely different paths in composition space.

Figure 36 shows the simulations of the transient exchange of $\text{H}^+/\text{Na}^+/\text{Zn}^{++}$ within DOWEX 50WX10 cation exchanger particle. Two scenarios are simulated. Figure 36a shows the results of the simulations when the particle is loaded with H^+ and is replaced $\text{Na}^+/\text{Zn}^{++}$. Also shown in Figure 36a are the experimental data from Figure 4 of Yoshida and Kataoka²⁴ for this scenario. There is good agreement between the experimental data and the simulated uptakes. The overshoot in the uptake of Na^+ is properly captured by the simulations. Figure 36b shows the simulations for the scenario in which the particle is loaded with $\text{Na}^+/\text{Zn}^{++}$ and is replaced H^+ . No overshoots or undershoots are experienced in this scenario. Also shown in Figure 36b are the experimental data in Figure 8 of Yoshida and Kataoka²⁴ for this scenario; there is good agreement between simulations and experiment. Figure 36c compares

the diffusion equilibration trajectories in composition space. The two scenarios follow completely different paths in composition space.

Figure 37 presents a comparison of uptakes of H^+ and Na^+ in the experiments as shown, respectively, in Figure 35a, and Figure 36a. We note that the uptake of Na^+ occurs faster than the uptake of H^+ . The rationalization of these observations is precisely the same as that presented earlier in the discussions on the Helfferich experiments in Figure 24a.

Let us analyze in more detail the overshoot in the uptake of Na^+ as witnessed in Figure 36a.

The radial distribution of equivalent fractions can be calculated from

$$(X(r,t) - X_{r=rc}) = [Q_{r,t}] (X_0 - X_{r=rc}); \quad [Q_{r,t}] \equiv \frac{2r_c}{\pi r} \sum_{m=1}^{\infty} \frac{(-1)^{m+1}}{m} \sin\left(\frac{m\pi r}{r_c}\right) \exp\left[-m^2\pi^2 \frac{[D]t}{r_c^2}\right] \quad (90)$$

Figures 38a,b,c shows the radial equivalent fraction profiles $\frac{z_i c_i}{c_{fixed}}$ for transient uptake of (a) H^+ , (b) Na^+ , and (c) Zn^{++} at times $t = 10$ s, 30 s, 40 s, and 500 s from the start of the uptake process. We note that Na^+ also experiences overshoots in the radial coordinate direction, that is a clear indication of uphill diffusion.

At any time t , equation (90) may be differentiated to give the gradients of the concentrations

$$\left(\frac{\partial X(r,t)}{\partial r}\right) = \frac{\partial [Q_{r,t}]}{\partial r} (X_0 - X_{r=rc}); \quad \frac{\partial [Q_{r,t}]}{\partial r} \equiv \sum_{m=1}^{\infty} \frac{(-1)^{m+1}}{m} \exp\left[-m^2\pi^2 \frac{[D]t}{r_c^2}\right] \frac{\partial}{\partial r} \left(\frac{2r_c}{\pi r} \sin\left(\frac{m\pi r}{r_c}\right) \right) \quad (91)$$

Equation (70) in combination with equation(91) allows the determination of the radial distribution of the electrostatic potential gradient. Figure 38d shows the radial profile for $\frac{F}{RT} \frac{\partial \Phi}{\partial(r/r_c)}$ at times $t = 10$ s, 30 s, 40 s, and 500 s from the start of the uptake process. The steep electrostatic potential gradients at the initial stages of the transient uptake are caused by the rapid efflux of the mobile H^+ . The steep gradients $\frac{F}{RT} \frac{\partial \Phi}{\partial(r/r_c)} = \frac{F}{RT} \frac{\partial \Phi}{\partial \eta}$ to enhance the influx of Na^+ ; this enhancement causes supra-equilibrium loadings to be achieved during the initial stages of the transient uptake. Figure 38e compares the ionic mole

concentration gradients $\frac{1}{c_{fixed}} \frac{\partial(z_i c_i)}{\partial(r/r_c)} = \frac{1}{c_{fixed}} \frac{\partial(z_i c_i)}{\partial\eta} = \frac{\partial(X_i)}{\partial\eta}$ for H^+ , Na^+ , and Zn^{++} with $\frac{F}{RT} \frac{\partial\Phi}{\partial\eta}$ at time $t = 30$ s from the start of the uptake process. Close to the surface of the particle, for $0.0 < \eta = r/r_c < 1$, we note that for Na^+ , the contribution of $\frac{F}{RT} \frac{\partial\Phi}{\partial\eta}$ is larger in magnitude and opposite in sign to the contribution of $\frac{1}{c_{fixed}} \frac{\partial(z_i c_i)}{\partial(r/r_c)} = \frac{1}{c_{fixed}} \frac{\partial(z_i c_i)}{\partial\eta} = \frac{\partial(X_i)}{\partial\eta}$. This is the root cause of the uphill diffusion experienced by Na^+ .

15. A simplified transient model for the Kraaijeveld-Wesselingh experiments

We now set up a simple model to describe the batch Kraaijeveld experiments for $H^+(1)/Na^+(2)$ between Lewatit S100 IEX particles of diameter 1 mm and the bulk electrolyte HCl/NaCl mixture; see Figure 15a. The data inputs are from Kraaijeveld and Wesselingh.²¹

Specifically, we simulate the experiments of Kraaijeveld and Wesselingh²¹ in which the bulk electrolyte concentration is 0.01 mol L⁻¹.

The nomenclature used in setting up the model equations are provided below

The volume of IEX resin particles = V_r ; units L

Fixed charge per L of IEX resin particle = c_{fixed} ; units equivalent L⁻¹

The volume of bulk electrolyte solution = V_L ; units L

Molar concentration of bulk electrolyte = c_L ; units mol L⁻¹; $c_L = 0.01$ mol L⁻¹

Equivalent fraction of component $H^+(1)$ in IEX resin X_r

Equivalent fraction of component $H^+(1)$ in bulk electrolyte X

In the Kraaijeveld experiments, the diffusion resistance dominated by transfer to/from the IEX particle to the bulk electrolyte.

The effective “film” thickness is δ ; units m

At any instant of time, the differential mass balance relation

$$V_r c_{fixed} \frac{dX_r}{dt} = -V_L c_L \frac{dX}{dt} \quad (92)$$

Equation (92) can be integrated between the initial state at $t = 0$, and the state at $t = t$.

$$\begin{aligned} X_r &= X_{r0} + \frac{c_L V_L}{c_{fixed} V_r} (X_0 - X); \\ X_r &= \left[X_{r0} + \frac{c_L V_L}{c_{fixed} V_r} X_0 \right] - \left[\frac{c_L V_L}{c_{fixed} V_R} \right] X; \quad X_r = A - BX \end{aligned} \quad (93)$$

Equation (93) relates the equivalent fraction of $H^+(1)$ in the resin to the equivalent fraction in the bulk electrolyte X .

The equivalent fraction at the interface between the IEX resin and the bulk electrolyte can be determined from the resin/electrolyte phase equilibrium. The equilibrium for $H^+(1)/Na^+(2)$ exchange between the resin and the bulk electrolyte is described in the manner explained by Wesselingh and Krishna:⁸

$$X_{interface} = \frac{X_r}{K_{eq1} + (1 - K_{eq1})X_r}; \quad K_{eq1} = \frac{1}{K_{eq2}} \quad (94)$$

The resin particle favor $Na^+(2)$. For a bulk electrolyte of concentration 0.01 mol L^{-1} in the simulated experiments, the value of

$$K_{eq2} = 1.38; \quad K_{eq1} = \frac{1}{K_{eq2}} \quad (95)$$

Combining equation (93) and (94) we obtain

$$X_{interface} = \frac{(A - BX)}{K_{eq1} + (1 - K_{eq1})(A - BX)} \quad (96)$$

Assuming quasi-steady state, the transfer flux of $H^+(1)$ can be calculated from the Turner-Snowden equation (54) where the interface composition at any time t is determined from equation (96) and the bulk composition at time t is X .

$$N_1 = \frac{D_1}{\delta} \frac{2c_L}{\left(1 + \left(\frac{D_1}{D_2} - 1\right)X_{10}\right) + \sqrt{\left(1 + \left(\frac{D_1}{D_2} - 1\right)X_{\text{interface}}\right)\left(1 + \left(\frac{D_1}{D_2} - 1\right)X\right)}} (X_{\text{interface}} - X) \quad (97)$$

The differential material balance is

$$\begin{aligned} V_L c_L \frac{dX}{dt} &= N_1 Area \\ &= \frac{D_1 Area}{\delta} \frac{2c_L}{\left(1 + \left(\frac{D_1}{D_2} - 1\right)X_{10}\right) + \sqrt{\left(1 + \left(\frac{D_1}{D_2} - 1\right)X_{\text{interface}}\right)\left(1 + \left(\frac{D_1}{D_2} - 1\right)X\right)}} (X_{\text{interface}} - X) \end{aligned} \quad (98)$$

where *Area* is the interfacial area between the suspended particles and the liquid. Let us define a cell constant β as

$$\beta = \frac{Area}{V_L \delta} \quad (99)$$

The value $\beta = 4000 \text{ m}^{-2}$ was chosen in the simulations.

The differential material balance takes the form

$$\frac{dX}{dt} = \beta D_1 \frac{2}{\left(1 + \left(\frac{D_1}{D_2} - 1\right)X_{10}\right) + \sqrt{\left(1 + \left(\frac{D_1}{D_2} - 1\right)X_{\text{interface}}\right)\left(1 + \left(\frac{D_1}{D_2} - 1\right)X\right)}} (X_{\text{interface}} - X) \quad (100)$$

Equation (100) can be solved using the Runge-Kutta ODE routine that is available in MathCad 15; the printout of the program is appended herewith. The continuous solid lines in Figure 39a are the solutions for the forward/reverse $\text{H}^+(1)/\text{Na}^+(2)$ exchanges, obtained using the MathCad program. The agreement is qualitatively correct and captures the essential asymmetry as observed in the experiments. The equilibration trajectories for the forward/reverse $\text{H}^+(1)/\text{Na}^+(2)$ exchanges are also compared in Figure 39b; the asymmetry is evident.

16. Notation

A	transfer area, m^2
c_i	molar concentration, mol m^{-3}
$\bar{c}_i(t)$	spatial-averaged concentration of species i inside particle, mol m^{-3}
c_t	total molar concentration of mixture, mol m^{-3}
c_{fixed}	molar concentration of fixed charges in ion exchanger particle, equiv m^{-3}
d_p	pore diameter, m
D_i	ion diffusivity, $\text{m}^2 \text{s}^{-1}$
D_{ij}	ion-ion diffusivity, $\text{m}^2 \text{s}^{-1}$
$D_{i,\text{eff}}$	effective ion diffusivity, $\text{m}^2 \text{s}^{-1}$
$[D]$	matrix of diffusivities, $\text{m}^2 \text{s}^{-1}$
F	Faraday constant, $9.65 \times 10^4 \text{ C mol}^{-1}$
L	length of packed bed adsorber, m
m	number of counter-ions, dimensionless
M	excess amount injected in Taylor dispersion experiment, mol
n	number of species in the mixture, dimensionless
r	radial direction coordinate, m
r_c	radius of ion-exchanger particle m
R	gas constant, $8.314 \text{ J mol}^{-1} \text{ K}^{-1}$
R	radius of tube in Taylor dispersion studies, m
t	time, s
T	absolute temperature, K
u	cross-sectional averaged velocity in tube, m s^{-1}
u_i	ion velocity, m s^{-1}
V	compartment volume, m^3
x_i	mole fraction of species i , dimensionless
X_i	ionic equivalent fraction of species i inside IEX particle, dimensionless
z	distance coordinate, m

z_i charge on species i , dimensionless

Greek letters

β	cell constant, m^{-2}
δ	diffusion film or membrane thickness, m
δ_{ij}	Kronecker delta, dimensionless
Φ	electrostatic potential, V
μ_i	molar chemical potential of component i , J mol^{-1}
σ	rate of entropy production, $\text{J m}^{-3} \text{ s}^{-1} \text{ K}^{-1}$

Subscripts

i	referring to component i
t	referring to total mixture
1	referring to species 1
2	referring to species 2

Table 1. Experimental data of Yoshida and Kataoka²⁴ for transient uptake of H⁺, Na⁺, and Zn⁺⁺. The experimental data are scanned from the Figure numbers, as specified in the last column of this Table 1.

Ion Exchanger	Initial equivalent fractions:			Final equilibrated equivalent fractions			Data scanned For Y-K paper
	H ⁺	Na ⁺	Zn ⁺⁺	H ⁺	Na ⁺	Zn ⁺⁺	
50WX8	1	0	0	0	0.5	0.5	Fig 3
SK116	1	0	0	0	0.5	0.5	Fig 5
50WX10	1	0	0	0	0.5	0.5	Fig 4
50WX10	0	1	0	0.5	0	0.5	Fig 6
50WX10	0	0	1	0.7	0.3	0	Fig 7
50WX10	0	0.5	0.5	1	0	0	Fig 8
50WX10	0.5	0	0.5	0	1	0	Fig 9

17. References

- (1) PTC MathCad 15.0. <http://www.ptc.com/>, PTC Corporate Headquarters, Needham, 3 November 2015.
- (2) Krishna, R. Uphill Diffusion in Multicomponent Mixtures. *Chem. Soc. Rev.* **2015**, *44*, 2812-2836.
- (3) Krishna, R. Serpentine Diffusion Trajectories and the Ouzo Effect in Partially Miscible Ternary Liquid Mixtures. *Phys. Chem. Chem. Phys.* **2015**, *17*, 27428-27436.
- (4) Seader, J. D.; Henley, E. J.; Roper, D. K. *Separation Process Principles*; 3rd Edition, John Wiley: New York, 2011.
- (5) Newman, J. *Electrochemical Systems*; 2nd Edition, Prentice Hall, Inc.: Englewood Cliffs, NJ, USA, 1991.
- (6) Helfferich, F. G. Ion Exchange Kinetics. III. Experimental Test of the Theory of Particle-Diffusion Controlled Ion Exchange. *J. Phys. Chem.* **1962**, *66*, 39-42.
- (7) Helfferich, F. G. *Ion Exchange Kinetics - Evolution of a Theory*. Mass Transfer and Kinetics of Ion Exchange; Edited by L. Liberti and F.G. Helfferich, Martinus Nijhoff Publishers: The Hague, 1983.
- (8) Wesselingh, J. A.; Krishna, R. *Mass transfer in multicomponent mixtures*; VSSD: Delft, 2000.
- (9) Lightfoot, E. N. *Transport phenomena and living systems*; John Wiley: New York, 1974.
- (10) Standart, G. L.; Taylor, R.; Krishna, R. The Maxwell-Stefan formulation of irreversible thermodynamics for simultaneous heat and mass transfer. *Chem. Eng. Commun.* **1979**, *3*, 277-289.
- (11) Kraaijeveld, G.; Wesselingh, J. A. Negative Maxwell-Stefan Diffusion Coefficients. *Ind. Eng. Chem. Res.* **1993**, *32*, 738-742.
- (12) Chakraborty, B. Sign Crossover in All Maxwell–Stefan Diffusivities for Molten Salt LiF-BeF₂: A Molecular Dynamics Study. *J. Phys. Chem. B* **2015**, *119*, 10652-10663.
- (13) Umino, S.; Newman, J. Diffusion of sulfuric acid in concentrated solutions. *J. Electrochem. Soc.* **1993**, *140*, 2217-2221.
- (14) Vinograd, J. R.; McBain, J. W. Diffusion of Electrolytes and Ions in their Mixtures. *J. Am. Chem. Soc.* **1941**, *63*, 2008-2015.
- (15) Taylor, R.; Krishna, R. *Multicomponent mass transfer*; John Wiley: New York, 1993.
- (16) Price, W. F. Theory of the Taylor Dispersion Technique for Three-component-system Diffusion Measurements. *J. Chem. Soc.-Faraday Trans. 1* **1988**, *84*, 2431-2439.
- (17) Rutten, P. W. M. *Diffusion in Liquids*. Ph.D. Dissertation, Delft University of Technology, Delft, 1992.
- (18) Yang, Y.; Pintauro, P. N. Multicomponent Space-Charge Transport Model for Ion-Exchange Membranes. *A.I.Ch.E.J.* **2000**, *46*, 1177-1190.
- (19) Sodaye, S.; Agarwal, C.; Goswami, A. N. Study on multicomponent diffusion of ions in poly(perfluorosulfonated) ion-exchange membrane using radiotracers. *J. Membr. Sci.* **2006**, *314*, 221-225.
- (20) Schlögl, R.; Helfferich, F. Comment on the Significance of the Diffusion Potentials in Ion Exchange Kinetics. *J. Chem. Phys.* **1957**, *26*, 5-7.
- (21) Kraaijeveld, G.; Wesselingh, J. A. The Kinetics of Film-Diffusion-Limited Ion Exchange. *Chem. Eng. Sci.* **1993**, *48*, 467-473.
- (22) Smith, T. G.; Dranoff, J. S. Film Diffusion-Controlled Kinetics in Binary Ion Exchange. *Ind. Eng. Chem. Fundamentals* **1964**, *5*, 195-200.

- (23) Turner, J. C. R.; Snowdon, C. B. Liquid-side Mass-Transfer Coefficients in Ion Exchange: An Examination of the Nernst-Planck Model. *Chem. Eng. Sci.* **1968**, *23*, 221-230.
- (24) Yoshida, H.; Kataoka, T. Intraparticle Ion-Exchange Mass Transfer in Ternary System. *Ind. Eng. Chem. Res.* **1987**, *26*, 1179-1184.
- (25) Jones, I. L.; Carta, G. Ion Exchange of Amino Acids and Dipeptides on Cation Resins with Varying Degree of Cross-Linking. 2. Intraparticle Transport. *Ind. Eng. Chem. Res.* **1993**, *32*, 117-125.
- (26) Hwang, Y.-L.; Helfferich, F. G. Generalized Model for Multispecies Ion-Exchange Kinetics Including Fast Reversible Reactions. *Reactive Polymers* **1987**, *5*, 237-253.
- (27) Varshney, K. G.; Pandith, A. H. Forward and Reverse Ion-Exchange Kinetics for Some Alkali and Alkaline Earth Metal Ions on Amorphous Zirconium(IV) Aluminophosphate. *Langmuir* **1999**, *15*, 7422-7425.
- (28) Graham, E. E.; Dranoff, J. S. Application of the Stefan-Maxwell Equations to Diffusion in Ion Exchangers. 1. Theory. *Ind. Eng. Chem. Res.* **1982**, *21*, 360-365.
- (29) Graham, E. E.; Dranoff, J. S. Application of the Stefan-Maxwell Equations to Diffusion in Ion Exchangers. 2. Experimental Results. *Ind. Eng. Chem. Res.* **1982**, *21*, 365-369.
- (30) Boyd, G. E.; Soldano, B. A. Self-Diffusion of Cations in and through Sulfonated Polystyrene Cation-Exchange Polymers. *J. Am. Chem. Soc.* **2010**, *75*, 6091-6099.

18. Caption for Figures

Figure 1. Maxwell-Stefan cation-water and anion-water diffusivities for various electrolyte systems at 293 K. Data from Wesselingh and Krishna.⁸

Figure 2. Maxwell-Stefan diffusivities in aqueous sulphuric acid system. Data from Umino and Newman.¹³

Figure 3. Maxwell-Stefan diffusivities in aqueous NaCl system. Data from Wesselingh and Krishna.⁸

Figure 4. Maxwell-Stefan plus-minus diffusivities for various electrolyte systems. Data from Wesselingh and Krishna.⁸

Figure 5. Relative contributions of ion-ion friction and ion-water friction in aqueous solution of sulphuric acid. Calculations using data from Umino and Newman.¹³

Figure 6. Co-diffusion of H^+ , Ba^{++} , and Cl^- between two well-mixed compartments. Experimental data of Vinograd and McBain¹⁴ for ionic diffusivities of H^+ , Ba^{++} , and Cl^- in a two-compartment diffusion cell. The continuous solid lines are the calculations using equations (26), (27), and (28).

Figure 7. Co-diffusion of H^+ , K^+ , and Cl^- between two well-mixed compartments. Experimental data of Vinograd and McBain¹⁴ for ionic diffusivities of H^+ , K^+ , and Cl^- in a two-compartment diffusion cell. The continuous solid lines are the calculations using equations (26), (27), and (28).

Figure 8. (a) Transient co-diffusion of H^+ , Ba^{++} , and Cl^- between Left and Right compartments. A bulk electrolyte solution is brought into contact with liquid water at time $t = 0$. (b) Transient co-diffusion of H^+ , NO_3^- , Na^+ , and Cl^- between Left and Right compartments. A bulk HNO_3/NaCl electrolyte solution, each with concentrations of 0.1 mol L^{-1} , is brought into contact with NaCl solution, also of concentration 0.1 mol L^{-1} , at time $t = 0$.

Figure 9. Taylor dispersion in a tube for pulse injection of 10^{-7} mol of HCl and 10^{-7} mol of BaCl_2 . In (a) the electrostatic leash contribution is included. In (b) the electrostatic leash contribution is neglected.

Figure 10. Counter-diffusion of H^+ , Ba^{++} , and Cl^- between two well-mixed compartments. The continuous solid lines are the calculations using equations (26), (27), and (34).

Figure 11. Counter-diffusion of between two well-mixed compartments. The continuous solid lines are the calculations using equations (26), (27), and (34).

Figure 12. (a) Experimental data of Yang and Pintauro¹⁸ for the transient equilibration of H^+ , Na^+ , and Cs^+ in the salt and acid compartments that are separated by a Nafion cation exchange membrane. (b) Simulations using equations (26), (27), and (34).

Figure 13. (a, b) Equilibration trajectories followed by H^+ , Na^+ , and Cs^+ in the left and right compartments, plotted in composition space. In (a) the left compartment contains Na_2SO_4 and Cs_2SO_4 and the right compartment contains H_2SO_4 . In (b) the left compartment contains Na_2SO_4 and the right compartment contains H_2SO_4 and Cs_2SO_4 .

Figure 14. Schematic showing an ion exchanger particle with fixed HSO_3^- charges. The surrounding liquid phase consists of a mixture of electrolytes. The electrolytes are fully ionized and the bulk liquid phase contains anion, and two counter-ions along with unionized water molecules. The schematic is redrawn using the information contained in Wesselingh and Krishna⁸

Figure 15. Asymmetry in forward/reverse exchange in systems limited by diffusion from bulk liquid electrolyte to the surface of the particle. Experimental data of Kraaijeveld and Wesselingh²¹ for (a) H^+/Na^+ , and (b) $\text{H}^+/\text{Ca}^{++}$ exchanges

Figure 16. (a) The effective diffusivities of H^+ , and Na^+ in bulk electrolyte HCl/NaCl liquid mixture phase surrounding ion exchanger particle. (b) The effective diffusivities of H^+ , and Ca^{++} in bulk electrolyte HCl/CaCl_2 liquid mixture phase surrounding ion exchanger particle.

Figure 17. Typical concentration profiles for H^+/Na^+ exchanges. (a) Transfer of H^+ is from particle to the bulk electrolyte liquid. (b) Transfer of Na^+ is from particle to the bulk electrolyte liquid.

Figure 18. Forward and reverse H^+/Na^+ exchange from ion exchange resin to bulk electrolyte HCl/NaCl liquid. Diffusion resistance outside the resin particle.

Figure 19. Calculations of the effective diffusivities for forward and reverse H^+/Na^+ exchange in the two scenarios shown in Figure 18.

Figure 20. Forward and reverse H^+/Ca^{++} exchange from ion exchange resin to bulk electrolyte HCl/CaCl₂ liquid. Diffusion resistance outside the resin particle.

Figure 21. Calculations of the effective diffusivities for forward and reverse H^+/ Ca^{++} exchange in the two scenarios shown in Figure 20.

Figure 22. Concentration trajectories for forward and reverse (a) H^+/Na^+ , and (b) H^+/ Ca^{++} exchange from ion exchange resin to bulk electrolyte liquid. Diffusion resistance outside the resin particle.

Figure 23. (a) The effective diffusivity of H^+/Na^+ counter-ions within ion exchanger particle. (b) The effective diffusivity of Na^+/Sr^{++} counter-ions within ion exchanger particle. Note that the y-axes

represent the intra-particle diffusivities divided by the square of the particle radius. Also note that the x -axis represents the ion equivalent fraction of the more mobile component 1, defined as $\frac{z_1 c_1}{c_{fixed}}$.

Figure 24. Experimental data reported by Helfferich^{6,7} for phenolsulphonic acid cation exchangers. (a) H^+ / Na^+ exchange, and (b) Na^+ / Sr^{++} exchange. (c) Comparison of the data for H^+ / Na^+ exchange, with Na^+ / Sr^{++} exchange.

Figure 25. Comparison with the ternary ion uptake results of Hwang and Helfferich²⁶, as reported in their Figure 1 of their paper using an exact numerical procedure, with our solution methodology implemented in MathCad 15. The match between the two sets is perfect.

Figure 26. Simulations of the H^+/Na^+ exchange within cation exchanger particle, compared with Helfferich^{6,7} experiments. Two scenarios are considered: (i) initially the particle is loaded with H^+ and is brought into contact with NaCl in the surrounding bulk liquid phase, and (ii) initially the particle is loaded with Na^+ and is brought into contact with HCl in the surrounding bulk liquid phase. (a) Ionic equivalent fractions $\frac{z_i c_i}{c_{fixed}}$ for the two scenarios. (b) The fractional conversions for the two scenarios. (c) Effective diffusivities in the two scenarios. (d) The electrostatic potential difference in the two scenarios.

Figure 27. Simulations of the $\text{Na}^+/\text{Sr}^{++}$ exchange within cation exchanger particle, compared with Helfferich^{6, 7} experiments. Two scenarios are considered: (i) initially the particle is loaded with Na^+ and is brought into contact with SrCl_2 in the surrounding bulk liquid phase, and (ii) initially the particle is loaded with Sr^{++} and is brought into contact with NaCl in the surrounding bulk liquid phase. (a) Ionic equivalent fractions $\frac{z_i c_i}{c_{fixed}}$ for the two scenarios. (b) The fractional conversions for the two scenarios. (c) Effective diffusivities in the two scenarios.

Figure 28. Comparison of the experimental data of Varshney and Pandith²⁷ with Nernst-Planck model for forward/reverse exchanges of (a) H^+/Li^+ , (b) $\text{H}^+/\text{Ca}^{++}$, (c) $\text{H}^+/\text{Mg}^{++}$, and (d) $\text{H}^+/\text{Sr}^{++}$.

Figure 29. Simulations of the Na^+/Cs^+ exchange within cation exchanger DOWEX 50X8 particle of radius 0.44 mm, compared with Graham and Dranoff^{28, 29} experiments.

Figure 30. Simulation of the transient exchange of $\text{Na}^+/\text{Cs}^+/\text{Zn}^{2+}$ within DOWEX cation exchanger particle of radius 0.4 mm. Two scenarios are simulated. (a) Initially the particle is loaded with Na^+ and is replaced $\text{Cs}^+/\text{Zn}^{2+}$. (b) Initially the particle is loaded with $\text{Cs}^+/\text{Zn}^{2+}$ and is replaced Na^+ . (c) Comparison of the potential difference for the scenarios (a) and (b). (d) Plots of the ionic equivalent fractions $\frac{z_i c_i}{c_{fixed}}$ in ternary composition space for the two scenarios.

Figure 31. Simulation of the transient exchange of $\text{Na}^+/\text{Cs}^+/\text{La}^{3+}$ within DOWEX cation exchanger particle of radius 0.4 mm. Two scenarios are simulated. (a) Initially the particle is loaded with Na^+ and

is replaced $\text{Cs}^+/\text{La}^{3+}$. (b) Initially the particle is loaded with $\text{Cs}^+/\text{La}^{3+}$ and is replaced Na^+ . (c) Comparison of the potential difference for the scenarios (a) and (b). (d) Plots of the ionic equivalent fractions $\frac{z_i c_i}{c_{fixed}}$ in ternary composition space for the two scenarios.

Figure 32. Simulation of the transient exchange of $\text{H}^+/\text{Na}^+/\text{Zn}^{++}$ within DOWEX 50WX8 cation exchanger particle of radius 0.4 mm. Two scenarios are simulated. (a) Initially the particle is loaded with H^+ and is replaced $\text{Na}^+/\text{Zn}^{++}$. Also shown in (a) are the experimental data in Figure 3 of Yoshida and Kataoka²⁴ for this scenario. (b) Initially the particle is loaded with $\text{Na}^+/\text{Zn}^{++}$ and is replaced H^+ . (c)

Plots of the ionic equivalent fractions $\frac{z_i c_i}{c_{fixed}}$ in ternary composition space for the two scenarios.

Figure 33. Simulation of the transient exchange of $\text{H}^+/\text{Na}^+/\text{Zn}^{++}$ within DIAION SK116 cation exchanger particle of radius 0.4 mm. Two scenarios are simulated. (a) Initially the particle is loaded with H^+ and is replaced $\text{Na}^+/\text{Zn}^{++}$. Also shown in (a) are the experimental data in Figure 5 of Yoshida and Kataoka²⁴ for this scenario. (b) Initially the particle is loaded with $\text{Na}^+/\text{Zn}^{++}$ and is replaced H^+ . (c)

Plots of the ionic equivalent fractions $\frac{z_i c_i}{c_{fixed}}$ in ternary composition space for the two scenarios.

Figure 34. Simulation of the transient exchange of $\text{H}^+/\text{Na}^+/\text{Zn}^{++}$ within DOWEX 50WX10 cation exchanger particle of radius 0.4 mm. Two scenarios are simulated. (a) Initially the particle is loaded with Zn^{++} and is replaced H^+/Na^+ . Also shown in (a) are the experimental data in Figure 7 of Yoshida and Kataoka²⁴ for this scenario. (b) Initially the particle is loaded with H^+/Na^+ and is replaced Zn^{++} . (c)

Plots of the ionic equivalent fractions $\frac{z_i c_i}{c_{fixed}}$ in ternary composition space for the two scenarios.

Figure 35. Simulation of the transient exchange of $\text{H}^+/\text{Na}^+/\text{Zn}^{++}$ within DOWEX 50WX10 cation exchanger particle of radius 0.4 mm. Two scenarios are simulated. (a) Initially the particle is loaded with Na^+ and is replaced $\text{H}^+/\text{Zn}^{++}$. Also shown in (a) are the experimental data in Figure 6 of Yoshida and Kataoka²⁴ for this scenario. (b) Initially the particle is loaded with $\text{H}^+/\text{Zn}^{++}$ and is replaced Na^+ . Also shown in (b) are the experimental data in Figure 9 of Yoshida and Kataoka²⁴ for this scenario. (c)

Plots of the ionic equivalent fractions $\frac{z_i c_i}{c_{fixed}}$ in ternary composition space for the two scenarios.

Figure 36. Simulation of the transient exchange of $\text{H}^+/\text{Na}^+/\text{Zn}^{++}$ within DOWEX 50WX10 cation exchanger particle of radius 0.4 mm. Two scenarios are simulated. (a) Initially the particle is loaded with H^+ and is replaced $\text{Na}^+/\text{Zn}^{++}$. Also shown in (a) are the experimental data in Figure 4 of Yoshida and Kataoka²⁴ for this scenario. (b) Initially the particle is loaded with $\text{Na}^+/\text{Zn}^{++}$ and is replaced H^+ . Also shown in (b) are the experimental data in Figure 8 of Yoshida and Kataoka²⁴ for this scenario. (c)

Plots of the ionic equivalent fractions $\frac{z_i c_i}{c_{fixed}}$ in ternary composition space for the two scenarios.

Figure 37. Comparison of uptakes of H^+ and Na^+ in the experiments shown, respectively, in Figure 35a, and Figure 36a.

Figure 38. (a) Radial ion equivalent fraction profiles $\frac{z_i c_i}{c_{fixed}}$ for transient uptake of (a) H^+ , (b) Na^+ , and (c) Zn^{++} within DOWEX 50WX10 cation exchanger particles of radius 0.4 mm. The profiles are monitored at times $t = 10$ s, 30 s, 40 s, and 500 s from the start of the equilibration process. (d) Radial profile of the electrostatic potential gradient, monitored at times $t = 10$ s, 30 s, 40 s, and 500 s from the start of the equilibration process. (e) Comparison of the ionic mole fraction gradients with the electrostatic potential gradient. Note that the dimensionless radial coordinate is indicated as $\eta \equiv r/r_c$.

Figure 39. Asymmetry in forward/reverse exchange in systems limited by diffusion from bulk liquid electrolyte to the surface of the particle. (a) Experimental data of Kraaijeveld and Wesselingh²¹ for H^+/Na^+ exchanges compared with model simulations (indicated by the continuous solid lines). The MathCad program is appended herewith. (b) Comparison of the simulated equilibration trajectories for forward/reverse exchanges.

Figure S1

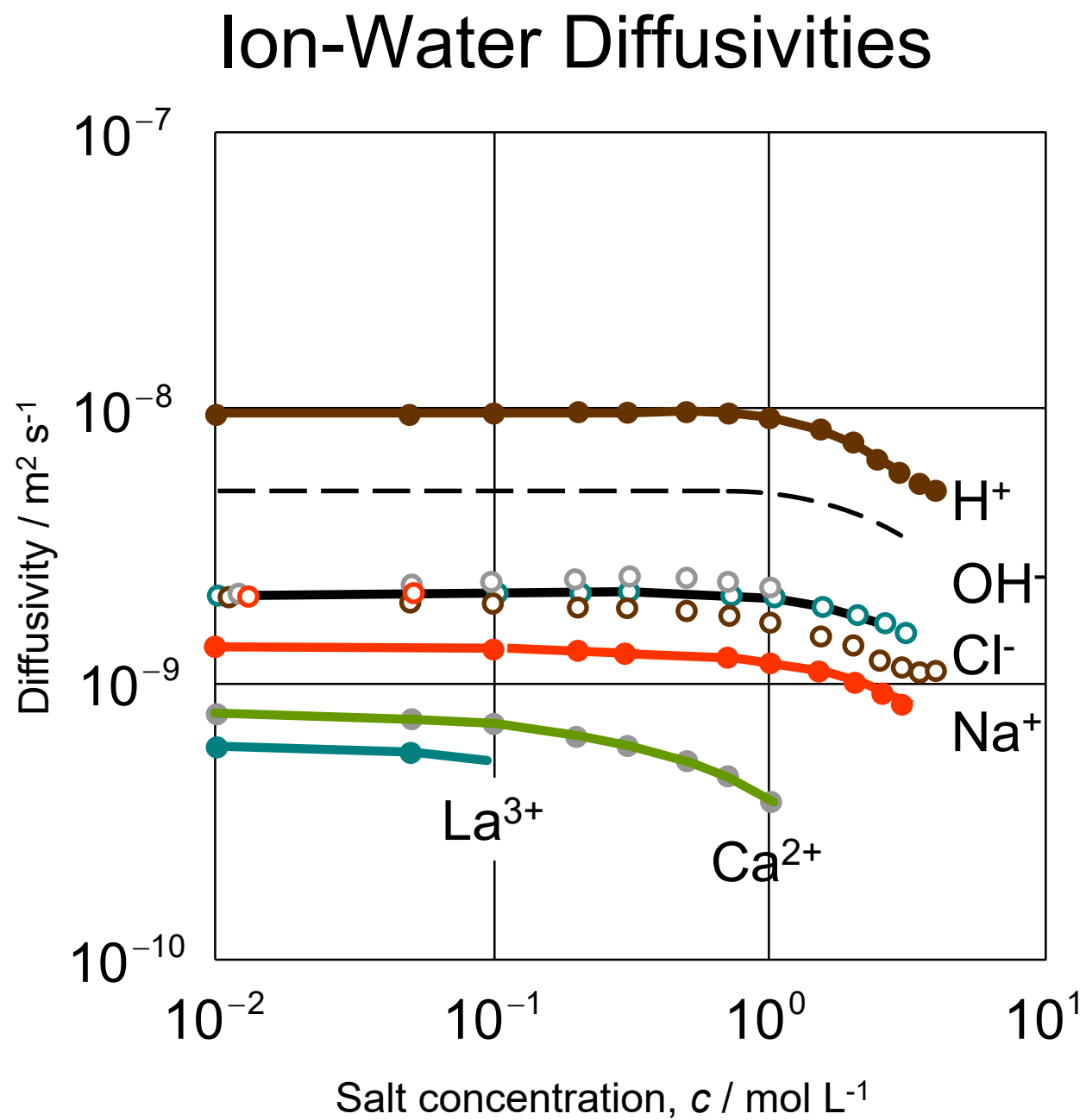


Figure S2

Diffusivities in aqueous H_2SO_4

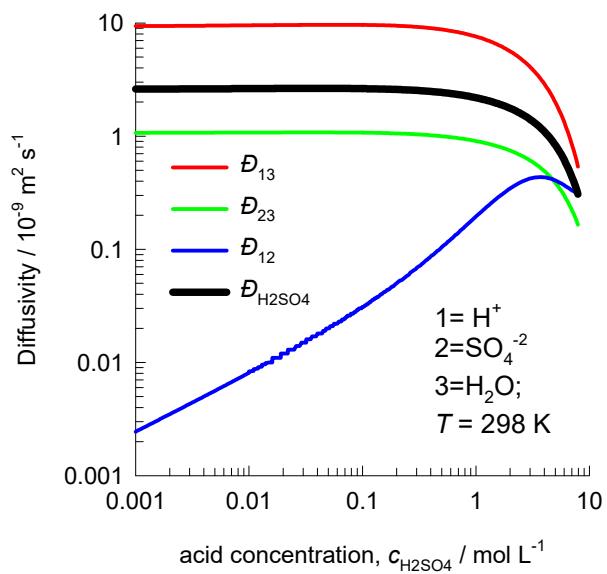


Figure S3

Diffusivities in aqueous NaCl

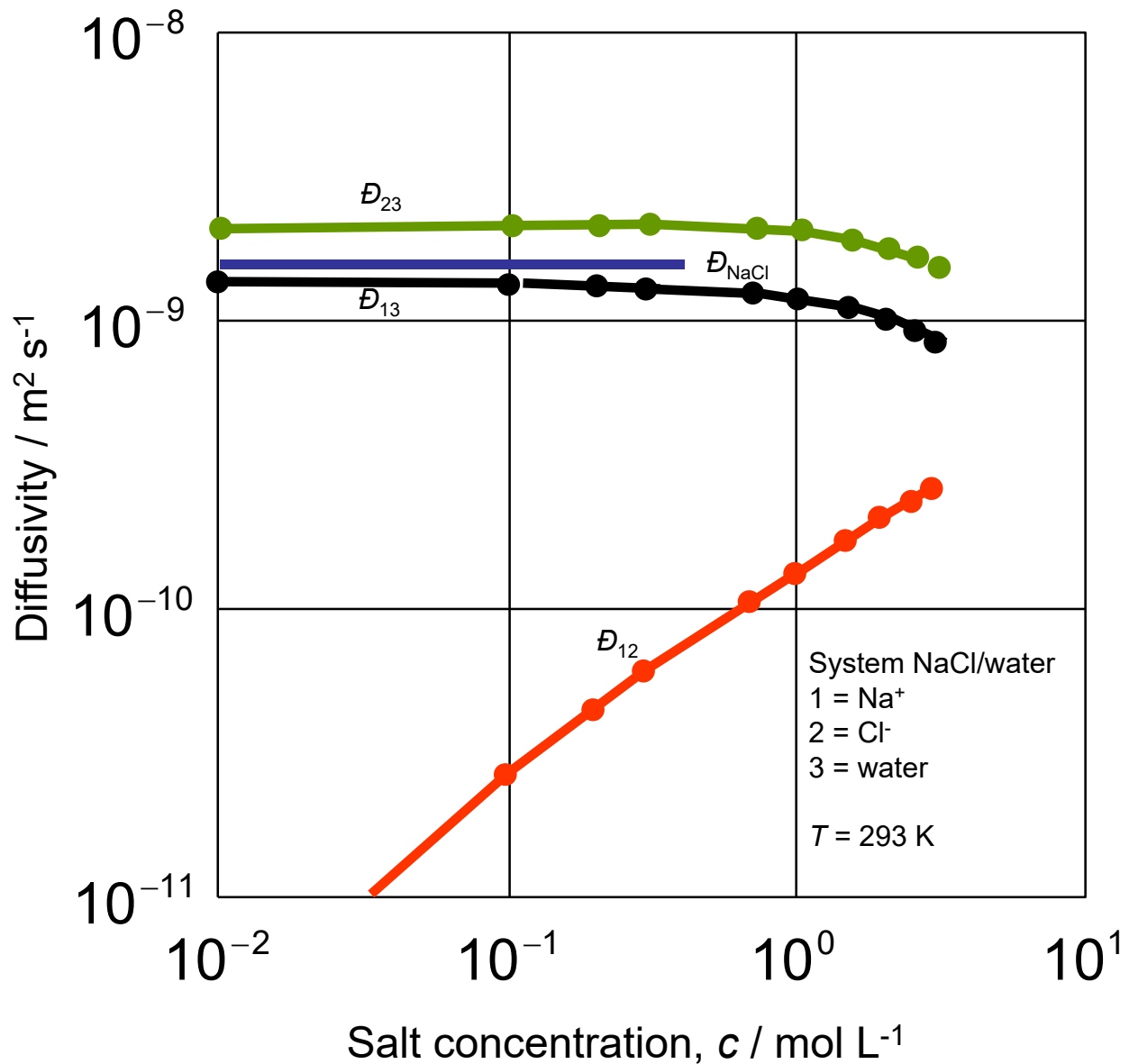


Figure S4

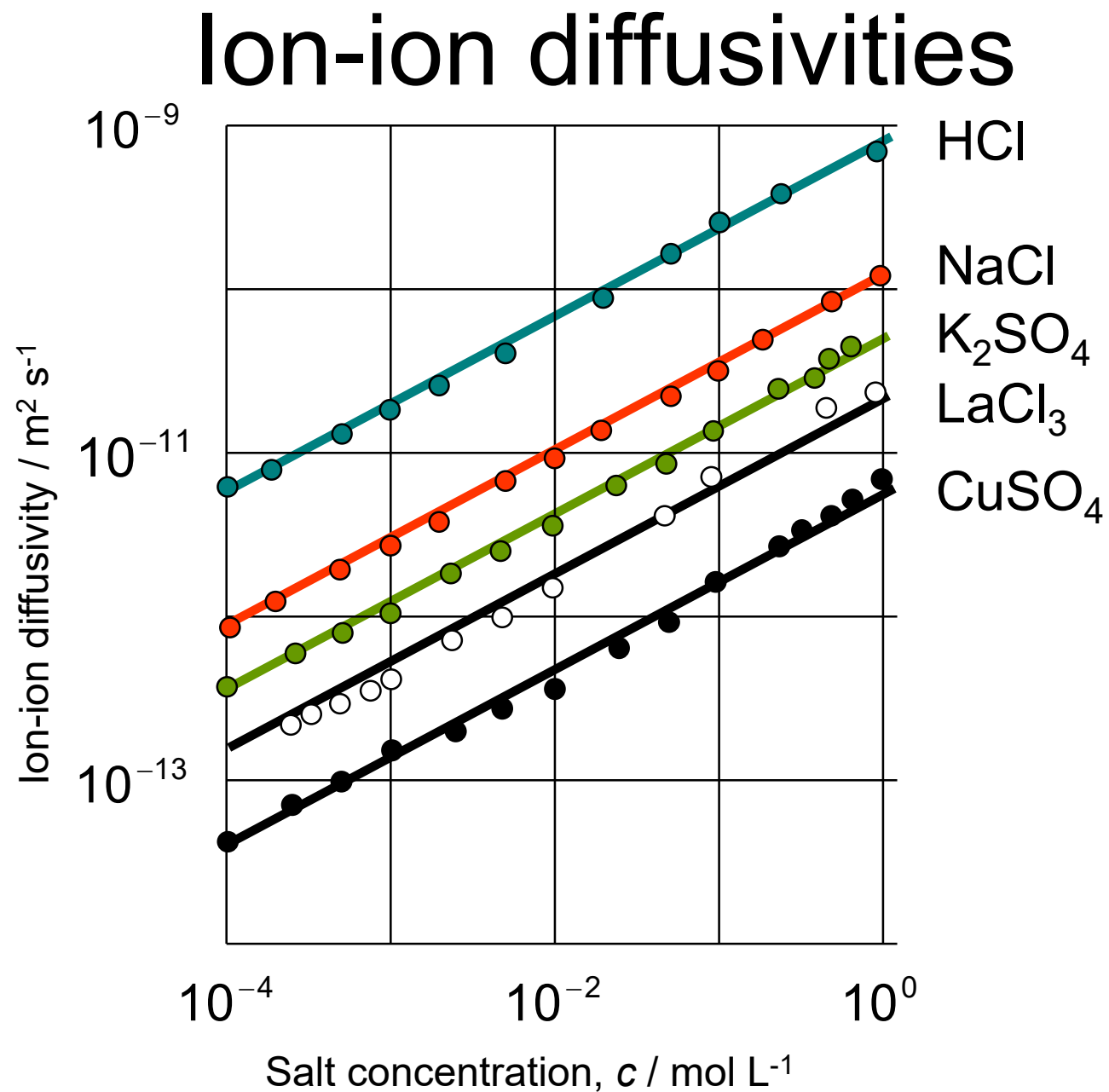


Figure S5

Relative importance of ion-ion and ion-water interactions

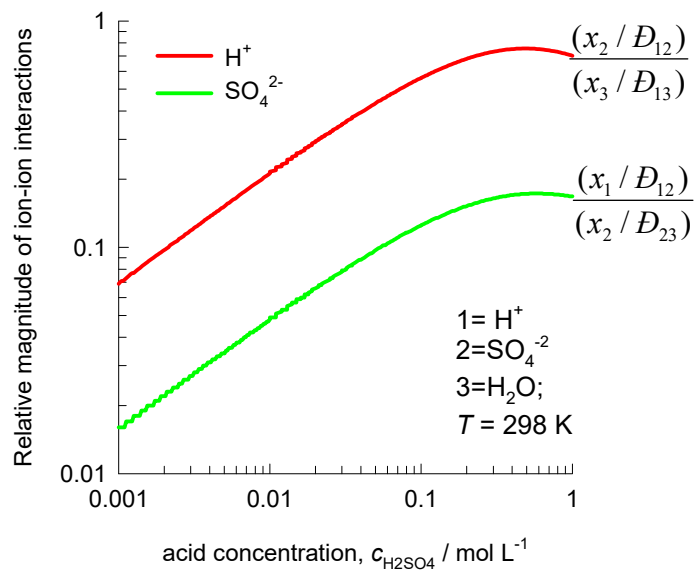
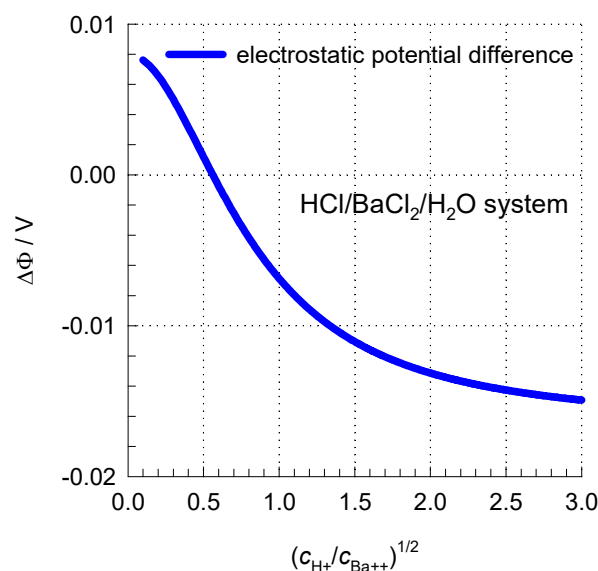
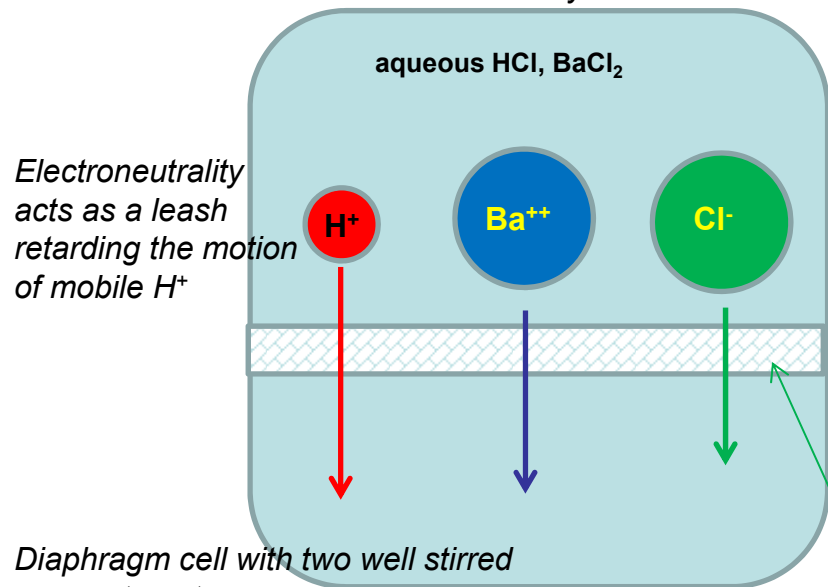


Figure S6

Co-diffusion of Mixed Ions

Electro-neutrality acts as a leash retarding the motion of tardy Ba⁺⁺



Note negative diffusivities

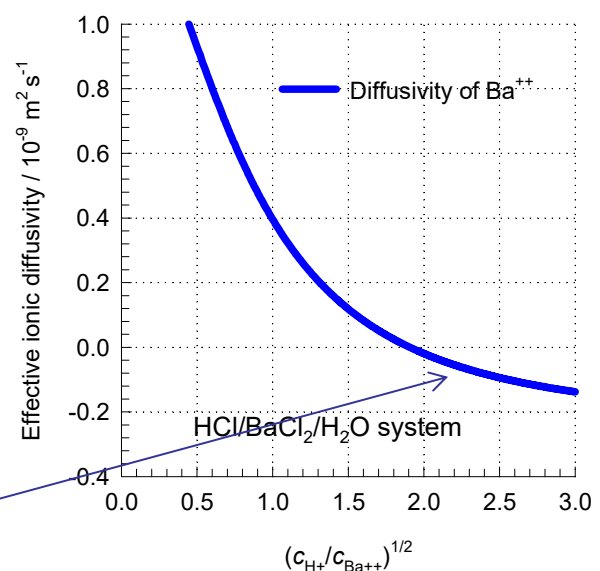
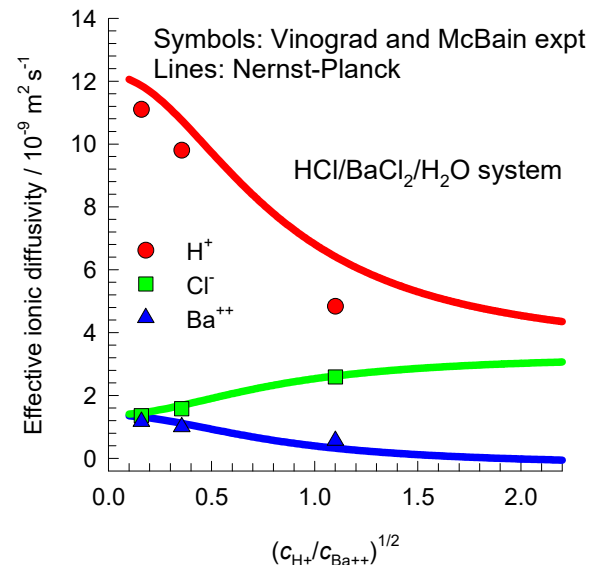


Figure S7

Co-diffusion of Mixed Ions

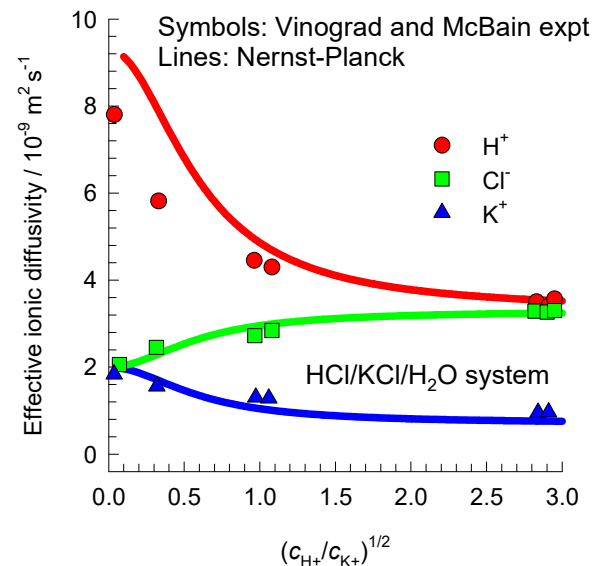
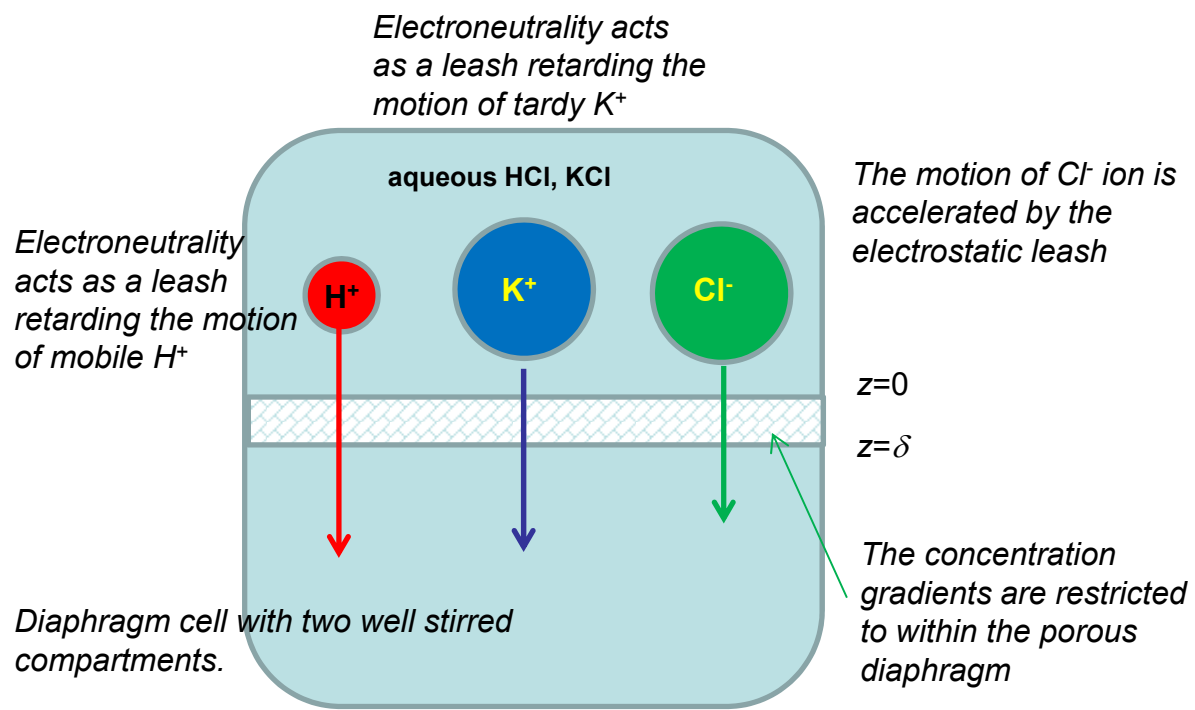
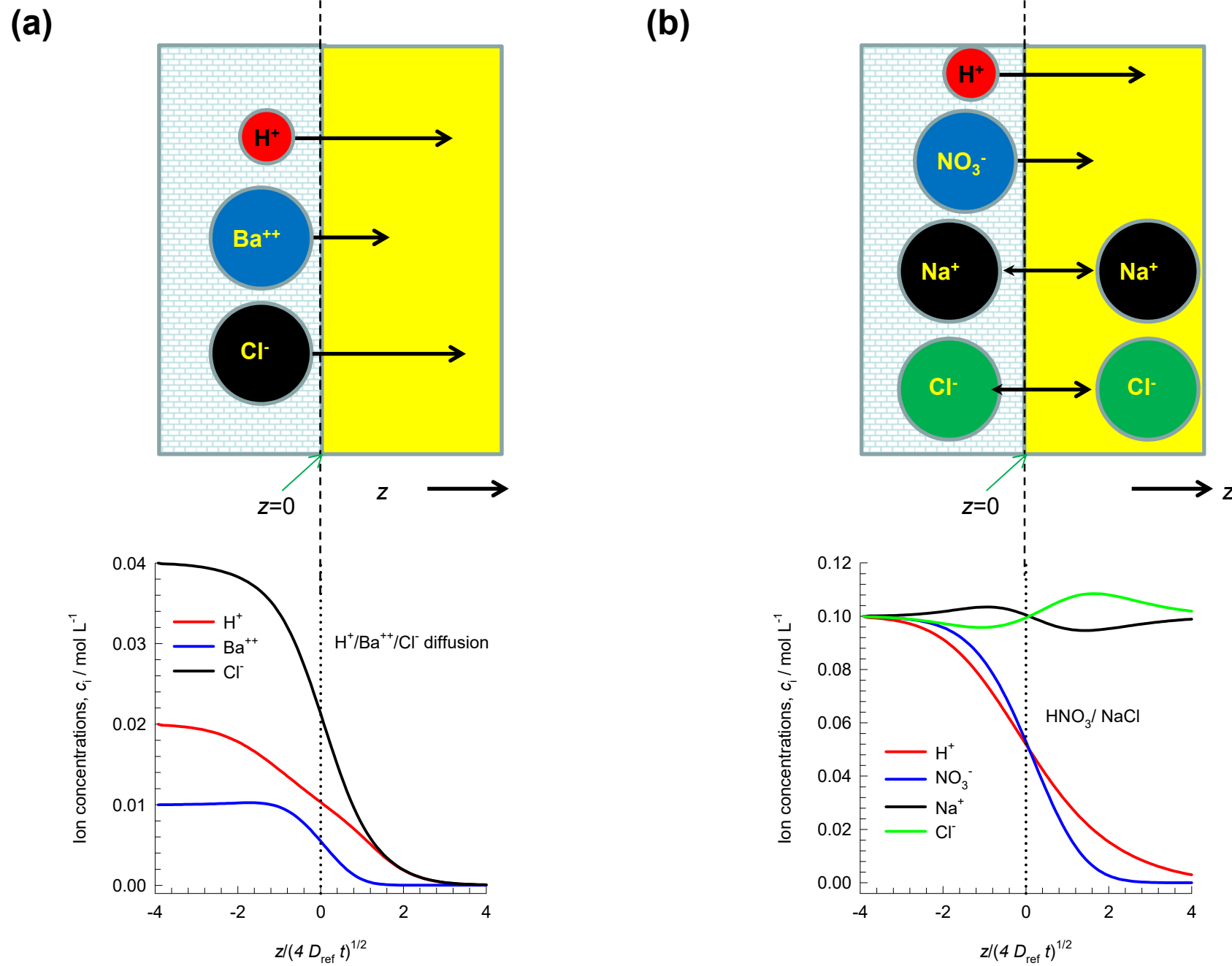


Figure S8

Co-diffusion of Mixed Ions

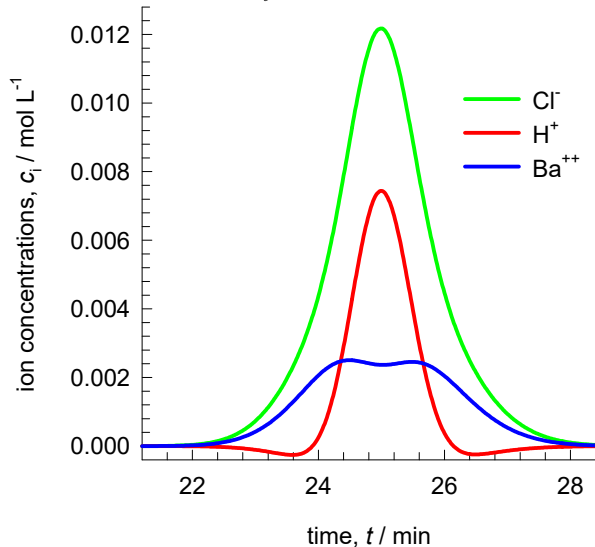


Taylor dispersion in a tube

Figure S9

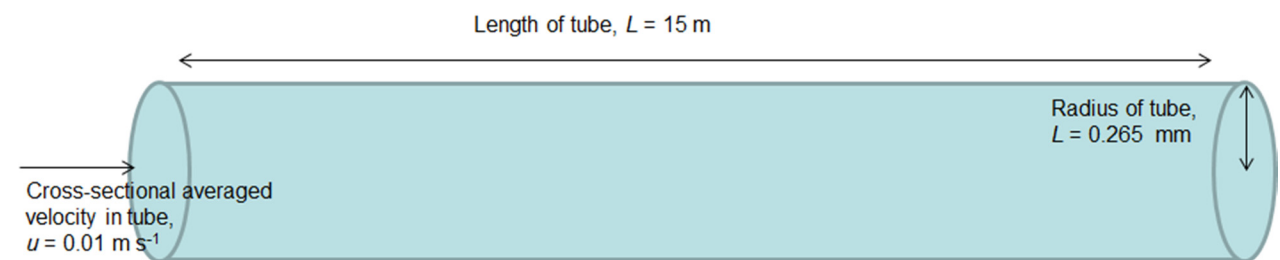
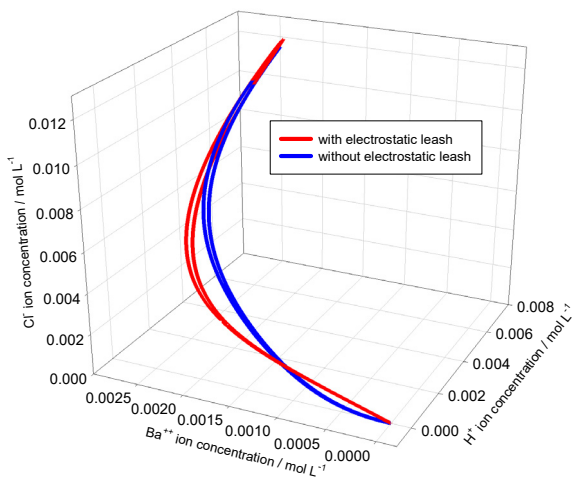
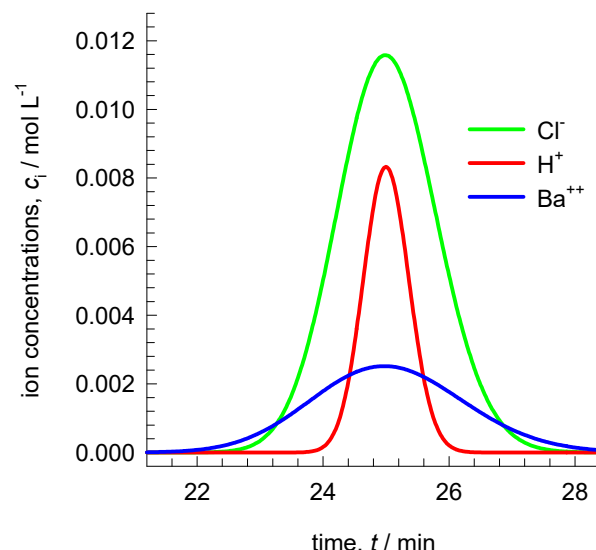
(a) With electrostatic leash

$$D_{ik} = D_i \delta_{ik} - \frac{(c_i z_i D_i)(z_k (D_k - D_{n-1}))}{\sum_{j=1}^{n-1} c_j z_j^2 D_j}; \quad i, k = 1, 2, \dots, n-2$$



(b) Neglecting electrostatic leash

$$D_{ik} = D_{iw} \delta_{ik}; \quad i, k = 1, 2, \dots, n-1$$



Counter-diffusion of Mixed Ions

Figure S10

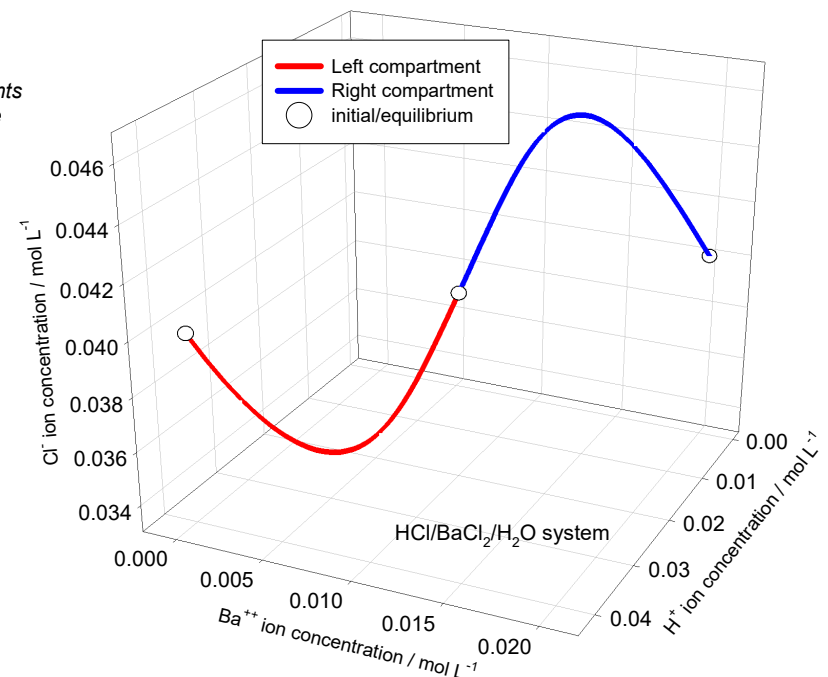
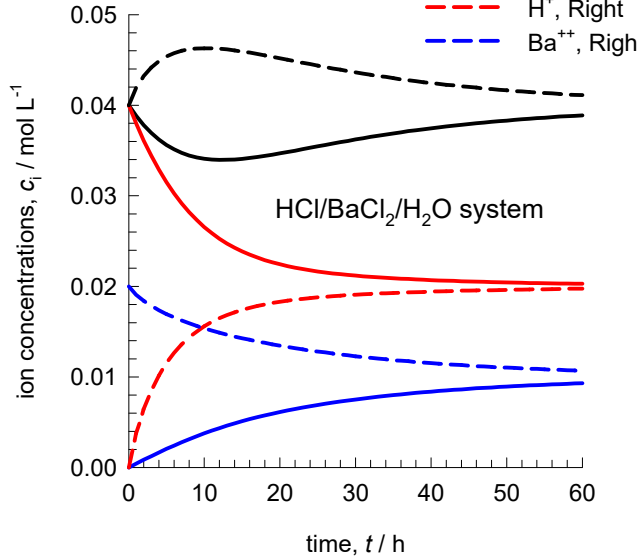
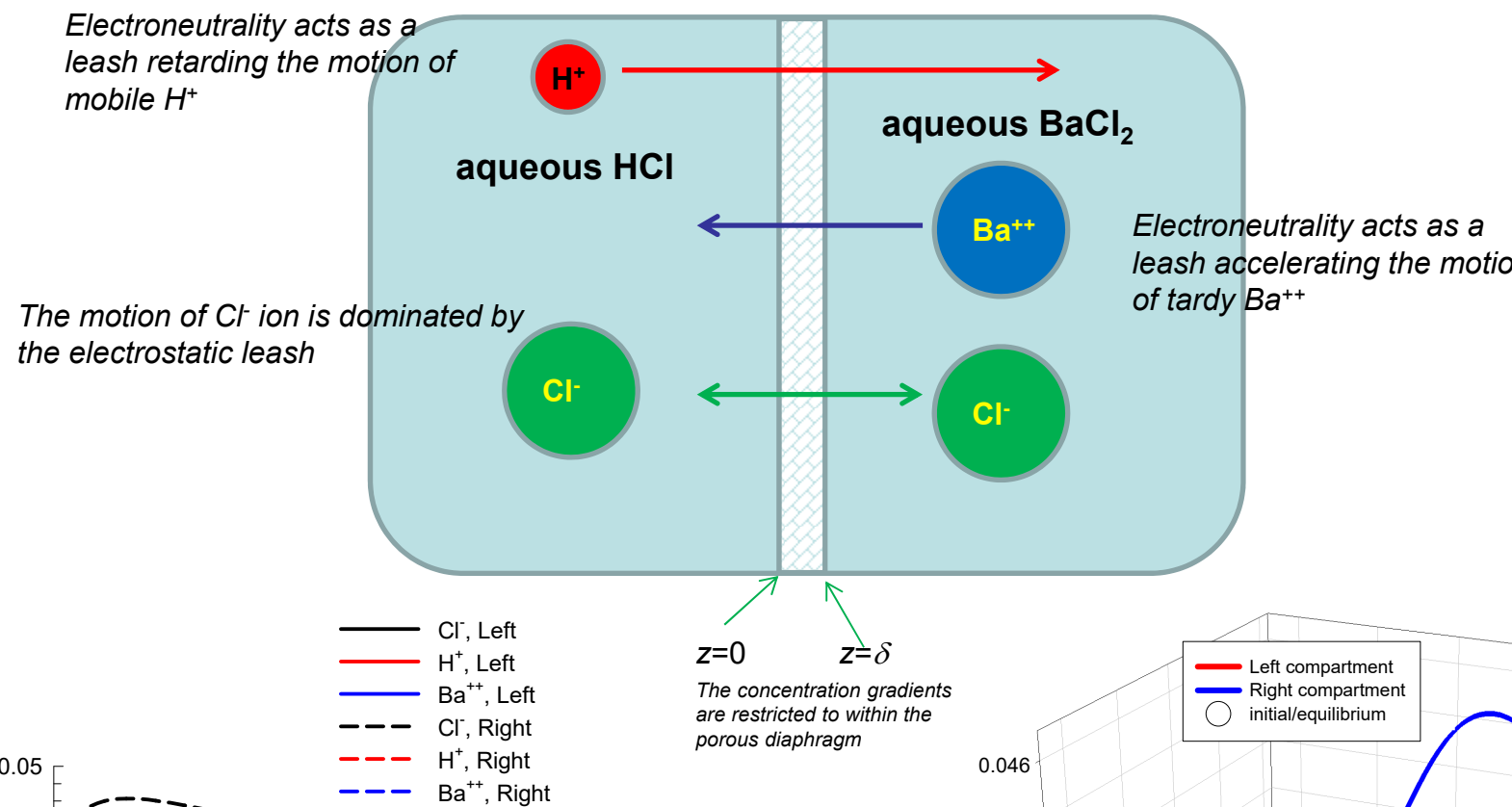


Figure S11

Counter-diffusion of Mixed Ions

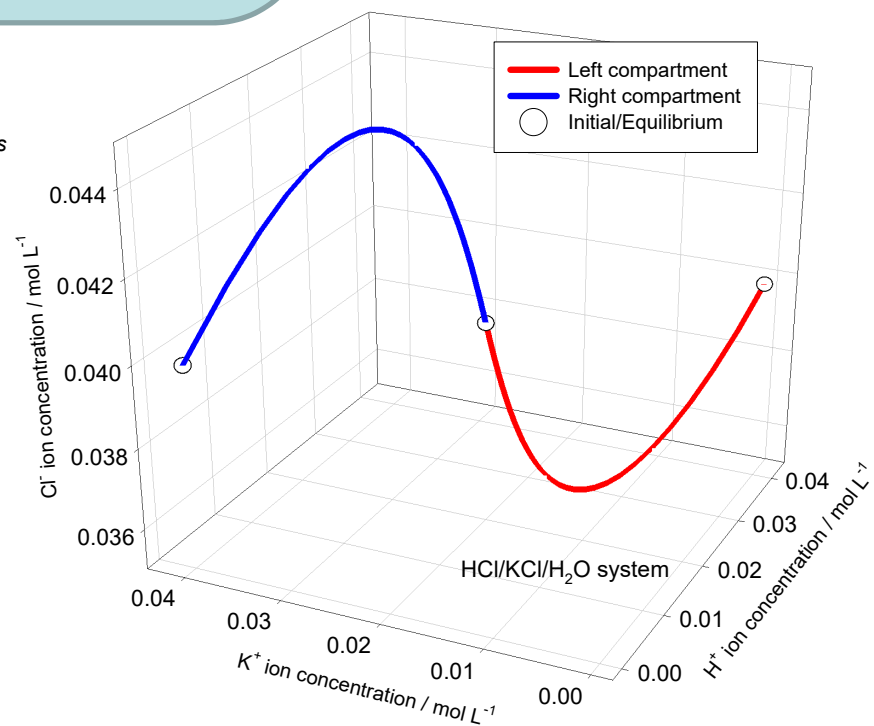
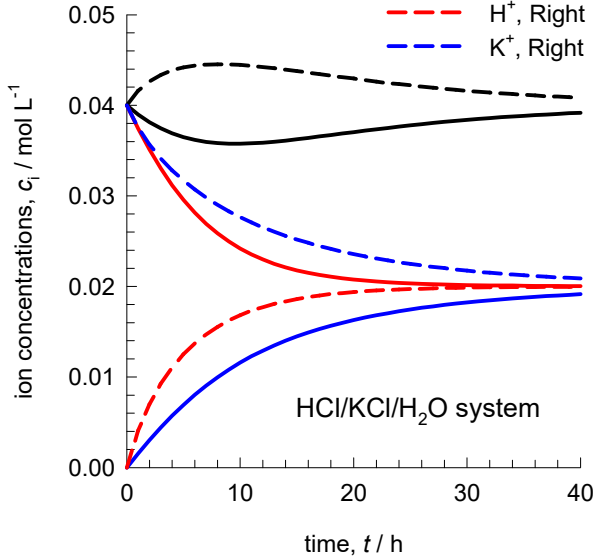
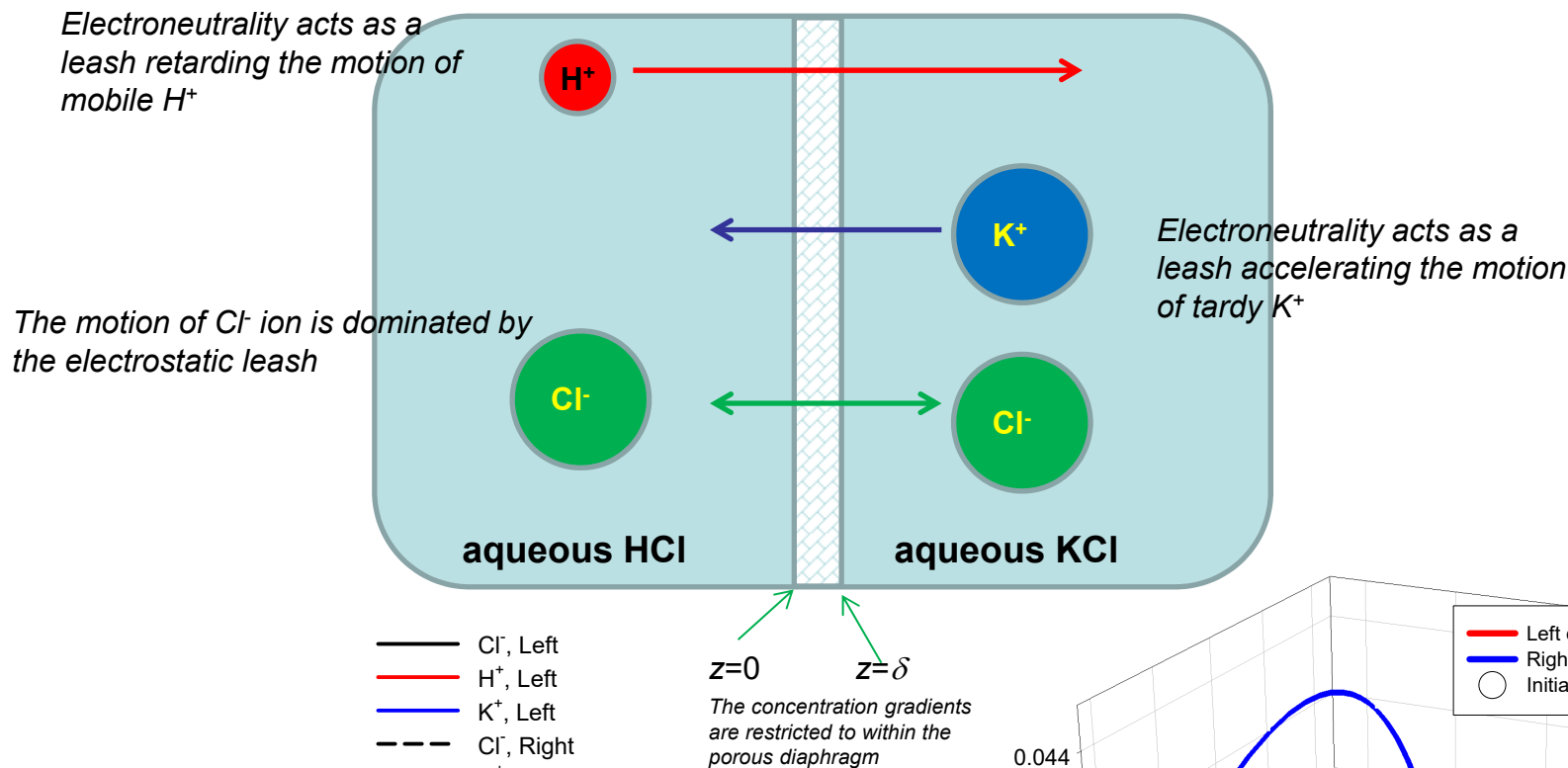
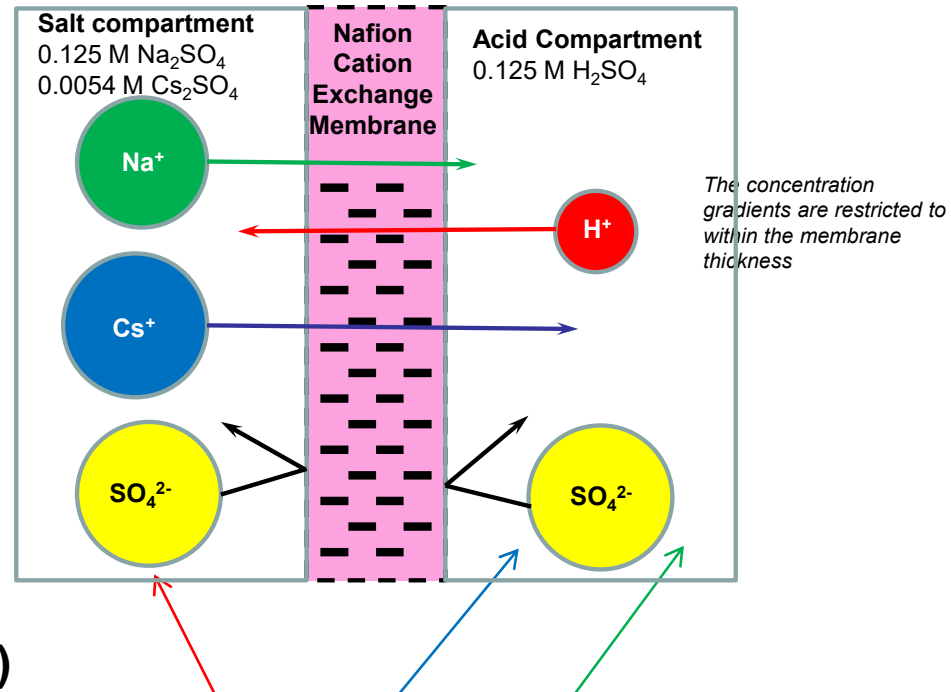
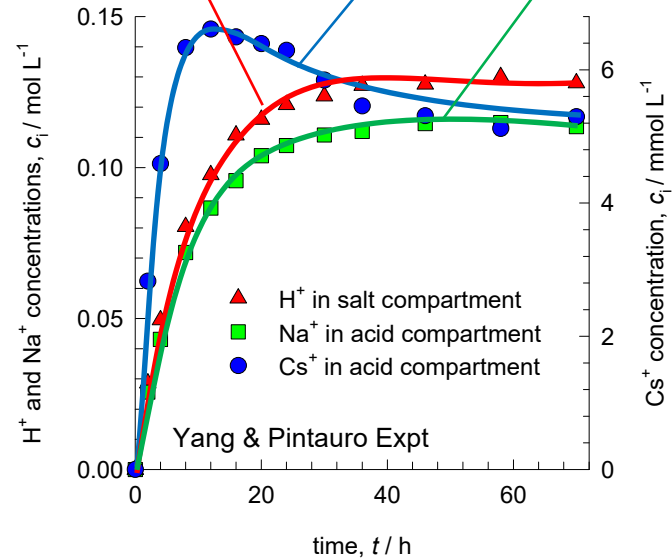


Figure S12

Transport across cation-exchange membrane



(a)



(b)

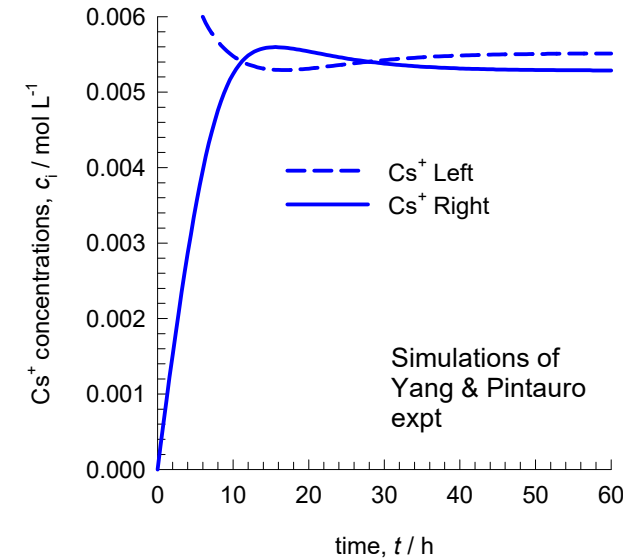
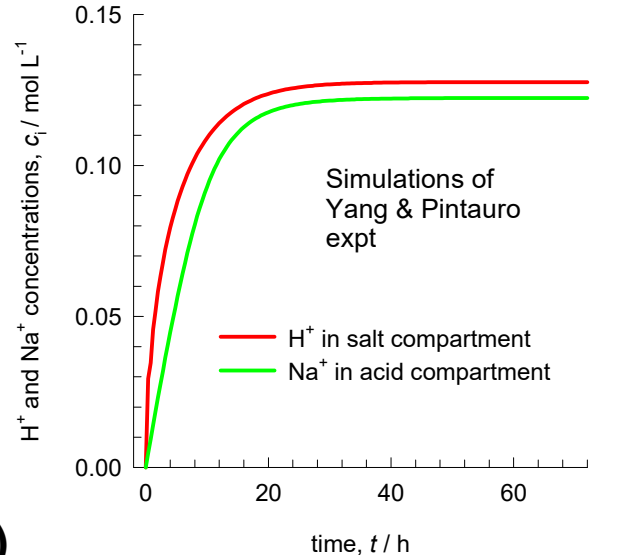


Figure S13

Transport across cation-exchange membrane

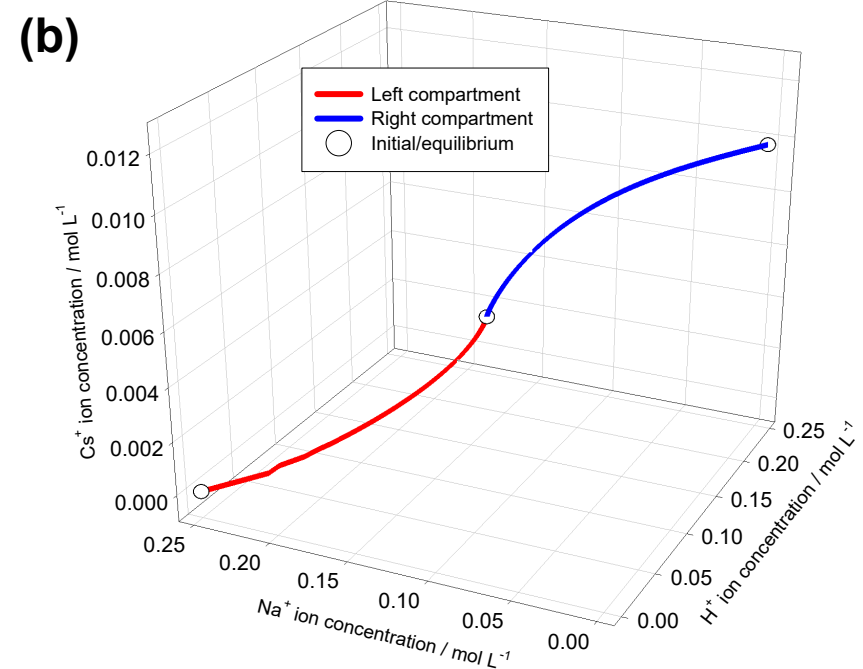
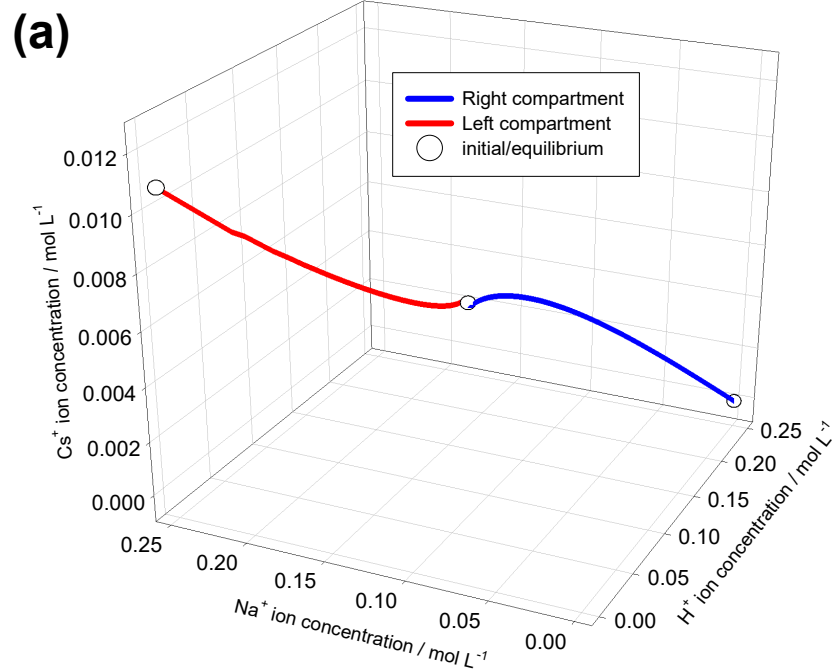
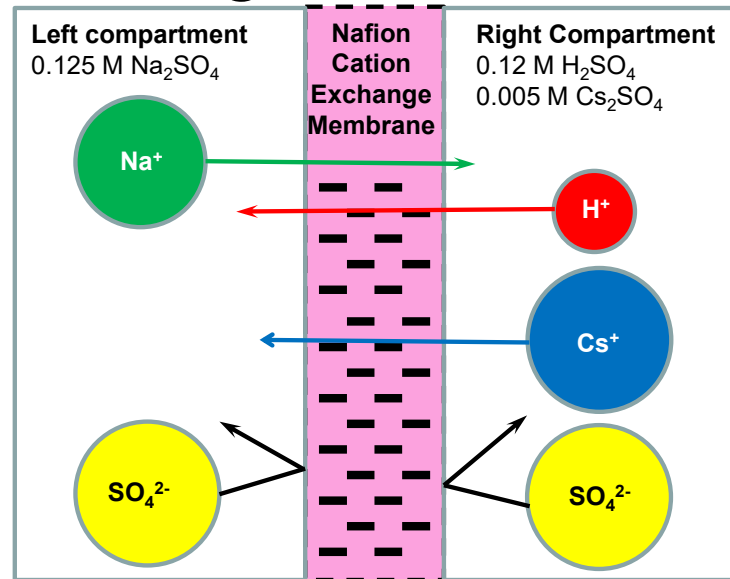
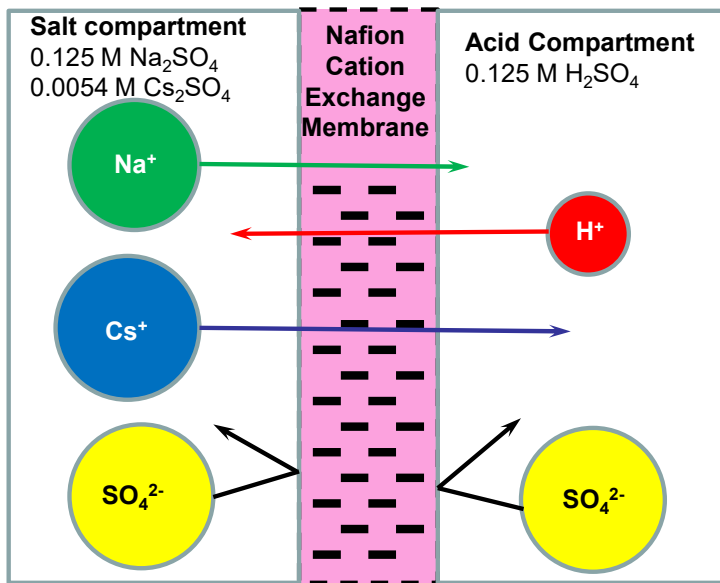


Figure S14

Ion-Exchange

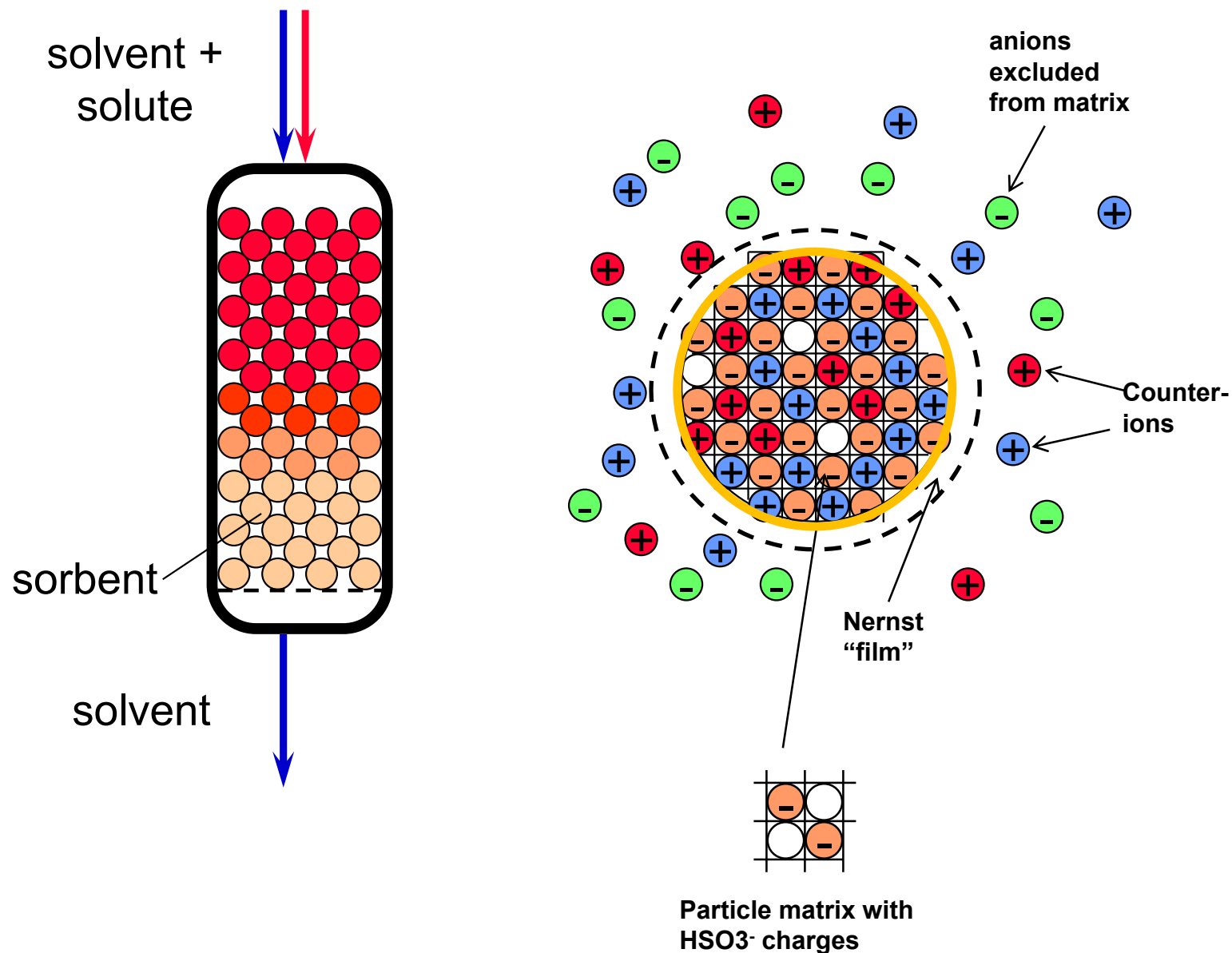


Figure S15

Asymmetry in Ion-Exchange Kinetics Limited by Transport of Ions from Bulk Liquid to Particle Surface

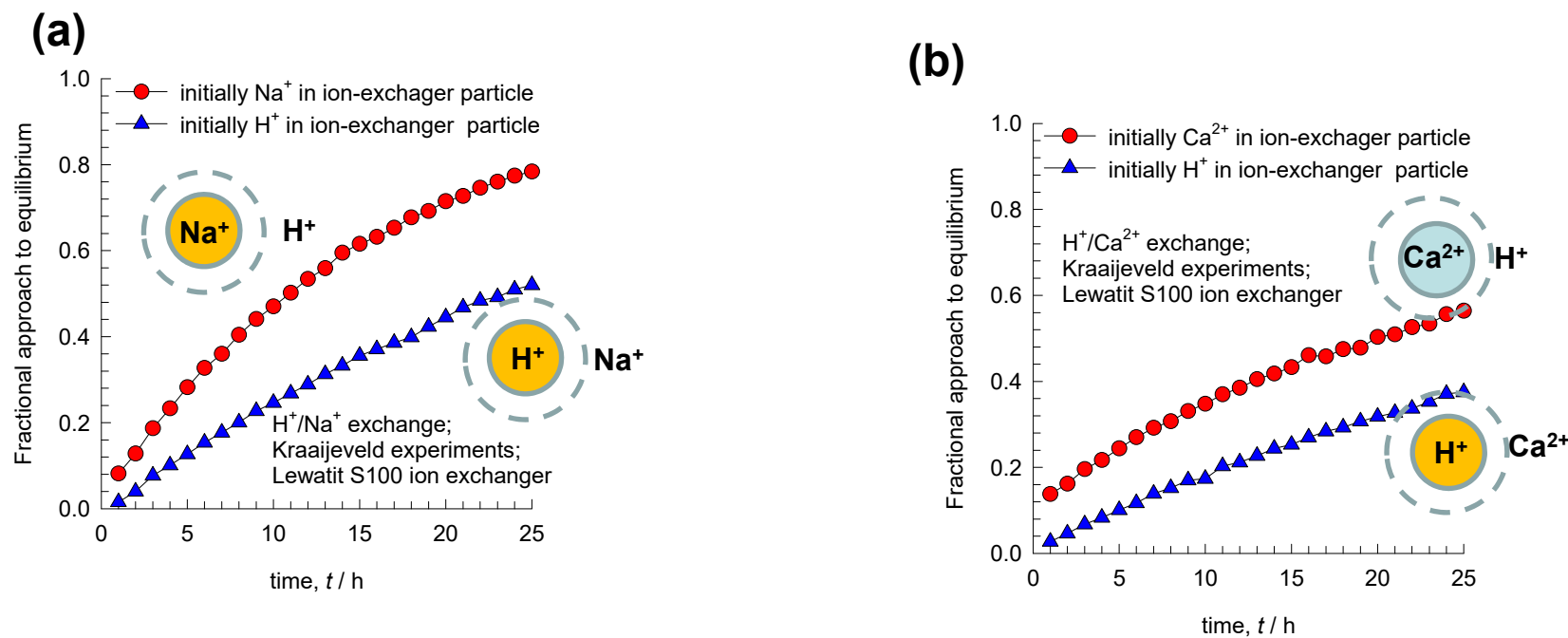
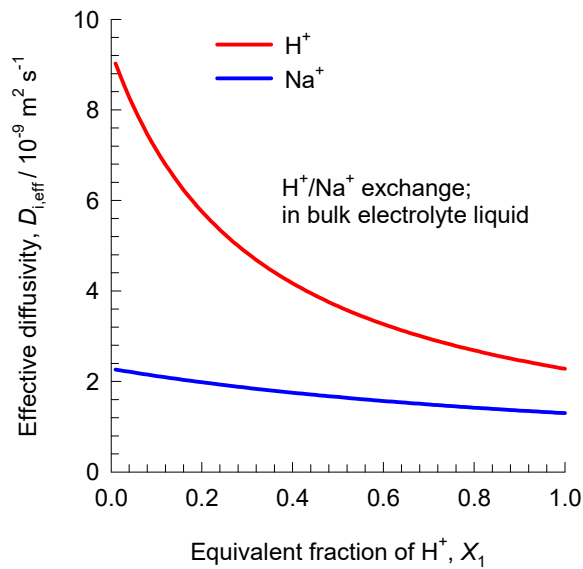


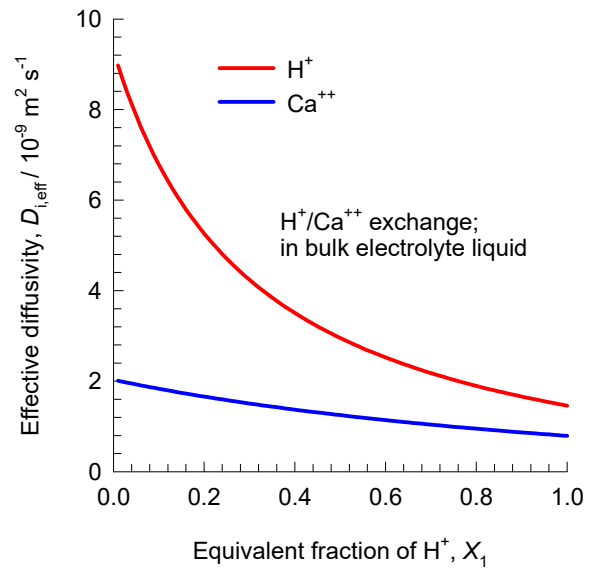
Figure S16

Minority rule for extra-particle exchange

(a)



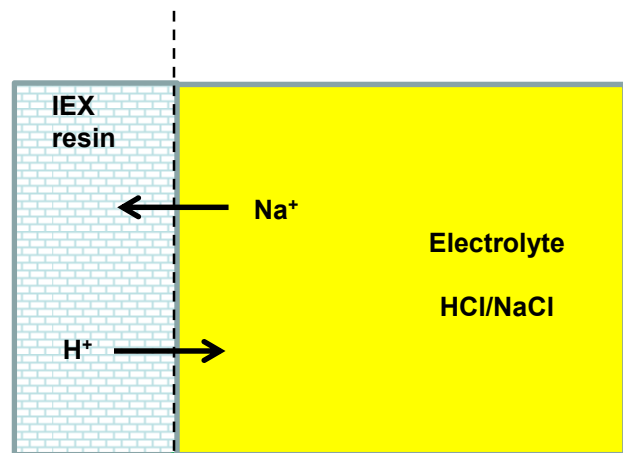
(b)



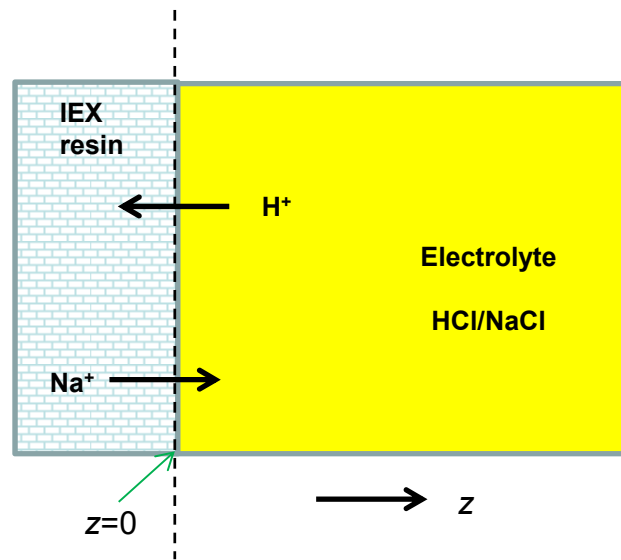
Asymmetry in Ion-Exchange Kinetics

Figure S17

(a)

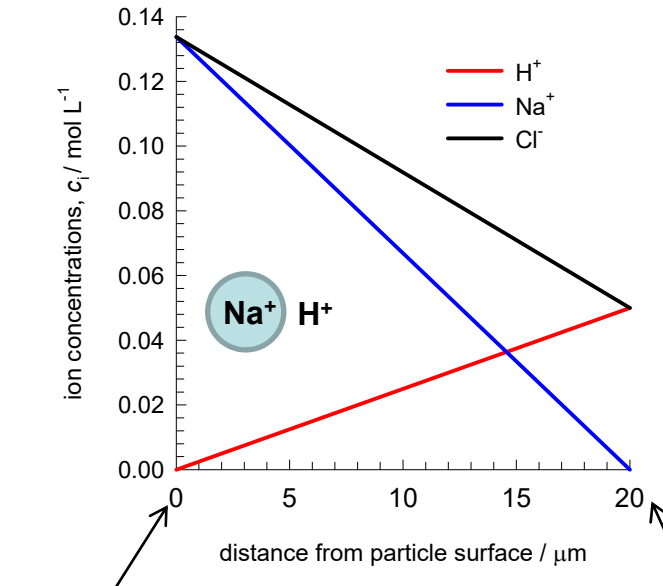
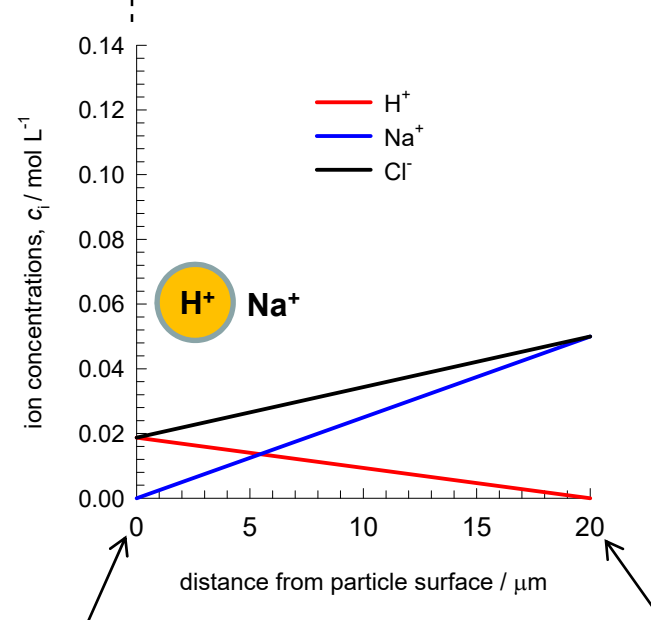


(b)



Particle/liquid interface
 $z=0$

Bulk electrolyte solutions
 $z=\delta$



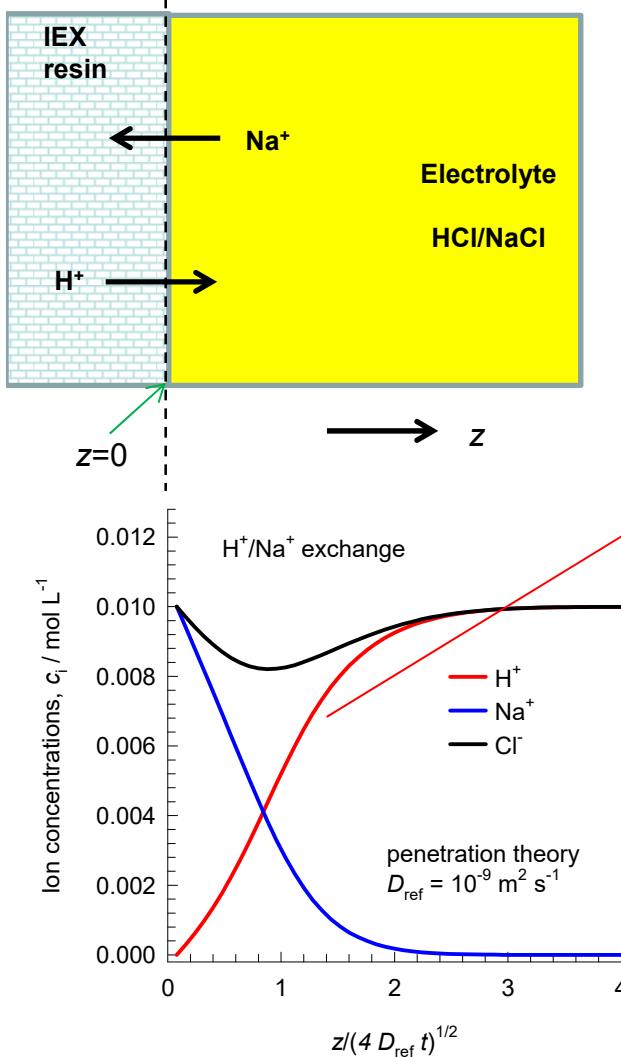
Particle/liquid interface
 $z=0$

Bulk electrolyte solutions
 $z=\delta$

Figure S18

Asymmetry

(a)



(b)

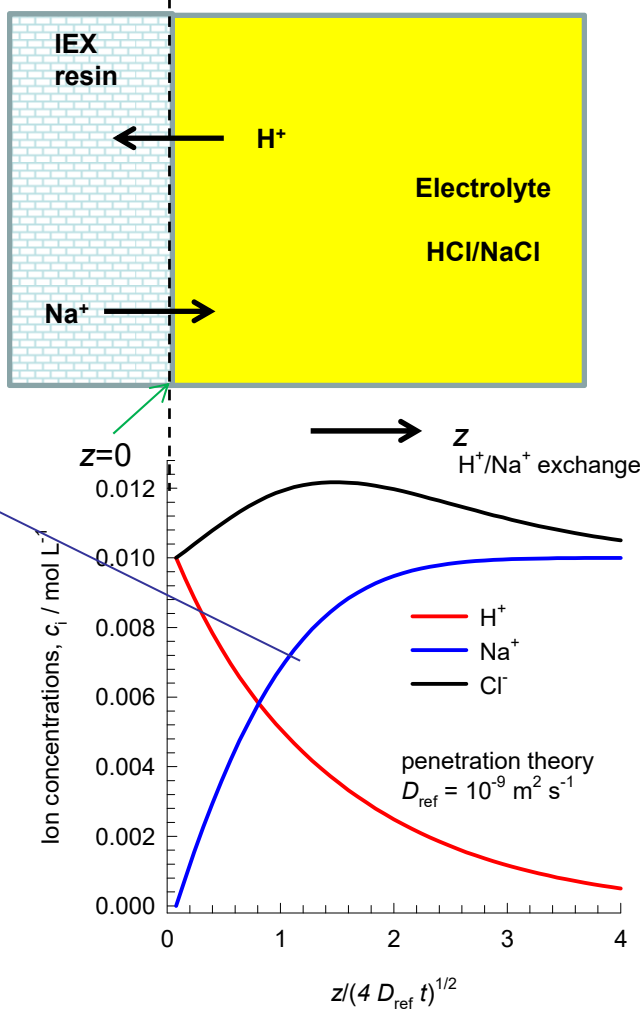
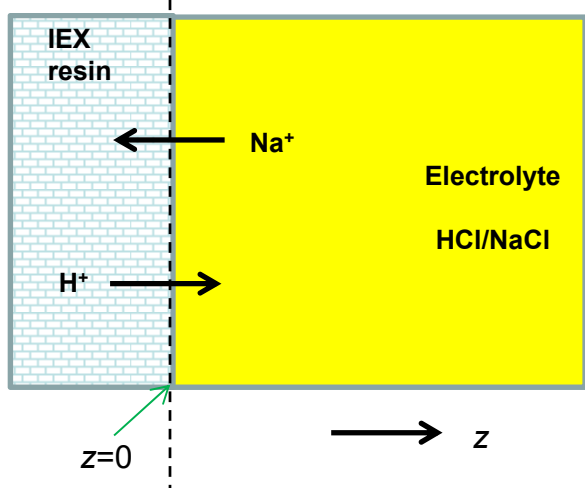


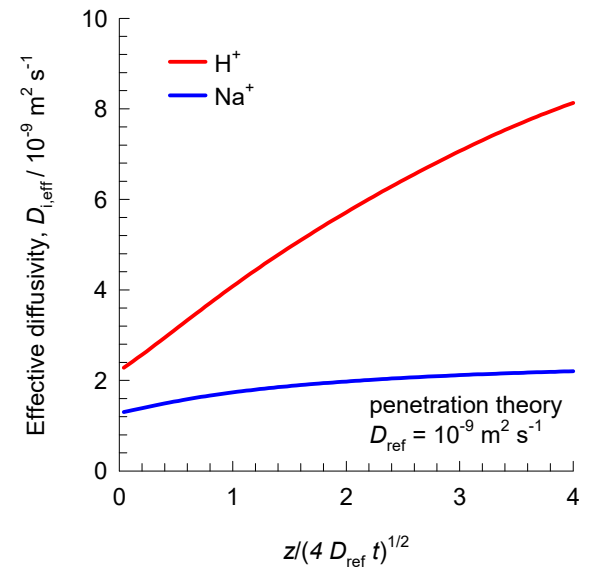
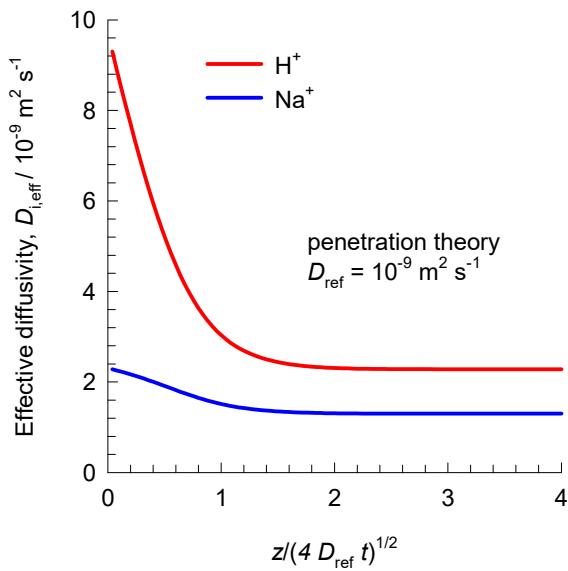
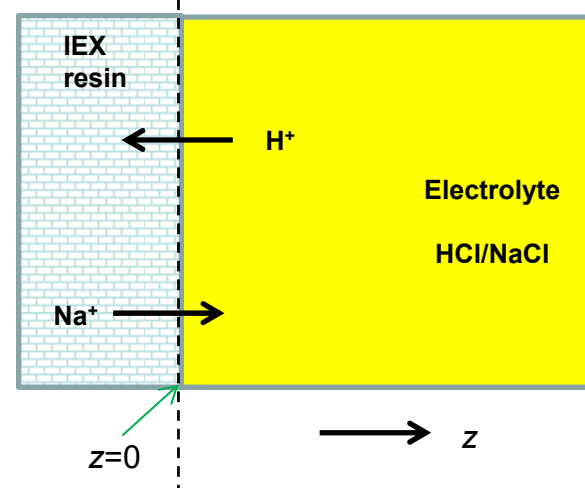
Figure S19

Effective diffusivities

(a)



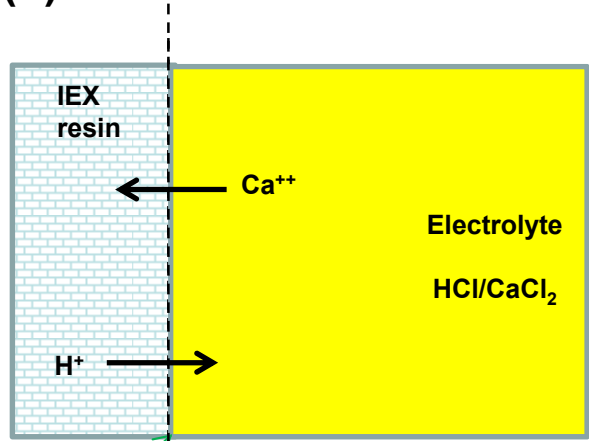
(b)



Asymmetry

Figure S20

(a)



(b)

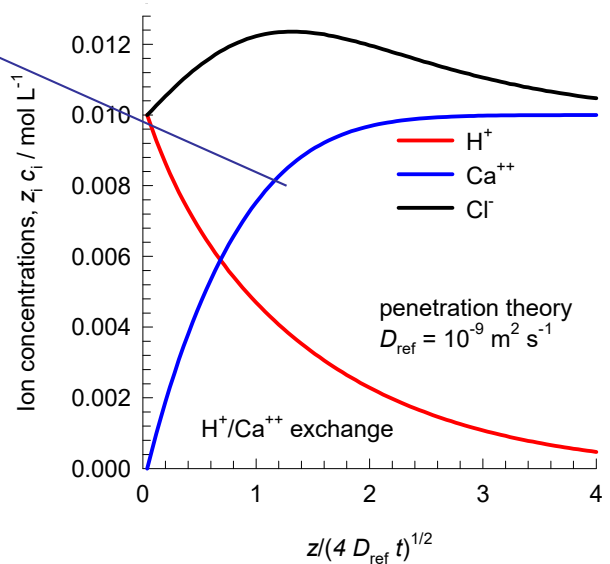
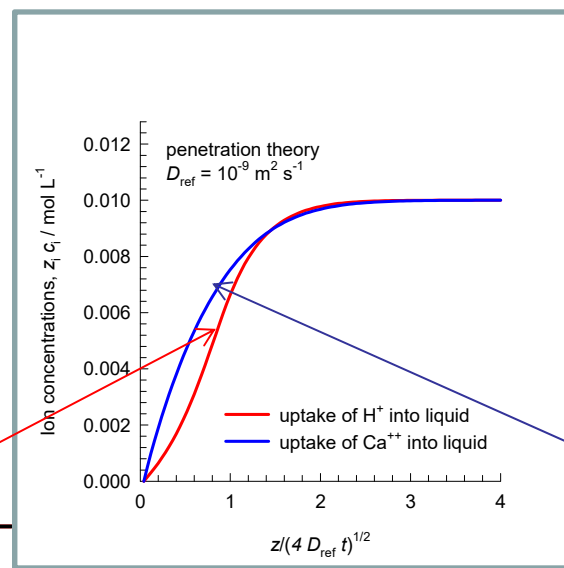
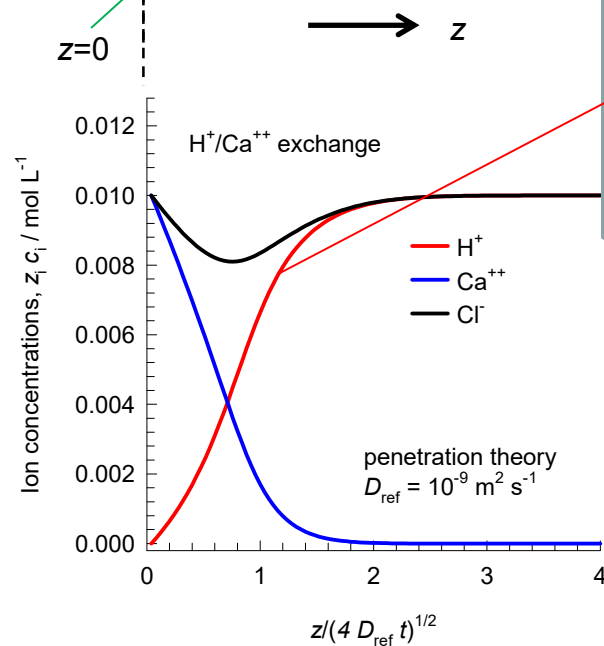
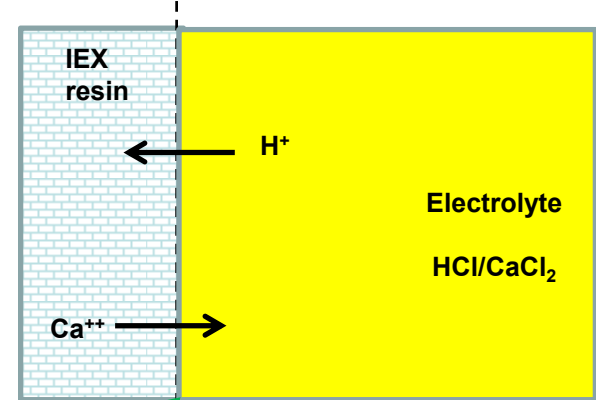
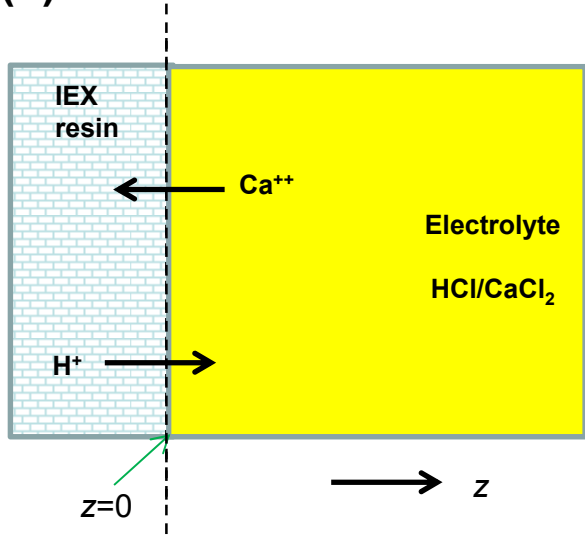


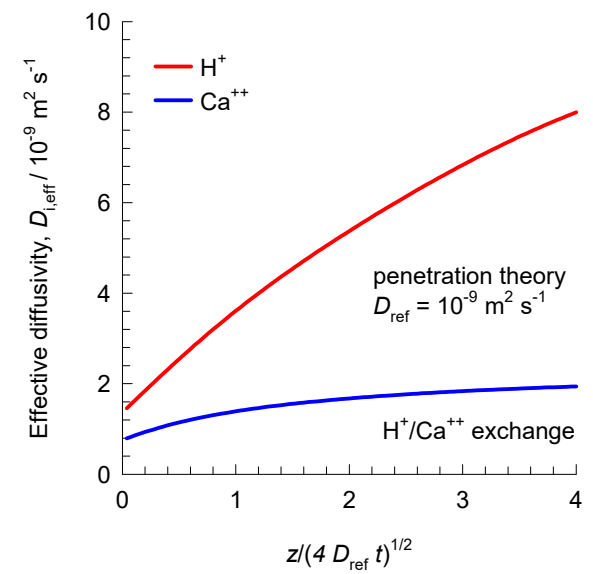
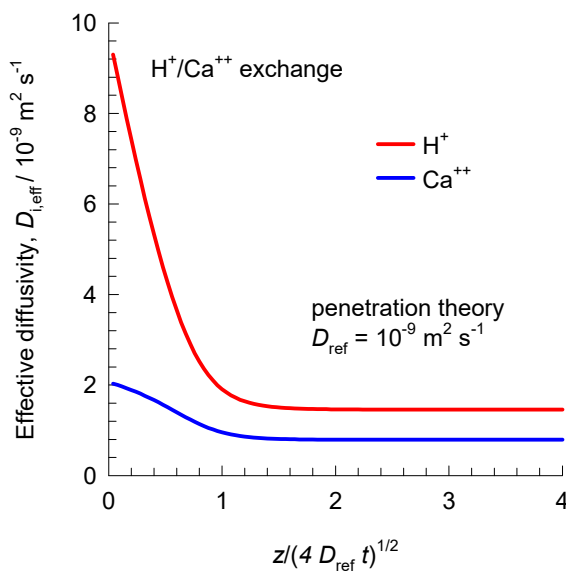
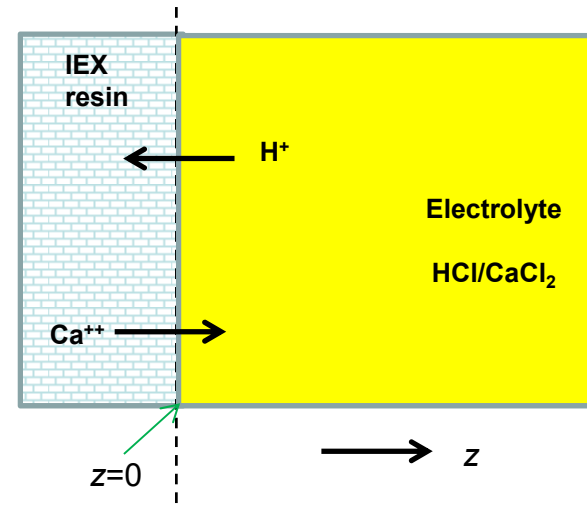
Figure S21

Effective diffusivities

(a)



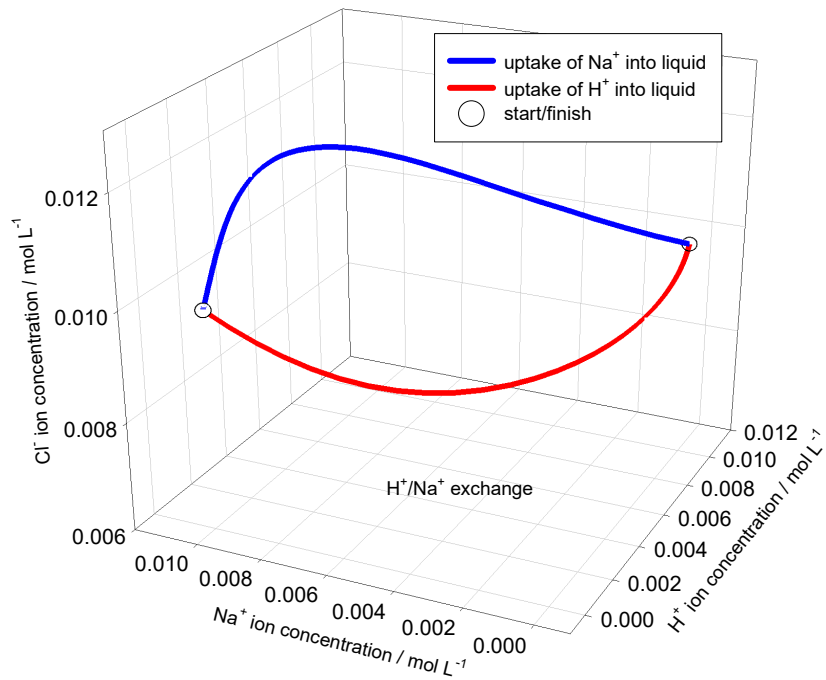
(b)



Asymmetric trajectories

Figure S22

(a)



(b)

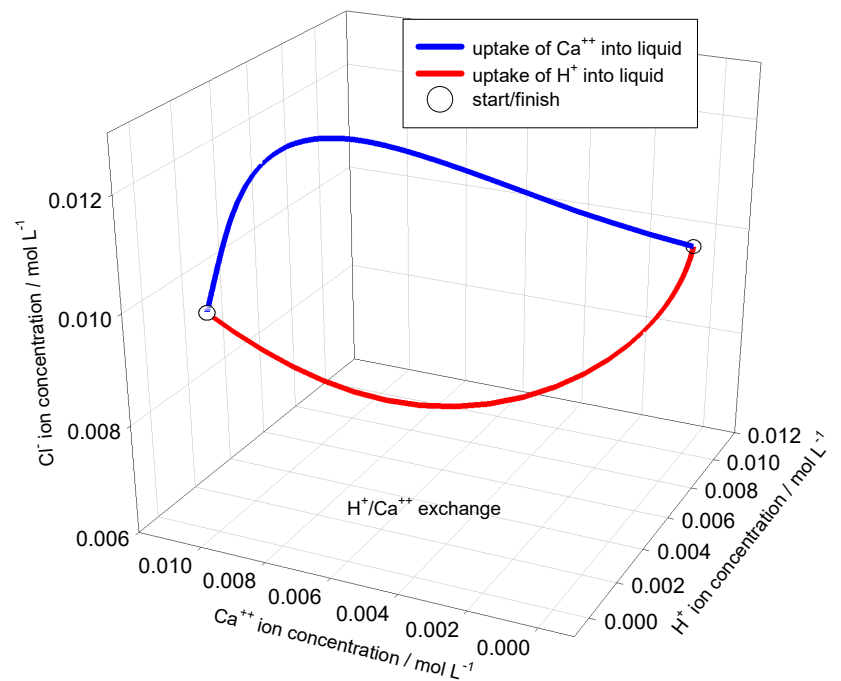
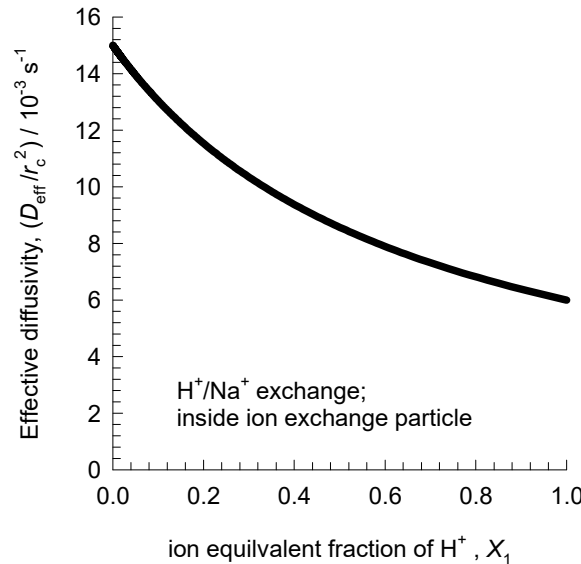


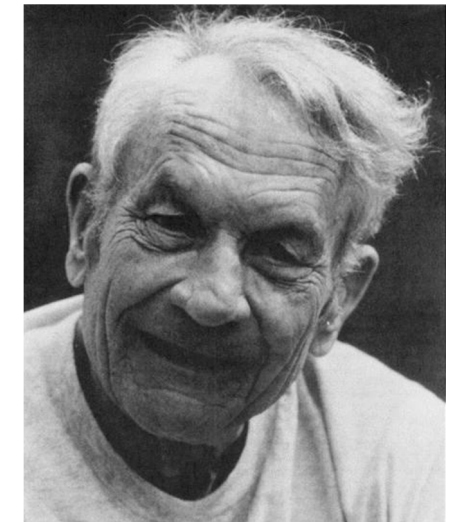
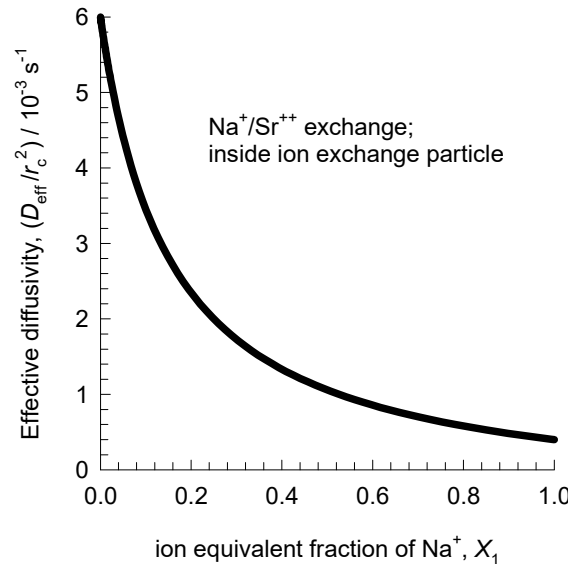
Figure S23

Minority rule for intra-particle exchange

(a)



(b)



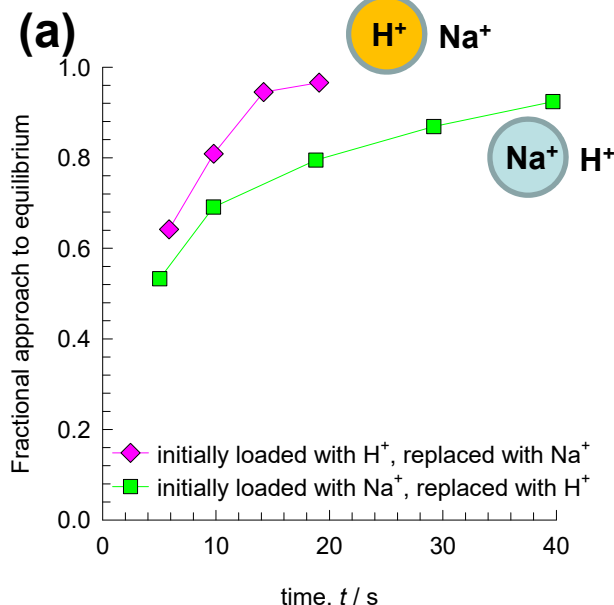
Friedrich Georg Helfferich
1922-1995

interdiffusion is not a democratic process but, in the parlance of the activist 1960's, is ruled by a participating minority!

F.G. Helfferich

Asymmetry in Ion-Exchange Kinetics^{Figure S24}

Diffusion Limitation inside Particle



(c)

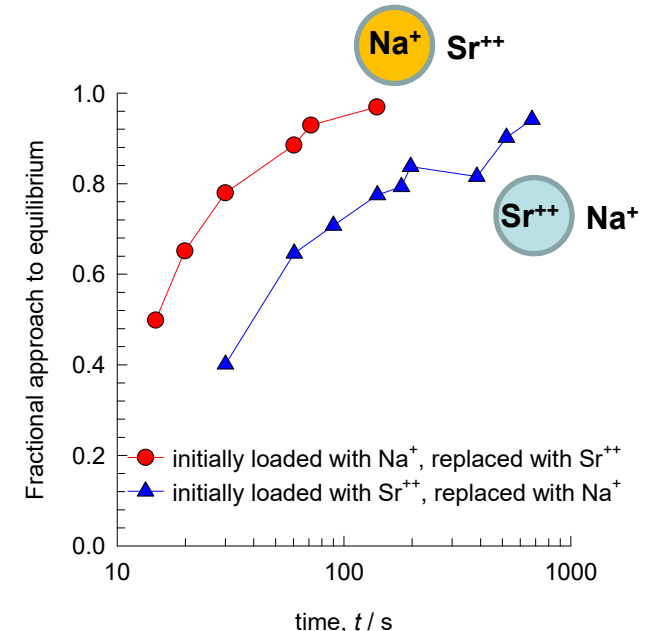
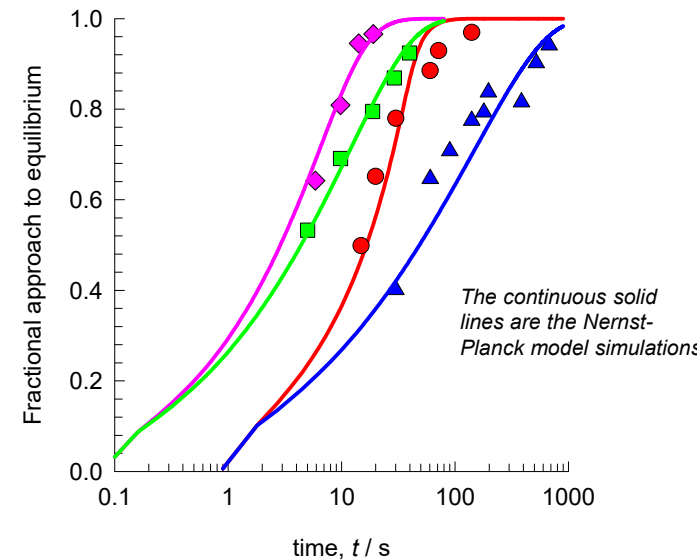
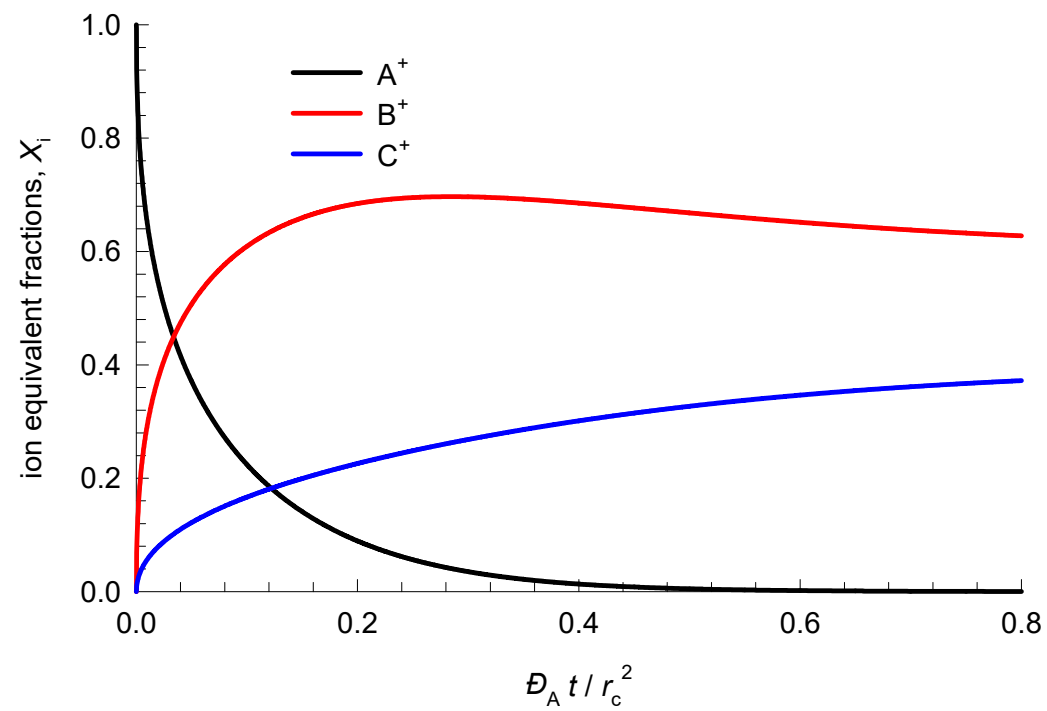
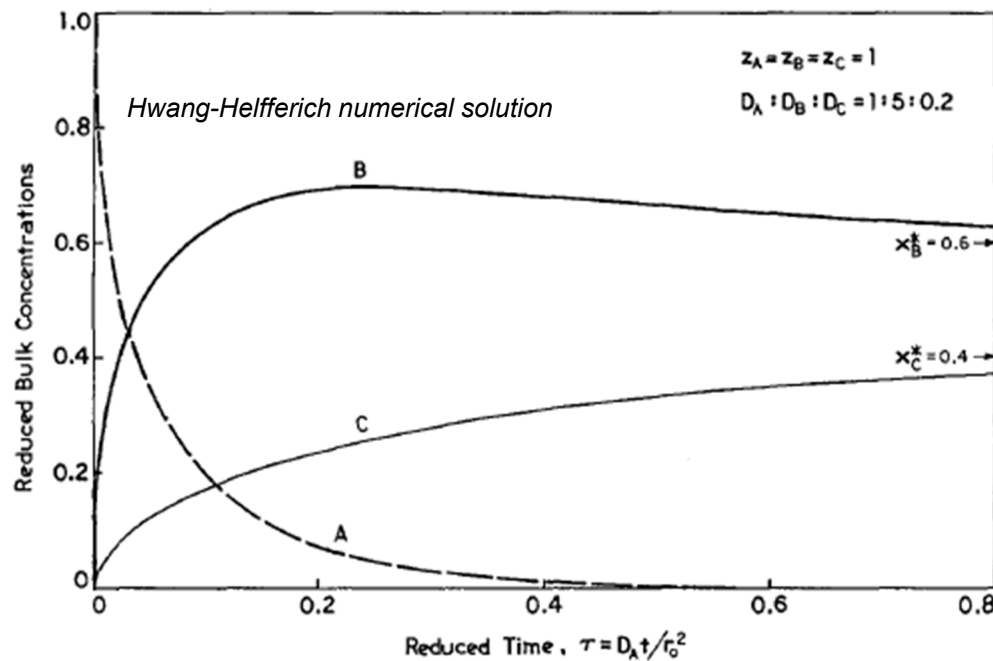


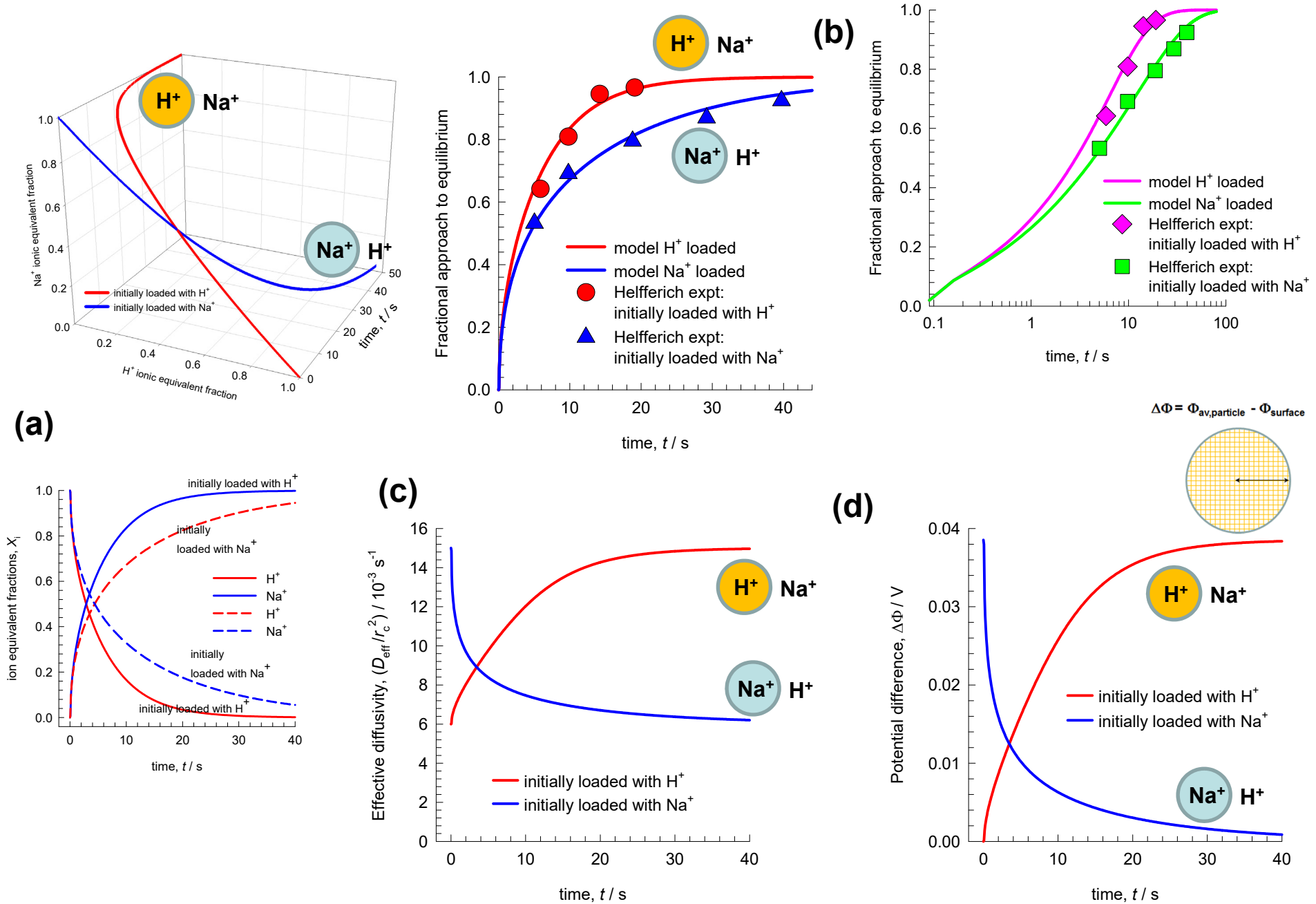
Figure S25

Accuracy of numerical procedure used in this work



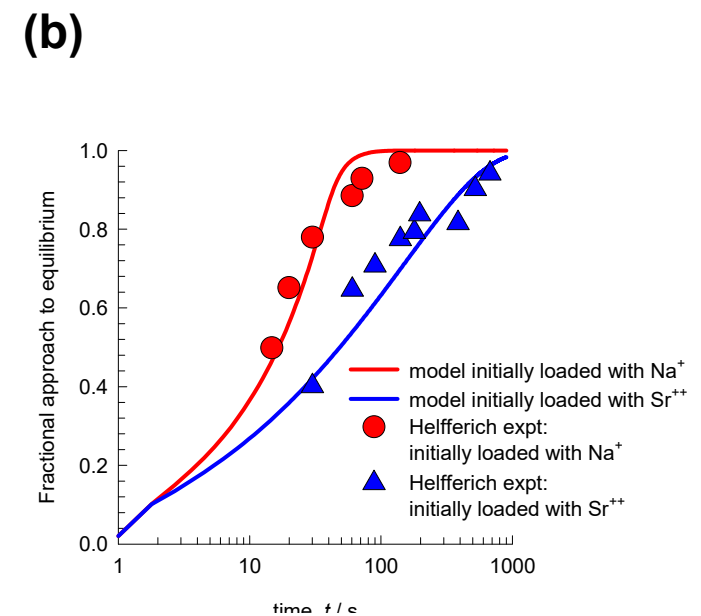
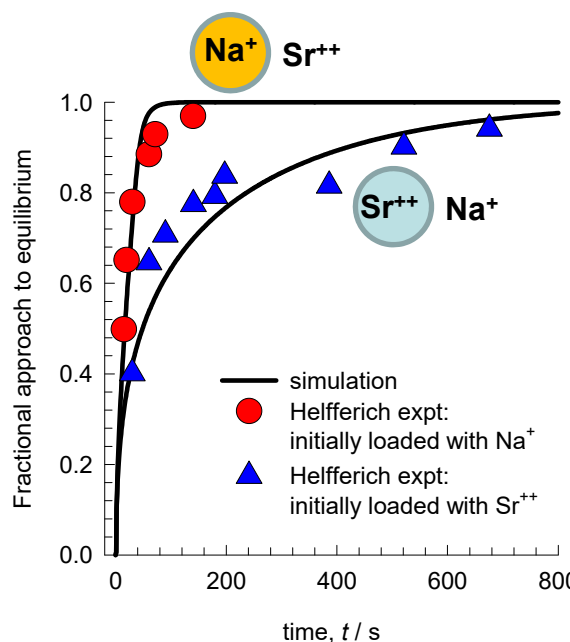
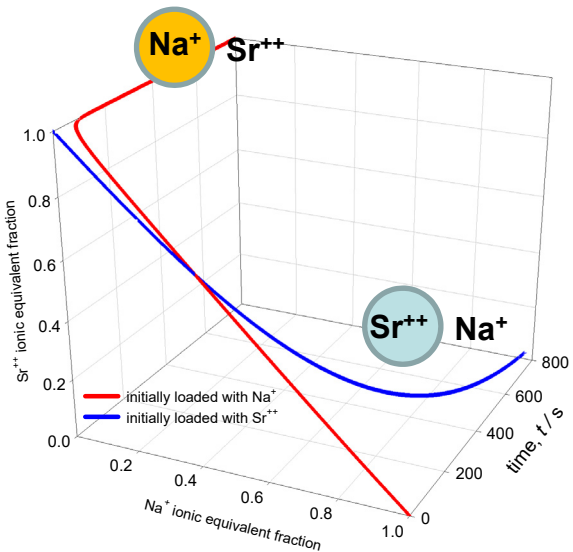
Asymmetry in Ion-Exchange Kinetics

Figure S26

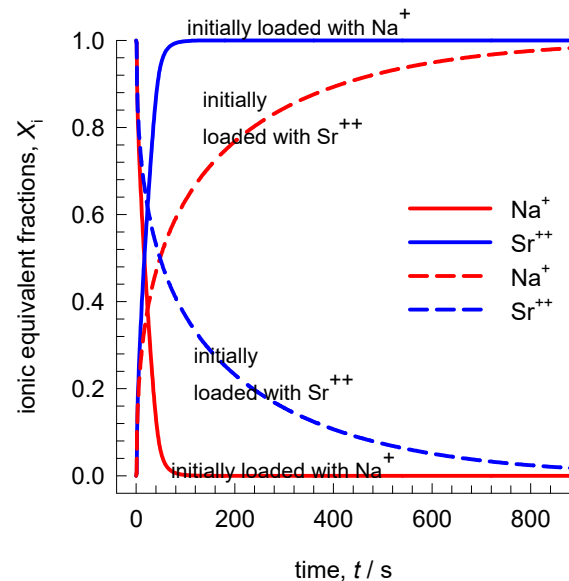


Asymmetry in Ion-Exchange Kinetics

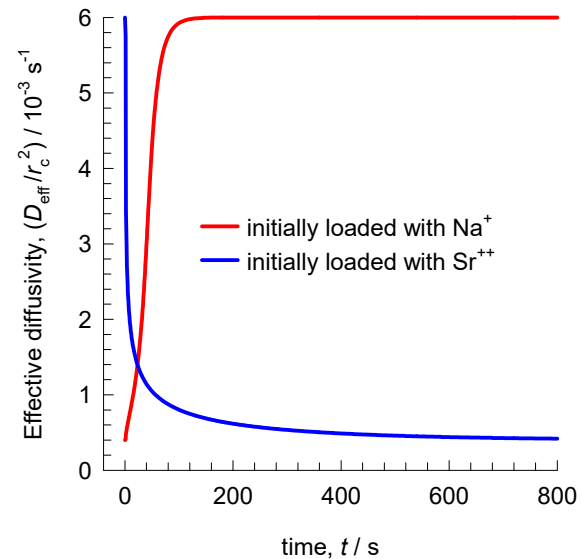
Figure S27



(a)

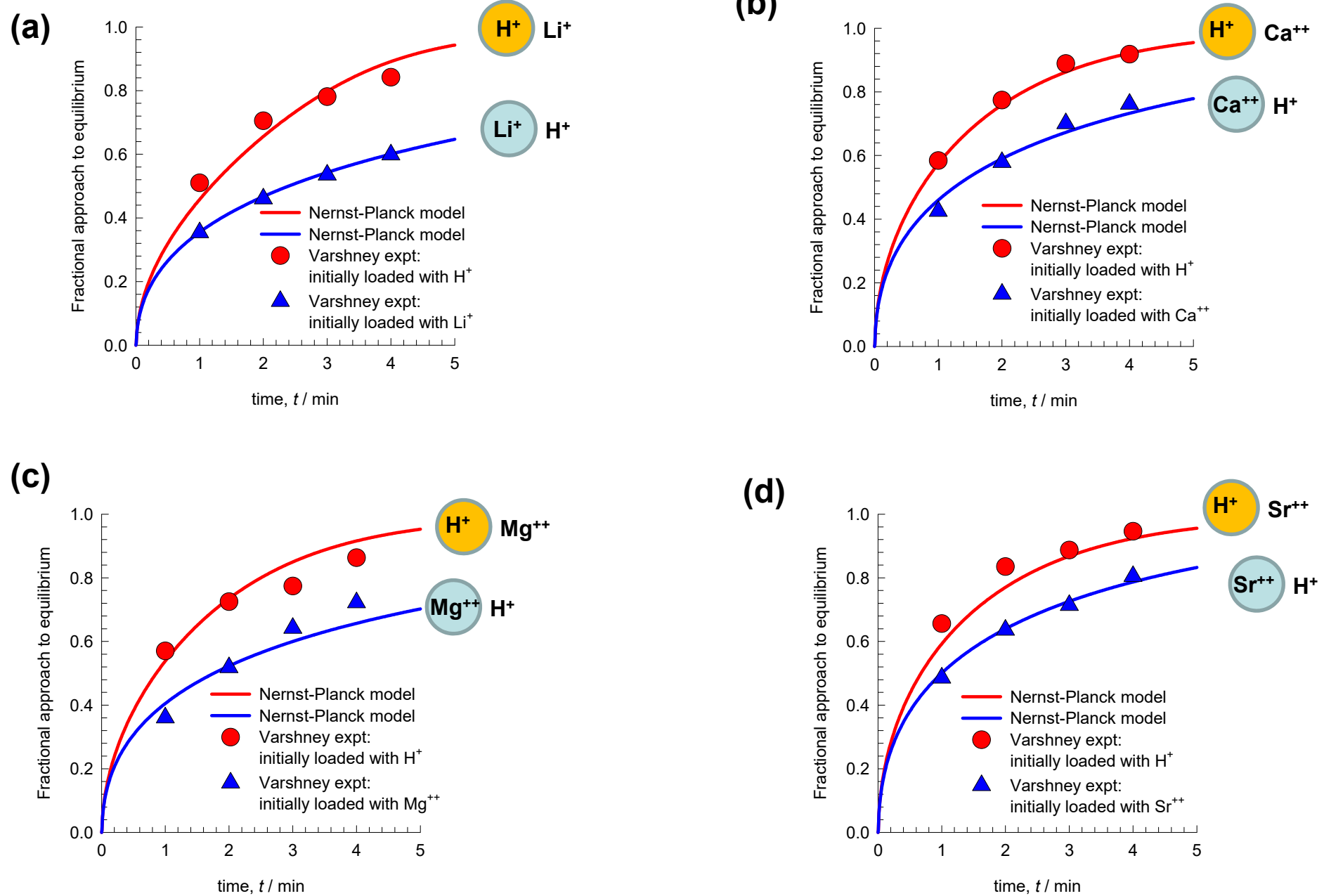


(c)



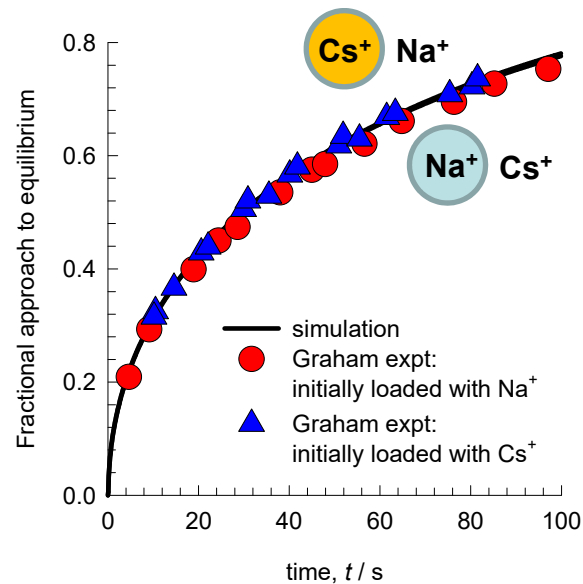
Asymmetry in Ion-Exchange Kinetics

Figure S28



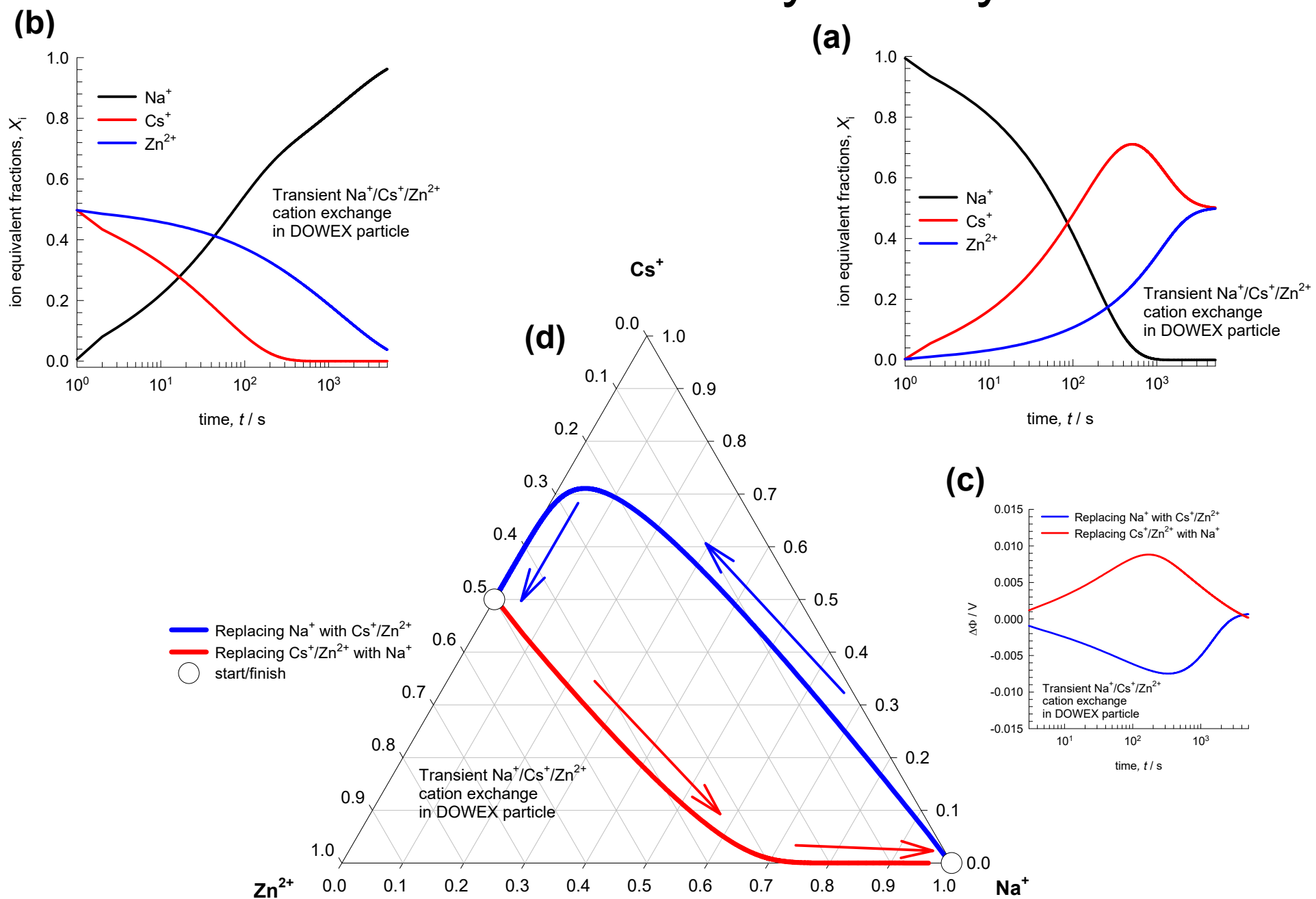
Ion-Exchange Kinetics Diffusion Limitation inside Particle

Figure S29



Overshoot and Asymmetry

Figure S30



Overshoot and Asymmetry

Figure S31

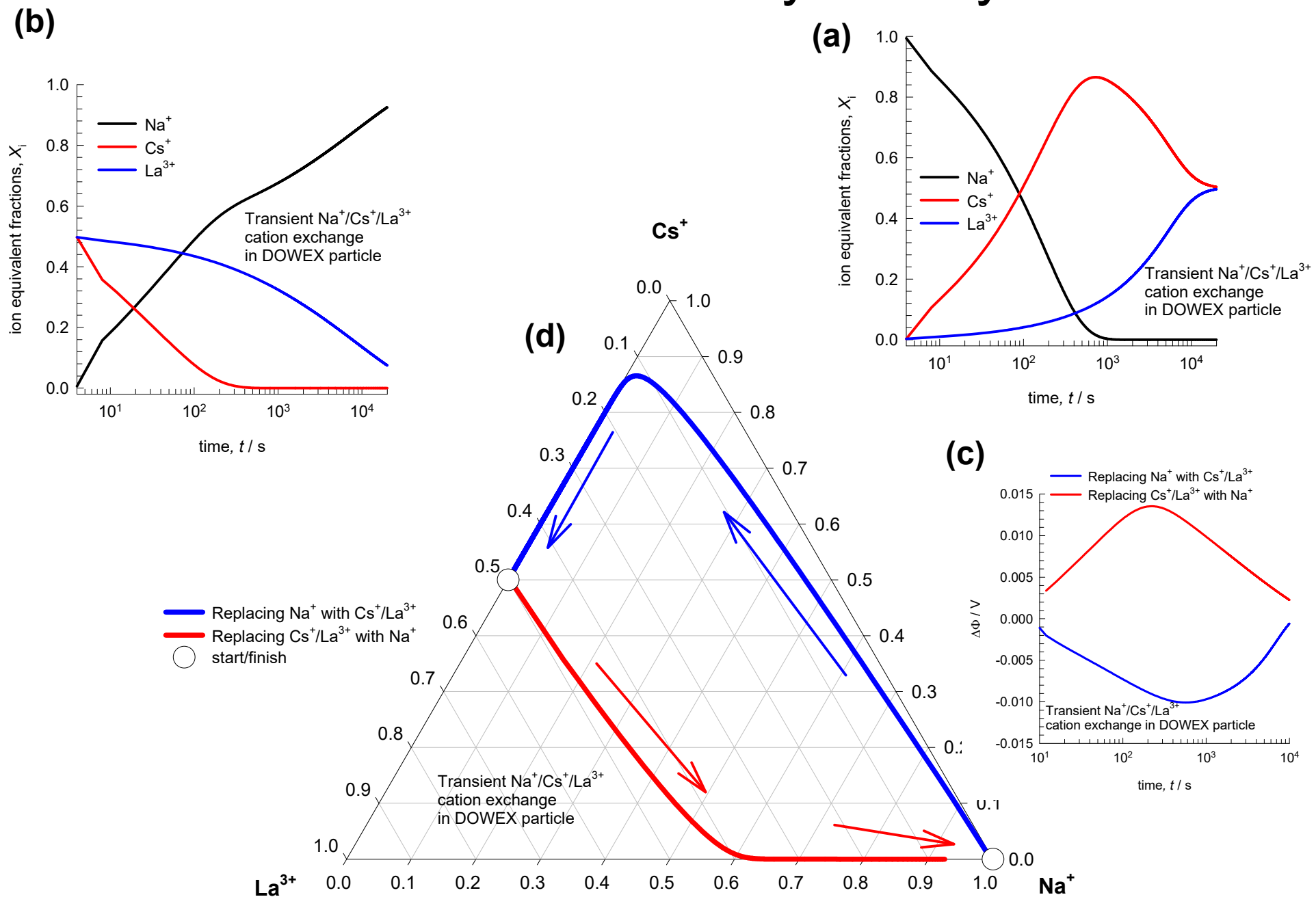
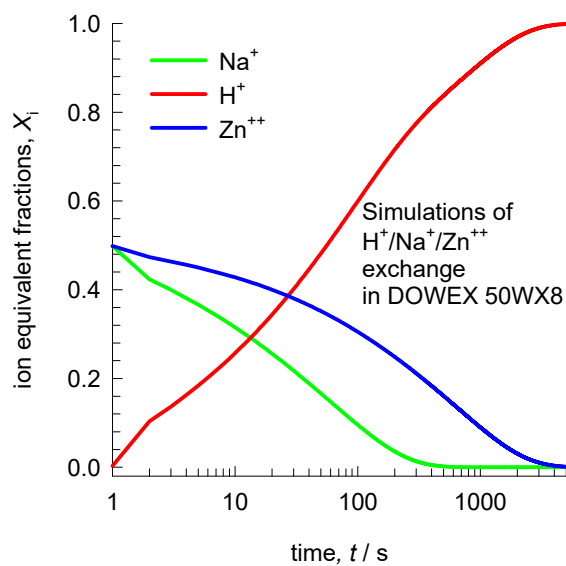
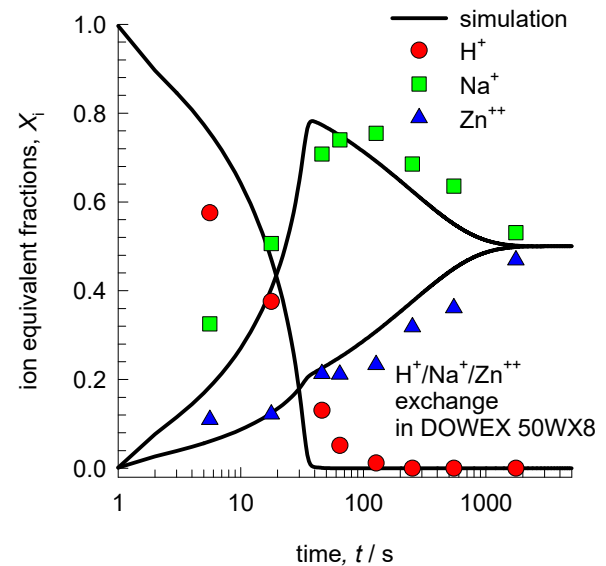


Figure S32

(b)



(a)



(c)

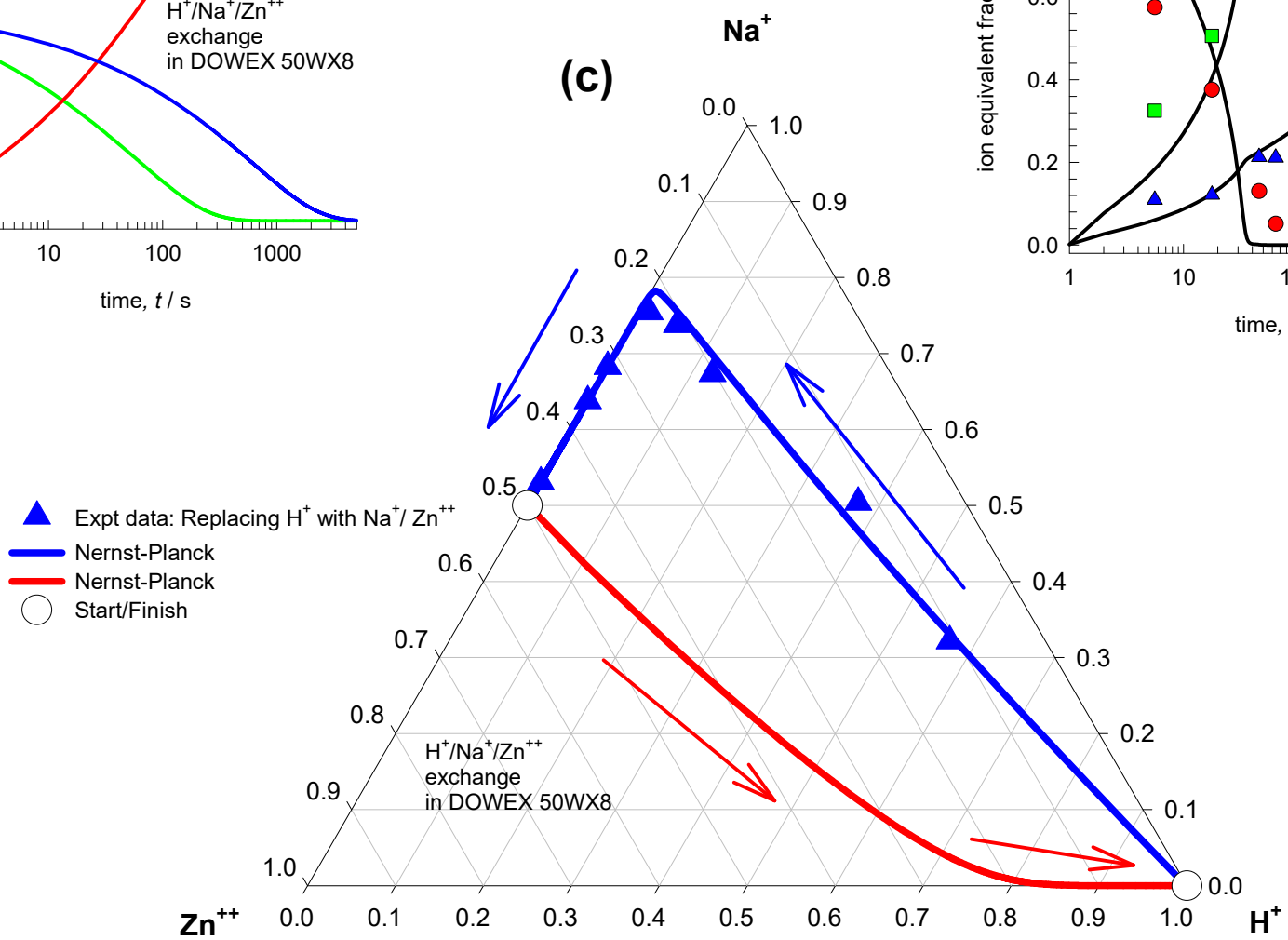
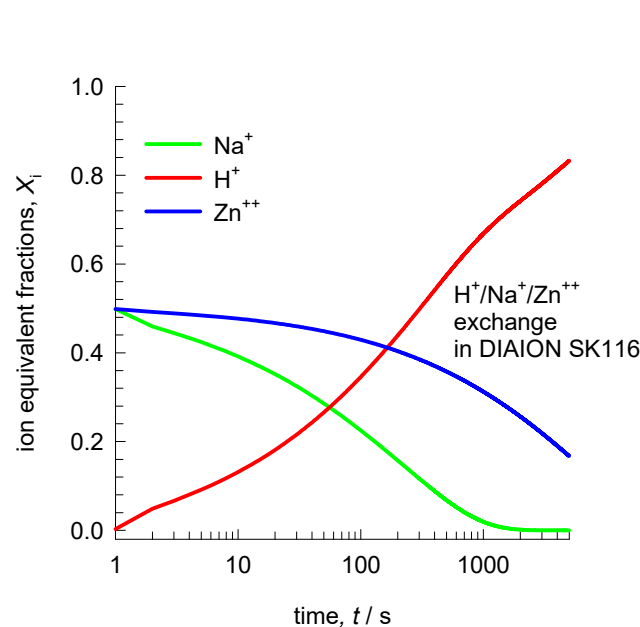


Figure S33

(b)

Transient uptake and asymmetry



- ▲ Expt data: Replacing H^+ with $\text{Na}^+/\text{Zn}^{++}$
- Nernst-Planck
- Nernst-Planck
- Start/Finish

(c)

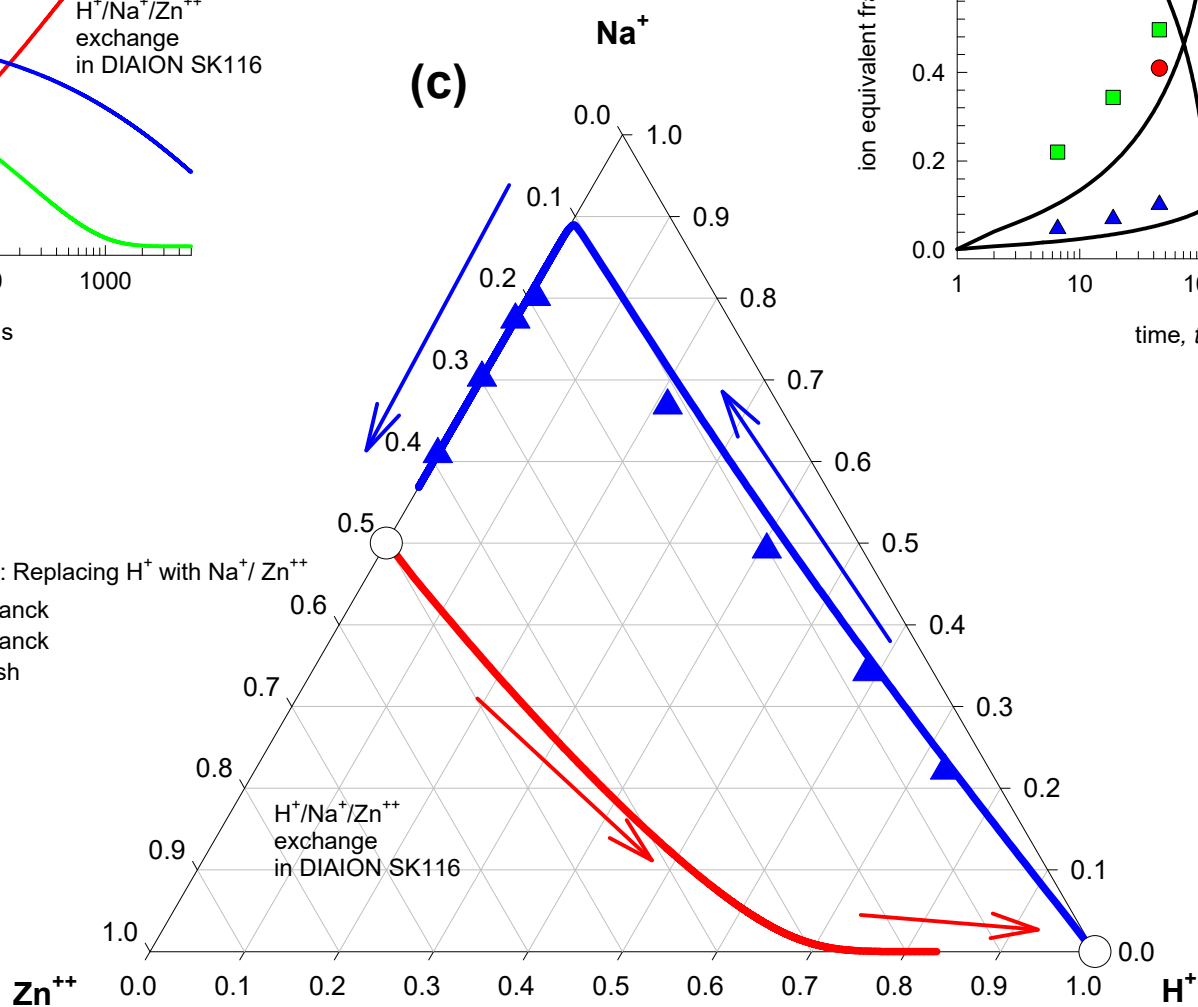
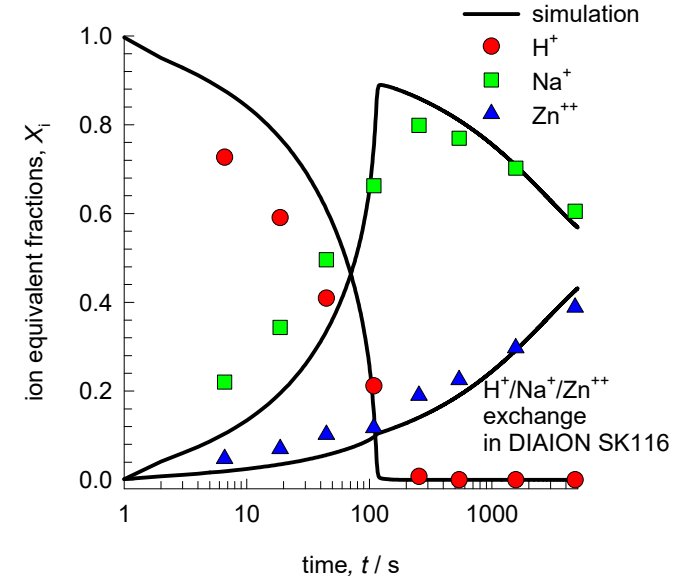
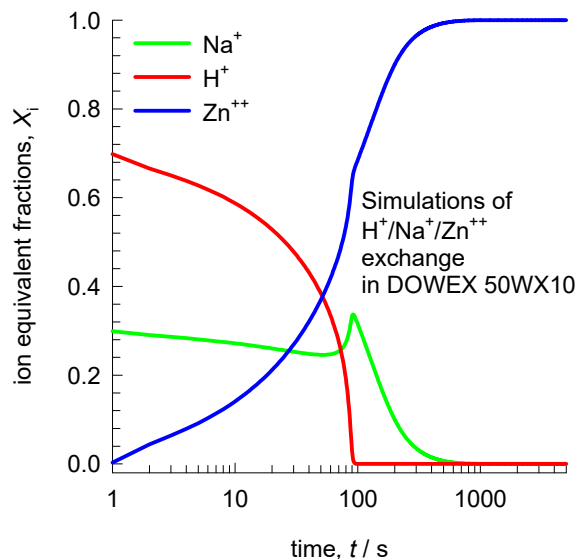
 (σ') 

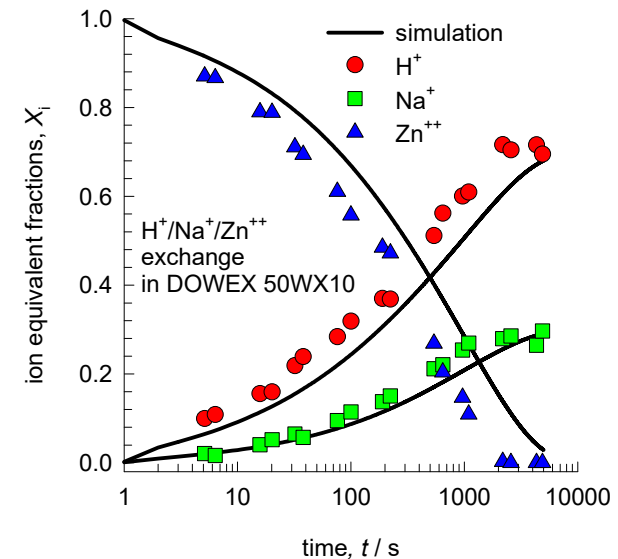
Figure S34

(b)



- Expt data: Replacing Zn^{++} with H^+/Na^+
- Nernst-Planck
- Nernst-Planck
- Start/Finish

(a)



(c)

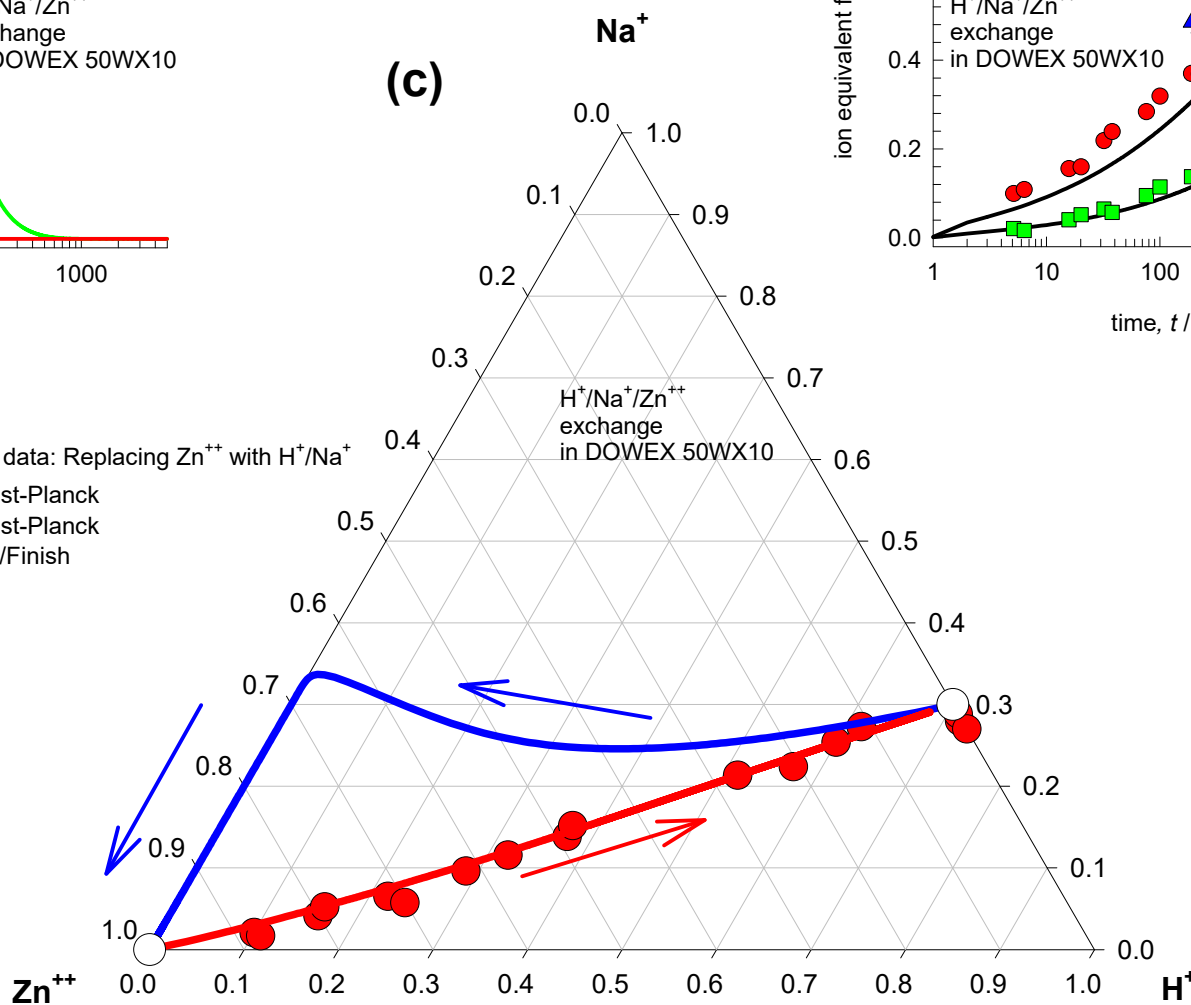
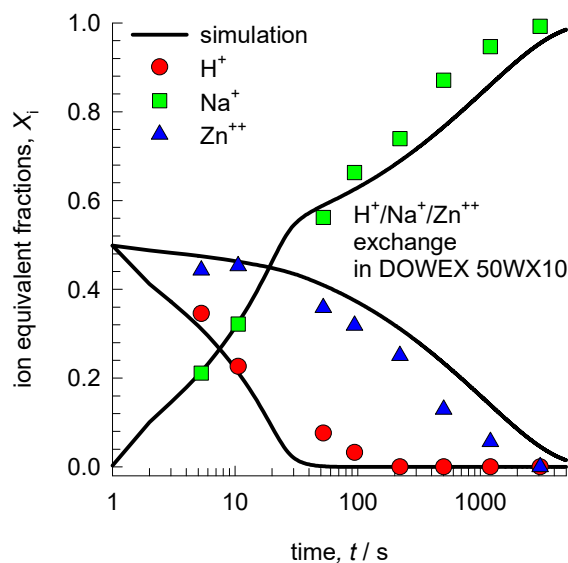
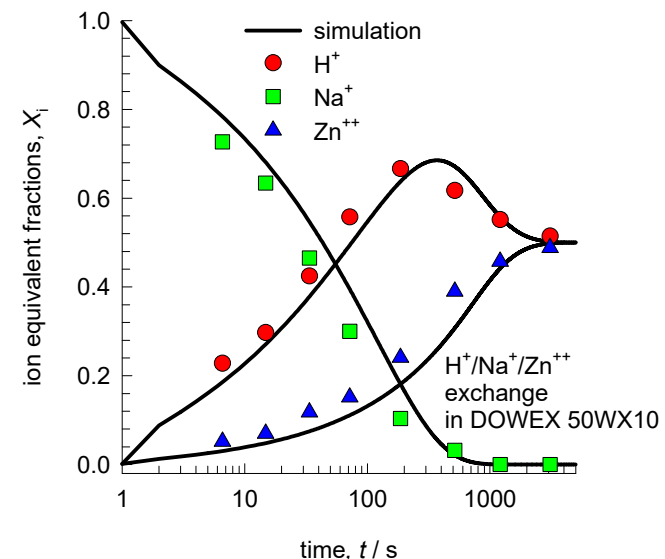


Figure S35

(b)



(a)



(c)

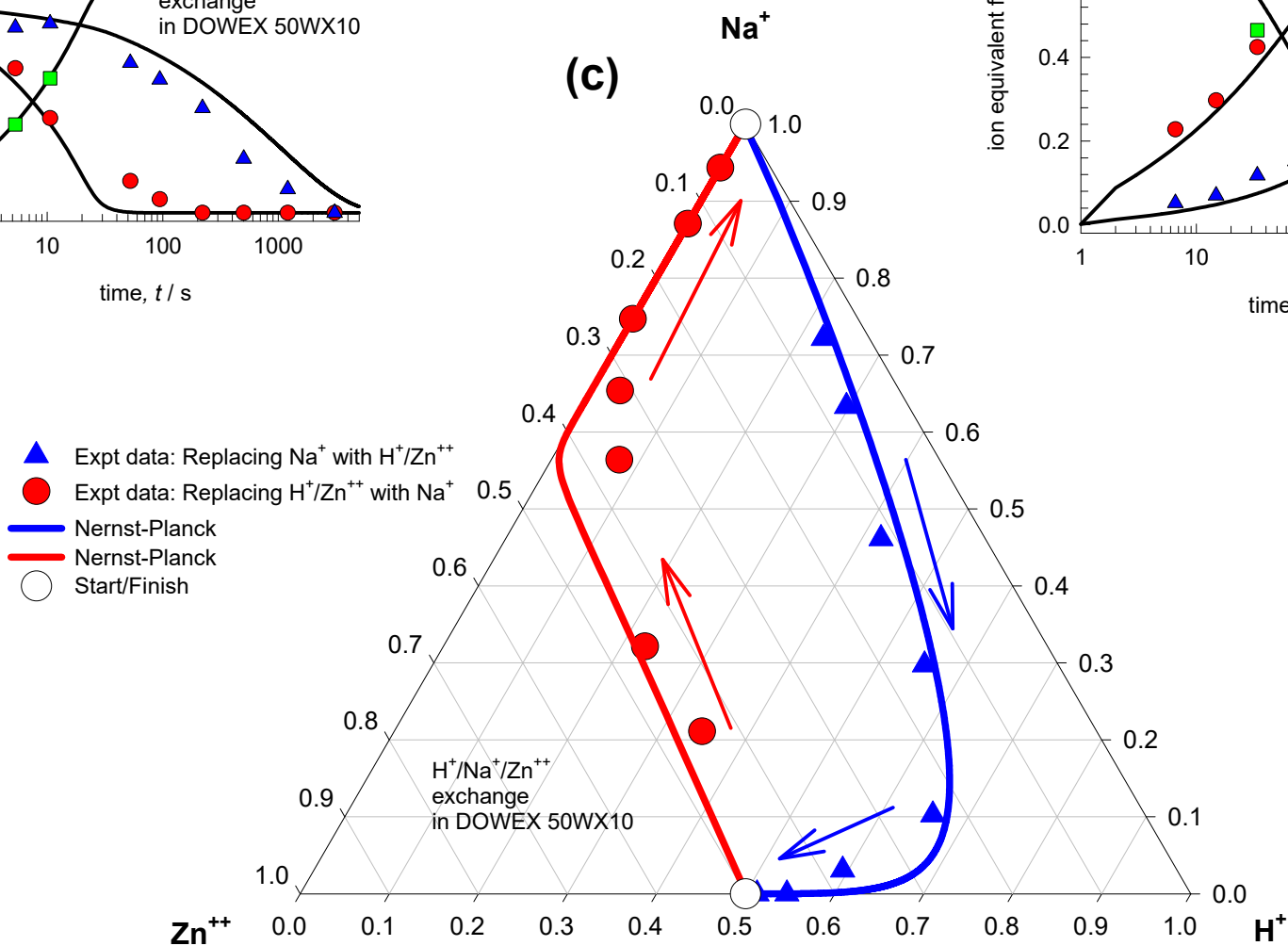
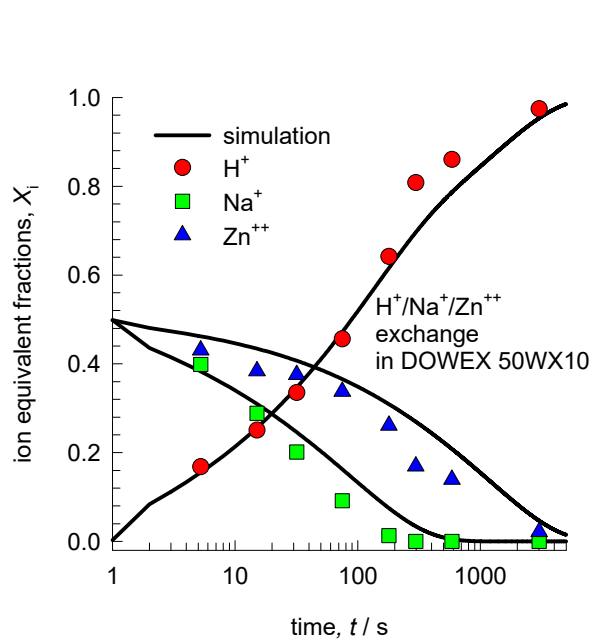


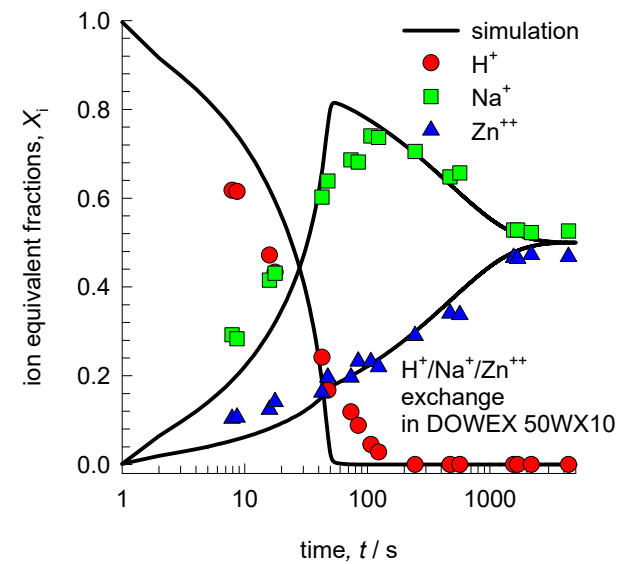
Figure S36

(b)

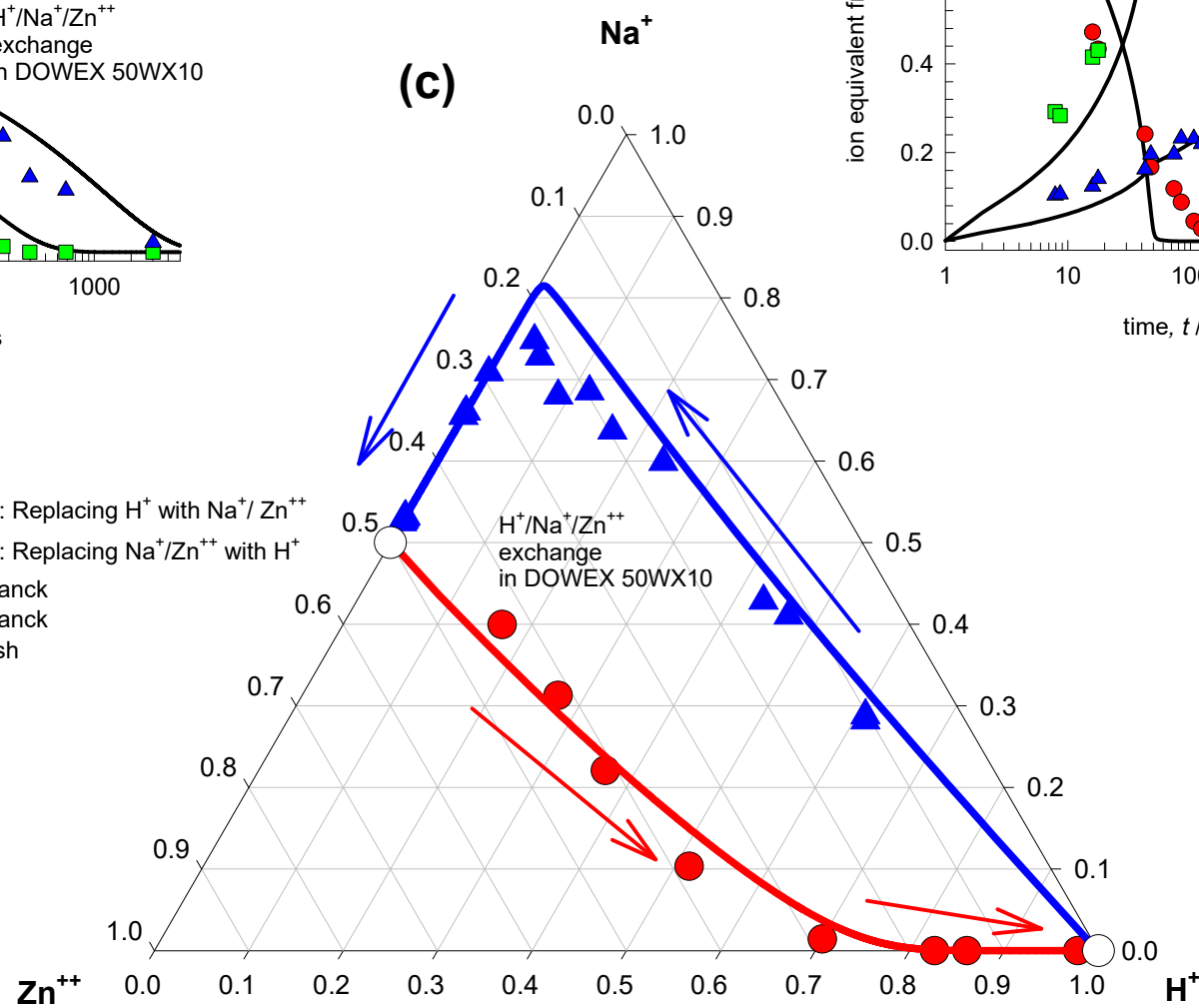


- Expt data: Replacing H^+ with Na^+/Zn^{++} (blue triangles)
- Expt data: Replacing Na^+/Zn^{++} with H^+ (red circles)
- Nernst-Planck (blue line)
- Nernst-Planck (red line)
- Start/Finish (white circle)

(a)

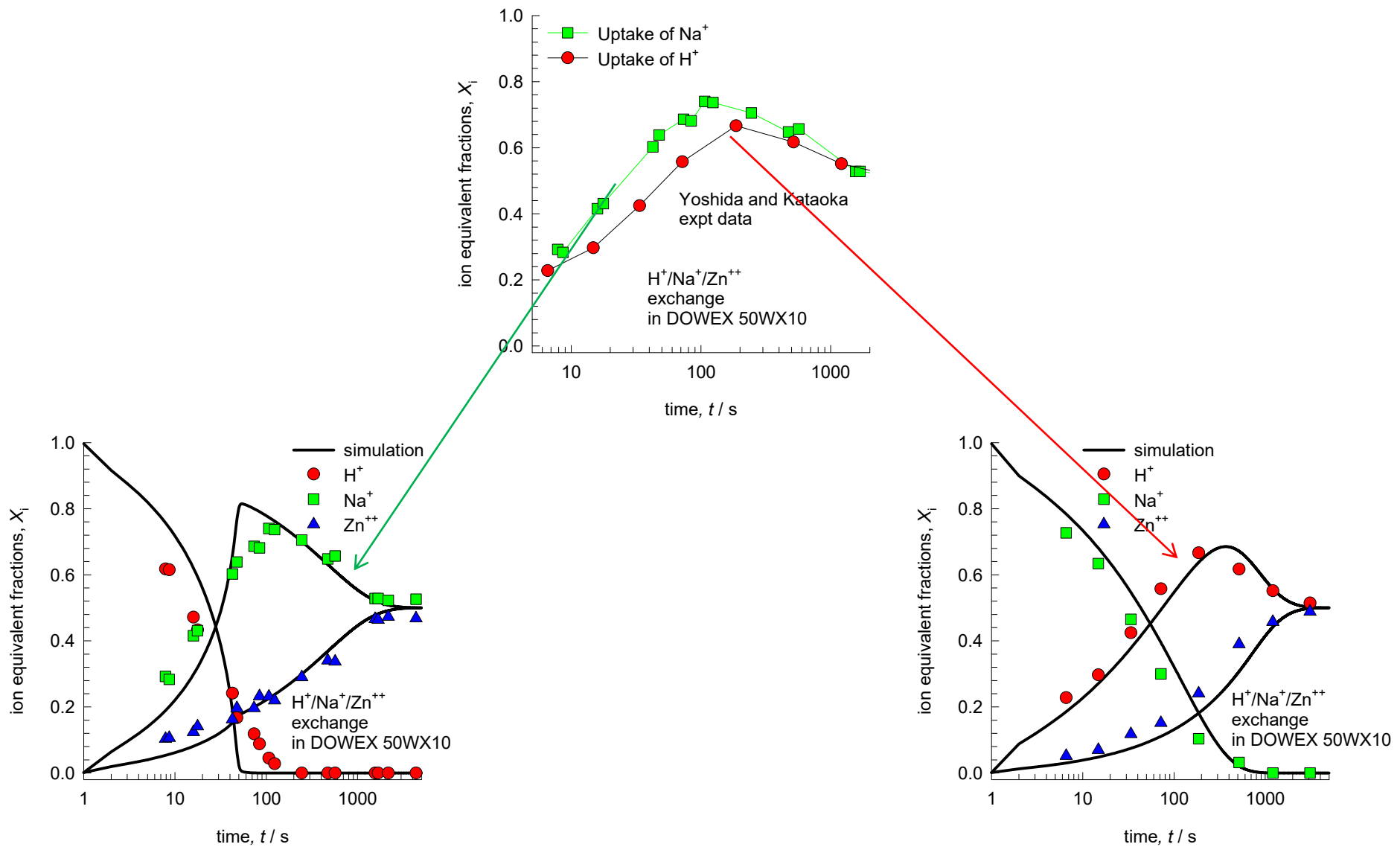


(c)



Comparisons of overshoots

Figure S37



Transient overshoot in ion exchanger

Figure S38

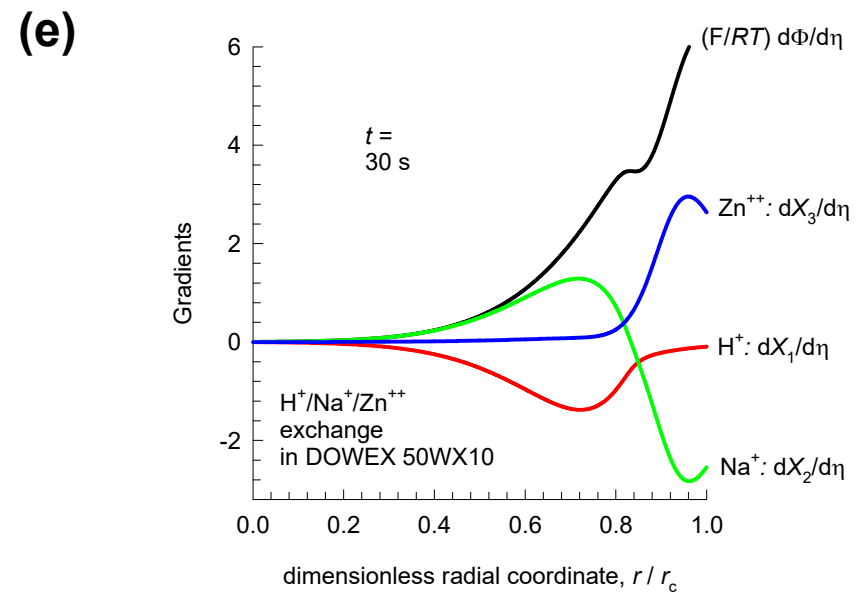
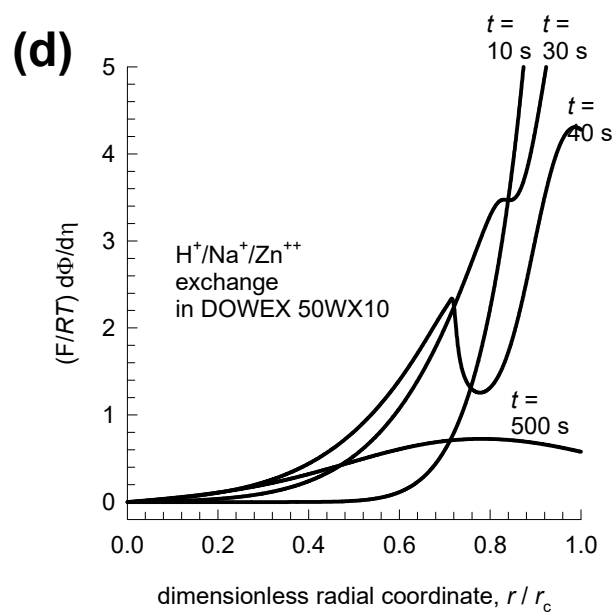
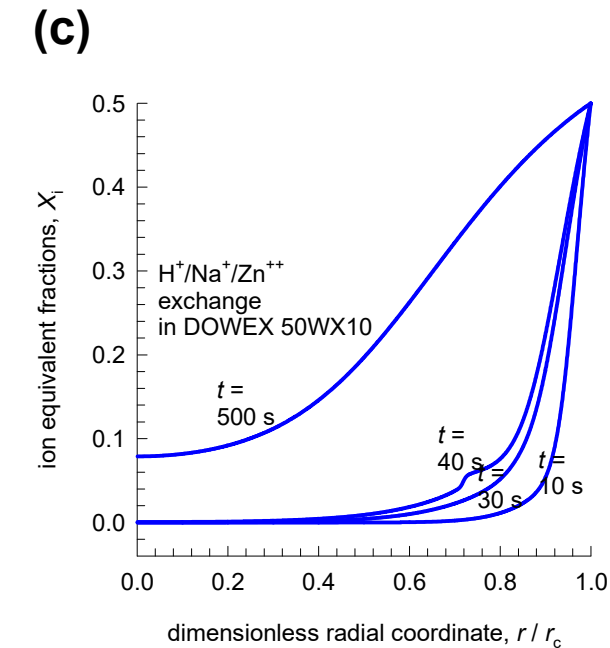
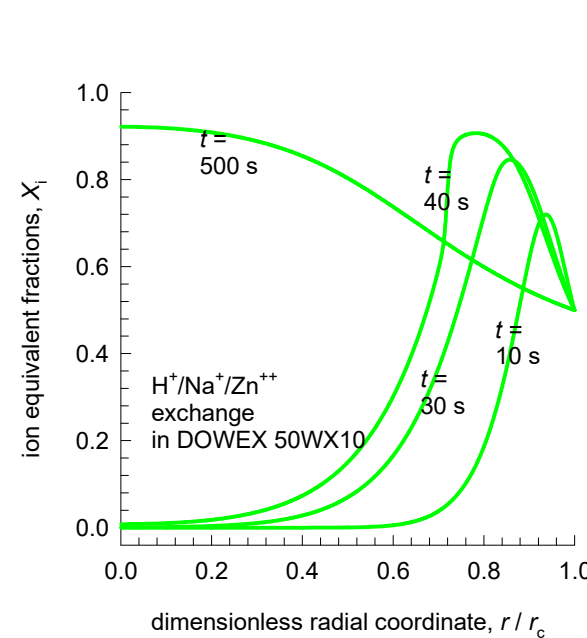
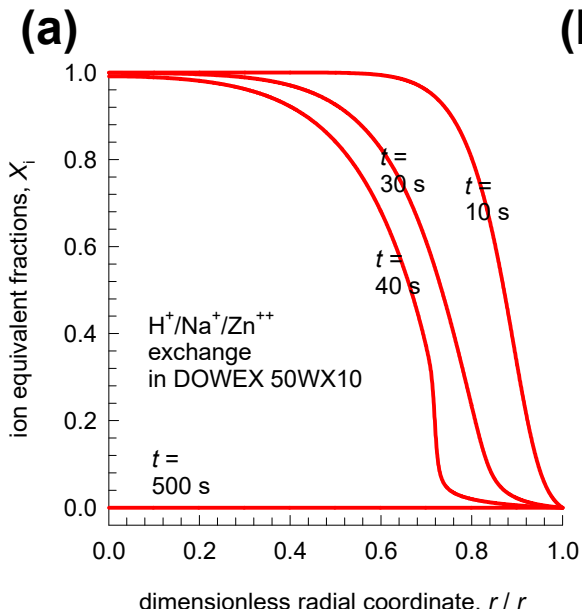
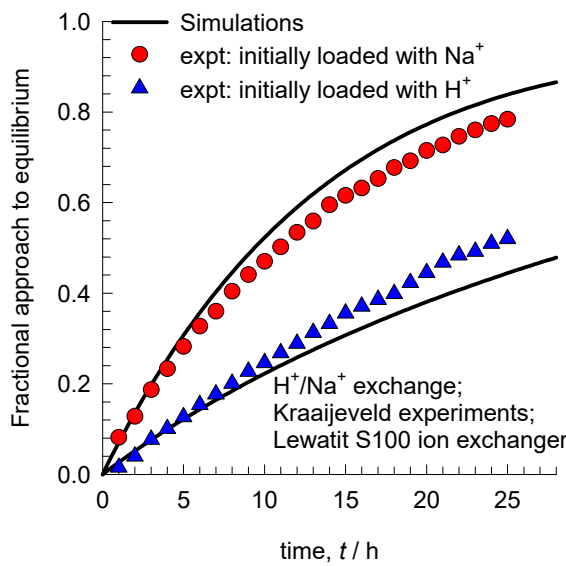


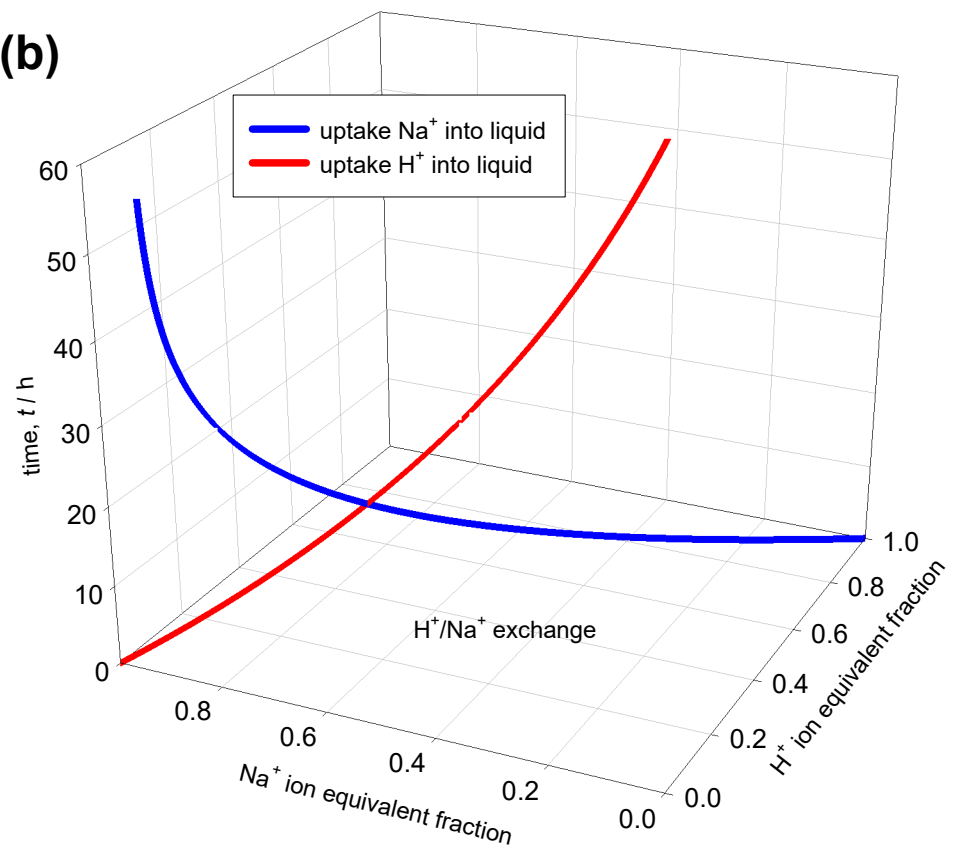
Figure S39

Asymmetry in Ion-Exchange Kinetics Limited by Transport of Ions from Bulk Liquid to Particle Surface

(a)



(b)



The calculations are those plotted in Figure S2 and Figure S5 of Supplementary Material

ORIGIN = 1

$$DMS(c) := \exp \left[-10.56 + \frac{0.1918\sqrt{c}}{1+\sqrt{c}} + (-0.3638)c + 0.1356c^{1.5} + (-0.03840)c^2 \right] \cdot 10^{-4}$$

$$Dplus(c) := \exp \left[-9.282 + \frac{0.3139\sqrt{c}}{1+\sqrt{c}} + (-0.4583)c + 0.1375c^{1.5} + (-0.03996)c^2 \right] \cdot 10^{-4}$$

$$Dmin(c) := \exp \left[-11.45 + \frac{0.1604\sqrt{c}}{1+\sqrt{c}} + (-0.3309)c + 0.1211c^{1.5} + (-0.03275)c^2 \right] \cdot 10^{-4}$$

$$Dplmin(c) := \exp \left[-14.09 + \frac{0.5634\sqrt{c}}{1+\sqrt{c}} + 1.456c + (-0.9512)c^{1.5} + 0.1535c^2 \right] \cdot \sqrt{c} \cdot 10^{-4}$$

i := 1 .. 391

$$t_i := 10^{-3+(i-1)\cdot 0.01}$$

$$zplus := 1 \quad zmin := -2$$

$$Dplus_i := Dplus(t_i) \cdot 10^9$$

$$Dmin_i := Dmin(t_i) \cdot 10^9$$

$$Dplmin_i := Dplmin(t_i) \cdot 10^9$$

$$D_i := DMS(t_i) \cdot 10^9$$

$$\text{sqrtc}_i := \sqrt(t_i)$$

$$Dsw_i := \frac{Dplus_i \cdot Dmin_i \cdot (zplus - zmin)}{zplus \cdot Dplus_i - zmin \cdot Dmin_i}$$

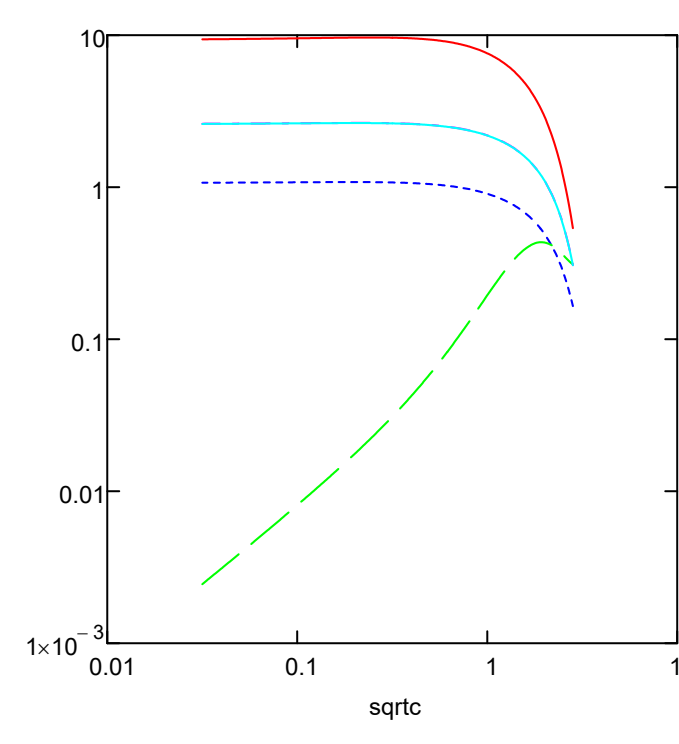
	1
1	1·10 ⁻³
2	1.023·10 ⁻³
3	1.047·10 ⁻³
4	1.072·10 ⁻³
5	1.096·10 ⁻³
6	1.122·10 ⁻³
7	1.148·10 ⁻³
8	1.175·10 ⁻³
9	1.202·10 ⁻³
10	1.23·10 ⁻³
11	1.259·10 ⁻³
12	1.288·10 ⁻³
13	1.318·10 ⁻³
14	1.349·10 ⁻³
15	1.38·10 ⁻³
16	...

	1
1	9.394
2	9.395
3	9.396
4	9.397
5	9.398
6	9.399
7	9.4
8	9.401
9	9.402
10	9.403
11	9.404
12	9.405
13	9.406
14	9.407
15	9.408
16	...

	1
1	1.07
2	1.07
3	1.07
4	1.07
5	1.07
6	1.07
7	1.07
8	1.07
9	1.07
10	1.07
11	1.07
12	1.07
13	1.07
14	1.071
15	1.071
16	...

	1
1	2.449·10 ⁻³
2	2.477·10 ⁻³
3	2.507·10 ⁻³
4	2.536·10 ⁻³
5	2.566·10 ⁻³
6	2.597·10 ⁻³
7	2.627·10 ⁻³
8	2.658·10 ⁻³
9	2.69·10 ⁻³
10	2.722·10 ⁻³
11	2.754·10 ⁻³
12	2.787·10 ⁻³
13	2.82·10 ⁻³
14	2.853·10 ⁻³
15	2.887·10 ⁻³
16	...

	1
1	2.608
2	2.608
3	2.608
4	2.608
5	2.608
6	2.608
7	2.609
8	2.609
9	2.609
10	2.609
11	2.609
12	2.609
13	2.61
14	2.61
15	2.61
16	...



Mwater := 18

ρwater := 1000

$$c_{water} := \frac{\rho_{water}}{M_{water}}$$

cwater = 55.556

$$\rho(c) := \exp \left[-0.002904 + (0.06814)c + (-0.007375)c^{1.5} + (-0.0001617)c^2 \right]$$

$$ct(c) := (c_{water} + c) \cdot \rho(c)$$

$$D(c) := DMS(c) \cdot \frac{ct(c)}{c_{water}} \cdot \Gamma(c)$$

$$xplus(c) := \frac{2 \cdot c}{ct(c)}$$

$$xmin(c) := \frac{c}{ct(c)}$$

$$xwat(c) := \frac{c_{water}}{ct(c)}$$

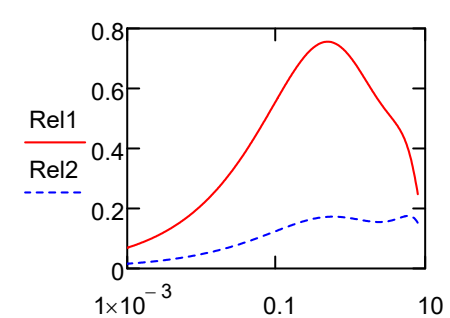
$$Rel1_i := \frac{xmin_i}{Dplmin_i}$$

$$Rel2_i := \frac{xplus_i}{Dmin_i}$$

$$Rel1 := \frac{xplus}{Dmin}$$

$$Rel2 := \frac{xplus}{Dmin}$$

	1
1	0.016
2	0.016
3	0.016
4	0.016
5	0.016
6	0.017
7	0.017
8	0.017
9	0.017
10	0.017
11	0.018
12	0.018
13	0.018
14	0.018
15	0.018
16	...



The calculations are those plotted in Figure S6 of Supplementary Material

System: 1: H+ 2: Cl- 3: Ba++ 4: H₂O

ORIGIN= 1

Charges

z1 := 1 z2 := -1 z3 := 2

Ionic diffusivities

D1 := 9.3·10⁻⁹ D2 := 2·10⁻⁹ D3 := 0.85·10⁻⁹F := 9.65·10⁴ T := 25 + 273.15 R := 8.3144

$$DW := \begin{pmatrix} D1 & 0 \\ 0 & D2 \end{pmatrix} \quad DLeash(c1, c2, c3) := \frac{\begin{bmatrix} c1 \cdot z1 \cdot D1 \cdot z1 \cdot (D1 - D3) & c1 \cdot z1 \cdot D1 \cdot z2 \cdot (D2 - D3) \\ c2 \cdot z2 \cdot D2 \cdot z1 \cdot (D1 - D3) & c2 \cdot z2 \cdot D2 \cdot z2 \cdot (D2 - D3) \end{bmatrix}}{(c1 \cdot z1^2 \cdot D1 + c2 \cdot z2^2 \cdot D2 + c3 \cdot z3^2 \cdot D3)}$$

D(c1, c2, c3) := DW + DLeash(c1, c2, c3)

$$\Delta\Phi(c1, c2, c3) := \frac{[-z1 \cdot D1 \cdot c1 + z2 \cdot D2 \cdot (c2) + z3 \cdot D3 \cdot (c3)]}{(c1 \cdot z1^2 \cdot D1 + c2 \cdot z2^2 \cdot D2 + c3 \cdot z3^2 \cdot D3) \cdot \frac{F}{R \cdot T}}$$

$$D1eff(c1, c2, c3) := DW_{1,1} + DLeash(c1, c2, c3)_{1,1} \cdot \frac{c1}{c1} + DLeash(c1, c2, c3)_{1,2} \cdot \frac{c2}{c1}$$

$$D2eff(c1, c2, c3) := DW_{2,2} + DLeash(c1, c2, c3)_{2,1} \cdot \frac{c1}{c2} + DLeash(c1, c2, c3)_{2,2} \cdot \frac{c2}{c2}$$

$$D3eff(c1, c2, c3) := D3 + c3 \cdot z3 \cdot D3 \cdot \frac{\frac{F}{R \cdot T}}{c3}$$

i := 1 .. 1000

r_i := i·0.01c3_i := 1c1_i := r_i c3_ic2_i := c1_i + 2·c3_i

$$D1_i := D1eff(c1_i, c2_i, c3_i) \cdot 10^9$$

$$D2_i := D2eff(c1_i, c2_i, c3_i) \cdot 10^9$$

$$D3_i := D3eff(c1_i, c2_i, c3_i) \cdot 10^9$$

$$\Delta\Phi_i := \Delta\Phi(c1_i, c2_i, c3_i)$$

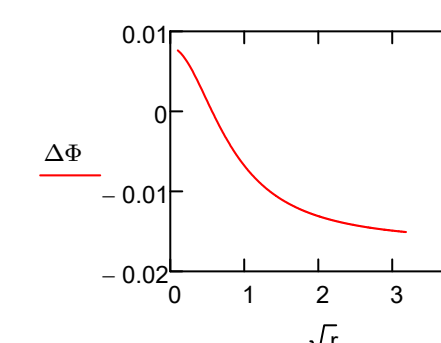
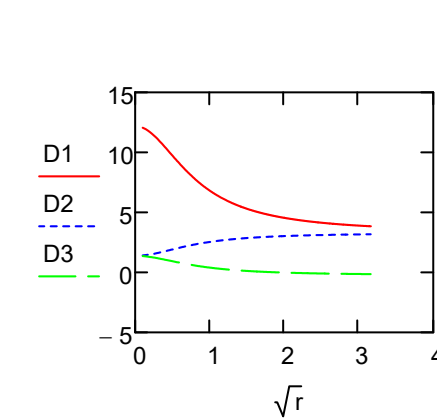
	1
1	0.01
2	0.02
3	0.03
4	0.04
5	0.05
6	0.06
7	0.07
8	0.08
9	0.09
10	0.1
11	0.11
12	0.12
13	0.13
14	0.14
15	0.15
16	...

	1
1	12.057
2	11.927
3	11.801
4	11.678
5	11.559
6	11.444
7	11.331
8	11.222
9	11.115
10	11.012
11	10.911
12	10.812
13	10.717
14	10.623
15	10.532
16	...

	1
1	1.407
2	1.435
3	1.462
4	1.489
5	1.514
6	1.539
7	1.563
8	1.587
9	1.61
10	1.632
11	1.654
12	1.675
13	1.695
14	1.715
15	1.735
16	...

	1
1	1.354
2	1.33
3	1.307
4	1.285
5	1.263
6	1.242
7	1.221
8	1.201
9	1.182
10	1.163
11	1.144
12	1.126
13	1.109
14	1.092
15	1.075
16	...

$$D3 = \begin{array}{l} 1 \\ \hline 1 & 7.61457 \cdot 10^{-3} \\ 2 & 7.25583 \cdot 10^{-3} \\ 3 & 6.90758 \cdot 10^{-3} \\ 4 & 6.56934 \cdot 10^{-3} \\ 5 & 6.2407 \cdot 10^{-3} \\ 6 & 5.92126 \cdot 10^{-3} \\ 7 & 5.61063 \cdot 10^{-3} \\ 8 & 5.30846 \cdot 10^{-3} \\ 9 & 5.0144 \cdot 10^{-3} \\ 10 & 4.72813 \cdot 10^{-3} \\ 11 & 4.44934 \cdot 10^{-3} \\ 12 & 4.17775 \cdot 10^{-3} \\ 13 & 3.91308 \cdot 10^{-3} \\ 14 & 3.65507 \cdot 10^{-3} \\ 15 & 3.40348 \cdot 10^{-3} \\ 16 & \dots \end{array}$$



The calculations are those plotted in Figure S7 of Supplementary Material

System: 1: H⁺ 2: Cl⁻ 3: K⁺ 4: H₂O

ORIGIN= 1

Charges

z1 := 1 z2 := -1 z3 := 1 z4 := 0

Ionic diffusivities

D1 := 9.3·10⁻⁹ D2 := 2·10⁻⁹ D3 := 2·10⁻⁹F_w := 9.65·10⁴ T_w := 25 + 273.15 R_w := 8.3144

$$DW := \begin{pmatrix} D1 & 0 \\ 0 & D2 \end{pmatrix}$$

$$DLeash(c1, c2, c3) := \frac{[c1 \cdot z1 \cdot D1 \cdot z1 \cdot (D1 - D3) \quad c1 \cdot z1 \cdot D1 \cdot z2 \cdot (D2 - D3)]}{[c2 \cdot z2 \cdot D2 \cdot z1 \cdot (D1 - D3) \quad c2 \cdot z2 \cdot D2 \cdot z2 \cdot (D2 - D3)]}$$

$$(c1 \cdot z1^2 \cdot D1 + c2 \cdot z2^2 \cdot D2 + c3 \cdot z3^2 \cdot D3)}$$

D(c1, c2, c3) := DW + DLeash(c1, c2, c3)

$$\Delta\Phi(c1, c2, c3) := \frac{-z1 \cdot D1 \cdot c1 + z2 \cdot D2 \cdot (c2) + z3 \cdot D3 \cdot (c3)}{(c1 \cdot z1^2 \cdot D1 + c2 \cdot z2^2 \cdot D2 + c3 \cdot z3^2 \cdot D3)} \cdot \frac{F}{R \cdot T}$$

$$D1eff(c1, c2, c3) := DW_{1,1} + DLeash(c1, c2, c3)_{1,1} \cdot \frac{c1}{c1} + DLeash(c1, c2, c3)_{1,2} \cdot \frac{c2}{c1}$$

$$D2eff(c1, c2, c3) := DW_{2,2} + DLeash(c1, c2, c3)_{2,1} \cdot \frac{c1}{c2} + DLeash(c1, c2, c3)_{2,2} \cdot \frac{c2}{c2}$$

$$D3eff(c1, c2, c3) := D3 + c3 \cdot z3 \cdot D3 \cdot \frac{F}{R \cdot T}$$

i := 1 .. 1000

r_i := i·0.01c3_i := 1c1_i := r_i·c3_ic2_i := c1_i + 1·c3_iD1_i := D1eff(c1_i, c2_i, c3_i) · 10⁹D2_i := D2eff(c1_i, c2_i, c3_i) · 10⁹D3_i := D3eff(c1_i, c2_i, c3_i) · 10⁹ΔΦ_i := ΔΦ(c1_i, c2_i, c3_i)

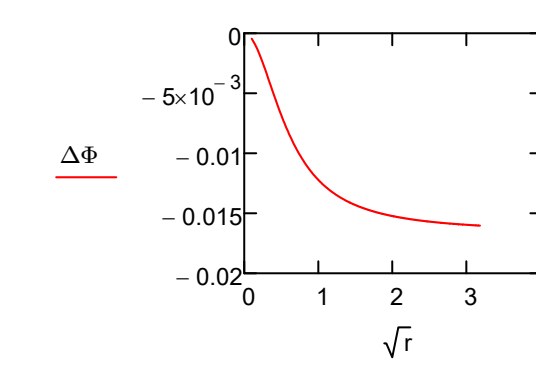
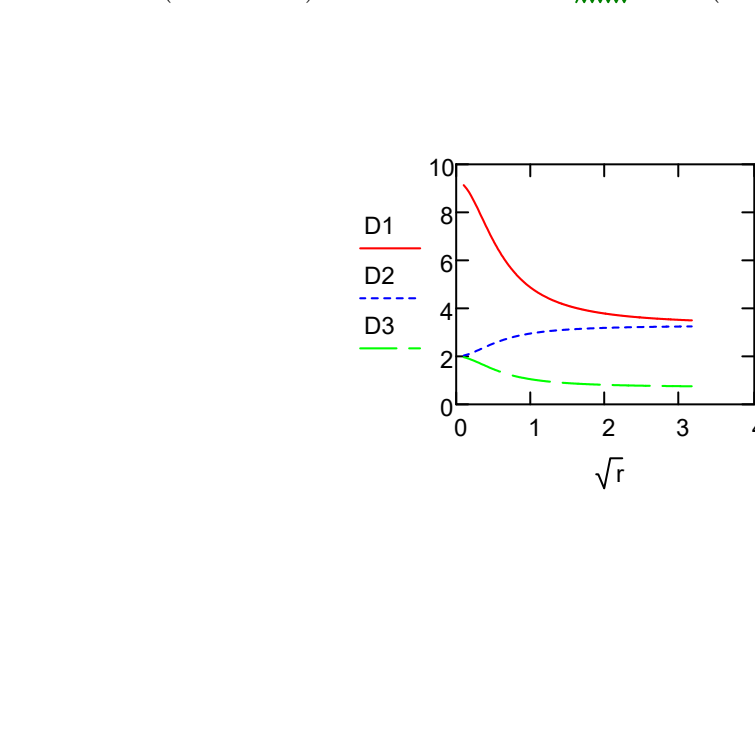
	1
1	0.01
2	0.02
3	0.03
4	0.04
5	0.05
6	0.06
7	0.07
8	0.08
9	0.09
10	0.1
11	0.11
12	0.12
13	0.13
14	0.14
15	0.15
16	...

	1
1	9.135
2	8.979
3	8.831
4	8.69
5	8.556
6	8.429
7	8.308
8	8.192
9	8.082
10	7.977
11	7.876
12	7.779
13	7.686
14	7.597
15	7.512
16	...

	1
1	2.035
2	2.069
3	2.101
4	2.131
5	2.16
6	2.187
7	2.213
8	2.238
9	2.262
10	2.285
11	2.306
12	2.327
13	2.347
14	2.366
15	2.385
16	...

	1
1	1.965
2	1.931
3	1.899
4	1.869
5	1.84
6	1.813
7	1.787
8	1.762
9	1.738
10	1.715
11	1.694
12	1.673
13	1.653
14	1.634
15	1.615
16	...

ΔΦ =



Transient diffusion between Left and Right compartments

The calculations are those plotted in Figure S8a of Supplementary Material

System: 1: H+ 2: Ba++ 3: Cl- 4: H₂O

ORIGIN= 1

Charges

$z1 := 1$ $z3 := -1$ $z2 := 2$

Ionic diffusivities

$$D1 := 9.3 \cdot 10^{-9} \quad D2 := 0.85 \cdot 10^{-9} \quad D3 := 2 \cdot 10^{-9}$$

$$F := 9.65 \cdot 10^4 \quad T := 25 + 273.15 \quad R := 8.3144$$

$$cHCl := 0.02 \quad cBaCl2 := 0.01$$

$$c1L := cHCl \quad c2L := cBaCl2 \quad c3L := cHCl + 2 \cdot cBaCl2$$

$$c1R := 0 \quad c2R := 0 \quad c3R := 0$$

$$c1eq := \frac{c1L + c1R}{2} \quad c2eq := \frac{c2L + c2R}{2} \quad c3eq := \frac{c3L + c3R}{2}$$

$$DW := \begin{pmatrix} D1 & 0 \\ 0 & D2 \end{pmatrix} \quad DLwash(c1, c2) := \frac{\begin{pmatrix} c1 \cdot z1 \cdot D1 \cdot z1 \cdot (D1 - D3) & c1 \cdot z1 \cdot D1 \cdot z2 \cdot (D2 - D3) \\ c2 \cdot z2 \cdot D2 \cdot z1 \cdot (D1 - D3) & c2 \cdot z2 \cdot D2 \cdot z2 \cdot (D2 - D3) \end{pmatrix}}{(c1 \cdot z1^2 \cdot D1 + c2 \cdot z2^2 \cdot D2 + c3(c1, c2) \cdot z3^2 \cdot D3)}$$

$$D(c1, c2) := DW + DLwash(c1, c2)$$

$$D1(c1, c2) := \text{eigenvals}(D(c1, c2))_1$$

$$D2(c1, c2) := \text{eigenvals}(D(c1, c2))_2$$

$$I := \begin{pmatrix} 1 & 0 \\ 0 & 1 \end{pmatrix} \quad f(D, z) := \begin{pmatrix} \text{erf}\left(\frac{z}{\sqrt{D}}\right) \\ 1 \end{pmatrix} \quad Dref := 1 \cdot 10^{-9}$$

$$Q(c1, c2, z) := \frac{f(D1(c1, c2), z) \cdot (D(c1, c2) - D2(c1, c2)) \cdot I}{(D1(c1, c2) - D2(c1, c2))} \dots \\ + \frac{f(D2(c1, c2), z) \cdot (D(c1, c2) - D1(c1, c2)) \cdot I}{(D2(c1, c2) - D1(c1, c2))}$$

$$zL := -4 \quad zR := 4$$

$$i := 1 .. 100$$

$$z_i := zL + \frac{(zR - zL) \cdot i}{100}$$

$$c1_1 := c1L \quad c2_1 := c2L \quad c3_1 := c3L$$

$$\begin{pmatrix} c1_{i+1} \\ c2_{i+1} \end{pmatrix} := Q(c1_i, c2_i, z_i) \begin{pmatrix} c1R - c1L \\ c2R - c2L \end{pmatrix} + \begin{pmatrix} c1R + c1L \\ c2R + c2L \end{pmatrix}$$

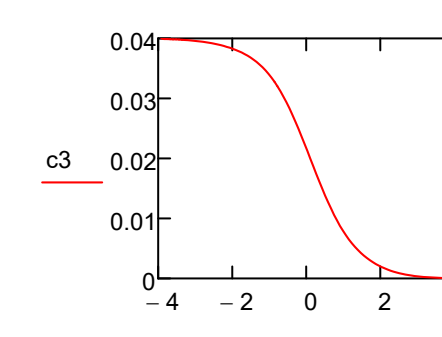
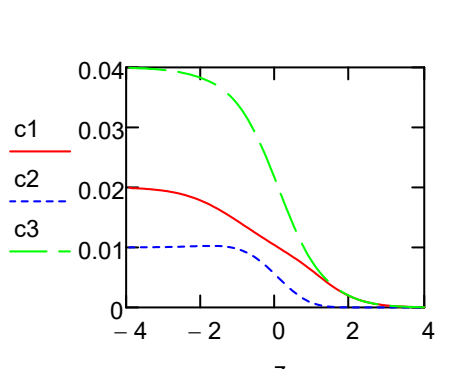
$$c3_i := c1_i + 2 \cdot c2_i$$

	1
1	-3.92
2	-3.84
3	-3.76
4	-3.68
5	-3.6
6	-3.52
7	-3.44
8	-3.36
9	-3.28
10	-3.2
11	-3.12
12	-3.04
13	-2.96
14	-2.88
15	-2.8
16	...

	1
1	0.02
2	0.01988
3	0.01986
4	0.01983
5	0.01981
6	0.01978
7	0.01974
8	0.0197
9	0.01966
10	0.01961
11	0.01956
12	0.01949
13	0.01942
14	0.01935
15	0.01926
16	...

	1
1	0.01
2	0.01001
3	0.01002
4	0.01002
5	0.01002
6	0.01003
7	0.01003
8	0.01003
9	0.01004
10	0.01004
11	0.01005
12	0.01006
13	0.01007
14	0.01007
15	0.01008
16	...

	1
1	0.04
2	0.0399
3	0.03989
4	0.03987
5	0.03985
6	0.03983
7	0.0398
8	0.03977
9	0.03974
10	0.0397
11	0.03966
12	0.03961
13	0.03956
14	0.0395
15	0.03943
16	...



The calculations are those plotted in Figure S8b of Supplementary Material

System: 1: H⁺2: NO₃⁻3: Na⁺4: Cl⁻

ORIGIN = 1

Charges

$$z1 := 1 \quad z2 := -1 \quad z3 := 1 \quad z4 := -1$$

Ionic diffusivities

$$D1 := 9.3 \cdot 10^{-9} \quad D2 := 1.9 \cdot 10^{-9} \quad D3 := 1.3 \cdot 10^{-9} \quad D4 := 2 \cdot 10^{-9}$$

$$F := 9.65 \cdot 10^4 \quad T := 25 + 273.15 \quad R := 8.3144$$

$$cHNO3 := 0.1$$

$$cNaCl := 0.1$$

$$c1R := 0 \quad c2R := 0 \quad c3R := cNaCl \quad c4R := cNaCl$$

$$c1L := cHNO3 \quad c2L := cHNO3 \quad c3L := cNaCl \quad c4L := cNaCl$$

$$c4(c1, c2, c3) := \frac{(z1 \cdot c1 + z2 \cdot c2 + z3 \cdot c3)}{-z4}$$

$$c1eq := \frac{c1L + c1R}{2} \quad c2eq := \frac{c2L + c2R}{2} \quad c3eq := \frac{c3L + c3R}{2} \quad c4eq := \frac{c4L + c4R}{2}$$

$$DW := \begin{pmatrix} D1 & 0 & 0 \\ 0 & D2 & 0 \\ 0 & 0 & D3 \end{pmatrix} \quad DLeash(c1, c2, c3) := \frac{\begin{bmatrix} c1 \cdot z1 \cdot D1 \cdot z1 \cdot (D1 - D4) & c1 \cdot z1 \cdot D1 \cdot z2 \cdot (D2 - D4) & c1 \cdot z1 \cdot D1 \cdot z3 \cdot (D3 - D4) \\ c2 \cdot z2 \cdot D2 \cdot [z1 \cdot (D1 - D4)] & c2 \cdot z2 \cdot D2 \cdot [z2 \cdot (D2 - D4)] & c2 \cdot z2 \cdot D2 \cdot [z3 \cdot (D3 - D4)] \\ c3 \cdot z3 \cdot D3 \cdot [z1 \cdot (D1 - D4)] & c3 \cdot z3 \cdot D3 \cdot [z2 \cdot (D2 - D4)] & c3 \cdot z3 \cdot D3 \cdot [z3 \cdot (D3 - D4)] \end{bmatrix}}{(c1 \cdot z1^2 \cdot D1 + c2 \cdot z2^2 \cdot D2 + c3 \cdot z3^2 \cdot D3 + c4(c1, c2, c3) \cdot z4^2 \cdot D4)}$$

$$D(c1, c2, c3) := DW + DLeash(c1, c2, c3)$$

$$\beta := 10000$$

$$I := \begin{pmatrix} 1 & 0 & 0 \\ 0 & 1 & 0 \\ 0 & 0 & 1 \end{pmatrix}$$

$$D1(c1, c2, c3) := \text{eigvals}(D(c1, c2, c3))_1$$

$$D2(c1, c2, c3) := \text{eigvals}(D(c1, c2, c3))_2$$

$$D3(c1, c2, c3) := \text{eigvals}(D(c1, c2, c3))_3$$

$$Dref := 1 \cdot 10^{-9} \quad f(D, z) := \left(\operatorname{erf} \left(\frac{z}{\sqrt{\frac{D}{Dref}}} \right) \right)$$

$$Q(c1, c2, c3, z) := \frac{f(D1(c1, c2, c3), z) \cdot (D(c1, c2, c3) - D2(c1, c2, c3) \cdot I) \cdot (D(c1, c2, c3) - D3(c1, c2, c3) \cdot I)}{(D1(c1, c2, c3) - D2(c1, c2, c3) \cdot I) \cdot (D1(c1, c2, c3) - D3(c1, c2, c3) \cdot I)} \dots$$

$$+ \frac{f(D2(c1, c2, c3), z) \cdot (D(c1, c2, c3) - D1(c1, c2, c3) \cdot I) \cdot (D(c1, c2, c3) - D3(c1, c2, c3) \cdot I)}{(D2(c1, c2, c3) - D1(c1, c2, c3) \cdot I) \cdot (D(c1, c2, c3) - D3(c1, c2, c3) \cdot I)} \dots$$

$$+ \frac{f(D3(c1, c2, c3), z) \cdot (D(c1, c2, c3) - D1(c1, c2, c3) \cdot I) \cdot (D(c1, c2, c3) - D2(c1, c2, c3) \cdot I)}{(D3(c1, c2, c3) - D1(c1, c2, c3) \cdot I) \cdot (D3(c1, c2, c3) - D2(c1, c2, c3) \cdot I)}$$

$$z1 := -4 \quad z2 := 4$$

$$i := 1..100$$

$$z_i := z1 + \frac{(z2 - z1)}{100} \cdot i$$

$$c1_1 := c1L$$

$$c2_1 := c2L$$

$$c3_1 := c3L$$

$$\begin{pmatrix} c1_{i+1} \\ c2_{i+1} \\ c3_{i+1} \end{pmatrix} := Q(c1_i, c2_i, c3_i, z_i) \cdot \begin{pmatrix} c1R - c1L \\ c2R - c2L \\ c3R - c3L \end{pmatrix} + \frac{1}{2} \begin{pmatrix} c1R + c1L \\ c2R + c2L \\ c3R + c3L \end{pmatrix}$$

$$c4 := c4(c1_i, c2_i, c3_i)$$

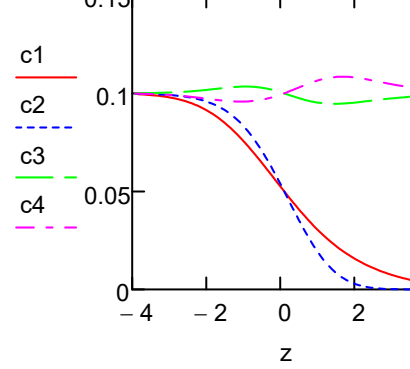
	1
1	-3.92
2	-3.84
3	-3.76
4	-3.68
5	-3.6
6	-3.52
7	-3.44
8	-3.36
9	-3.28
10	-3.2
11	-3.12
12	-3.04
13	-2.96
14	-2.88
15	-2.8
16	...

	1
1	0.1
2	0.09955
3	0.09947
4	0.09938
5	0.09928
6	0.09916
7	0.09903
8	0.09888
9	0.09871
10	0.09853
11	0.09831
12	0.09807
13	0.0978
14	0.0975
15	0.09717
16	...

	1
1	0.1
2	0.09983
3	0.0998
4	0.09976
5	0.09972
6	0.09968
7	0.09963
8	0.09957
9	0.0995
10	0.09942
11	0.09933
12	0.09923
13	0.09912
14	0.09899
15	0.09884
16	...

	1
1	0.1
2	0.1001
3	0.10011
4	0.10013
5	0.10015
6	0.10018
7	0.1002
8	0.10024
9	0.10027
10	0.10031
11	0.10036
12	0.10041
13	0.10046
14	0.10053
15	0.1006
16	...

	1
1	0.1
2	0.09981
3	0.09978
4	0.09975
5	0.09971
6	0.09966
7	0.09961
8	0.09955
9	0.09949
10	0.09941
11	0.09933
12	0.09925
13	0.09915
14	0.09904
15	0.09892
16	...



The calculations are those plotted in Figure S9 of Supplementary Material

System: 1: H+ 2: Ba++ 3: Cl- 4: H2O

ORIGIN= 1

Charges

z1 := 1 z3 := -1 z2 := 2

Ionic diffusivities

$$D1 := 9.3 \cdot 10^{-9} \quad D2 := 0.85 \cdot 10^{-9} \quad D3 := 2 \cdot 10^{-9}$$

$$F_w = 9.65 \cdot 10^4 \quad T_w := 25 + 273.15 \quad R_w = 8.3144$$

$$cHCl := 0.01 \quad cBaCl2 := 0.01$$

$$c1 := cHCl \quad c3 := cHCl + 2 \cdot cBaCl2 \quad c2 := cBaCl2$$

$$c1 = 0.01 \quad c2 = 0.01 \quad c3 = 0.03$$

$$c3(c1, c2) := z1 \cdot c1 + z2 \cdot c2$$

$$DW := \begin{pmatrix} D1 & 0 \\ 0 & D2 \end{pmatrix} \quad DLeash(c1, c2) := \frac{\begin{bmatrix} c1 \cdot z1 \cdot D1 \cdot z1 \cdot (D1 - D3) & c1 \cdot z1 \cdot D1 \cdot z2 \cdot (D2 - D3) \\ c2 \cdot z2 \cdot D2 \cdot z1 \cdot (D1 - D3) & c2 \cdot z2 \cdot D2 \cdot z2 \cdot (D2 - D3) \end{bmatrix}}{(c1 \cdot z1^2 \cdot D1 + c2 \cdot z2^2 \cdot D2 + c3(c1, c2) \cdot z3^2 \cdot D3)}$$

$$D(c1, c2) := DW + DLeash(c1, c2)$$

$$D1(c1, c2) := \text{eigenvals}(D(c1, c2))_1$$

$$D2(c1, c2) := \text{eigenvals}(D(c1, c2))_2$$

$$r := 0.265 \cdot 10^{-3} \quad u := 0.01 \quad L := 15$$

$$Q := u \cdot \pi \cdot r^2 \quad Q = 2.20618 \times 10^{-9}$$

$$\sigma(D) := \frac{u^2 \cdot r^2}{48 \cdot D}$$

$$f(D, t) := \frac{1}{2 \cdot \pi \cdot r^2 \cdot \sqrt{\pi \cdot \sigma(D) \cdot t}} \cdot \exp\left[-\frac{(L - u \cdot t)^2}{4 \cdot \sigma(D) \cdot t}\right] \quad I := \begin{pmatrix} 1 & 0 \\ 0 & 1 \end{pmatrix}$$

$$QQ(t) := \frac{f(D1(c1, c2), t) \cdot (D(c1, c2) - D2(c1, c2) \cdot I)}{(D1(c1, c2) - D2(c1, c2))} \dots$$

$$+ \frac{f(D2(c1, c2), t) \cdot (D(c1, c2) - D1(c1, c2) \cdot I)}{(D2(c1, c2) - D1(c1, c2))}$$

$$M1 := 1 \cdot M2 \quad M2 := 10^{-9}$$

$$M3 := M1 + 2 \cdot M2$$

$$j := 1 \dots 500$$

$$t_j := 1250 + j \cdot 1$$

$$c(t) := QQ(t) \begin{pmatrix} M1 \\ M2 \end{pmatrix}$$

$$c1_{1j} := c(t_j)_1$$

$$c2_{1j} := c(t_j)_2$$

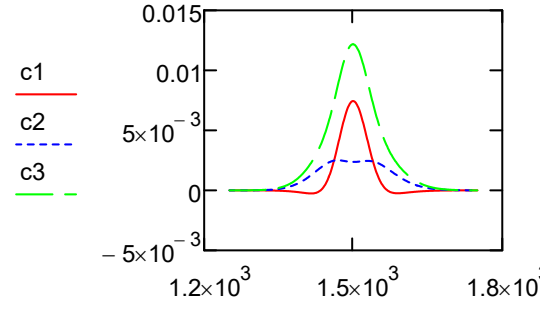
$$c3_{1j} := c1_j + 2 \cdot c2_j$$

	1
1	1.251 \cdot 10^3
2	1.252 \cdot 10^3
3	1.253 \cdot 10^3
4	1.254 \cdot 10^3
5	1.255 \cdot 10^3
6	1.256 \cdot 10^3
7	1.257 \cdot 10^3
8	1.258 \cdot 10^3
9	1.259 \cdot 10^3
10	1.26 \cdot 10^3
11	1.261 \cdot 10^3
12	1.262 \cdot 10^3
13	1.263 \cdot 10^3
14	1.264 \cdot 10^3
15	1.265 \cdot 10^3
16	...

	1
1	-3.05348 \cdot 10^{-8}
2	-3.34559 \cdot 10^{-8}
3	-3.66388 \cdot 10^{-8}
4	-4.01052 \cdot 10^{-8}
5	-4.38786 \cdot 10^{-8}
6	-4.7984 \cdot 10^{-8}
7	-5.24486 \cdot 10^{-8}
8	-5.73012 \cdot 10^{-8}
9	-6.25731 \cdot 10^{-8}
10	-6.82977 \cdot 10^{-8}
11	-7.45108 \cdot 10^{-8}
12	-8.12507 \cdot 10^{-8}
13	-8.85587 \cdot 10^{-8}
14	-9.64787 \cdot 10^{-8}
15	-1.05058 \cdot 10^{-7}
16	...

	1
1	1.1851 \cdot 10^{-7}
2	1.29847 \cdot 10^{-7}
3	1.422 \cdot 10^{-7}
4	1.55654 \cdot 10^{-7}
5	1.70299 \cdot 10^{-7}
6	1.86233 \cdot 10^{-7}
7	2.0356 \cdot 10^{-7}
8	2.22394 \cdot 10^{-7}
9	2.42855 \cdot 10^{-7}
10	2.65073 \cdot 10^{-7}
11	2.89186 \cdot 10^{-7}
12	3.15345 \cdot 10^{-7}
13	3.43708 \cdot 10^{-7}
14	3.74447 \cdot 10^{-7}
15	4.07744 \cdot 10^{-7}
16	...

	1
1	2.06484 \cdot 10^{-7}
2	2.26238 \cdot 10^{-7}
3	2.47761 \cdot 10^{-7}
4	2.71202 \cdot 10^{-7}
5	2.96719 \cdot 10^{-7}
6	3.24481 \cdot 10^{-7}
7	3.54671 \cdot 10^{-7}
8	3.87486 \cdot 10^{-7}
9	4.23136 \cdot 10^{-7}
10	4.61847 \cdot 10^{-7}
11	5.03862 \cdot 10^{-7}
12	5.49439 \cdot 10^{-7}
13	5.98858 \cdot 10^{-7}
14	6.52415 \cdot 10^{-7}
15	7.1043 \cdot 10^{-7}
16	...



Equilibration in Left and Right compartments separated by a porous diaphragm

The calculations are those plotted in Figure S10 of Supplementary Material

System: 1: H+ 3: Cl- 2: Ba++ 4: H2O

ORIGIN = 1

Charges

$z1 := 1$ $z3 := -1$ $z2 := 2$ $z4 := 0$

Ionic diffusivities

$D1 := 9.3 \cdot 10^{-9}$ $D3 := 2 \cdot 10^{-9}$ $D2 := 0.85 \cdot 10^{-9}$

$F := 9.65 \cdot 10^4$ $T := 25 + 273.15$ $R := 8.3144$

$cHCl := 0.04$

$cBaCl2 := 0.02$

$c1L0 := cHCl$ $c3L0 := cHCl$ $c2L0 := 0$

$c1R0 := 0$ $c3R0 := 2 \cdot cBaCl2$ $c2R0 := cBaCl2$

$$c1eq := \frac{(c1L0 + c1R0)}{2} \quad c2eq := \frac{(c2L0 + c2R0)}{2} \quad c3eq := \frac{(c3L0 + c3R0)}{2}$$

$c1eq = 0.02$

$c2eq = 0.01$

$c3eq = 0.04$

$c3(c1, c2) := z1 \cdot c1 + z2 \cdot c2$

$DW = \begin{pmatrix} D1 & 0 \\ 0 & D2 \end{pmatrix}$

$$DLeash(c1, c2) := \frac{\begin{bmatrix} c1 \cdot z1 \cdot D1 \cdot z1 \cdot (D1 - D3) & c1 \cdot z1 \cdot D1 \cdot z2 \cdot (D2 - D3) \\ c2 \cdot z2 \cdot D2 \cdot z1 \cdot (D1 - D3) & c2 \cdot z2 \cdot D2 \cdot z2 \cdot (D2 - D3) \end{bmatrix}}{(c1 \cdot z1^2 \cdot D1 + c2 \cdot z2^2 \cdot D2 + c3(c1, c2) \cdot z3^2 \cdot D3)}$$

$D(c1, c2) := DW + DLeash(c1, c2)$

$D1(c1, c2) := \text{eigvals}(D(c1, c2))_1$

$D2(c1, c2) := \text{eigvals}(D(c1, c2))_2$

$\beta := 10000$

$$I := \begin{pmatrix} 1 & 0 \\ 0 & 1 \end{pmatrix}$$

$f(D, t) := \exp(-\beta \cdot D \cdot t)$

$i := 1..100$

$t_i := (i - 1) \cdot 3600$

Equilibration in Left compartment

$c1 := c1L0$ $c2 := c2L0$ $c3 := c3L0$

$$\begin{pmatrix} c1_{i+1} \\ c2_{i+1} \end{pmatrix} := Q \left(\frac{c1_i + c1eq}{2}, \frac{c2_i + c2eq}{2}, t_i \right) \begin{pmatrix} c1L0 - c1eq \\ c2L0 - c2eq \end{pmatrix} + \begin{pmatrix} c1eq \\ c2eq \end{pmatrix}$$

$c3_i := c1_i + 2 \cdot c2_i$

$c3(c1, c2) := z1 \cdot c1 + z2 \cdot c2$

$$\Delta\Phi_L(c1, c2) := \frac{-z1 \cdot D1 \cdot (c1 - c1L0) - z2 \cdot D2 \cdot (c2 - c2L0) - z3 \cdot D3 \cdot (c3(c1, c2) - c3L0)}{(c1 \cdot z1^2 \cdot D1 + c2 \cdot z2^2 \cdot D2 + c3(c1, c2) \cdot z3^2 \cdot D3)} \cdot \frac{F}{R \cdot T}$$

$$\Delta\Phi_{L,i} := \Delta\Phi_L \left(\frac{c1_i + c1eq}{2}, \frac{c2_i + c2eq}{2} \right)$$

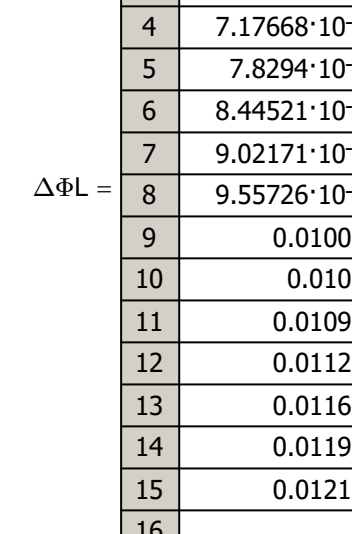
t	1
1	0
2	1
3	2
4	3
5	4
6	5
7	6
8	7
9	8
10	9
11	10
12	11
13	12
14	13
15	14
16	...
3600	

t	1
1	0.04
2	0.04
3	0.03795
4	0.03609
5	0.0344
6	0.03288
7	0.03151
8	0.03027
9	0.02917
10	0.02819
11	0.02732
12	0.02655
13	0.02587
14	0.02527
15	0.02474
16	...

t	1
1	0
2	0
3	4.30267 \cdot 10^{-4}
4	8.52417 \cdot 10^{-4}
5	1.2648 \cdot 10^{-3}
6	1.66587 \cdot 10^{-3}
7	2.05423 \cdot 10^{-3}
8	2.42872 \cdot 10^{-3}
9	2.78842 \cdot 10^{-3}
10	3.1327 \cdot 10^{-3}
11	3.46121 \cdot 10^{-3}
12	3.77384 \cdot 10^{-3}
13	4.07074 \cdot 10^{-3}
14	4.35226 \cdot 10^{-3}
15	4.61889 \cdot 10^{-3}
16	...

t	1
1	0.04
2	0.04
3	0.03881
4	0.03779
5	0.03693
6	0.03621
7	0.03561
8	0.03513
9	0.03475
10	0.03446
11	0.03424
12	0.0341
13	0.03401
14	0.03397
15	0.03398
16	...

t	1
1	5.77308 \cdot 10^{-3}
2	5.77308 \cdot 10^{-3}
3	6.49007 \cdot 10^{-3}
4	7.17668 \cdot 10^{-3}
5	7.8294 \cdot 10^{-3}
6	8.44521 \cdot 10^{-3}
7	9.02171 \cdot 10^{-3}
8	9.55726 \cdot 10^{-3}
9	0.01005
10	0.0105
11	0.01091
12	0.01128
13	0.01162
14	0.01192
15	0.01218
16	...



$c3(c1, c2) := z1 \cdot c1 + z2 \cdot c2$

$$\Delta\Phi_R(c1, c2) := \frac{-z1 \cdot D1 \cdot (c1 - c1R0) - z2 \cdot D2 \cdot (c2 - c2R0) - z3 \cdot D3 \cdot (c3(c1, c2) - c3R0)}{(c1 \cdot z1^2 \cdot D1 + c2 \cdot z2^2 \cdot D2 + c3(c1, c2) \cdot z3^2 \cdot D3)} \cdot \frac{F}{R \cdot T}$$

$$\Delta\Phi_{R,i} := \Delta\Phi_R \left(\frac{c1_i + c1eq}{2}, \frac{c2_i + c2eq}{2} \right)$$

t	1
1	0
2	1
3	2
4	3
5	4
6	5
7	6
8	7
9	8
10	9
11	10
12	11
13	12
14	13
15	14
16	...
3600	

t	1
1	0
2	0
3	3.74807 \cdot 10^{-3}
4	6.42407 \cdot 10^{-3}
5	8.49955 \cdot 10^{-3}
6	0.01016
7	0.01152
8	0.01264
9	0.01357
10	0.01436
11	0.01502
12	0.01559
13	0.01607
14	0.01648
15	0.01683
16	...

t	1
1	0.02
2	0.02
3	0.01908
4	0.01839
5	0.01783
6	0.01735
7	0.01693
8	0.01656
9	0.01622
10	0.0159
11	0.01562
12	0.01535
13	0.01511
14	0.01487
15	0.01466
16	...

t	1

<tbl

Equilibration in Left and Right compartments separated by a porous diaphragm

The calculations are those plotted in Figure S11 of Supplementary Material

System: 1: H+ 2: Cl- 3: K+ 4: H2O

ORIGIN = 1

Charges

$z1 := 1 \quad z3 := -1 \quad z2 := 1 \quad z4 := 0$

Ionic diffusivities

$D1 := 9.3 \cdot 10^{-9} \quad D3 := 2 \cdot 10^{-9} \quad D2 := 1.9 \cdot 10^{-9}$

$F := 9.65 \cdot 10^4$

$T := 25 + 273.15 \quad R := 8.3144$

$cHCl := 0.04$

$cKCl := 0.04$

$c1L0 := cHCl \quad c3L0 := cHCl \quad c2L0 := 0$

$c1R0 := 0 \quad c3R0 := cKCl \quad c2R0 := cKCl$

$$c1eq := \frac{(c1L0 + c1R0)}{2} \quad c2eq := \frac{(c2L0 + c2R0)}{2} \quad c3eq := \frac{(c3L0 + c3R0)}{2}$$

$c1eq = 0.02$

$c2eq = 0.02$

$c3eq = 0.04$

$c3(c1, c2) := z1 \cdot c1 + z2 \cdot c2$

$DW = \begin{pmatrix} D1 & 0 \\ 0 & D2 \end{pmatrix}$

$$DLeash(c1, c2) := \frac{\begin{bmatrix} c1 \cdot z1 \cdot D1 \cdot z1 \cdot (D1 - D3) & c1 \cdot z1 \cdot D1 \cdot z2 \cdot (D2 - D3) \\ c2 \cdot z2 \cdot D2 \cdot z1 \cdot (D1 - D3) & c2 \cdot z2 \cdot D2 \cdot z2 \cdot (D2 - D3) \end{bmatrix}}{(c1 \cdot z1^2 \cdot D1 + c2 \cdot z2^2 \cdot D2 + c3(c1, c2) \cdot z3^2 \cdot D3)}$$

$D(c1, c2) := DW + DLeash(c1, c2)$

$D1(c1, c2) := \text{eigvals}(D(c1, c2))_1$

$D2(c1, c2) := \text{eigvals}(D(c1, c2))_2$

$\beta := 10000$

$$I := \begin{pmatrix} 1 & 0 \\ 0 & 1 \end{pmatrix}$$

$f(D, t) := \exp(-\beta \cdot D \cdot t)$

$i := 1..100$

$t_i := (i - 1) \cdot 3600$

Equilibration in Left compartment

$c1 := c1L0 \quad c2 := c2L0 \quad c3 := c3L0$

$$\begin{pmatrix} c1_{i+1} \\ c2_{i+1} \end{pmatrix} := Q \left(\frac{c1_i + c1eq}{2}, \frac{c2_i + c2eq}{2}, t_i \right) \begin{pmatrix} c1L0 - c1eq \\ c2L0 - c2eq \end{pmatrix} + \begin{pmatrix} c1eq \\ c2eq \end{pmatrix}$$

$c3_i := c1_i + 1 \cdot c2_i$

$$\Delta\Phi_L(c1, c2) := \frac{-z1 \cdot D1 \cdot (c1 - c1L0) - z2 \cdot D2 \cdot (c2 - c2L0) - z3 \cdot D3 \cdot (c3(c1, c2) - c3L0)}{(c1 \cdot z1^2 \cdot D1 + c2 \cdot z2^2 \cdot D2 + c3(c1, c2) \cdot z3^2 \cdot D3)} \cdot \frac{F}{R \cdot T}$$

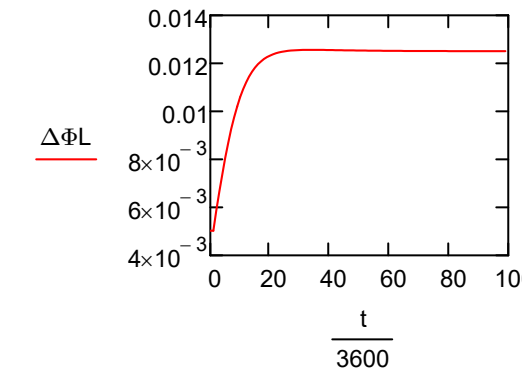
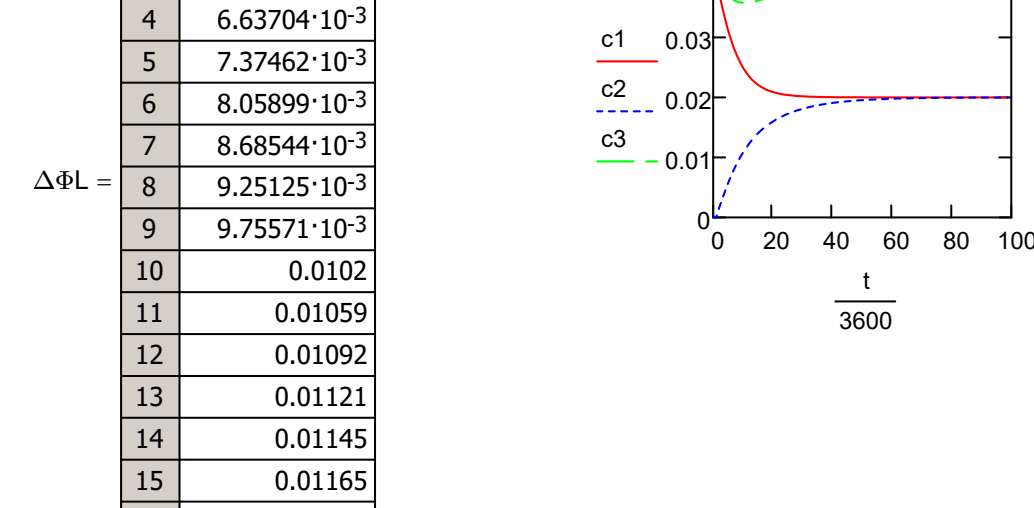
t	1	0
1	0	
2	1	
3	2	
4	3	
5	4	
6	5	
7	6	
8	7	
9	8	
10	9	
11	10	
12	11	
13	12	
14	13	
15	14	
16	...	

t	1	0.04
1	0.04	
2	0.04	
3	0.03742	
4	0.0351	
5	0.03302	
6	0.03118	
7	0.02957	
8	0.02815	
9	0.02692	
10	0.02586	
11	0.02496	
12	0.02418	
13	0.02353	
14	0.02297	
15	0.0225	
16	...	

t	1	0
1	0	
2	0	
3	0.03742	
4	0.0351	
5	0.03302	
6	0.03118	
7	0.02957	
8	0.02815	
9	0.02692	
10	0.02586	
11	0.02496	
12	0.02418	
13	0.02353	
14	0.02297	
15	0.0225	
16	...	

t	1	0.04
1	0.04	
2	0.04	
3	1.56394 \cdot 10^{-3}	
4	3.04123 \cdot 10^{-3}	
5	4.42788 \cdot 10^{-3}	
6	5.72128 \cdot 10^{-3}	
7	6.92041 \cdot 10^{-3}	
8	8.02596 \cdot 10^{-3}	
9	9.04027 \cdot 10^{-3}	
10	10.96713 \cdot 10^{-3}	
11	0.01081	
12	0.01158	
13	0.01228	
14	0.01291	
15	0.01348	
16	...	

t	1	0.04
1	0.04	
2	0.04	
3	0.03898	
4	0.03814	
5	0.03745	
6	0.03691	
7	0.03649	
8	0.03618	
9	0.03596	
10	0.03583	
11	0.03577	
12	0.03576	
13	0.0358	
14	0.03588	
15	0.03598	
16	...	



$c3(c1, c2) := z1 \cdot c1 + z2 \cdot c2$

$$\Delta\Phi_R(c1, c2) := \frac{-z1 \cdot D1 \cdot (c1 - c1R0) - z2 \cdot D2 \cdot (c2 - c2R0) - z3 \cdot D3 \cdot (c3(c1, c2) - c3R0)}{(c1 \cdot z1^2 \cdot D1 + c2 \cdot z2^2 \cdot D2 + c3(c1, c2) \cdot z3^2 \cdot D3)} \cdot \frac{F}{R \cdot T}$$

t	1	0
1	0	
2	1	
3	2	
4	3	
5	4	
6	5	
7	6	
8	7	
9	8	
10	9	
11	10	
12	11	
13	12	
14	13	
15	14	
16	...	

t	1	0
1	0	
2	0	
3	4.06175 \cdot 10^{-3}	
4	6.97746 \cdot 10^{-3}	
5	9.23551 \cdot 10^{-3}	
6	0.01104	
7	0.0125	
8	0.0137	
9	0.0147	
10	0.01553	
11	0.01622	
12	0.01681	
13	0.0173	
14	0.01771	
15	0.01806	
16	...	

t	1	0.04
1	0.04	
2	0.04	
3	0.03754	
4	0.03657	
5	0.03413	
6	0.03282	
7	0.03168	
8</		

Simulations of the Yang-Pintauro experiments for two compartments separated by cation exchange membrane. We assume that the diffusion resistance is in the bulk electrolyte liquids in either compartment.

The calculations are those plotted in Figure S12 and Figure 13a of Supplementary Material

System: 1: H+ 2: Na+ 3: Cs+ 4: SO4-

ORIGIN=1

Charges

$z1 := 1$ $z2 := 1$ $z3 := 1$ $z4 := -2$

Ionic diffusivities

$D1 := 9.3 \cdot 10^{-9}$ $D2 := 1.33 \cdot 10^{-9}$ $D3 := 2.06 \cdot 10^{-9}$ $D4 := 1.33 \cdot 10^{-9}$

$F := 9.65 \cdot 10^4$

$T_w = 25 + 273.15$

$R_w = 8.3144$

$c_{Na2SO4} := 0.125$ $c_{Cs2SO4} := 0.0054$ $c_{H2SO4} := 0.125$

$c_{1L0} := 0$ $c_{2L0} := 2 \cdot c_{Na2SO4}$ $c_{3L0} := 2 \cdot c_{Cs2SO4}$ $c_{4L0} := c_{Na2SO4} + c_{Cs2SO4}$

$c_{1R0} := 2 \cdot c_{H2SO4}$ $c_{2R0} := 0$ $c_{3R0} := 0$ $c_{4R0} := c_{H2SO4}$

$$c_{1eq} := \frac{(c_{1L0} + c_{1R0})}{2} \quad c_{2eq} := \frac{(c_{2L0} + c_{2R0})}{2} \quad c_{3eq} := \frac{(c_{3L0} + c_{3R0})}{2} \quad c_{4eq} := \frac{(c_{4L0} + c_{4R0})}{2}$$

$c_{1eq} = 0.125$

$c_{2eq} = 0.125$

$c_{3eq} = 5.4 \times 10^{-3}$

$c_{4eq} = 0.1277$

$c1 := c1eq$ $c2 := c2eq$ $c3 := c3eq$ $c4 := c4eq$

$$Dw := \begin{pmatrix} D1 & 0 & 0 \\ 0 & D2 & 0 \\ 0 & 0 & D3 \end{pmatrix}$$

$$D_{Leash}(c1, c2, c3) := \frac{\begin{bmatrix} c1 \cdot z1 \cdot D1 \cdot z1 \cdot D1 & c1 \cdot z1 \cdot (D1 \cdot z2 \cdot D2) & c1 \cdot z1 \cdot (D1 \cdot z3 \cdot D3) \\ c2 \cdot z2 \cdot D2 \cdot (z1 \cdot D1) & c2 \cdot z2 \cdot (D2 \cdot z2 \cdot D2) & c2 \cdot z2 \cdot (D2 \cdot z3 \cdot D3) \\ c3 \cdot z3 \cdot D3 \cdot (z1 \cdot D1) & c3 \cdot z3 \cdot (D3 \cdot z2 \cdot D2) & c3 \cdot z3 \cdot (D3 \cdot z3 \cdot D3) \end{bmatrix}}{(c1 \cdot z1^2 \cdot D1 + c2 \cdot z2^2 \cdot D2 + c3 \cdot z3^2 \cdot D3)}$$

$$D(c1, c2, c3) := Dw + D_{Leash}(c1, c2, c3)$$

$$\Delta \Phi := \frac{z1 \cdot (c1L0 - c1R0) + z2 \cdot (c2L0 - c2R0) + z3 \cdot (c3L0 - c3R0)}{-(c1 \cdot z1 + c2 \cdot z2 + c3 \cdot z3) \cdot z4 \cdot \frac{F}{R \cdot T}}$$

$\beta := 20000$

$f(D, t) := \exp(-\beta \cdot D \cdot t)$

$$I := \begin{pmatrix} 1 & 0 & 0 \\ 0 & 1 & 0 \\ 0 & 0 & 1 \end{pmatrix}$$

$D1(c1, c2, c3) := \text{eigenvals}(D(c1, c2, c3))_1$

$D2(c1, c2, c3) := \text{eigenvals}(D(c1, c2, c3))_2$

$D3(c1, c2, c3) := \text{eigenvals}(D(c1, c2, c3))_3$

$$Q(c1, c2, c3, t) := \frac{f(D1(c1, c2, c3), t) \cdot (D(c1, c2, c3) - D2(c1, c2, c3) \cdot I) \cdot (D(c1, c2, c3) - D3(c1, c2, c3) \cdot I)}{(D1(c1, c2, c3) - D2(c1, c2, c3)) \cdot (D(c1, c2, c3) - D3(c1, c2, c3))} \\ + \frac{f(D2(c1, c2, c3), t) \cdot (D(c1, c2, c3) - D1(c1, c2, c3) \cdot I) \cdot (D(c1, c2, c3) - D3(c1, c2, c3) \cdot I)}{(D2(c1, c2, c3) - D1(c1, c2, c3)) \cdot (D(c1, c2, c3) - D3(c1, c2, c3))} \\ + \frac{f(D3(c1, c2, c3), t) \cdot (D(c1, c2, c3) - D1(c1, c2, c3) \cdot I) \cdot (D(c1, c2, c3) - D2(c1, c2, c3) \cdot I)}{(D3(c1, c2, c3) - D1(c1, c2, c3)) \cdot (D3(c1, c2, c3) - D2(c1, c2, c3)))}$$

These are the simulations for the Left compartment

$i := 1..200$

$t_i := (i - 1) \cdot 3600 \cdot 0.4$

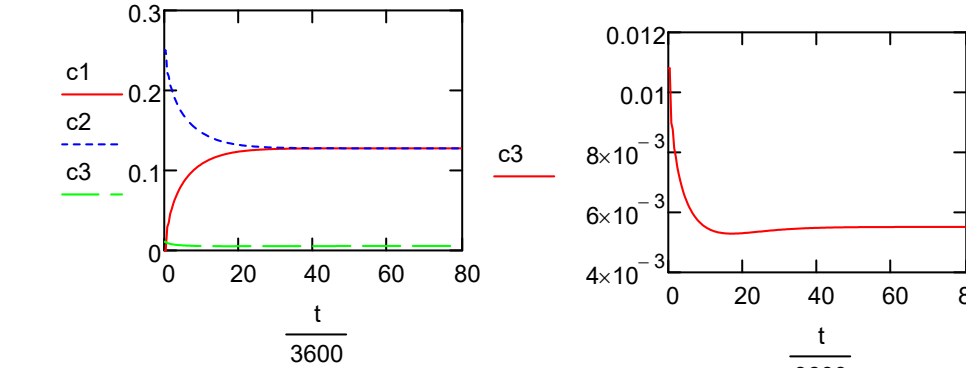
$c1_i := c1L0$ $c2_i := c2L0$ $c3_i := c3L0$

$$\begin{pmatrix} c1_{i+1} \\ c2_{i+1} \\ c3_{i+1} \end{pmatrix} := Q(c1_i, c2_i, c3_i, t_i) \cdot \begin{pmatrix} c1L0 - c1eq \\ c2L0 - c2eq \\ c3L0 - c3eq \end{pmatrix} + \begin{pmatrix} c1eq \\ c2eq \\ c3eq \end{pmatrix}$$

	1
1	0
2	0.4
3	0.8
4	1.2
5	1.6
6	2
7	2.4
8	2.8
9	3.2
10	3.6
11	4
12	4.4
13	4.8
14	5.2
15	5.6
16	...

	1
1	0
2	0.25
3	0.0293712
4	0.0346703
5	0.0457209
6	0.0517277
7	0.058232
8	0.0633111
9	0.0680683
10	0.0722282
11	0.0760331
12	0.0794807
13	0.0826431
14	0.0855485
15	0.0882304
16	...

	1
1	0.25
2	0.25
3	0.2224522
4	0.2173658
5	0.206941
6	0.2012205
7	0.1950494
8	0.1902106
9	0.1856792
10	0.1817087
11	0.1780741
12	0.1747762
13	0.1717478
14	0.1689623
15	0.1663881
16	...



These are the simulations for the Right compartment

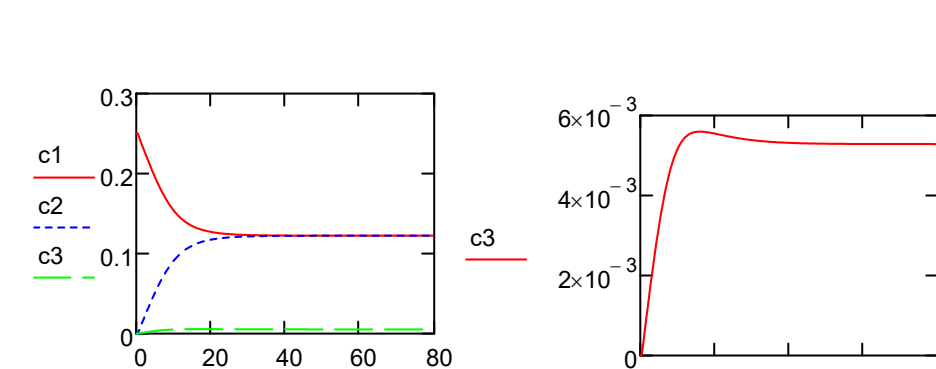
$c1 := c1R0$ $c2 := c2R0$ $c3 := c3R0$

$$\begin{pmatrix} c1_{i+1} \\ c2_{i+1} \\ c3_{i+1} \end{pmatrix} := Q(c1_i, c2_i, c3_i, t_i) \cdot \begin{pmatrix} c1R0 - c1eq \\ c2R0 - c2eq \\ c3R0 - c3eq \end{pmatrix} + \begin{pmatrix} c1eq \\ c2eq \\ c3eq \end{pmatrix}$$

	1
1	0
2	0.4
3	0.8
4	1.2
5	1.6
6	2
7	2.4
8	2.8
9	3.2
10	3.6
11	4
12	4.4
13	4.8
14	5.2
15	5.6
16	...

	1
1	0.25
2	0.25
3	0.2449915
4	0.2400199
5	0.2350907
6	0.2302101
7	0.2253845
8	0.2206209
9	0.2159266
10	0.2113094
11	0.2067774
12	0.2023387
13	0.1980019
14	0.1937753
15	0.1896675
16	...

	1
1	0
2	0
3	4.6974599 \cdot 10^{-3}
4	9.3615722 \cdot 10^{-3}
5	0.0139874
6	0.0185696
7	0.0231023
8	0.0275794
9	0.0319944
10	0.0363401
11	0.0406093
12	0.0447946
13	0.0488882
14	0.0528822
15	0.0567691
16	...



Simulations of the Yang-Pintauro experiments for two compartments separated by cation exchange membrane. We assume that the diffusion resistance is in the bulk electrolyte liquids in either compartment.

The calculations are those plotted in Figure S13b of Supplementary Material

System: 1: H+ 2: Na+ 3: Cs+ 4: SO4-

ORIGIN = 1

Charges

$z1 := 1$ $z2 := 1$ $z3 := 1$ $z4 := -2$

Ionic diffusivities

$D1 := 9.3 \cdot 10^{-9}$ $D2 := 1.33 \cdot 10^{-9}$ $D3 := 2.06 \cdot 10^{-9}$ $D4 := 1.33 \cdot 10^{-9}$

$F := 9.65 \cdot 10^4$

$T := 25 + 273.15$

$R := 8.3144$

$cNa2SO4 := 0.125$

$cCs2SO4 := 0.005$

$cH2SO4 := 0.12$

$c1L0 := 0$

$c2L0 := 2 \cdot cNa2SO4$

$c2L0 := 0.25$

$c3L0 := 0$

$c4L0 := cNa2SO4$

$c1R0 := 2 \cdot cH2SO4$

$c2R0 := 0$

$c3R0 := 2 \cdot cCs2SO4$

$c4R0 := cH2SO4 + cCs2SO4$

$c1eq := \frac{(c1L0 + c1R0)}{2}$

$c2eq := \frac{(c2L0 + c2R0)}{2}$

$c3eq := \frac{(c3L0 + c3R0)}{2}$

$c4eq := \frac{(c4L0 + c4R0)}{2}$

$c1eq = 0.12$

$c2eq = 0.125$

$c3eq = 5 \times 10^{-3}$

$c4eq = 0.125$

$c1 := c1eq$

$c2 := c2eq$

$c3 := c3eq$

$c4 := c4eq$

$DW := \begin{pmatrix} D1 & 0 & 0 \\ 0 & D2 & 0 \\ 0 & 0 & D3 \end{pmatrix}$

$DLeash(c1, c2, c3) := \frac{\begin{bmatrix} c1 \cdot z1 \cdot D1 \cdot z1 \cdot D1 & c1 \cdot z1 \cdot (D1 \cdot z2 \cdot D2) & c1 \cdot z1 \cdot (D1 \cdot z3 \cdot D3) \\ c2 \cdot z2 \cdot D2 \cdot (z1 \cdot D1) & c2 \cdot z2 \cdot (D2 \cdot z2 \cdot D2) & c2 \cdot z2 \cdot (D2 \cdot z3 \cdot D3) \\ c3 \cdot z3 \cdot D3 \cdot (z1 \cdot D1) & c3 \cdot z3 \cdot (D3 \cdot z2 \cdot D2) & c3 \cdot z3 \cdot (D3 \cdot z3 \cdot D3) \end{bmatrix}}{(c1 \cdot z1)^2 \cdot D1 + c2 \cdot z2^2 \cdot D2 + c3 \cdot z3^2 \cdot D3}$

$D(c1, c2, c3) := DW + DLeash(c1, c2, c3)$

$\Delta\Phi := \frac{z1 \cdot (c1L0 - c1R0) + z2 \cdot (c2L0 - c2R0) + z3 \cdot (c3L0 - c3R0)}{-(c1 \cdot z1 + c2 \cdot z2 + c3 \cdot z3) \cdot z4 \cdot \frac{F}{R \cdot T}}$

$\beta := 20000$

$f(D, t) := \exp(-\beta \cdot D \cdot t)$

$I := \begin{pmatrix} 1 & 0 & 0 \\ 0 & 1 & 0 \\ 0 & 0 & 1 \end{pmatrix}$

$D1(c1, c2, c3) := \text{eigenvals}(D(c1, c2, c3))_1$

$D2(c1, c2, c3) := \text{eigenvals}(D(c1, c2, c3))_2$

$D3(c1, c2, c3) := \text{eigenvals}(D(c1, c2, c3))_3$

$Q(c1, c2, c3, t) := \frac{f(D1(c1, c2, c3), t) \cdot (D(c1, c2, c3) - D2(c1, c2, c3) \cdot I) \cdot (D(c1, c2, c3) - D3(c1, c2, c3) \cdot I)}{(D1(c1, c2, c3) - D2(c1, c2, c3)) \cdot (D1(c1, c2, c3) - D3(c1, c2, c3)) \dots}$

$+ \frac{f(D2(c1, c2, c3), t) \cdot (D(c1, c2, c3) - D1(c1, c2, c3) \cdot I) \cdot (D(c1, c2, c3) - D3(c1, c2, c3) \cdot I)}{(D2(c1, c2, c3) - D1(c1, c2, c3)) \cdot (D2(c1, c2, c3) - D3(c1, c2, c3)) \dots}$

$+ \frac{f(D3(c1, c2, c3), t) \cdot (D(c1, c2, c3) - D1(c1, c2, c3) \cdot I) \cdot (D(c1, c2, c3) - D2(c1, c2, c3) \cdot I)}{(D3(c1, c2, c3) - D1(c1, c2, c3)) \cdot (D3(c1, c2, c3) - D2(c1, c2, c3)) \dots}$

These are the simulations for the Left compartment

$i := 1 \dots 200$

$t_i := (i - 1) \cdot 3600 \cdot 0.4$

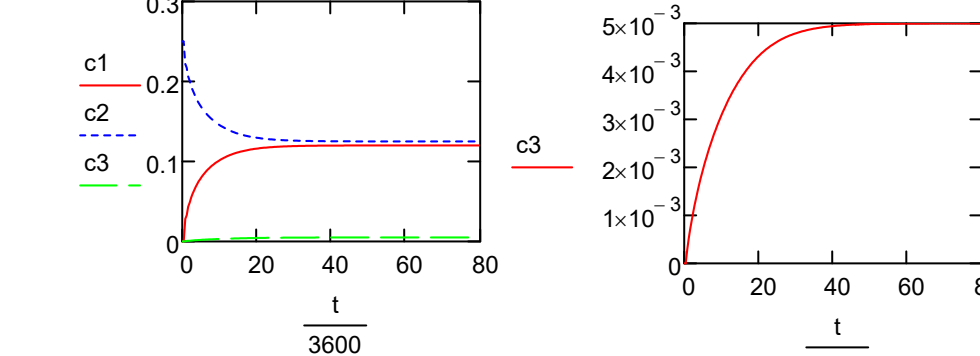
$c1 := c1L0$ $c2 := c2L0$ $c3 := c3L0$

$\begin{pmatrix} c1_{i+1} \\ c2_{i+1} \\ c3_{i+1} \end{pmatrix} := Q(c1_i, c2_i, c3_i, t_i) \begin{pmatrix} c1L0 - c1eq \\ c2L0 - c2eq \\ c3L0 - c3eq \end{pmatrix} + \begin{pmatrix} c1eq \\ c2eq \\ c3eq \end{pmatrix}$

	1
1	0
2	0.4
3	0.8
4	1.2
5	1.6
6	2
7	2.4
8	2.8
9	3.2
10	3.6
11	4
12	4.4
13	4.8
14	5.2
15	5.6
16	...

	1
1	0
2	0
3	0.0281964
4	0.0327582
5	0.043389
6	0.0488797
7	0.05050567
8	0.0597731
9	0.0642472
10	0.068129
11	0.0716915
12	0.0749118
13	0.0778673
14	0.0805804
15	0.0830846
16	...

	1
1	0.25
2	0.25
3	0.2215156
4	0.2167298
5	0.2059039
6	0.200227
7	0.1938842
8	0.1890089
9	0.1843876
10	0.1803655
11	0.1766705
12	0.1733238
13	0.1702477
14	0.1674191
15	0.1648043
16	...



These are the simulations for the Right compartment

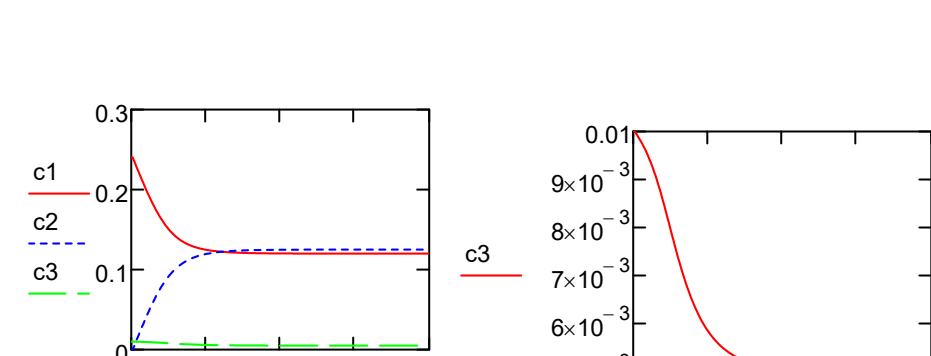
$c1 := c1R0$ $c2 := c2R0$ $c3 := c3R0$

$\begin{pmatrix} c1_{i+1} \\ c2_{i+1} \\ c3_{i+1} \end{pmatrix} := Q(c1_i, c2_i, c3_i, t_i) \begin{pmatrix} c1R0 - c1eq \\ c2R0 - c2eq \\ c3R0 - c3eq \end{pmatrix} + \begin{pmatrix} c1eq \\ c2eq \\ c3eq \end{pmatrix}$

	1
1	0
2	0.4
3	0.8
4	1.2
5	1.6
6	2
7	2.4
8	2.8
9	3.2
10	3.6
11	4
12	4.4
13	4.8
14	5.2
15	5.6
16	...

	1
1	0.24
2	0.24
3	0.2353499
4	0.2307335
5	0.2261561
6	0.2216234
7	0.2171414
8	0.2127164
9	0.2083553
10	0.2040653
11	0.1998535
12	0.1957277
13	0.1916954
14	0.1877644
15	0.1839421
16	...

	1
1	0.01
2	0.01
3	9.9526658 \cdot 10^{-3}
4	9.9039158 \cdot 10^{-3}
5	9.8533547 \cdot 10^{-3}
6	9.8005836 \cdot 10^{-3}
7	9.745206 \cdot 10^{-3}
8	9.6868345 \cdot 10^{-3}
9	9.6250996 \cdot 10^{-3}
10	9.5596585 \cdot 10^{-3}
11	9.4902047 \cdot 10^{-3}
12	9.4164783 \cdot 10^{-3}
13	9.3382765 \cdot 10^{-3}
14	9.2554635 \cdot 10^{-3}
15	9.1679792 \cdot 10^{-3}
16	...



These are steady-state flux calculations when diffusion resistance is external to the IEX particle

The calculations are for two different scenarios

The calculations are those plotted in Figure S17 of Supplementary Material

System: 1: H+ 2: Na+ 3: Cl- 4: H2O

ORIGIN = 1

Charges

$z1 := 1$ $z2 := 1$ $z3 := -1$ $z4 := 0$

Ionic diffusivities

$D2 := 1.3 \cdot 10^{-9}$ $D1 := 9.3 \cdot 10^{-9}$ $D3 := 2 \cdot 10^{-9}$

$\Delta := 9.65 \cdot 10^{-4}$ $T := 25 + 273.15$ $R := 8.3144$

$\delta := 20 \cdot 10^{-6}$

$c3(c1, c2) := \frac{z1 \cdot c1 + z2 \cdot c2}{-z3}$ This is the electroneutrality

$$D1eff(c1, c2) := \frac{c1 \cdot z1^2 + c2 \cdot z2^2 + c3(c1, c2) \cdot z3^2}{\frac{c1 \cdot z1^2}{D2} + \frac{(c2 \cdot z2^2 + c3(c1, c2) \cdot z3^2)}{D1}}$$

$$D2eff(c1, c2) := \frac{c1 \cdot z1^2 + c2 \cdot z2^2 + c3(c1, c2) \cdot z3^2}{\frac{c2 \cdot z2^2}{D1} + \frac{(c1 \cdot z1^2 + c3(c1, c2) \cdot z3^2)}{D2}}$$

$$f(c1L, c1R, c2L, c2R) := z1 \left[\frac{D1eff\left(\frac{c1L + c1R}{2}, \frac{c2L + c2R}{2}\right)}{\delta} \cdot (c1L - c1R) \right] + z2 \left[\frac{D2eff\left(\frac{c1L + c1R}{2}, \frac{c2L + c2R}{2}\right)}{\delta} \cdot (c2L - c2R) \right]$$

These are the calculations are for Scenario 1

$c1R := 0.0$

$c2L := 0.0$ $c2R := 0.05$

$c1L := 0.05$ This is guess value

$c3L := c1L + c2L$ $c3R := c1R + c2R$

$c11L(c2L, c1R, c2R) := \text{root}(f(c1L, c1R, c2L, c2R), c1L)$

$c11L(0, 0.0, 0.05) = 0.01869$

$$N1(c2L, c1R, c2R) := \frac{D1eff\left(\frac{c11L(c2L, c1R, c2R) + c1R}{2}, \frac{c2L + c2R}{2}\right)}{\delta} \cdot (c11L(c2L, c1R, c2R) - c1R)$$

$$N2(c2L, c1R, c2R) := \frac{D2eff\left(\frac{c11L(c2L, c1R, c2R) + c1R}{2}, \frac{c2L + c2R}{2}\right)}{\delta} \cdot (c2L - c2R)$$

$N1(0, 0.0, 0.05) = 4.73113 \times 10^{-6}$

$N2(0, 0.0, 0.05) = -4.73113 \times 10^{-6}$

These are the calculations are for Scenario 2

$c1L := 0$ $c1R := 0.05$

$c2R := 0$

$c2L := 0.5$ This is guess value

$c3L := c1L + c2L$ $c3R := c1R + c2R$

$c22L(c1L, c1R, c2R) := \text{root}(f(c1L, c1R, c2L, c2R), c2L)$

$c22L(0, 0.05, 0) = 0.13373$

$$N1(c1L, c1R, c2R) := \frac{D1eff\left(\frac{c1L + c1R}{2}, \frac{c22L(c1L, c1R, c2R) + c2R}{2}\right)}{\delta} \cdot (c1L - c1R)$$

$$N2(c1L, c1R, c2R) := \frac{D2eff\left(\frac{c1L + c1R}{2}, \frac{c22L(c1L, c1R, c2R) + c2R}{2}\right)}{\delta} \cdot (c22L(c1L, c1R, c2R) - c2R)$$

$N1(c1L, c1R, c2R) = -1.26542 \times 10^{-5}$

$N2(c1L, c1R, c2R) = 1.26542 \times 10^{-5}$

These are the calculations of the effective diffusivities

$ctotal := 0.05$

$i := 1 .. 99$

$x1_i := i \cdot 0.01$

$c1_i := x1_i \cdot ctotal$ $c2_i := (1 - x1_i) \cdot ctotal$ $c3_i := c1_i + c2_i$

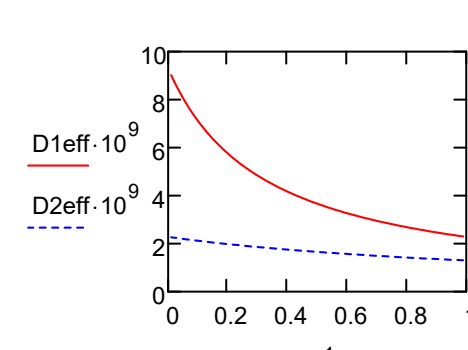
$D1eff := D1eff(c1_i, c2_i)$

$D2eff := D2eff(c1_i, c2_i)$

	1
1	0.01
2	0.02
3	0.03
4	0.04
5	0.05
6	0.06
7	0.07
8	0.08
9	0.09
10	0.1
11	0.11
12	0.12
13	0.13
14	0.14
15	0.15
16	...

	1
1	9.02239
2	8.76087
3	8.51408
4	8.28082
5	8.06
6	7.85065
7	7.6519
8	7.46296
9	7.28313
10	7.11176
11	6.94828
12	6.79213
13	6.64286
14	6.5
15	6.36316
16	...

	1
1	2.26404
2	2.24721
3	2.23063
4	2.21429
5	2.19818
6	2.18231
7	2.16667
8	2.15125
9	2.13604
10	2.12105
11	2.10627
12	2.0917
13	2.07732
14	2.06314
15	2.04915
16	...



These are simulations of the penetration model for transient diffusion into the right compartment; two scenarios are simulated

The calculations are those plotted in Figure S18, Figure 19, and Figure 22a of Supplementary Material

System: 1: H+ 2: Na+ 3: Cl+ 4: H2O

ORIGIN=1

Charges

$z1 := 1 \quad z2 := 1 \quad z3 := -1 \quad z4 := 0$

Ionic diffusivities

$D1 := 9.3 \cdot 10^{-9} \quad D2 := 1.3 \cdot 10^{-9} \quad D3 := 2 \cdot 10^{-9}$

$F := 9.65 \cdot 10^4 \quad T := 25 + 273.15 \quad R := 8.3144$

$c3(c1, c2) := \frac{z1 \cdot c1 + z2 \cdot c2}{-z3} \quad \text{This is the electroneutrality}$

$$D1eff(c1, c2) := \frac{c1 \cdot z1^2 + c2 \cdot z2^2 + c3(c1, c2) \cdot z3^2}{c1 \cdot z1^2 + (c2 \cdot z2^2 + c3(c1, c2) \cdot z3^2)} \quad D2eff(c1, c2) := \frac{c1 \cdot z1^2 + c2 \cdot z2^2 + c3(c1, c2) \cdot z3^2}{c2 \cdot z2^2 + (c1 \cdot z1^2 + c3(c1, c2) \cdot z3^2)}$$

$$f(D, z) := \left(\operatorname{erf} \left(\frac{z}{\sqrt{Dref}} \right) \right)$$

$Dref := 10^{-9}$

$$Q1eff(c1, c2, z) := f(D1eff(c1, c2), z) \quad Q2eff(c1, c2, z) := f(D2eff(c1, c2), z)$$

$$Q(c1, c2, z) := \begin{pmatrix} Q1eff(c1, c2, z) & 0 \\ 0 & Q2eff(c1, c2, z) \end{pmatrix}$$

$zL := 0 \quad zR := 8$

$i := 1 \dots 100$

$$z_i := zL + \frac{(zR - zL)}{100} \cdot i$$

These are simulations for uptake of H+ into the liquid from the IEX particle

$$c1L := 0.0 \quad c2L := 0.01 \quad c3L := z1 \cdot c1L + z2 \cdot c2L \quad c3L = 0.01$$

$$c1R := 0.01 \quad c2R := 0.0 \quad c3R := z2 \cdot c1R + z1 \cdot c2R \quad c3R = 0.01$$

$$c1eq := \frac{(c1L + c1R)}{2} \quad c2eq := \frac{(c2L + c2R)}{2} \quad c3eq := \frac{(c3L + c3R)}{2}$$

$$c1_1 := c1L \quad c2_1 := c2L$$

$$\begin{pmatrix} c1_{i+1} \\ c2_{i+1} \end{pmatrix} := Q(c1_i, c2_i, z_i) \begin{pmatrix} c1R - c1L \\ c2R - c2L \end{pmatrix} + \begin{pmatrix} c1L \\ c2L \end{pmatrix}$$

$$DD1eff_i := D1eff(c1_i, c2_i)$$

$$DD2eff_i := D2eff(c1_i, c2_i)$$

$$c3_i := z1 \cdot c1_i + z2 \cdot c2_i$$

	1
1	0.08
2	0.16
3	0.24
4	0.32
5	0.4
6	0.48
7	0.56
8	0.64
9	0.72
10	0.8
11	0.88
12	0.96
13	1.04
14	1.12
15	1.2
16	...

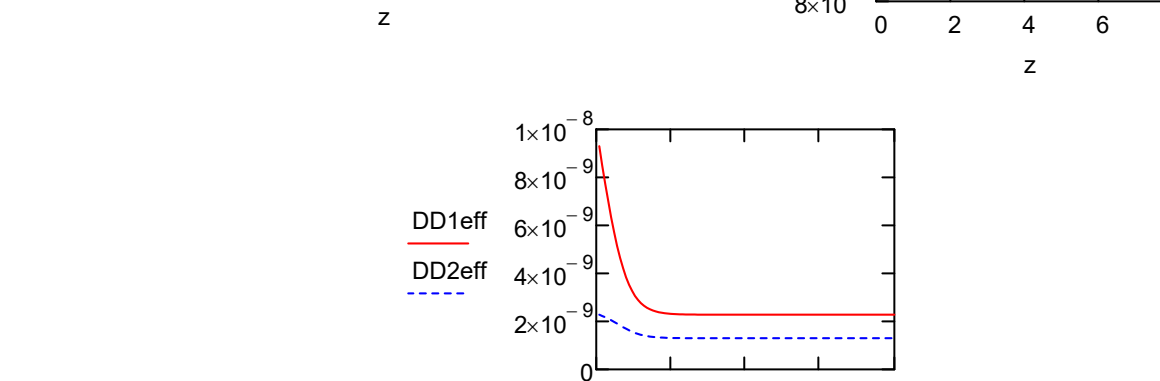
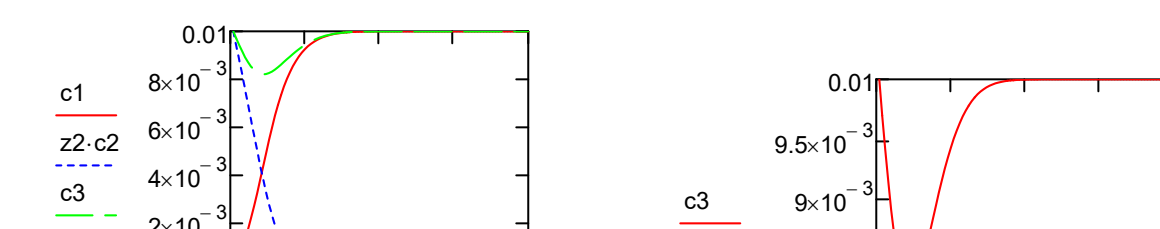
	1
1	0
2	$2.9594 \cdot 10^{-4}$
3	$6.18563 \cdot 10^{-4}$
4	$9.71251 \cdot 10^{-4}$
5	$1.35713 \cdot 10^{-3}$
6	$1.77858 \cdot 10^{-3}$
7	$2.23653 \cdot 10^{-3}$
8	$2.72973 \cdot 10^{-3}$
9	$3.254 \cdot 10^{-3}$
10	$3.80184 \cdot 10^{-3}$
11	$4.36267 \cdot 10^{-3}$
12	$4.92376 \cdot 10^{-3}$
13	$5.47184 \cdot 10^{-3}$
14	$5.99486 \cdot 10^{-3}$
15	$6.4835 \cdot 10^{-3}$
16	...

	1
1	0.01
2	$9.40288 \cdot 10^{-3}$
3	$8.79556 \cdot 10^{-3}$
4	$8.17914 \cdot 10^{-3}$
5	$7.55494 \cdot 10^{-3}$
6	$6.9249 \cdot 10^{-3}$
7	$6.29191 \cdot 10^{-3}$
8	$5.66031 \cdot 10^{-3}$
9	$5.03619 \cdot 10^{-3}$
10	$4.42747 \cdot 10^{-3}$
11	$3.8434 \cdot 10^{-3}$
12	$3.29367 \cdot 10^{-3}$
13	$2.787 \cdot 10^{-3}$
14	$2.32995 \cdot 10^{-3}$
15	$1.92611 \cdot 10^{-3}$
16	...

	1
1	0.01
2	$9.69882 \cdot 10^{-3}$
3	$9.41413 \cdot 10^{-3}$
4	$9.15039 \cdot 10^{-3}$
5	$8.91207 \cdot 10^{-3}$
6	$8.70348 \cdot 10^{-3}$
7	$8.52844 \cdot 10^{-3}$
8	$8.39004 \cdot 10^{-3}$
9	$8.29019 \cdot 10^{-3}$
10	$8.22931 \cdot 10^{-3}$
11	$8.20608 \cdot 10^{-3}$
12	$8.21743 \cdot 10^{-3}$
13	$8.25883 \cdot 10^{-3}$
14	$8.32482 \cdot 10^{-3}$
15	$8.4096 \cdot 10^{-3}$
16	...

	1
1	9.3
2	8.5018
3	7.736
4	7.01043
5	6.33276
6	5.7098
7	5.14692
8	4.64747
9	4.21247
10	3.84059
11	3.52832
12	3.27045
13	3.06063
14	2.89201
15	2.75785
16	...

	1
1	2.28113
2	2.22978
3	2.17336
4	2.11195
5	2.04599
6	1.97633
7	1.90424
8	1.83143
9	1.75981
10	1.69139
11	1.62794
12	1.57079
13	1.52072
14	1.47791
15	1.44206
16	...



These are simulations for uptake of Na+ into the liquid from the IEX particle

$$c1L := 0.01 \quad c2L := 0.0 \quad c3L := c1L + 1 \cdot c2L \quad c3L = 0.01$$

$$c1R := 0.0 \quad c2R := 0.01 \quad c3R := c1R + 1 \cdot c2R \quad c3R = 0.01$$

$$c1eq := \frac{(c1L + c1R)}{2} \quad c2eq := \frac{(c2L + c2R)}{2} \quad c3eq := \frac{(c3L + c3R)}{2}$$

$$c1eq = 5 \times 10^{-3} \quad c2eq = 5 \times 10^{-3} \quad c3eq = 0.01$$

$$c1_1 := c1L \quad c2_1 := c2L$$

$$\begin{pmatrix} c1_{i+1} \\ c2_{i+1} \end{pmatrix} := Q(c1_i, c2_i, z_i) \begin{pmatrix} c1R - c1L \\ c2R - c2L \end{pmatrix} + \begin{pmatrix} c1L \\ c2L \end{pmatrix}$$

$$c3_i := c1_i + 1 \cdot c2_i$$

$$DD1eff_i := D1eff(c1_i, c2_i) \quad DD2eff_i := D2eff(c1_i, c2_i)$$

$$DD1eff := D1eff(c1, c2) \quad DD2eff := D2eff(c1, c2)$$

	1
1	0.08
2	0.16
3	0.24
4	0.32
5	0.4
6	0.48
7	0.56
8	0.64
9	0.72
10	0.8
11	0.88
12	0.96
13	1.04
14	1.12
15	1.2
16	...

	1
1	0.01
2	$9.40288 \cdot 10^{-3}$
3	$8.84421 \cdot 10^{-3}$
4	$$

These are simulations of the penetration model for transient diffusion into the right compartment; two scenarios are simulated

The calculations are those plotted in Figure S20, Figure 21, and Figure 22b of Supplementary Material

System: 1: H+ 2: Ca+ 3: Cl+ 4: H2O

ORIGIN = 1

Charges

$z1 := 1$ $z2 := 2$ $z3 := -1$ $z4 := 0$

Ionic diffusivities

$D1 := 9.3 \cdot 10^{-9}$ $D2 := 0.792 \cdot 10^{-9}$ $D3 := 2 \cdot 10^{-9}$

$\bar{E}_W := 9.65 \cdot 10^4$ $\bar{T}_W := 25 + 273.15$ $\bar{R}_W := 8.3144$

$c3(c1, c2) := \frac{z1 \cdot c1 + z2 \cdot c2}{-z3}$ This is the electroneutrality

$$D1eff(c1, c2) := \frac{-c1 \cdot z1^2 + c2 \cdot z2^2 + c3(c1, c2) \cdot z3^2}{\frac{c1 \cdot z1^2}{D2} + \frac{c2 \cdot z2^2}{D1} + \frac{c3(c1, c2) \cdot z3^2}{D1}}$$

$$D2eff(c1, c2) := \frac{c1 \cdot z1^2 + c2 \cdot z2^2 + c3(c1, c2) \cdot z3^2}{\frac{c2 \cdot z2^2}{D1} + \frac{(c1 \cdot z1^2 + c3(c1, c2) \cdot z3^2)}{D2}}$$

$$Dref := 10^{-9}$$

$$f(D, z) := \left(\operatorname{erf} \left(\frac{z}{\sqrt{\frac{D}{Dref}}} \right) \right)$$

$$Q1eff(c1, c2, z) := f(D1eff(c1, c2), z)$$

$$Q(c1, c2, z) := \begin{pmatrix} Q1eff(c1, c2, z) & 0 \\ 0 & Q2eff(c1, c2, z) \end{pmatrix}$$

$$Q2eff(c1, c2, z) := f(D2eff(c1, c2), z)$$

$$zL := 0$$

$$zR := 8$$

$$i := 1..100$$

$$z_i := zL + \frac{(zR - zL)}{100} \cdot i$$

These are simulations for uptake of H+ into the liquid from the IEX particle

$$c1L := 0.0$$

$$c2L := 0.005$$

$$c3L := c1L + z2 \cdot c2L$$

$$c3L = 0.01$$

$$c1R := 0.01$$

$$c2R := 0.0$$

$$c3R := c1R + z2 \cdot c2R$$

$$c3R = 0.01$$

$$c1eq := \frac{(c1L + c1R)}{2}$$

$$c2eq := \frac{(c2L + c2R)}{2}$$

$$c3eq := \frac{(c3L + c3R)}{2}$$

$$c1_1 := c1L$$

$$c2_1 := c2L$$

$$\begin{pmatrix} c1_{i+1} \\ c2_{i+1} \end{pmatrix} := Q(c1_i, c2_i, z_i) \begin{pmatrix} c1R - c1L \\ c2R - c2L \end{pmatrix} + \begin{pmatrix} c1L \\ c2L \end{pmatrix}$$

$$DD1eff_i := D1eff(c1_i, c2_i)$$

$$DD2eff_i := D2eff(c1_i, c2_i)$$

$$c3_i := c1_i + z2 \cdot c2_i$$

	1
1	0.08
2	0.16
3	0.24
4	0.32
5	0.4
6	0.48
7	0.56
8	0.64
9	0.72
10	0.8
11	0.88
12	0.96
13	1.04
14	1.12
15	1.2
16	...

	1
1	0
2	2.9594 \cdot 10^{-4}
3	6.23316 \cdot 10^{-4}
4	9.88062 \cdot 10^{-4}
5	1.39682 \cdot 10^{-3}
6	1.85653 \cdot 10^{-3}
7	2.37354 \cdot 10^{-3}
8	2.95206 \cdot 10^{-3}
9	3.59177 \cdot 10^{-3}
10	4.28468 \cdot 10^{-3}
11	5.01226 \cdot 10^{-3}
12	5.74473 \cdot 10^{-3}
13	6.44537 \cdot 10^{-3}
14	7.08002 \cdot 10^{-3}
15	7.62734 \cdot 10^{-3}
16	...

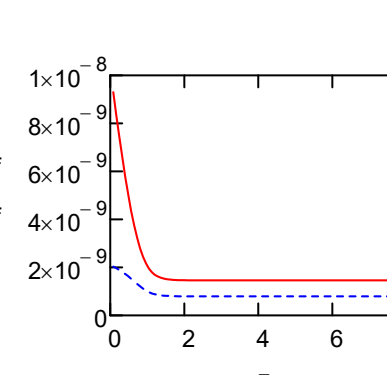
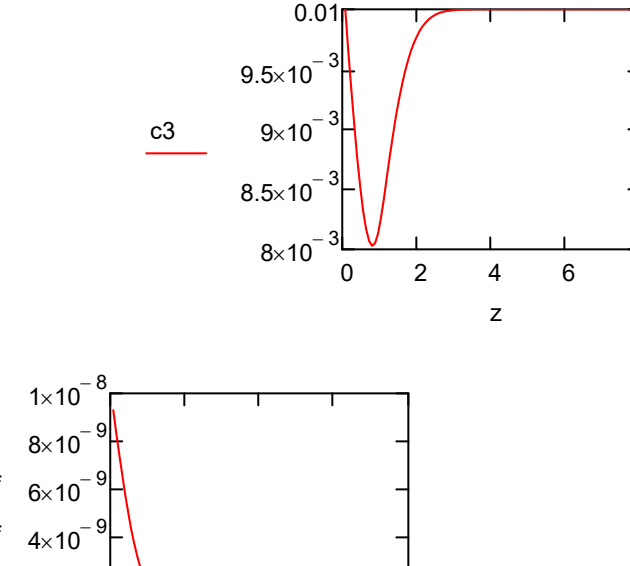
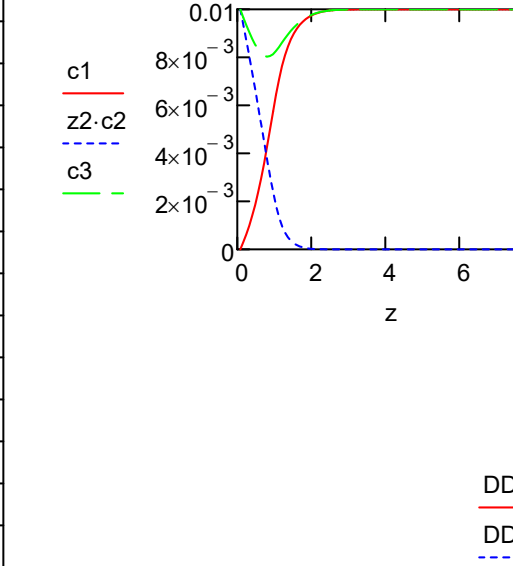
	1
1	0.01
2	9.36712 \cdot 10^{-3}
3	8.71821 \cdot 10^{-3}
4	8.05269 \cdot 10^{-3}
5	7.36977 \cdot 10^{-3}
6	6.66889 \cdot 10^{-3}
7	5.95055 \cdot 10^{-3}
8	5.21772 \cdot 10^{-3}
9	4.4774 \cdot 10^{-3}
10	3.7444 \cdot 10^{-3}
11	3.03895 \cdot 10^{-3}
12	2.38829 \cdot 10^{-3}
13	1.81891 \cdot 10^{-3}
14	1.34839 \cdot 10^{-3}
15	9.79627 \cdot 10^{-4}
16	...

	1
1	0.01
2	8.37237
3	7.47369
4	6.61384
5	5.80325
6	5.05214
7	4.36974
8	3.76355
9	3.23873
10	2.79755
11	2.13302
12	1.5867
13	1.04815
14	0.79615
15	0.68981
16	...

$$DD1eff \cdot 10^9 =$$

$$DD2eff \cdot 10^9 =$$

	1
1	2.03021
2	1.96678
3	1.8954
4	1.81558
5	1.72727
6	1.63104
7	1.5283
8	1.42153
9	1.31428
10	1.21095
11	1.11626
12	1.03428
13	0.96749
14	0.91616
15	0.87855
16	...



These are simulations for uptake of Ca++ into the liquid from the IEX particle

$$c1L := 0.01$$

$$c2L := 0.0$$

$$c3L := c1L + 2 \cdot c2L$$

$$c3L = 0.01$$

$$c1R := 0.0$$

$$c2R := 0.005$$

$$c3R := c1R + 2 \cdot c2R$$

$$c3R = 0.01$$

$$c1eq := \frac{(c1L + c1R)}{2}$$

$$c2eq := \frac{(c2L + c2R)}{2}$$

$$c3eq := \frac{(c3L + c3R)}{2}$$

$$c1eq = 5 \times 10^{-3}$$

$$c2eq = 2.5 \times 10^{-3}$$

$$c3eq = 0.01$$

$$c1_1 := c1L$$

$$c2_1 := c2L$$

$$\begin{pmatrix} c1_{i+1} \\ c2_{i+1} \end{pmatrix} := Q(c1_i, c2_i, z_i) \begin{pmatrix} c1R - c1L \\ c2R - c2L \end{pmatrix} + \begin{pmatrix} c1L \\ c2L \end{pmatrix}$$

$$c3_i := c1_i + 2 \cdot c2_i$$

$$DD1eff_i := D1eff(c1_i, c2_i)$$

$$DD2eff_i := D2eff(c1_i, c2_i)$$

	1
1	0.08
2	0.16
3	0.24
4	0.32
5	0.4
6	0.48
7	0.56
8	0.64
9	0.72
10	0.8
11	0.88
12	0.96
13	1.04
14	1.12
15	1.2
16	...

These simulations are for comparisons with Hwang-Helfferich numerical solution

The calculations are those plotted in Figure S25 of Supplementary Material

ORIGIN = 1

Charges

$z_1 := 1$ $z_2 := 1$ $z_3 := 1$

Ionic diffusivities

$$D_1 := 1 \cdot 10^{-11} \quad D_2 := 5 \cdot 10^{-11} \quad D_3 := 0.2 \cdot 10^{-11}$$

$$F := 9.65 \cdot 10^4 \quad T := 25 + 273.15 \quad R := 8.3144$$

$$x_{1L0} := \frac{1}{z_1} \quad x_{2L0} := \frac{0.0}{z_2} \quad x_{3L0} := \frac{(1 - z_1 \cdot x_{1L0} - z_2 \cdot x_{2L0})}{z_3}$$

$$x_{1R0} := \frac{0}{z_1} \quad x_{2R0} := \frac{0.0}{z_2} \quad x_{3R0} := \frac{(1 - z_1 \cdot x_{1R0} - z_2 \cdot x_{2R0})}{z_3}$$

$$D(x_1, x_2, x_3) := \begin{pmatrix} D_1 & 0 \\ 0 & D_2 \end{pmatrix} - \frac{1}{(x_1 \cdot z_1^2 \cdot D_1 + x_2 \cdot z_2^2 \cdot D_2 + x_3 \cdot z_3^2 \cdot D_3)} \begin{bmatrix} x_1 \cdot z_1^2 \cdot D_1 \cdot (D_1 - D_3) & x_1 \cdot z_1 \cdot z_2 \cdot D_1 \cdot (D_2 - D_3) \\ x_2 \cdot z_2 \cdot z_1 \cdot D_2 \cdot (D_1 - D_3) & x_2 \cdot z_2^2 \cdot D_2 \cdot (D_2 - D_3) \end{bmatrix}$$

$$\Delta\Phi(x_1, x_2, x_3) := \frac{[z_1 \cdot (D_1 - D_3) \cdot (x_1 - x_{1L0}) + z_2 \cdot (D_2 - D_3) \cdot (x_2 - x_{2L0})]}{(x_1 \cdot z_1^2 \cdot D_1 + x_2 \cdot z_2^2 \cdot D_2 + x_3 \cdot z_3^2 \cdot D_3) \cdot \frac{F}{R \cdot T}}$$

$$rc := 0.4 \cdot 10^{-3}$$

$$m := 1..100$$

$$I := \begin{pmatrix} 1 & 0 \\ 0 & 1 \end{pmatrix}$$

$$fexp(m, D, t) := \exp\left[-\left(m^2 \cdot \pi^2 \cdot \frac{D \cdot t}{rc^2}\right)\right] \cdot \frac{1}{m^2}$$

$$f(D, t) := \frac{6}{\pi^2} \sum_m (fexp(m, D, t))$$

$$D1(x_1, x_2, x_3) := \text{eigenvals}(D(x_1, x_2, x_3))_1$$

$$D2(x_1, x_2, x_3) := \text{eigenvals}(D(x_1, x_2, x_3))_2$$

$$i := 1 .. 5000$$

$$Q(x_1, x_2, x_3, t) := \frac{f(D1(x_1, x_2, x_3), t) \cdot (D(x_1, x_2, x_3) - D2(x_1, x_2, x_3) \cdot I)}{(D(x_1, x_2, x_3) - D2(x_1, x_2, x_3)) \dots} \\ + \frac{f(D2(x_1, x_2, x_3), t) \cdot (D(x_1, x_2, x_3) - D1(x_1, x_2, x_3) \cdot I)}{(D2(x_1, x_2, x_3) - D1(x_1, x_2, x_3))}$$

$$t_i := (i - 1) \cdot 4$$

$$x_{11} := x_{1L0}$$

$$x_{21} := x_{2L0}$$

$$x_{31} := x_{3L0}$$

$$Fo_i := \frac{D1 \cdot t_i}{rc^2}$$

$$\begin{pmatrix} x_{1i+1} \\ x_{2i+1} \end{pmatrix} := Q \left[x_{1i}, x_{2i}, \frac{(1 - z_1 \cdot x_{1i} - z_2 \cdot x_{2i})}{z_3}, t_i \right] \cdot \begin{pmatrix} x_{1L0} - x_{1R0} \\ x_{2L0} - x_{2R0} \end{pmatrix} + \begin{pmatrix} x_{1R0} \\ x_{2R0} \end{pmatrix}$$

$$x_{3i+1} := \frac{(1 - z_1 \cdot x_{1i+1} - z_2 \cdot x_{2i+1})}{z_3}$$

$$\Delta\Phi_{1i+1} := \Delta\Phi \left[x_{1i}, x_{2i}, \frac{(1 - z_1 \cdot x_{1i} - z_2 \cdot x_{2i})}{z_3} \right]$$

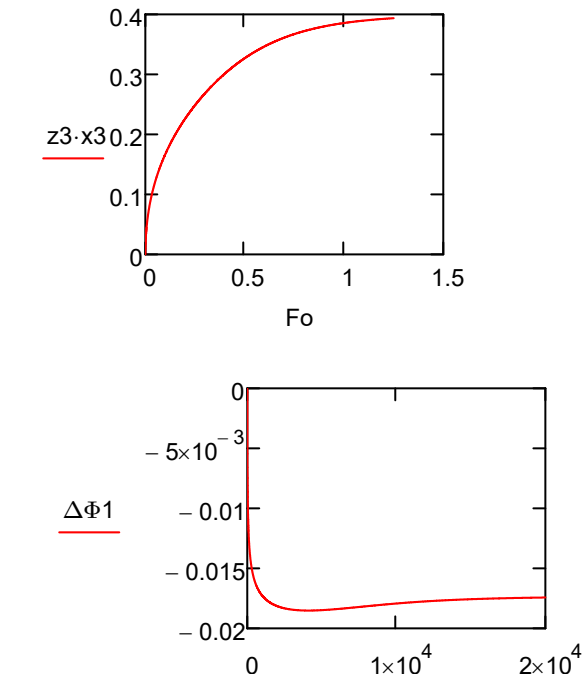
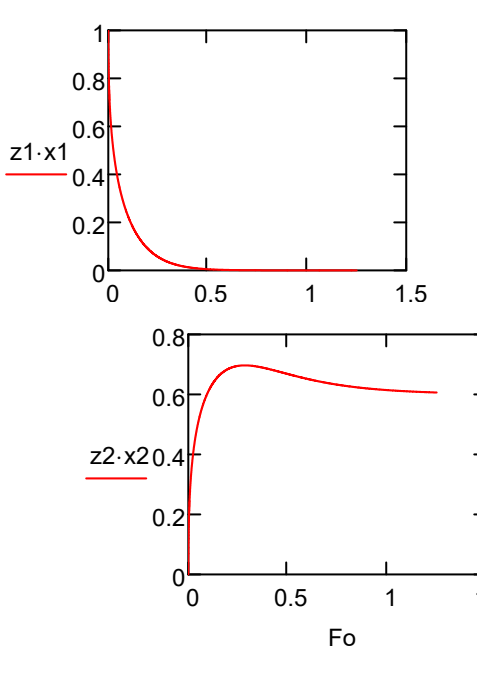
	1
1	0
2	$2.5 \cdot 10^{-4}$
3	$5 \cdot 10^{-4}$
4	$7.5 \cdot 10^{-4}$
5	$1 \cdot 10^{-3}$
6	$1.25 \cdot 10^{-3}$
7	$1.5 \cdot 10^{-3}$
8	$1.75 \cdot 10^{-3}$
9	$2 \cdot 10^{-3}$
10	$2.25 \cdot 10^{-3}$
11	$2.5 \cdot 10^{-3}$
12	$2.75 \cdot 10^{-3}$
13	$3 \cdot 10^{-3}$
14	$3.25 \cdot 10^{-3}$
15	$3.5 \cdot 10^{-3}$
16	...

	1
1	1
2	0.993951
3	0.9213111
4	0.8977628
5	0.878071
6	0.8621614
7	0.8484517
8	0.8363155
9	0.8253576
10	0.8153245
11	0.8060405
12	0.7973786
13	0.7892434
14	0.7815612
15	0.7742737
16	...

	1
1	0
2	$3.6293856 \cdot 10^{-3}$
3	0.069186
4	0.0888761
5	0.1056215
6	0.1190581
7	0.1305978
8	0.140779
9	0.1499448
10	0.1583148
11	0.1660408
12	0.1732328
13	0.1799732
14	0.1863257
15	0.1923405
16	...

	1
1	0
2	$2.4195904 \cdot 10^{-3}$
3	$9.502887 \cdot 10^{-3}$
4	0.0133611
5	0.0163075
6	0.0187805
7	0.0209505
8	0.0229054
9	0.0246975
10	$-9.4301684 \cdot 10^{-3}$
11	$-9.7543845 \cdot 10^{-3}$
12	-0.0100422
13	-0.0103008
14	-0.0105354
15	-0.0107499
16	...

	1
1	0
2	0
3	$-3.1919308 \cdot 10^{-4}$
4	$-5.4476527 \cdot 10^{-3}$
5	$-6.5866187 \cdot 10^{-3}$
6	$-7.4624617 \cdot 10^{-3}$
7	$-8.1081781 \cdot 10^{-3}$
8	$-8.6268735 \cdot 10^{-3}$
9	$-9.0593911 \cdot 10^{-3}$
10	$-9.4301684 \cdot 10^{-3}$
11	$-9.7543845 \cdot 10^{-3}$
12	-0.0100422
13	-0.0103008
14	-0.0105354
15	-0.0107499
16	...



These are the simulations for transient diffusion of counter-ions inside IEX particle; two scenarios are simulated

The calculations are those plotted in Figure S26 of Supplementary Material

ORIGIN = 1

System: 1: H+ 2: Na+ 3: Cl-

Charges

$z1 := 1$ $z2 := 1$

Ionic diffusivities

$$\begin{aligned} D1 &:= 15 \cdot 10^{-9} & D2 &:= 6 \cdot 10^{-9} & R &:= 8.3144 \\ rc &:= 1 \cdot 10^{-3} & \frac{D1}{rc^2} &= 0.015 & \frac{D2}{rc^2} &= 6 \cdot 10^{-3} \\ D1 & & D2 & & D1 &= 2.5 \end{aligned}$$

$$F_i := 9.65 \cdot 10^4$$

$$T := 25 + 273.15$$

$$Deff(x1, x2) := D1 - x1 \cdot z1 \cdot D1 \cdot \frac{z1 \cdot (D1 - D2)}{(x1 \cdot z1^2 \cdot D1 + x2 \cdot z2^2 \cdot D2)}$$

$$m := 1 \dots 100$$

$$fexp(m, D, t) := \exp\left[-\left(\frac{m^2 \cdot \pi^2 \cdot D}{rc^2}\right) \cdot t\right] \cdot \frac{1}{m^2}$$

$$f(D, t) := \frac{6}{\pi^2} \sum_m (fexp(m, D, t))$$

$$Q(x1, x2, t) := f(Deff(x1, x2), t)$$

$$i := 1 \dots 1000$$

$$t_i := (i - 1) \cdot 0.08$$

In this scenario, the particle is initially loaded with Na+

$$x1L0 := 0$$

$$x2L0 := 1 - x1L0$$

$$x1R0 := 1$$

$$x2R0 := 1 - x1R0$$

$$x1 := x1L0$$

$$x2 := x2L0$$

$$\Delta\Phi(x1, x2) := \frac{-z1 \cdot D1 \cdot (x1 - x1R0) + z2 \cdot D2 \cdot (x2 - x2R0)}{(x1 \cdot z1^2 \cdot D1 + x2 \cdot z2^2 \cdot D2) \cdot \frac{F}{R \cdot T}}$$

$$\begin{pmatrix} x1_{i+1} \\ x2_{i+1} \end{pmatrix} := Q \left[\frac{(x1_i + x1R0)}{2}, \frac{(x2_i + x2R0)}{2}, t_i \right] \cdot \begin{pmatrix} x1L0 - x1R0 \\ x2L0 - x2R0 \end{pmatrix} + \begin{pmatrix} x1R0 \\ x2R0 \end{pmatrix}$$

$$D1eff_i := Deff(x1_i, x2_i)$$

$$\Delta\Phi1_i := \Delta\Phi(x1_i, x2_i)$$

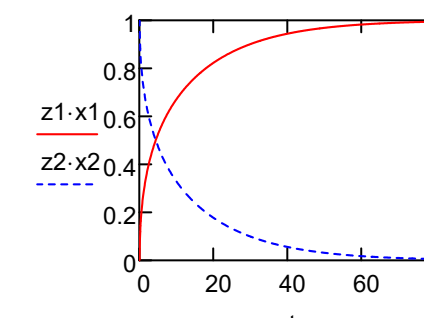
	1
1	0
2	0.08
3	0.16
4	0.24
5	0.32
6	0.4
7	0.48
8	0.56
9	0.64
10	0.72
11	0.8
12	0.88
13	0.96
14	1.04
15	1.12
16	...

	1
1	0
2	6.04898 \cdot 10^{-3}
3	0.08648
4	0.11913
5	0.14389
6	0.16431
7	0.18197
8	0.19768
9	0.21191
10	0.22497
11	0.23708
12	0.2484
13	0.25905
14	0.26911
15	0.27866
16	0.27134

	1
1	1
2	0.99395
3	0.91352
4	0.88087
5	0.85611
6	0.83569
7	0.81803
8	0.80232
9	0.78809
10	0.77503
11	0.76292
12	0.7516
13	0.74095
14	0.73089
15	0.72134
16	...

	1
1	15
2	14.86512
3	13.27768
4	12.72588
5	12.33723
6	12.03402
7	11.78356
8	11.56943
9	11.38206
10	11.21531
11	11.06501
12	10.92814
13	10.80249
14	10.68636
15	10.57839
16	...

	1
1	0.03853
2	0.03796
3	0.03116
4	0.0288
5	0.02713
6	0.02583
7	0.02476
8	0.02385
9	0.02304
10	0.02233
11	0.02169
12	0.0211
13	0.02056
14	0.02006
15	0.0196
16	...



In this scenario, the particle is initially loaded with H+

$$x1L0 := 1$$

$$x2L0 := 1 - x1L0$$

$$x1R0 := 0$$

$$x2R0 := 1 - x1R0$$

$$x1 := x1L0$$

$$x2 := x2L0$$

$$D1eff_i := Deff(x1_i, x2_i)$$

$$\Delta\Phi1_i := \Delta\Phi(x1_i, x2_i)$$

	1
1	0
2	0.08
3	0.16
4	0.24
5	0.32
6	0.4
7	0.48
8	0.56
9	0.64
10	0.72
11	0.8
12	0.88
13	0.96
14	1.04
15	1.12
16	...

	1
1	1
2	0.99395
3	0.9133
4	0.87652
5	0.84875
6	0.82547
7	0.80505
8	0.78665
9	0.7698
10	0.75417
11	0.73954
12	0.72575
13	0.71268
14	0.70023
15	0.68833
16	...

	1
1	0
2	6.04898 \cdot 10^{-3}
3	0.0867
4	0.12348
5	0.15125
6	0.17453
7	0.19495
8	0.21335
9	0.2302
10	0.24583
11	0.26046
12	0.27425
13	0.28732
14	0.29977
15	0.31167
16	...

	1
1	0
2	9.3573 \cdot 10^{-5}
3	1.40958 \cdot 10^{-3}
4	2.05557 \cdot 10^{-3}
5	2.56391 \cdot 10^{-3}
6	3.00469 \cdot 10^{-3}
7	3.40286 \cdot 10^{-3}
8	3.77104 \cdot 10^{-3}
9	4.11665 \cdot 10^{-3}
10	4.44454 \cdot 10^{-3}
11	4.75805 \cdot 10^{-3}
12	5.05959 \cdot 10^{-3}
13	5.351 \cdot 10^{-3}
14	5.6337 \cdot 10^{-3}
15	

These are the simulations for transient diffusion of counter-ions inside IEX particle; two scenarios are simulated

The calculations are those plotted in Figure S27 of Supplementary Material

ORIGIN= 1

System: 1: Na+ 2: Sr+ 3: Cl-

Charges

$z1 := 1$ $z2 := 2$

Ionic diffusivities

$$\begin{aligned} D1 &:= 6 \cdot 10^{-9} & D2 &:= 0.4 \cdot 10^{-9} & R &:= 8.3144 \\ rc &:= 1 \cdot 10^{-3} & \frac{D1}{rc^2} &= 6 \times 10^{-3} & \frac{D2}{rc^2} &= 4 \times 10^{-4} \\ F &:= 9.65 \cdot 10^4 & & & \frac{D1}{D2} &= 15 \end{aligned}$$

$$T_w = 25 + 273.15$$

$$Deff(x1, x2) := D1 - x1 \cdot z1 \cdot D1 \cdot \frac{z1 \cdot (D1 - D2)}{(x1 \cdot z1)^2 \cdot D1 + x2 \cdot z2^2 \cdot D2}$$

$$m := 1..100$$

$$fexp(m, D, t) := \exp\left[-\left(\frac{m^2 \pi^2}{rc^2} \cdot \frac{D}{t}\right)\right] \cdot \frac{1}{m^2}$$

$$f(D, t) := \frac{6}{\pi^2} \sum_m (fexp(m, D, t))$$

$$Q(x1, x2, t) := f(Deff(x1, x2), t)$$

$$i := 1..1000$$

$$t_i := (i - 1) \cdot 0.9$$

In this scenario, the particle is initially loaded with Sr++

$$\begin{aligned} x1L0 &:= 0 & x2L0 &:= \frac{(1 - z1 \cdot x1L0)}{z2} & x1R0 &:= 1 & x2R0 &:= \frac{1 - z1 \cdot x1R0}{2} \\ x1_1 &:= x1L0 & x2_1 &:= x2L0 & x1L0 &:= 0.5 & x2L0 &:= 0.5 \\ x2R0 &:= 0 & & & & & & \\ \left(\frac{x1_{i+1}}{x2_{i+1}}\right) &:= Q\left[\frac{(x1_i + x1R0)}{2}, \frac{(x2_i + x2R0)}{2}, t_i\right] \cdot \left(\frac{x1L0 - x1R0}{x2L0 - x2R0}\right) + \left(\frac{x1R0}{x2R0}\right) & & & & & & \\ D1eff \cdot 10^9 &:= & \Delta\Phi(x1, x2) &:= \frac{-z1 \cdot D1 \cdot (x1 - x1R0) + z2 \cdot D2 \cdot (x2 - x2R0)}{(x1 \cdot z1^2 \cdot D1 + x2 \cdot z2^2 \cdot D2) \cdot \frac{F}{R \cdot T}} & & & & \\ & & D1eff_i := Deff(x1_i, x2_i) & & & & & \\ & & \Delta\Phi1_i := \Delta\Phi(x1_i, x2_i) & & & & & \end{aligned}$$

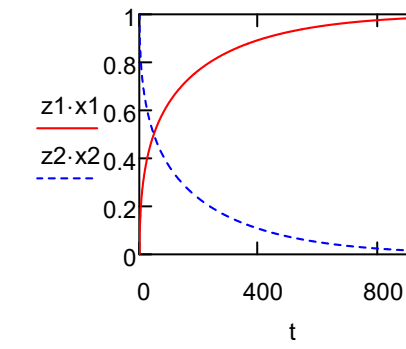
	1
1	0
2	0.9
3	1.8
4	2.7
5	3.6
6	4.5
7	5.4
8	6.3
9	7.2
10	8.1
11	9
12	9.9
13	10.8
14	11.7
15	12.6
16	...

	1
1	0
2	6.04898 \cdot 10^{-3}
3	0.10131
4	0.13482
5	0.16099
6	0.18221
7	0.20038
8	0.21638
9	0.23076
10	0.24386
11	0.25594
12	0.26715
13	0.27764
14	0.28751
15	0.29683
16	...

	1
1	1
2	0.99395
3	0.89869
4	0.86518
5	0.83901
6	0.81779
7	0.79962
8	0.78362
9	0.76924
10	0.75614
11	0.74406
12	0.73285
13	0.72236
14	0.71249
15	0.70317
16	...

	1
1	6
2	5.75555
3	3.4344
4	2.98219
5	2.69594
6	2.49655
7	2.34485
8	2.22354
9	2.12315
10	2.03797
11	1.96433
12	1.89971
13	1.8423
14	1.79081
15	1.74422
16	...

	1
1	0.17982
2	0.17197
3	0.09744
4	0.08292
5	0.07372
6	0.06732
7	0.06245
8	0.05855
9	0.05533
10	0.0526
11	0.05023
12	0.04816
13	0.04631
14	0.04466
15	0.04316
16	...



In this scenario, the particle is initially loaded with Na+

$$\begin{aligned} x1L0 &:= 1 & x2L0 &:= \frac{(1 - z1 \cdot x1L0)}{z2} & x1R0 &:= 0 & x2R0 &:= \frac{1 - z1 \cdot x1R0}{2} \\ x1_1 &:= x1L0 & x2_1 &:= x2L0 & x1L0 &:= 0 & x2L0 &:= 0.5 \\ x2R0 &:= 0.5 & & & & & & \end{aligned}$$

$$\left(\frac{x1_{i+1}}{x2_{i+1}}\right) := Q\left[\frac{(x1_i + x1R0)}{2}, \frac{(x2_i + x2R0)}{2}, t_i\right] \cdot \left(\frac{x1L0 - x1R0}{x2L0 - x2R0}\right) + \left(\frac{x1R0}{x2R0}\right)$$

$$D1eff_i := Deff(x1_i, x2_i)$$

$$\Delta\Phi1_i := \Delta\Phi(x1_i, x2_i)$$

	1
1	0
2	0.9
3	1.8
4	2.7
5	3.6
6	4.5
7	5.4
8	6.3
9	7.2
10	8.1
11	9
12	9.9
13	10.8
14	11.7
15	12.6
16	...

	1
1	1
2	0.99395
3	0.89803
4	0.84991
5	0.81305
6	0.78149
7	0.75322
8	0.72724
9	0.70298
10	0.68007
11	0.65824
12	0.63731
13	0.61713
14	0.59761
15	0.57864
16	...

	1
1	0
2	6.04898 \cdot 10^{-3}
3	0.10197
4	0.15009
5	0.18695
6	0.21851
7	0.24678
8	0.27276
9	0.29702
10	0.31993
11	0.34176
12	0.36269
13	0.38287
14	0.40239
15	0.42136
16	...

	1
1	0.4
2	0.40454
3	0.48352
4	0.52882
5	0.56658
6	0.60127
7	0.6344
8	0.66671
9	0.69865
10	0.73053
11	0.76257
12	0.79496
13	0.82784
14	0.86134
15	0.8956
16	...

	1

<tbl_r cells="2" ix="5" maxcspan="1" maxrspan="1" usedcols="

Both adsorption and desorption cycles are simulated

The calculations are those plotted in Figure S30 of Supplementary Material

ORIGIN = 1

Charges

$z1 := 1$ $z2 := 1$ $z3 := 2$

Ionic diffusivities

$D1 := 9.44 \cdot 10^{-11}$ $D2 := 17.7 \cdot 10^{-11}$ $D3 := 0.63 \cdot 10^{-11}$

$F := 9.65 \cdot 10^4$

$T := 25 + 273.15$

$R := 8.3144$

$$D(x1, x2, x3) := \begin{pmatrix} D1 & 0 \\ 0 & D2 \end{pmatrix} - \frac{1}{(x1 \cdot z1^2 \cdot D1 + x2 \cdot z2^2 \cdot D2 + x3 \cdot z3^2 \cdot D3)} \begin{bmatrix} x1 \cdot z1^2 \cdot D1 \cdot (D1 - D3) & x1 \cdot z1 \cdot z2 \cdot D1 \cdot (D2 - D3) \\ x2 \cdot z2 \cdot z1 \cdot D2 \cdot (D1 - D3) & x2 \cdot z2^2 \cdot D2 \cdot (D2 - D3) \end{bmatrix}$$

$$rc := 0.4 \cdot 10^{-3}$$

$m := 1 .. 100$

$$fexp(m, D, t) := \exp\left[-\left(\frac{m^2 \cdot \pi^2 \cdot D \cdot t}{rc^2}\right)\right] \cdot \frac{1}{m^2}$$

$$f(D, t) := \frac{6}{\pi^2} \sum_m (fexp(m, D, t))$$

$D1(x1, x2, x3) := \text{eigenvals}(D(x1, x2, x3))_1$

$D2(x1, x2, x3) := \text{eigenvals}(D(x1, x2, x3))_2$

$$Q(x1, x2, x3, t) := \frac{f(D1(x1, x2, x3), t) \cdot (D(x1, x2, x3) - D2(x1, x2, x3)) \cdot I}{(D1(x1, x2, x3) - D2(x1, x2, x3))} \dots$$

$$+ \frac{f(D2(x1, x2, x3), t) \cdot (D(x1, x2, x3) - D1(x1, x2, x3)) \cdot I}{(D2(x1, x2, x3) - D1(x1, x2, x3))}$$

$i := 1 .. 5000$

$t_i := (i - 1) \cdot 1$

Adsorption of Na+

$$x1L0 := \frac{0}{z1} \quad x2L0 := \frac{0.5}{z2} \quad x3L0 := \frac{(1 - z1 \cdot x1L0 - z2 \cdot x2L0)}{z3}$$

$$x1R0 := \frac{1}{z1} \quad x2R0 := \frac{0.0}{z2} \quad x3R0 := \frac{(1 - z1 \cdot x1R0 - z2 \cdot x2R0)}{z3}$$

$$\Delta\Phi(x1, x2, x3) := \frac{[z1 \cdot (D1 - D3) \cdot (x1 - x1L0) + z2 \cdot (D2 - D3) \cdot (x2 - x2L0)]}{(x1 \cdot z1^2 \cdot D1 + x2 \cdot z2^2 \cdot D2 + x3 \cdot z3^2 \cdot D3)} \cdot \frac{F}{R \cdot T}$$

$x1 := x1L0$

$x2 := x2L0$

$x3 := x3L0$

$$\begin{pmatrix} x1_{i+1} \\ x2_{i+1} \end{pmatrix} := Q \left[x1_i, x2_i, \frac{(1 - z1 \cdot x1_i - z2 \cdot x2_i)}{z3}, t_i \right] \begin{pmatrix} x1L0 - x1R0 \\ x2L0 - x2R0 \end{pmatrix} + \begin{pmatrix} x1R0 \\ x2R0 \end{pmatrix}$$

$$x3_{i+1} := \frac{(1 - z1 \cdot x1_{i+1} - z2 \cdot x2_{i+1})}{z3}$$

$$\Delta\Phi_{i+1} := \Delta\Phi \left[x1_i, x2_i, \frac{(1 - z1 \cdot x1_i - z2 \cdot x2_i)}{z3} \right]$$

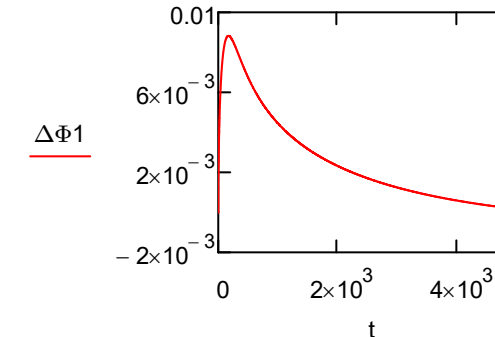
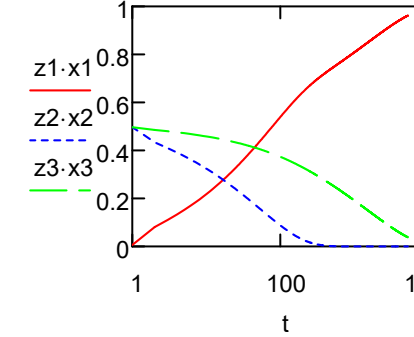
	1
1	0
2	1
3	2
4	3
5	4
6	5
7	6
8	7
9	8
10	9
11	10
12	11
13	12
14	13
15	14
16	...

	1
1	0
2	6.048976 · 10 ⁻³
3	0.0803465
4	0.1106865
5	0.133626
6	0.1525051
7	0.168792
8	0.1832384
9	0.1962919
10	0.2082442
11	0.2192981
12	0.2296011
13	0.2392645
14	0.2483748
15	0.2570009
16	...

	1
1	0.5
2	0.4969755
3	0.4340009
4	0.4094834
5	0.3909796
6	0.3758177
7	0.3627879
8	0.3512715
9	0.3409002
10	0.3314338
11	0.3227054
12	0.3145935
13	0.3070066
14	0.2998734
15	0.2931373
16	...

	1
1	0.5
2	0.4965526
3	0.4856247
4	0.47983
5	0.4753944
6	0.4716773
7	0.4684202
8	0.452715
9	0.4465901
10	0.4314338
11	0.4227054
12	0.4158054
13	0.40537289
14	0.4017518
15	0.40498618
16	...

	1
1	0
2	0
3	-4.5077074 · 10 ⁻⁶
4	1.1883378 · 10 ⁻³
5	1.6456247 · 10 ⁻³
6	2.0002901 · 10 ⁻³
7	2.2956638 · 10 ⁻³
8	2.5529037 · 10 ⁻³
9	2.762831 · 10 ⁻³
10	2.9919165 · 10 ⁻³
11	3.1843937 · 10 ⁻³
12	3.3632133 · 10 ⁻³
13	3.5305305 · 10 ⁻³
14	3.6879771 · 10 ⁻³
15	3.8368242 · 10 ⁻³
16	...



	1
1	0
2	1
3	2
4	3
5	4
6	5
7	6
8	7
9	8
10	9
11	10
12	11
13	12
14	13
15	14
16	...

	1
1	1
2	0.993951
3	0.9347167
4	0.9072125
5	0.8864994
6	0.8691699
7	0.8539934
8	0.8403456
9	0.8278568
10	0.8162864
11	0.805467
12	0.7952772
13	0.785625
14	0.7764391
15	0.7676626
16	...

	1
1	0
2	3.024488 · 10 ⁻³
3	0.054695
4	0.077782
5	0.0951028
6	0.1095714
7	0.1222263
8	0.1359533
9	0.1439838
10	0.1536004
11	0.1625839
12	0.1710368
13	0.1790363
14	0.1866427
15	0.1939037
16	...

	1
1	0
2	0
3</td	

Both adsorption and desorption cycles are simulated

The calculations are those plotted in Figure S31 of Supplementary Material

ORIGIN = 1

Charges

$z1 := 1$ $z2 := 1$ $z3 := 3$

Ionic diffusivities

$$D1 := 9.44 \cdot 10^{-11} \quad D2 := 17.7 \cdot 10^{-11} \quad D3 := 0.092 \cdot 10^{-11}$$

$$F := 9.65 \cdot 10^4$$

$$T := 25 + 273.15$$

$$R := 8.3144$$

$$D(x1, x2, x3) := \begin{pmatrix} D1 & 0 \\ 0 & D2 \end{pmatrix} - \frac{1}{(x1 \cdot z1^2 \cdot D1 + x2 \cdot z2^2 \cdot D2 + x3 \cdot z3^2 \cdot D3)} \begin{bmatrix} x1 \cdot z1^2 \cdot D1 \cdot (D1 - D3) & x1 \cdot z1 \cdot z2 \cdot D1 \cdot (D2 - D3) \\ x2 \cdot z2 \cdot z1 \cdot D2 \cdot (D1 - D3) & x2 \cdot z2^2 \cdot D2 \cdot (D2 - D3) \end{bmatrix}$$

$$rc := 0.4 \cdot 10^{-3}$$

$$m := 1 \dots 100$$

$$fexp(m, D, t) := \exp\left[-\left(\frac{m^2 \cdot \pi^2 \cdot D \cdot t}{rc^2}\right)\right] \cdot \frac{1}{m^2}$$

$$f(D, t) := \frac{6}{\pi^2} \sum_m (fexp(m, D, t))$$

$$D1(x1, x2, x3) := \text{eigenvals}(D(x1, x2, x3))_1$$

$$D2(x1, x2, x3) := \text{eigenvals}(D(x1, x2, x3))_2$$

$$Q(x1, x2, x3, t) := \frac{f(D1(x1, x2, x3), t) \cdot (D(x1, x2, x3) - D2(x1, x2, x3) \cdot I)}{(D1(x1, x2, x3) - D2(x1, x2, x3)) \dots} \\ + \frac{f(D2(x1, x2, x3), t) \cdot (D(x1, x2, x3) - D1(x1, x2, x3) \cdot I)}{(D2(x1, x2, x3) - D1(x1, x2, x3))}$$

$$i := 1 \dots 5000$$

Adsorption of Na+

$$t_i := (i - 1) \cdot 4$$

$$x1L0 := \frac{0}{z1} \quad x2L0 := \frac{0.5}{z2} \quad x3L0 := \frac{(1 - z1 \cdot x1L0 - z2 \cdot x2L0)}{z3}$$

$$x1R0 := \frac{1}{z1} \quad x2R0 := \frac{0.0}{z2} \quad x3R0 := \frac{(1 - z1 \cdot x1R0 - z2 \cdot x2R0)}{z3}$$

$$\Delta\Phi(x1, x2, x3) := \frac{[-z1 \cdot (D1 - D3) \cdot (x1 - x1L0) + z2 \cdot (D2 - D3) \cdot (x2 - x2L0)]}{(x1 \cdot z1^2 \cdot D1 + x2 \cdot z2^2 \cdot D2 + x3 \cdot z3^2 \cdot D3) \cdot \frac{F}{R \cdot T}}$$

$$x1 := x1L0$$

$$x2 := x2L0$$

$$x3 := x3L0$$

$$\begin{pmatrix} x1_{i+1} \\ x2_{i+1} \end{pmatrix} := Q \left[x1_i, x2_i, \frac{(1 - z1 \cdot x1_i - z2 \cdot x2_i)}{z3}, t_i \right] \begin{pmatrix} x1L0 - x1R0 \\ x2L0 - x2R0 \end{pmatrix} + \begin{pmatrix} x1R0 \\ x2R0 \end{pmatrix}$$

$$x3_{i+1} := \frac{(1 - z1 \cdot x1_{i+1} - z2 \cdot x2_{i+1})}{z3}$$

$$\Delta\Phi_{i+1} := \Delta\Phi \left[x1_i, x2_i, \frac{(1 - z1 \cdot x1_i - z2 \cdot x2_i)}{z3} \right]$$

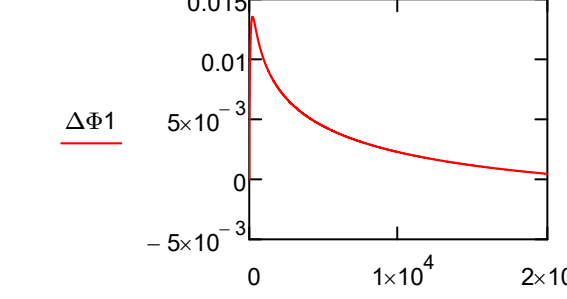
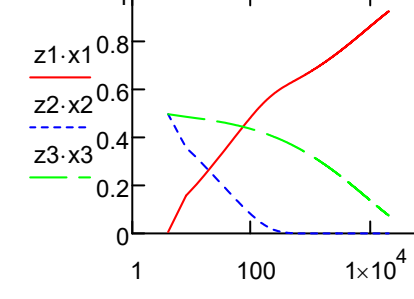
	1
1	0
2	4
3	8
4	12
5	16
6	20
7	24
8	28
9	32
10	36
11	40
12	44
13	48
14	52
15	56
16	...

	1
1	0
2	6.048976 $\cdot 10^{-3}$
3	0.1570061
4	0.2046636
5	0.2415403
6	0.2704014
7	0.2944493
8	0.315079
9	0.3331562
10	0.3492379
11	0.3637101
12	0.3768525
13	0.3888749
14	0.3999395
15	0.4101745
16	...

	1
1	0.5
2	0.4969755
3	0.3571686
4	0.3152413
5	0.2827065
6	0.2574802
7	0.2366104
8	0.2188345
9	0.2033649
10	0.1896958
11	0.1774766
12	0.1664538
13	0.1564369
14	0.147279
15	0.1388641
16	...

	1
1	0.5
2	0.4858253
3	0.4800951
4	0.4757532
5	0.4721184
6	0.4689402
7	0.4660865
8	0.4634789
9	0.4610663
10	0.4588133
11	0.4566937
12	0.4546682
13	0.4527815
14	0.4509615
15	0.4491538
16	...

	1
1	0
2	-9.4020817 $\cdot 10^{-6}$
3	3.3891055 $\cdot 10^{-3}$
4	4.5031566 $\cdot 10^{-3}$
5	5.432555 $\cdot 10^{-3}$
6	6.1826395 $\cdot 10^{-3}$
7	6.62838697 $\cdot 10^{-3}$
8	7.3862142 $\cdot 10^{-3}$
9	8.3302589 $\cdot 10^{-3}$
10	7.8824686 $\cdot 10^{-3}$
11	8.3302589 $\cdot 10^{-3}$
12	8.7362142 $\cdot 10^{-3}$
13	9.1066138 $\cdot 10^{-3}$
14	9.4462684 $\cdot 10^{-3}$
15	9.7589679 $\cdot 10^{-3}$
16	...



	1
1	0
2	4
3	8
4	12
5	16
6	20
7	24
8	28
9	32
10	36
11	40
12	44
13	48
14	52
15	56
16	...

	1
1	1
2	0.993951
3	0.8857259
4	0.8346437
5	0.7969591
6	0.7565483
7	0.7383442
8	0.7138852
9	0.6915898
10	0.6710152
11	0.6518542
12	0.6338832
13	0.6169329
14	0.6008719
15	0.5855954
16	...

	1
1	0
2	3.024488 $\cdot 10^{-3}$
3	8.1574209 $\cdot 10^{-3}$
4	0.0115345
5	0.0141663
6	0.016394
7	0.0183625
8	0.0201469
9	0.0217919
10	0.0233266
11	0.0247712
12	0.0261403
13	0.027445
14	0.028694
15	0.029894
16	...

	1

<tbl_r cells="2" ix="5" maxcspan="1" maxrspan="1" usedcols="

System: 1: H+ 2: Na+ 3: Cl- 4: H2O

These are the results presented in Figure S39 of the Supplementary Material

ORIGIN= 0

Charges

$z1 := 1$ $z2 := 1$ $z3 := -1$ $z4 := 0$

Ionic diffusivities

$D2 := 1.3 \cdot 10^{-9}$ $D1 := 9.3 \cdot 10^{-9}$ $D3 := 2 \cdot 10^{-9}$

$F := 9.65 \cdot 10^4$ $T := 25 + 273.15$ $R := 8.3144$

$x1L0 := 0$ $x1R0 := 1$ $x2L0 := 1 - x1L0$ $x2R0 := 1 - x1R0$

$c_{fixed1} := 4.754$ meq per g

$\rho := 1.28$ g per mL

$c_{fixed} := 4.754 \cdot 1.28$ eq per L

$mass_resin := 20$ g

$VR := \frac{20 \cdot 10^{-6}}{1.28}$ m³
 $VL := 400 \cdot 10^{-6}$ m²

$CL := 0.01$ eq per L $VR = 1.5625 \times 10^{-5}$ $K := \frac{1}{1.38}$

$x1L0 := 0$ $x1R0 := 1$ $x2L0 := 1 - x1L0$ $x2R0 := 1 - x1R0$

$$\begin{aligned} A &:= x1L0 + \frac{(CL \cdot VL)}{c_{fixed} \cdot VR} \cdot x1R0 & \frac{(CL \cdot VL)}{c_{fixed} \cdot VR} &= 0.04207 & \alpha &:= \frac{D1}{D2} - 1 & r &:= \frac{D1}{D2} \\ A &= 0.04207 & & & & & & \\ B &:= \frac{CL \cdot VL}{c_{fixed} \cdot VR} & B &= 0.04207 & \frac{A}{B} &= 1 & & \\ \beta &:= 4000 & & & & & & \end{aligned}$$

$t0 := 0$ $t1 := 2 \cdot 10^5$

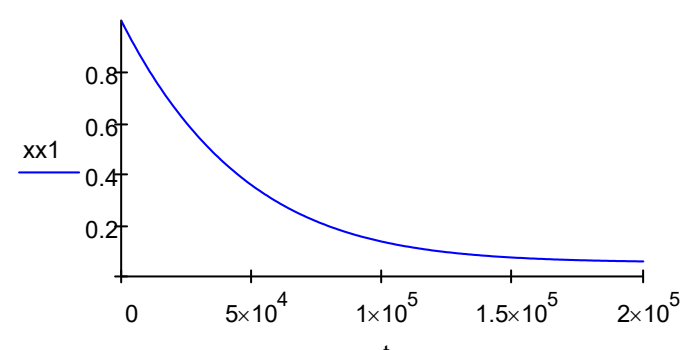
$ic_0 := 1$

$$D(t, x) := \beta \left[D1 \cdot \frac{2}{\left[1 + \alpha \cdot \frac{A - B \cdot x}{K + (1 - K) \cdot (A - B \cdot x)} \right] + \sqrt{\left[1 + \alpha \cdot \frac{A - B \cdot x}{K + (1 - K) \cdot (A - B \cdot x)} \right] \cdot (1 + \alpha \cdot x)}} \right] \left[\frac{A - B \cdot x}{K + (1 - K) \cdot (A - B \cdot x)} - x \right]$$

$S := rkfixed(ic, t0, t1, 200, D)$

$t := s^{(0)}$

$xx1 := s^{(1)}$



	0
0	0
1	0.27778
2	0.55556
3	0.83333
4	1.11111
5	1.38889
6	1.66667
7	1.94444
8	2.22222
9	2.5
10	2.77778
11	3.05556
12	3.33333
13	3.61111
14	3.88889
15	...

	0
0	1
1	0.97995
2	0.96029
3	0.94101
4	0.92211
5	0.90357
6	0.88539
7	0.86757
8	0.85008
9	0.83293
10	0.81612
11	0.79963
12	0.78345
13	0.76759
14	0.75204
15	...

$x1L0 := 1$ $x1R0 := 0$ $x2L0 := 1 - x1L0$ $x2R0 := 1 - x1R0$

$$\begin{aligned} A &:= x1L0 + \frac{(CL \cdot VL)}{c_{fixed} \cdot VR} \cdot x1R0 & \frac{(CL \cdot VL)}{c_{fixed} \cdot VR} &= 0.04207 \\ A &= 1 & & \\ B &:= \frac{CL \cdot VL}{c_{fixed} \cdot VR} & B &= 0.04207 \end{aligned}$$

$\beta = 4 \times 10^3$

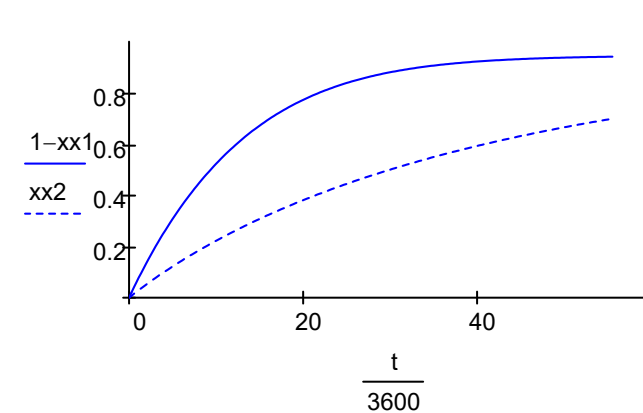
$ic_0 := 0$

$$D(t, x) := \beta \left[D1 \cdot \frac{2}{\left[1 + \alpha \cdot \frac{A - B \cdot x}{K + (1 - K) \cdot (A - B \cdot x)} \right] + \sqrt{\left[1 + \alpha \cdot \frac{A - B \cdot x}{K + (1 - K) \cdot (A - B \cdot x)} \right] \cdot (1 + \alpha \cdot x)}} \right] \left[\frac{A - B \cdot x}{K + (1 - K) \cdot (A - B \cdot x)} - x \right]$$

$S := rkfixed(ic, t0, t1, 200, D)$

$t := s^{(0)}$

$xx2 := s^{(1)}$



	0
0	0
1	0.27778
2	0.55556
3	0.83333
4	1.11111
5	1.38889
6	1.66667
7	1.94444
8	2.22222
9	2.5
10	2.77778
11	3.05556
12	3.33333
13	3.61111
14	3.88889
15	...

	0
0	0
1	7.51758 \cdot 10^{-3}
2	0.01493
3	0.02225
4	0.02947
5	0.0366
6	0.04364
7	0.05059
8	0.05746
9	0.06425
10	0.07096
11	0.07758
12	0.08414
13	0.09061
14	0.09702
15	...